Near Infrared Spectrophotometry and the 2.2 Micron Galactic Survey

by

Peter Laurence Hammersley

Astrophysics Group

Blackett Laboratory

Imperial College of Science, Technology and Medicine

London SW7

A thesis submitted for the degree of

Doctor of Philosophy of the University of London

and for the

Diploma of Membership of the Imperial College

January 1990

Abstract

This report describes two separate near infrared astronomical projects: the development of high quality spectrophotometry for use with the infrared flux method (IRFM) and the initiation of the 2.2μm galactic survey.

The IRFM is acknowledged as potentially the most accurate method of determining stellar temperatures and angular diameters. However, it is limited by uncertainty in the absolute flux calibration and the infrared stellar spectra, particularly line blocking. In July 1987 the ICSTM cooled grating spectrometer (CGS1) was used on the 1m JKT (La Palma) to obtain an absolute calibration of Vega: the 2.250μm flux is $3.81 \times 10^{-10} Wm^{-2}\mu m^{-1}$ $\pm 4\%$. CGS1 on the 1.5m TCS (Tenerife) and CGSII on UKIRT have been used to obtain high quality spectra of non-variable, single, bright stars in the near infrared. The IRFM is applied to CGS1 spectra and gives similar results to previous photometric data. The spectra demonstrates problems with the models between 1.4 and 1.8μm, implying that the H window is unsuitable for the IRFM. Blocking features in the K window are shown to have a measureable effect on previous IRFM results.

The 2.2μm galactic survey is a long term collaboration between ICSTM and the Instituto de Astrofisica de Canarias (Tenerife). The project will map large parts of the galactic bulge and plane using the ICSTM 7 channel linear infrared camera on the 1.5m TCS (Tenerife). The aim is to examine large scale star distribution in the galaxy and to fill the wavelength gap between the I plate and IRAS surveys for probably the most interesting part of the sky. The development of the observational aspects of the project is described with a brief outline of the data reduction.

The development of existing ICSTM instrumentation for the projects outlined above are described in detail, particularly their data acquisition systems.

Contents

List of Figures

List of Tables

Acknowledgements

I wish to acknowledge the people who have helped me over the last three years and made my work both possible and enjoyable. Primarily, I wish to thank my Ph.D. supervisor, Dr Mike Selby, for his invaluable advice and guidance in all the aspects of the projects with which I have been involved. I have benefited immensely from his extensive knowledge of near infrared instrumentation and observational techniques, which have enabled me to avoid many of the pitfalls inherent in this field. I would also like to thank Ian Hepburn for his help in initiating me into the joys of infrared astronomy during my first year.

I have found Imperial College a stimulating place in which to work. This is due to the wide variety of projects being pursued and the friendly atmosphere within the astrophysics group. I would particularly like to thank the technical staff who were always prepared to help with the minor and not so minor problems. In this respect I would like to thank Bill Stannard, Mark Hooker and Victor DeMenezes.

I have had particular help with the infrared flux method from Prof. Blackwell and Dr Booth, from Oxford, who instigated the absolute calibration reported on in chapter 3. Also, I would like to thank Dr Lynas-Gray for his help with the model spectra.

The most memorable part of the ~~the~~ work has been the observing trips to Tenerife and Hawaii. I am greatly indebted to the staff at the Instituto de Astrofisica de Canarias (IAC) in Tenerife. In particular, I would like to thank Dr Francisco (Paco) Gazon and Dr Santiago Arribas for their support, especially during the many long nights spent observing cloud on the 1.5m TCS (originally the IRFC). I would also like to acknowledge the staff at the Joint Astronomy Center, Hilo, Hawaii, in particular, Dr T. Gaballe and Dr G. Wright for their help when using CGSII.

I acknowledge the SERC who funded me during the three years.

Finally, I would like to thank my family and friends for their constant support during the course of my studies. I am particularly grateful to my mother for reading this thesis and removing the worst mistakes.

The bodies that occupy the celestial vault,

These give rise to wise men's uncertainties;

Take care not to lose your grip on the thread of wisdom,

Since the Powers That Be themselves are in a spin.

Verse 9 of the Ruba'iyat Of Omar Khayyam

Translated by Peter Avery & John Heath-Stubbs

Chapter 1

Near Infrared Spectrometry and the Infrared Flux Method

The study of stars has been fundamental to astronomy since pre-historic times, but our understanding of them is still severely limited. There has been a temptation for perhaps the last century to say that although there are still some minor problems with stellar models, the fundamental properties of stars are well known. Certainly the crude parameters for the various stellar classes are now well documented. However, when individual stars are considered, there can be large discrepancies between the expected and actual stellar parameters. The most closely studied star of all, the sun, is still producing unexpected results (eg the low neutrino flux) and this is meant to be a relatively 'well behaved' G2V star. Arcturus is another well studied bright star and yet its mass is still uncertain to about a factor of 10. It is therefore important to astrophysics as a whole that improved models and observations of 'normal' stars continue to be made.

1.1 Defining Stellar Parameters

Stars are spherical hot plasmas, having atmospheres and not solid surfaces, so initially it may seem impossible to define parameters such as a diameter, surface gravity, or temperature.

Virtually all the radiation of a star comes from a relatively small section in the stellar atmosphere, the photosphere. This is essentially the surface of last scattering for radiation leaving a star and is generally taken as being where the optical depth drops from 10 to 0.0001. The thickness of the photosphere varies between 0.01% of the stellar radius for a dwarf star, and 0.1% for a giant, hence the diameter can be well defined.

The temperature of a star varies with radius so it cannot be uniquely defined. Even over the relatively short distance through the photosphere the temperature varies by typically a factor of two. So that a single value of temperature can be assigned to a star the 'effective temperature' T_e is used. This is the temperature that a black body of the same size as the star would require to produce the same total flux.

$$F_S = \sigma T_e^4 \tag{1.1}$$

F_S =Total surface stellar flux (Wm^{-2})

σ = Stefans constant

Although the T_e is not a true thermodynamic temperature, it is a convenient way to estimate the radiated energy output.

The surface gravity of the star is given as

$$g = \frac{GM}{R^2} \tag{1.2}$$

Where G is the gravitational constant, M the mass and R the stellar radius. The range of surface gravities is from about 2 cms^{-2} for M giants up to 10^4 cms^{-2} for B dwarfs. g is usually expressed in terms of $\log g$.

1.2 Measurement of Stellar Angular Diameter

The lack of accurate parallax measurements means that the diameters of stars are usually given in terms of the angle subtended by the star at the earth and not an actual diameter.

1.2.1 Direct Measurements

Interferometric Techniques

The earliest determination of angular diameters was made by Michelson and Pease in 1921 using a phase coherent Michelson interferometer with a 20m base line. They measured 6 late type (K and M) giants and obtained diameters of 20-50 milliarcsec and accuracies of 10-20%.

A two telescope stellar interferometer at CERGA, France, with a base line of 6 to 67m has been used in the visible (Faucherre et al 1983) and near infrared (Di Benedetto et al 1983) to measure giant stars. Angular diameters down to 8 ± 1 milliarcseconds were obtained, but fringe visibility and the scintillation effects make the systematic errors large so the measurements uncertain.

The intensity interferometer was first used by Hanbury Brown and Twiss in 1956. The long base lines possible with this instrument have allowed 32 stars with diameters down to 0.4 milliarcsec to be measured with accuracies of 2 to 14% (Hanbury Brown et al, 1974). The method has the advantage that it is not subject to atmospheric turbulence, but only bright ($< +2$ mag) hot (> 4000K) stars can be measured.

Speckle interferometry has been used by Gezari,Labeyrie and Stachnik (1972) to obtain resolutions down to 16 milliarcsec with an accuracy of 10%.

Although interferometric techniques are direct methods of measuring angular diameters they do rely on stellar models to predict limb darkening.

Lunar Occultations

This relies on measuring the diffraction pattern produced by a star as it passes behind the moon. Resolutions of 3 milliarcsec are possible with a 1 to 2 metre telescope. There have been many published results in both the visible (Cousins et al and Evans et al 1953) and near infrared (Ridgway et al 1977,1979,1980 and 1982) which are generally in good agreement with those from other methods. Potentially this is an accurate method for the

determination of angular diameters. However, there are only a few stars which can be measured.

Eclipsing Binaries

Linear stellar diameters of about 60 stars have been measured using eclipsing spectroscopic binary systems to an accuracy of 10% (Popper 1967,1980).

1.2.2 Indirect Methods for Determining Angular Diameters

Integrated Flux Using the Effective Temperature

If the effective temperature (T_e) and the total flux (F_E) received at the earth from a star are known, then the angular diameter (θ) can be calculated from

$$F_E = \frac{\theta^2}{4} \sigma T_e^4 \tag{1.3}$$

Predicting effective temperatures from spectral type is very inaccurate so only a crude estimate of the angular diameters can be made.

Surface Brightness-Colour Relationships

This is a statistical method for finding angular diameters. A relationship is derived for a set of calibration stars between their directly measured angular diameters and, typically, their visual magnitudes . This is then used to calculate the angular diameters of other stars (Wesselink et al 1972). Standard errors for this technique are estimated at 8 to 12%.

Stellar Atmospheres

Gray (1967) developed a photometric method of combining observed ($F_{E\lambda}$) and modelled stellar surface ($F_{S\lambda}$) monochromatic fluxes.

$$F_{E\lambda} = \frac{\theta^2}{4} F_{S\lambda} \tag{1.4}$$

He used the visible region to measure 80 normal stars with an accuracy of about 8%.

1.3 Measurement of Stellar Effective Temperatures

1.3.1 Direct Methods

Direct methods rely on measuring the angular diameter directly then combining with flux measurements to calculate the effective temperature. Code et al (1976) used the angular diameters of the 32 stars measured by the intensity interferometer in conjunction with their total fluxes to calculate the effective temperatures (using equation 1.1). Ridgway has published effective temperatures for 31 stars of luminosity class III and II in the spectral range G9 to M6, using the angular diameters obtained from lunar occultations together with infrared and visible photometry.

1.3.2 Indirect Methods

These methods use model atmosphere calculations to analyse various aspects of stellar spectra in terms of effective temperature. A number of features in the stellar spectra have been used including the energy distribution in the UV and optical, the Balmer discontinuity, the slope of the Paschen continuum and hydrogen and helium lines. These indirect methods typically claim accuracies of 200K to 500K but since they are often looking at non LTE effects the modelling can be difficult.

Strecker et al (1979) fitted model flux curves to low resolution 1.2-5 micron CVF spectra. He observed 13 mainly late stars.

Gustafsson and Bell (1989) have developed a method of comparing synthetic and measured infrared colour differences to calculate the effective temperature of stars. They have applied the technique to 96 G and K stars.

1.4 The Infrared Flux Method for the Determination of Stellar Effective Temperatures and Angular Diameters

The infrared flux method (IRFM) was developed at Oxford in the late 70's by Professor Blackwell and colleagues. It is a photometric method similar to that of Gray's in that it uses theoretical stellar atmospheres. However, it does not make as many assumptions as some other indirect methods: for this reason it is sometimes classed as being a semi-direct method.

Since the middle 70's the Oxford group has been measuring atomic oscillator strengths to an accuracy of 5% (Blackwell et al 1975,1976). If these strengths are to be used effectively for stellar spectroscopy, then a technique for a more accurate determination of effective temperature and angular diameter is required. Ideally an accuracy of 15K in 4500K is required to match the error in the oscillator strengths for low extinction lines (Blackwell et all 1977). At present this is not possible and a more realistic target accuracy for the IRFM is to determine effective temperature and angular diameters to better than 2%.

When more accurate parallax measurements become available the angular diameters will be converted to linear diameters. When these are combined with surface gravity measurements the masses of the stars can be calculated. This will offer the most accurate method for the determination of the mass of single stars.

1.4.1 The Theory

The IRFM determines angular diameter(θ) and effective temperature (T_e) by simultaneously solving the following 2 equations
Total flux at the earth

$$F_E = \frac{\theta^2}{4}\sigma T_e^4 \tag{1.5}$$

Monochromatic flux at the earth

$$F_{E\lambda} = \frac{\theta^2}{4} f(T_e, g, \lambda, m) \tag{1.6}$$

F_E = Total flux at the earth (Wm^{-2})

$F_{E\lambda}$ = Flux per micron ($Wm^{-2}\mu m^{-1}$)

$f(T_e, g, \lambda, m)$ = Model stellar surface monochromatic flux ($Wm^{-2}\mu m^{-1}$)

λ = Wavelength

m = Metal abundance

The solution is found by iteration. Values for T_e and g are estimated from the star's spectral type. These are used in equation 1.6 together with the measured monochromatic flux to give a value of angular diameter. This is entered into equation 1.5 together with the integrated flux to calculate a better approximation of T_e, which is used in the next iteration. The process rapidly converges to a unique solution for angular diameter and effective temperature.

The solution is very insensitive to the surface gravity so, usually, only an approximate value of $\log g$ needs to be used (eg from Allen's Astrophysical quantities). The metalicity has only been accurately determined for a very few stars, so in general, a solar abundance is assumed. This can lead to problems with certain stars. When the method is applied to Ap stars it is found that changing the metalicity alters the angular diameter by up to a factor of two.

1.4.2 Model Stellar Atmospheres

The IRFM can use any model stellar atmosphere. In the past the models by Carbon and Gingerich (1969) and Kurucz and Peytremann (1974) have been used. Recently the IRFM has tended to use the models of Gustafsson or Kurucz depending on the temperature range. Between 3500K and 7000K the MARCS code (Gustafsson et al 1975) is used, whilst above 7000K the model of Kurucz (1979) is preferred. The MARCS code lacks the ionised species' opacity sources so cannot be used above 7000K whereas the Kurucz model lacks the molecular opacities so should not be used below 6000K. In general, the IRFM is insensitive to the model used.

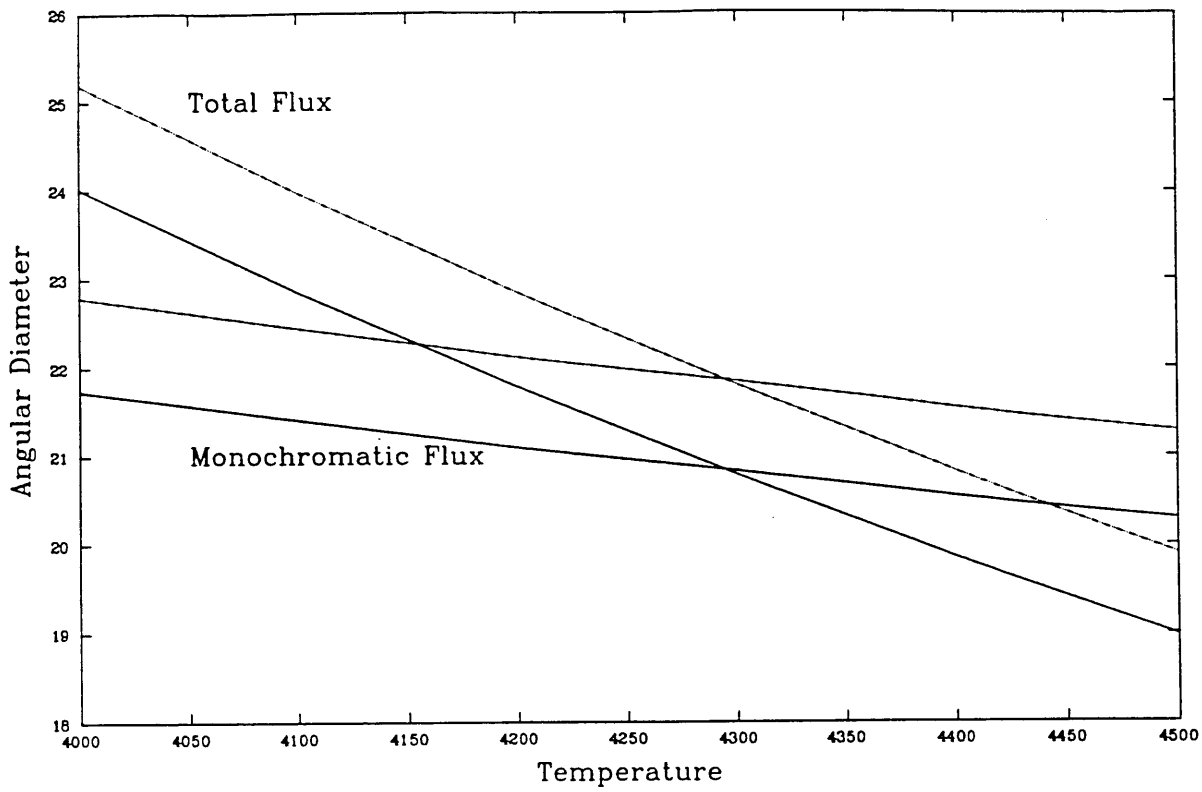

Figure 1.1: The IRFM Applied to αBoo

The solid lines show the application of the IRFM at 3.6μm using data taken from Blackwell et al (1989). The lines for total flux and monochromatic flux intersect sharply giving a clearly defined solution. The dashed lines show the effect of increasing the total and monochromatic fluxes by 10%.

1.4.3 Wavelength Region for the Determination of the Monochromatic Flux

The values of angular diameter and effective temperatures are best defined when the graphs of T_e verses angular diameter for equations 1.5 and 1.6 intersect with the greatest angle between them. The total integrated flux is strongly dependent on effective temperature ($\propto T_e^4$). Therefore the monochromatic flux must be measured in the wavelength range in which it is least sensitive to temperature. This is on the Rayleigh-Jeans part of the flux curve (monochromatic flux is approximately proportional to temperature). In general, this wavelength region is in the infrared although it will extend into the visible for the hotter stars. Figure 1.1 shows a diagram prepared using the observations and models of the K1III star αBoo at 3.6 microns. It gives a well defined solution for T_e and angular diameter.

The opacity of a star comes from a number of sources. The continuum opacities are dominated by bound-free transitions shortward of about 1.6μm and free-free transitions at longer wavelengths. The other major contributions to the opacities come from atomic and molecular absorption lines. In general, the model stellar atmospheres accurately predict the continuum opacities which are strictly in good local thermodynamic equilibrium. However, it is considerably more difficult to model the blocking features as they could contain non LTE effects. In the infrared, blocking features are considerably weaker than in the visible or UV, so the errors introduced will not be as large.

The IRFM does not directly take into account flux that is lost by interstellar extinction or circumstellar dust clouds. By working in the infrared, the extinction will be considerably smaller than at shorter wavelengths. To ascertain whether the losses will be significant, the B-V index of the star is compared with the expected values for that star type. (By using a visible colour difference the amount of extinction will be more easily determined.) If they are comparable then interstellar in the infrared will be negligible.

1.4.4 A Second Version of the IRFM

A second version of the IRFM was developed to make numerical working simpler. The angular diameter is eliminated from equations 1.5 and 1.6 to produce a ratio

$$R = \frac{F_E}{F_{E\lambda}} = \frac{\sigma T_e^4}{f(T_e, g, \lambda, m)} \tag{1.7}$$

The ratio is calculated using model atmospheres for various values of T_e, g, m and wavelength to produce a table. The observed values for F_E and $F_{E\lambda}$ are used to calculate R. Assuming g and m are known, the effective temperature is found by interpolating over the relevant part of the table.

On the Rayleigh-Jeans part of the flux curve the monochromatic flux is approximately proportional to $T_e\lambda^{-4}$.
Hence from equation 1.7

$$R \propto T_e^3\lambda^4 \tag{1.8}$$

for constant values of g and m.

By creating the table using $\log R$, $\log T_e$ and $\log \lambda$ the interpolation is made considerably simpler and more accurate.

1.4.5 Accuracy of the IRFM

The aim of the IRFM is to measure effective temperatures and angular diameters to better then 2%. Is this possible?

Assuming that the ratio R is proportional to T_e^3 then if R can be measured to 4%, which should be possible, the error in T_e is about 1%.
Substituting in equation 1.6 gives the angular diameter

$$\theta^2 \propto \frac{F_{E\lambda}}{f(g, T_e, \lambda, m)} \propto \frac{F_{E\lambda}}{R^{-\frac{1}{3}}} \tag{1.9}$$

so the error in θ goes as $F_{E\lambda}^{\frac{1}{2}} R^{\frac{1}{6}}$, ie is dominated by the flux. Hence, if the flux is accurate to 2%, which is again possible, the error in the angular diameter is only 1%.

There are problems with this simple analysis which will be explained in the next few sections, but in principle, the IRFM is at least as accurate as other methods for the determination of angular diameters and effective temperatures of stars.

1.4.6 Measuring the Total Flux

The measurement of the total integrated flux from a star relies on published energy distributions taken from a number of sources, therefore the final wavelength coverage and the accuracy is not always good. In the most recent paper, Blackwell et al (1989), the fluxes were taken from the following sources:

0-337nm The TD1 satellite (Thompson et al 1978).

337nm-380nm 13 colour photometry together with the absolute calibration of Johnson & Mitchell.

380nm-900nm The Oxford integrating photometer linked to the absolute flux calibration of Vega by Oke & Shield (1970) and by Hayes & Latham (1975).

900nm-1.24μm Model fluxes from the MARCS code linked to the absolute calibration at 1.247 microns and 13 colour photometry of Johnson and Mitchell.

1.24-3.786μm Narrow band photometry at 1.2467μm, 2.2135μm and 3.7825μm taken with the ICSTM 4 channel photometer linked with observational and model flux calibrations of Vega.

3.783-12.43μm Integration of the model atmosphere fluxes generated using the MARCS code.

12.34μm-infinity Integration of the Plank function at each effective temperature.

When determining the total flux a detailed knowledge of the UV line blocking is is not required since it only alters the flux distribution, not the integrated flux. However, accurate models are required for filling the 'gaps' in the wavelength coverage where there are no observations.

The total integrated flux and the monochromatic fluxes suffer from uncertainty in the absolute calibration. In the visible the absolute flux is known to about 3% but at other wavelengths it is considerably less accurate, being as high as 35% in the UV. This causes particular problems for the method when applied to hot stars. Cool stars have approximately 50% of the total flux in the IR and 50% in the visible, so errors introduced by the relatively poor monochromatic IR flux calibration (about 5%) will be reduced, because half the total flux will be subject to the same error, so partly cancels when ratioed. Since hot stars have nearly all their flux in the UV/visible, the error produced by the IR monochromatic flux calibration will not be reduced. Further, hot stars suffer from the inaccurate UV absolute flux calibration which dominates the error in their total flux.

The IRFM assumes that no flux is absorbed or scattered between the star and the earth, so when calculating the total flux, an allowance has to be made for interstellar extinction. In the infrared this is small, typically 0.2 mag per Kpc at 2.2μm, but rises rapidly with decreasing wavelength. In the UV, extinction causes a significant loss of flux for distances beyond about 100pc and it has proved difficult to calculate the loss with any accuracy. With the exception of the closest stars, interstellar extinction in the UV limits the use of the IRFM to stars with a temperature less than about 8000 K.

1.4.7 The Monochromatic Near Infrared Fluxes

The model stellar atmospheres only accurately predict the continuum fluxes and not necessarily the strength of the blocking features. Therefore, the observations must also only measure the continuum flux, as contamination by blocking features will introduce errors. In general, the near infrared windows contain relatively few blocking features and so the first applications of the IRFM used broad band filters. However, as will be shown in chapter 5, there are some relatively strong near infrared absorption lines, particularly hydrogen in the hot stars and CO in the cooler ones. The most recent published IRFM data was taken using narrow band filters: these have profiles that miss the strongest blocking features and use the best parts of the atmospheric windows. The use of narrow band filters also makes the conversion from the integrated signal over the filter profile to a monochromatic flux considerably simpler.

The absolute flux calibration comes from observations and models of Vega. This is a major source of uncertainty for the IRFM and will be discussed in more detail in chapter 3.

1.4.8 Applications of the IRFM

To date the majority of the data published on the IRFM has come from the Oxford/ICSTM collaboration led by D.E.Blackwell and M.J.Selby. They have applied the IRFM to over 200 stars between B9 and M3. Their most recent paper calculates the effective temperatures to about 1% and angular diameters to 3% for 114 A3V to M2.5III stars, assuming the absolute flux calibrations of Vega are correct.

Tsusji (1978,1981a,b,c) has applied the method to carbon stars.

Underhill (1979,1980,1981,1982,1983) has used the method with early type stars and Wolf-Rayet stars.

Saxner and Hammerback (1985) measured 31 F dwarf stars.

Bell and Gustafsson used the method as part of an analysis based on synthetic colours for 95 G and K stars.

1.4.9 Conclusion

The IRFM is currently at least as accurate as any of the direct methods for the determination of stellar effective temperatures and angular diameters and it can be applied to a far greater range of stars. Better models, observations and absolute flux calibrations will improve the accuracy of the IRFM still further.

1.5 Near Infrared Spectroscopy

The near infrared spectral region is at the transition between the stellar spectra being dominated by atomic lines and by molecular features. At near infrared energies, the atomic transition probabilities are sufficient to produce clearly visible lines, mainly hydrogen in the hotter stars and the neutral metals in the cooler ones, although they are considerably weaker than the equivalent optical or UV features. The near infrared contains a large number of molecular features which dominate the spectra of the cooler stars in some windows; the most common being the CO rotation/vibration bands around 2.3 microns.

Near infrared spectrometers with resolutions of 50 to 10^4 have been available for at least 20 years, but there are still surprisingly few published spectra beyond 1 micron. In general, infrared spectrometers are used to observe spectral lines because it has proved difficult to obtain high quality near infrared spectrophotometry over large spectral ranges.

1.6 Common Near Infrared Spectrometers

1.6.1 The CVF

These are probably the most common type of near infrared spectrometers and typically have resolutions in the range 50-100. In comparison with some other spectrometers they are relatively simple to construct and operate, and probably the majority of published spectrophotometry has been taken using these instruments. Having such low resolutions only the strongest features show above the continuum.

1.6.2 Cooled Grating Spectrometer

These have spectral resolutions from 100 up to 1500, or higher, depending on the grating. They are generally operated with a resolution of about 500 which allow many lines, such as the neutral metals, to be identified. However, the lines are not resolved and there can be problems with blending, particularly for molecular lines. Cooled grating spectrometers are becoming more important with the advent of infrared detector arrays which allow simultaneous measurement at many wavelengths. Eventually arrays will become available which will allow the coverage of complete windows at spectral resolutions of 500 or more. This has a number of advantages over single channel instruments.

- By not moving the grating there will be fewer problems with wavelength registration between the raw spectra.
- Spectra will take a far shorter time to complete.
- It will be possible to work in far poorer observing conditions. If a cloud passes through the beam whilst using a single channel scanning instrument, then the signal in one part of the spectrum will be reduced. This may not be noticed, particularly when working at low S/N. By simultaneously measuring all the wavelengths the reduction in signal will be obvious and measurable. If the reduction in signal is the same at all wavelengths then the shape of the spectra will not be affected, only the absolute flux. If it is not constant, then the samples taken at a lower than expected signal can be rejected. Whilst it may not be possible to obtain high quality spectrophotometry in poor conditions, it will be possible to measure the relative strengths of lines.

1.6.3 Fabry-Perot Interferometers

These generally have resolutions from about 80 to 10^4, depending on the distance between the plates. The resolution (R) of the FP is calculated, using $R = nN$, where n is the order and N the finesse. In the infrared the finesse is typically about 40 to 50. Fabry-Perots are ideal for line mapping since they can be used in front of 2D camera arrays. FP's do have some serious draw backs: generally the mirror coatings are only good for one infrared window so 3 or 4 would be needed to cover 1 to 5 microns. At higher (eg 800) resolutions

there will be many orders across a standard filter profile so many narrow band filters will be needed for each window. Also, their line profiles are relatively poor, having wide wings.

1.6.4 Fourier Transform Spectrometers

These have a wide range of possible resolutions depending on the optical path difference. Recent observations taken using FT spectrometers have had resolutions of about 10^4 so allow lines to be resolved (Kleinmann 1986). The high resolution means that to scan whole windows can take hours and the working magnitude limit is about +2. FT spectrometers do have some serious disadvantages. They are operated warm so producing high backgrounds, particularly at longer wavelengths. Also the whole filter band pass is simultaneously sampled, so the noise will tend to be dominated by the shot noise from the highest signals, making it more difficult to observe the fainter parts of the spectrum.

1.7 The Use of Near Infrared Spectrophotometry with the IRFM

High quality near infrared spectrophotometry can be used to improve the IRFM in a number of ways.

The IRFM can be applied directly to the spectra to produce plots of T_e and angular diameter against wavelength. Any problems with the model stellar atmospheres, particularly at the transition in the continuum opacities being dominated by bound-free to free-free, will be more easily identified by the trends in the plots. Narrow band photometry may give individual points more accurately but it cannot show the trends.

The spectra can be used to estimate the effect of the line blocking with star type over the filter profiles used for previous photometry. This will allow the photometry to be modified so that it gives the continuum fluxes.

Chapter 2

The ICSTM Cooled Grating Spectrometer

The ICSTM cooled grating spectrometer mark 1 (CGS1) was designed and built by M.J. Selby and C.M.Mountain at Imperial College in the early 1980's and was the first cooled grating infrared spectrometer built in the UK. It has been operated successfully for a number of years on the 1.5m TCS (Tenerife) and on the JKT (La Palma), both for scanning spectrometry and narrow band photometry.

2.1 The Optical Layout

The optical layout has to be compact in order to fit onto the 7 inch cold surface with the grating encoder and electronics.

The optical configuration is an up-down Newtonian Lithrow mount (figure 2.2). This has the advantage that the grating is operated in its most efficient mode and all the optics are on axis which reduces the aberrations and allows spherical optics to be used. The shadowing of the telescope secondary allows the Newtonian flat to be used without loss of throughput, and a cooled stop is placed near the collimator so the detector can only see a 77K black body in this central hole. Two CaF_2 lenses are used to convert the f13.8 beam from the 1.5m telescope to the f4.28 needed to keep the optics as compact as possible.

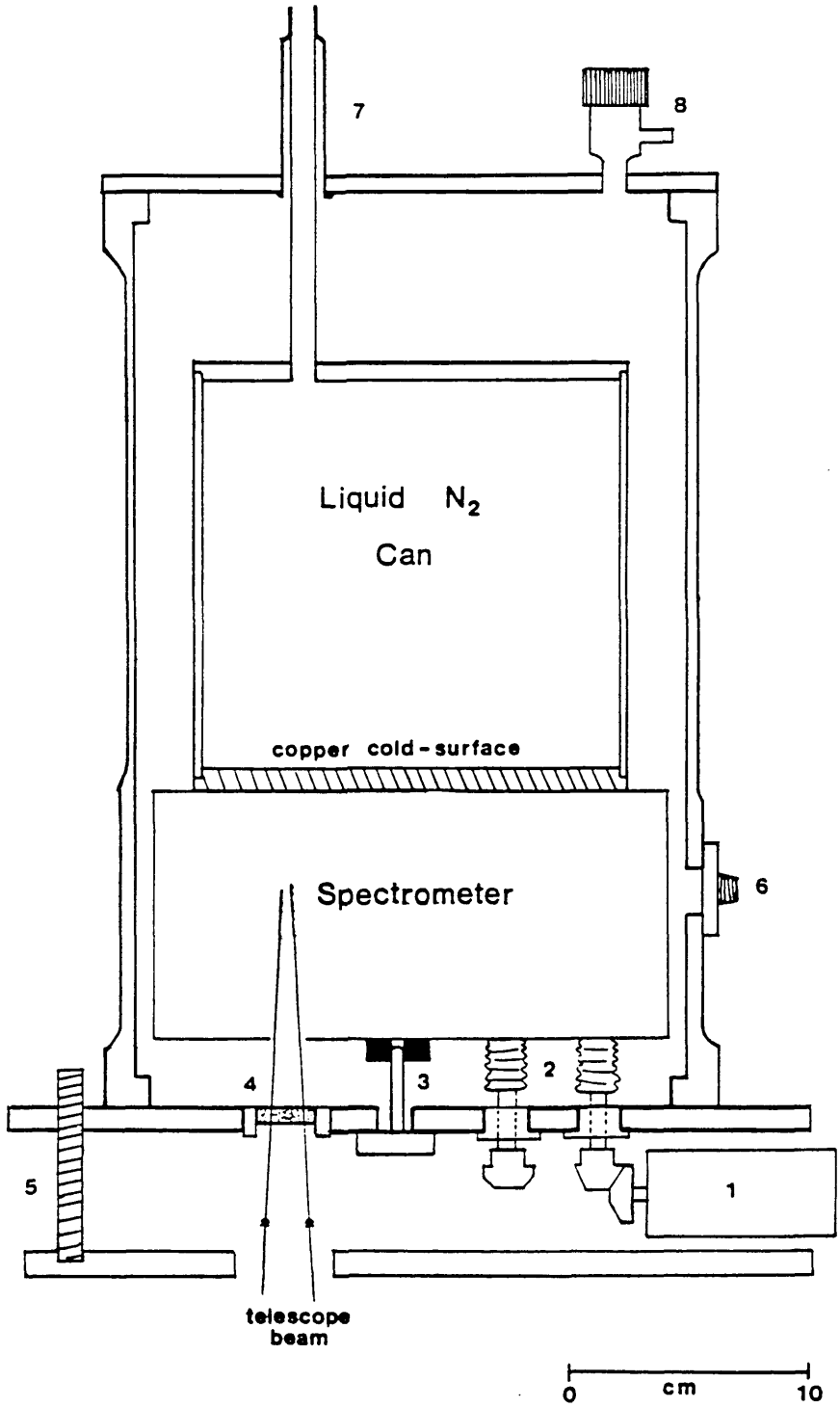

1. - grating drive motor 2. - flexible 'Bellow Couplings' and corresponding Wilson Seals 3. - centring pin 4. - CaF window 5. - spectrometer tilt and support screws 6. - Amphenol electrical connector 7. - fill tube 8. - vacuum valve

Figure 2.1: The Spectrometer Cryostat

(Taken from the thesis of C.M.Mountain.)

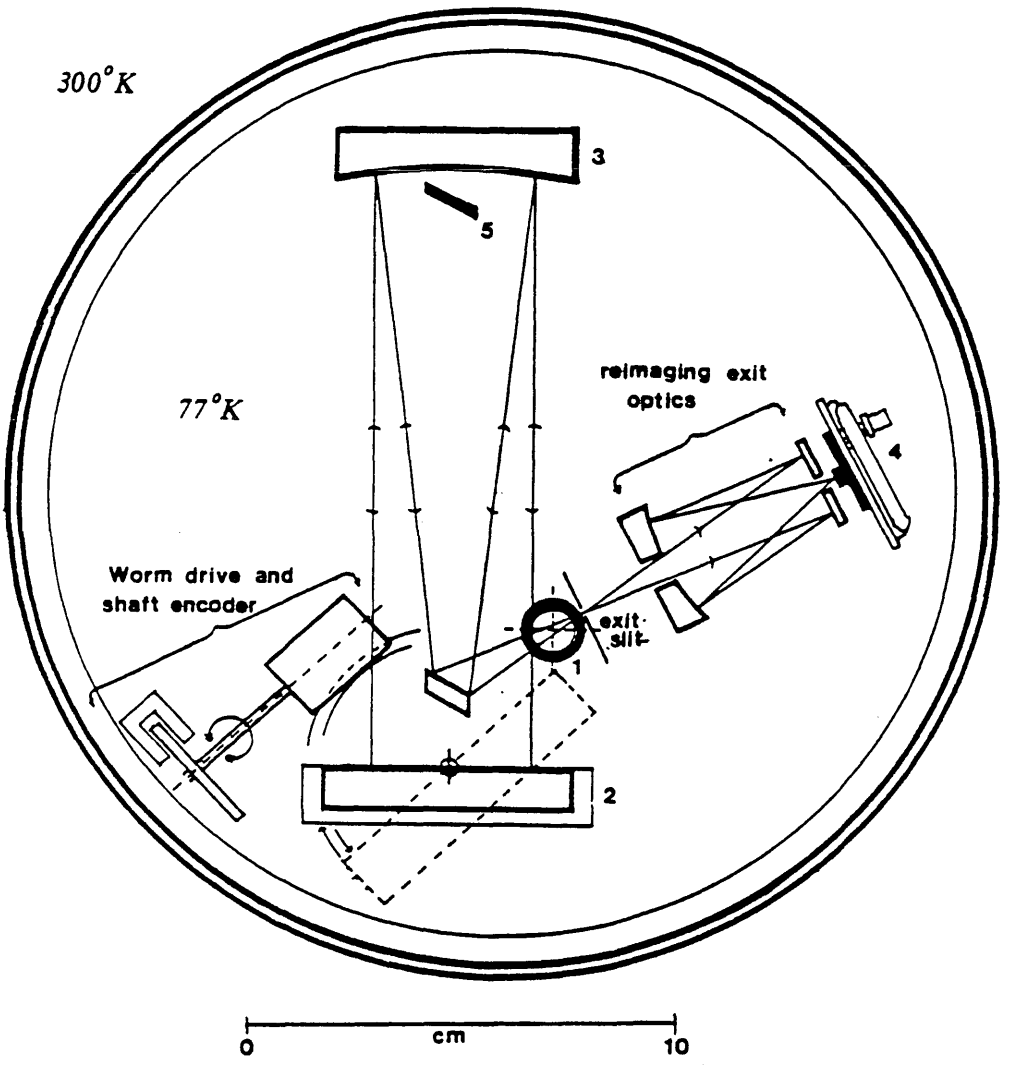

1. Input optics and blocking filters

2. Grating Cell

3. Collimator (spherical)

4. Detector and Pre-amp

5. Central stop

Figure 2.2: The Optical Configuration

(Adapted from the thesis of C.M.Mountain.)

Table 2.1: The Spectral Resolution of CGS1.

Wavelength (μm)	Spectral Order	Angle degrees	Resolution (nominal)
J 1.1	3	29.7	390
H 1.6	2	28.7	374
K 2.2	2	41.3	601
L 3.8	1	34.7	475
M 5.0	1	48.6	776

These lenses also act as field optics which significantly improve the instrument's image profiles. The collimating mirror has a focal length of 154mm so there is a clear aperture on the grating and collimator of 36mm. All the mirrors are gold coated to reduce the loss of signal.

The sky aperture is defined by a circular pin hole at the focus of the collimator. Generally, a sky aperture of 15" is used when it is operated on the TCS, although this could be changed.

The grating is a gold coated Brauch and Lomb replica on a glass substrate. It has 300 lines per mm and is blazed at 4μm so allows the full 1-5μm region to be covered with a nominal spectral resolution of between 400 and 800 (see table 2.1).

The filter wheel is directly under the copper can, so no unfiltered light can scatter onto the detector. There are 7 filters plus a blank as listed in table 2.2.

As with normal photometry, the filters must have no short wave leaks. The flux from a star is approximately proportional to λ^{-4} in the near infrared, ie the flux at 1μm is approximately 64 times that at 4μm. So if an L filter has a 1% short wave leak, one third of the detected signal would be from short wave.

From the grating equation

$$2d \sin\theta = N\lambda \tag{2.1}$$

it can been seen that specific values of grating angle will produce the series of wavelengths

Table 2.2: Filter Positions.

Filter Position	Filter	Approx. Band Pass
1	Blank	
2	J	1 to 1.3 microns
3	M	4.5 to 5.3 microns
4	1.5 Cut On	1.5 to 5 microns
5	2.5 Cut On	2.5 to 5 microns
6	H	1.4 to 1.8 microns
7	K	1.95 to 2.45 microns
8	L'	2.7 to 4.2 microns

$\theta, \frac{\theta}{2}, \frac{\theta}{3}, \frac{\theta}{4}$ ..... Care must be taken when choosing the filter profiles that only one wavelength is transmitted at the grating angles to be used. When two or more orders are transmitted then there is 'order overlap' and confusion occurs between them. Unfortunately, this happens in the J window. Figure 2.3 shows the ratio of three K stars with Vega in the J window. The emission lines are actually the hydrogen blocking lines in the Vega spectra. The hydrogen lines present are listed in table 2.3.

The confusion between the two orders means that beyond about 1.2 μm the data is virtually unusable. It was expected that there would be some order overlap, but only on the very edges of the J window. However, wavelengths as low as 0.9 microns are being detected when, according to the published profiles, the cut off should be at about 1 μm. This suggests that there is a serious defect in the J filter.

2.2 The Grating Drive and Support

The grating is mounted perpendicular to the wheel of a high precision P.I.C antibacklash worm and wheel. The grating is supported by two frictionless cross-spring hinges. A variable speed D.C motor, external to the cryostat, drives the grating. The warm motor drive shaft passes through a Wilson seal in the bottom cryostat plate, then connects to the cold drive shaft via a Servometer flexible bellows coupling. This is necessary to allow

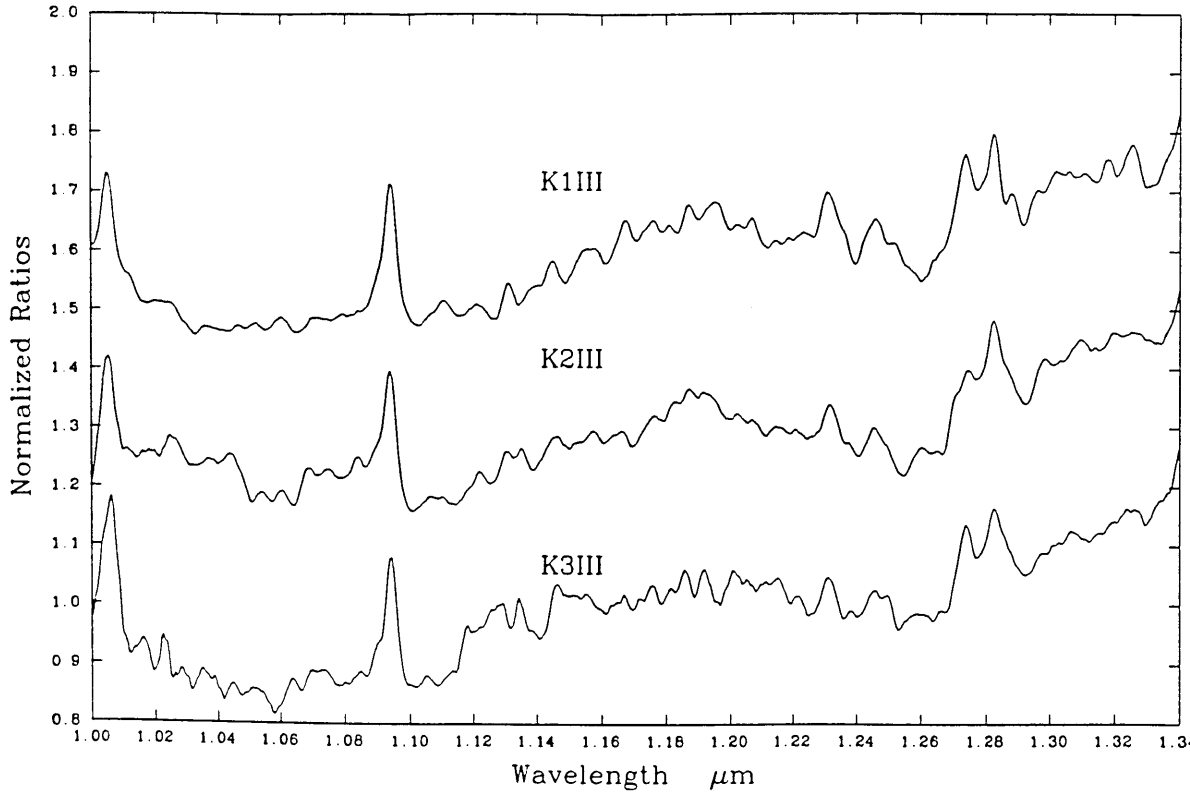

Figure 2.3: K Stars Ratioed with Vega

Table 2.3: Order Overlap.

Apparent Wavelength	Actual Wavelength	Order
1.0052 μm	1.0052 μm	3
1.0941 μm	1.0941 μm	3
1.2024 μm	0.9017 μm	4
1.2308 μm	0.9231 μm	4
1.2731 μm	0.9548 μm	4
1.2822 μm	1.2822 μm	3
1.3402 μm	1.0052 μm	4

contraction as the cryostat cools.

At present there are no lubricants that work in a vacuum at 77K, so all the bearings have to operate dry. This causes one of the major problems in the operation of CGS1, which is the tendency for the grating drive to jam. Although there is no total solution, steps are taken to reduce the risk.

- Extra support has been given to the bevel gear arrangement just outside the Wilson seal. Without the extra support, the drive shaft is only held by the Wilson seal so tends to twist when the motor operates. This in turn puts extra pressure on the internal bearings so making them more likely to seize.
- The whole cryostat is kept as dust free as possible: in particular, the worm, wheel and all internal bearings must be totally clean. As clean a room as possible is used when aligning the cryostat. When completed, the worm, wheel and bearings are washed with clean alcohol and all other parts of the cryostat checked for dust before it is re-assembled.
- The spring in the antibacklash wheel is to hold the teeth of the wheel onto the worm. The tension is kept as small as possible whilst still holding the teeth on the wheel, otherwise friction in the system rises rapidly, particularly when it gets cold.
- The bevel gears must be properly meshed.

2.3 Grating Position Registration

Probably the most difficult part in the design of any spectrometer is to make the wavelength registration sufficiently accurate. This is not for line identification (although it does help) but for the accurate removal of the telluric features when spectra are ratioed (see chapter 4). The errors arise from slight shifts in the relative positions of the edges of the lines. Here a small change in wavelength causes a large change in signal, especially for the deeper features, eg at 2 microns. The acceptable amount of relative shift depends on the signal to noise ratio of the scan, but generally it is around 1% to 2% of the spectral resolution. If it is greater than this then spikes appear in the ratio. Figure 2.4 shows the effect of ratioing a spectra with itself after shifting it by various amounts.

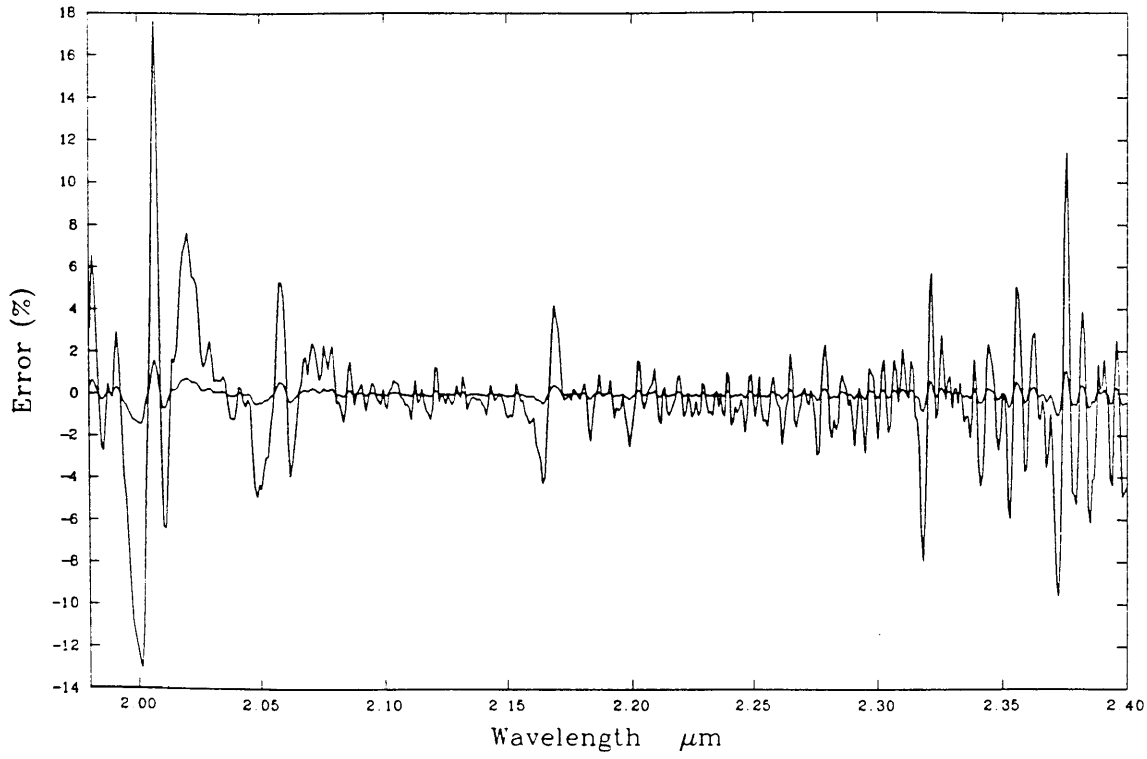

Figure 2.4: The Introduction of Shifts into the Ratioed Spectra

The above is the result of ratioing a K window spectrum with itself after introducing shifts of 0.001μm and 0.0001μm (20% and 2% of the spectral resolution).

CGS1 has two grating position encoders:

The coarse encoder is a potentiometer attached directly to the motor, which produces a binary coded decimal output between 00.00 and 20.00. Motion of the grating between its end stops changes the reading by about 13. The purpose of the coarse encoder is to allow the approximate position of the grating to be quickly determined.

The fine encoder is a capacitive device developed by Roger Sidey of Imperial College. It consists of two circular plates about 1mm apart: the stator is fixed to the base whilst the rota is attached directly to the worm's drive shaft. One quarter of a rotation of the rota produces a complete cycle of the encoder's output (0 to 4095), and it requires about 55 complete cycles of the fine encoder's output to move between the grating end stops. In principle, the wavelength registration should be accurate to better than 0.00001 μm at 2 microns or about $\frac{1}{1000}$th of the spectral resolution.

The advantage of having an absolute encoder directly attached to the worm, rather than external to the cryostat, is that it allows flexible bellows couplings to be used to connect the cold and warm drive shafts without concern about 'wind-up', especially at the torques typically required to move the grating when cold. Also, it means slippage between the motor and the grating will not affect the wavelength registration.

2.4 The Detector

The present detector is a 0.5mm square InSb photovoltaic detector from Cincinnati Electonics, which is operated in a Hall type transimpedence amplifier circuit. Unlike previous detectors from Santa Barbara, the impedence is not altered by J flashing and it can operate at relatively high bias voltages without causing extra noise.

There is a choice of 3 outputs from the pre amp. x1, x10, and x10 smoothed with a 20 Hz Filter. Generally, x10 smoothed is used when observing as it reduces the effect of pick up.

2.5 The Spectrometer Control Modules

The current spectrometer modules are designed to allow the spectrometer to be controlled by a 6502 microprocessor based computer system. They plug into a standard 19.5 inch rack using the ICSTM 'Astrobus' data bus system. (Here I have only included those modules specific to the spectrometer.)

The Motor Amp This provides the power to drive the DC motor. It requires too high a current to work using a standard rack so is generally powered from a stabilised power supply.

The Spectrometer Interface This interfaces the motor control and the fine encoder modules with the computer system.

The Motor Controller This sets the motor speed and direction either using the computer interface or the hand set. When controlled from the computer the speed is

set using a single byte two complement number (& 80 is stopped & FF is full forward and 00 full reverse). This module also has the grating end stop cutouts, which prevent the motor driving the grating into the end stops so damaging the grating support.

The Fine Encoder Module This has a 3 digit hexadecimal readout. The most significant 4 bits of the most significant byte are always 1111.

The Coarse Encoder Module This has a 3.5 digit binary coded decimal readout.

2.6 The Data Acquisition Systems

The spectrometer is currently operated using its third data acquisition system and already the fourth is being developed. Each version has been a vast improvement on its predecessor, allowing easier control of the instrument, better data storage, etc. Probably the most important feature of each new system has been the increase in computer power.

2.6.1 Computers in Data Acquisition Systems

One of the most important improvements to astronomical instrumentation in the last 10 years has been the enormous increase in computer power. Many small desk top computers now have more memory, better storage facilities, are considerably faster and are a fraction of the price of the main frame and mini computers 10 years ago.

Computers are excellent at controlling instruments. They can be made to control the electronic gains, the grating position, the filter wheel, the sky chopper, etc., as well as taking the data. In fact, much of the more recent instrumentation can only operate under the control of computers (eg CCDs). Computers can dramatically reduce the amount of time the observer needs to spend actually controlling the instrument, whilst also improving the accuracy of the recorded information (eg gains, time, airmass) and making damage to the instrument less likely by avoiding dangerous situations.

Computers are now becoming powerful enough to offer a large amount of on-line data reduction, which is of particular value for near infrared spectrophotometry. Generally,

the only guide to the quality of the observations as they are taken, has been the chart recording. Whilst this will show any major problems, a number of potentially serious ones (eg not being fully peaked up) could go un-noticed until the data is reduced. By being able to reduce the data on-line, direct comparisons can be made with previous data sets, as well as spectra taken on that night. Most problems, particularly with airmass calibration scans, will be obvious, so repeats can be made as necessary. This will dramatically reduce the amount of data that is found to be unusable when it is analysed. Also, if an interesting effect is discovered, the observer will be able to take repeat observations immediately.

2.6.2 The Micro-Nova System

The original data acquisition system had a AIM65 microcomputer (based on a 6502 micro processor) controlling the spectrometer, with the data being transferred to the Micro-Nova, where it was stored on punch tape. The spectrometer at this point used an optical fine encoder system. The signal was passed through a post amplifier and then an analogue PSD unit synchronised to the chopper before being read by a DVM.

2.6.3 The 4 Channel Data Acquisition System

When the 4 channel photometer's data acquisition system was built, it was also designed to control the spectrometer. This was again based on an AIM65 microcomputer, but the data was now dumped to a Cristie digital tape recorder. The phase sensitive detection was done digitally; the signal being converted to a frequency using a V to F converter before being passed to up/down counters. The phase of the counters and the sky chopper was controlled by the computer using interrupts.

The system required a lot of user interaction. The setting up of scans had to be done manually using the hand set, and the computer had to be told when to end each scan.

The data is sent to the Cristie in ASCII. The format is

The scan counter (4 digit in hex)

Then for every point in the spectra

AAAA;BBBBBB;CCCC;DDDDLFCR

AAAA is the position counter (4 digit in hex).

BBBBBB is the signal (6 digit in hex).

CCCC is the coarse encoder (4 digit in binary coded decimal).

DDDD is the fine encode (4 digit in hex).

LFCR line feed and carriage return at the end of each line.

2.7 The 7 Channel Data Acquisition System

When the 7 channel data acquisition system became available software was developed to allow it to control the spectrometer. The aim was for the first time to put the grating under full computer control making the spectrometer far simpler to operate. The 7 channel data acquisition system is based around two computers. The digital rack or single board computer (SBC) controls the cryostat, amplifiers, chopper, etc. Like the 4 channel it has a 6502 microprocessor and uses the Astrobus data bus. The second computer is at present a BBC micro computer: it is used for the data storage, user interface, and any online reduction. The computers communicate using a RS232 serial interface at 9600 baud. Full details of the 7 channel data acquisition system are in chapter 7. This section will only deal with the software required to run the spectrometer. I wrote both the SBC and BBC programs using as a guide the 7 channel SBC program written by Mick Bartholomew, the 7 channel BBC software written by M. Hooker and the 4 channel software written by A. Zadrosny.

2.7.1 The SBC Software

The most important job for the SBC is to control the timing for the chopping and data collection. Other tasks take second place to this.

The Interrupt Routines

The interrupt routine maintains the phase difference between the up/down counter and the chopper, and reads then resets the counter after a pre-defined number of chops. The

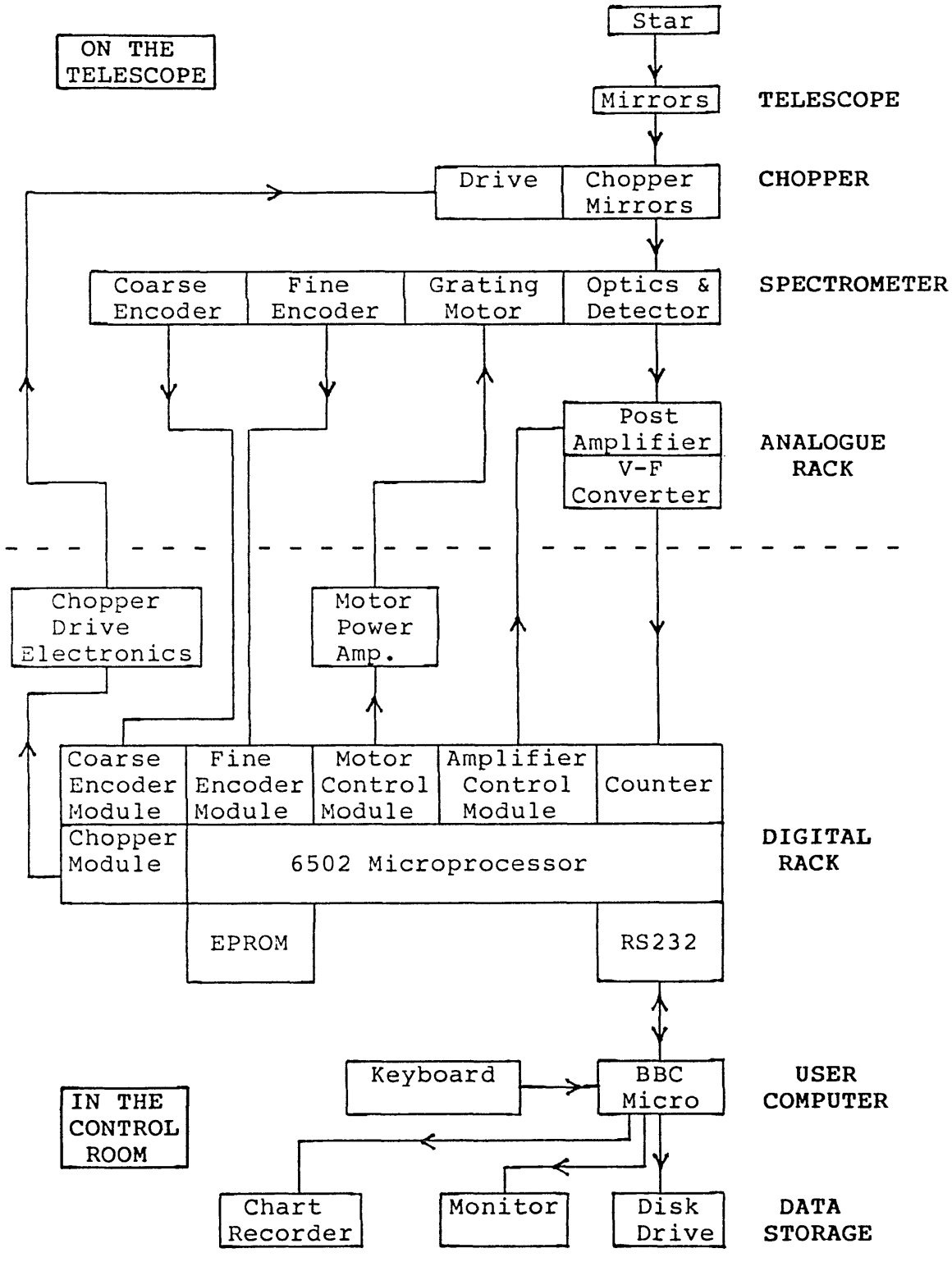

Figure 2.5: Information Flow in CGS1's Data Acquisition System

timing comes from hardware decremental counters which at present allow 16 chop rates between 60 Hz and 7Hz. The system is usually operated at 9.38Hz, with the signal being read every 10 cycles.

Every time the up/down counter interrupt is called (about 20 times per second) the fine encoder position is read. By registering when the value changes from & FFF to 000 the SBC can keep track of the absolute position of the fine encoder.

Data is transferred to the BBC every time the signal is read. The data is read into a software buffer and the interrupt, which senses when the RS232's output buffer is empty, is enabled. The interrupt routine gets the next character to be sent, from the software buffer. The interrupt is turned off when all the data has been transferred.

The None Interrupt Routine

This receives the commands from the RS232 then acts on them. It has routines for setting the gains, chopper frequency, phase, motor speed, etc.

The routine for setting a specific grating position is performed without using interrupts. First the interrupts concerned with outputing data are disabled to allow the SBC the maximum length of time to read the fine encoder. The grating is then moved at full speed until it is about one cycle of the fine encoder below the desired position. The grating is then moved slowly until the position is reached. Wind-up in the coupling bellows will mean that the grating will continue to move after the motor has stopped. The amount of overshoot can be calibrated, giving a final accuracy of 2 on the fine encoder.

2.7.2 The BBC to SBC Commands

The commands all start with an ASCII character and then the data where necessary. (x represents a real number and y an ASCII character.)

S Starts the timers. Must be the first command sent.

G y Cr Sets the post amplifier gain. y is the ASCII value of the gain number and varies between 0 and 7. Cr is a carriage return.

g x Sets all 7 amplifier gains. To reduce possible crosstalk it is advisable to set the channels not being used to a gain of 1.

C x Sets the chop frequency. x varies from 0 to 15.

I x Sets the number of half chop cycles before the signal is read. x must be even and in the range 2 to 254.

F Allows the phase to be set. Enter 1 or 2 to alter the phase between the counter enable and the chopper. When satisfied enter 'Return' to leave the routine.

U The up/down counters only count up (ie working DC).

D The up/down counters count up and down (ie chopping).

R Prevents further commands being accepted until **r** is entered. This is to prevent gains, etc. being altered whilst data is being taken.

H Halts the grating.

A x Defines the absolute cycle of the fine encoder.

M x Motor speed.

E x1 x2 Cycle of fine encoder which has the end stops. x1 is the upper end stop and x2 is the lower end stop.

L x1 x2 x3 x4 Send the grating to a position. x1 is the fine encoder cycle, x2 and x3 are the fine encoder reading, x4 is the check sum.

2.7.3 The SBC to BBC Data Packet

When the SBC is ready to send data it repeatedly outputs &36 on the RS232 until the BBC acknowledges by replying 06. The data is then sent.

Byte number

1	Number of bytes in the packet
2-4	Signal
5-6	Coarse encoder

7	Fine encoder cycle number
8-9	Fine encoder reading
10	Post amplifier gain
11	Motor speed

If a command was sent to the SBC since the previous data packet was transferred it is is now echoed back to the user computer. For example, if the gain number had been set to 4 then

12	G
13	4
14	CR

2.7.4 The BBC Software

The Acorn BBC micro computer is again based on a 6502 CPU. It provides the user interface and data storage. The BBC has the advantage of being a simple computer to program, but only having 32k of RAM and being relatively slow it allows very little on line data reduction, and necessitates the use of a large number of 'tricks' to fit the programs in. Various programs have been developed to make the operation of the system as simple as possible, particularly the setting up (ie defining the wavelength limits, chop rates, chopper/counter enable phase, etc.). However, I will only describe the software for taking data.

The Interrupt Routine

The BBC communicates with the SBC using the RS232 at 9600 baud without handshaking, and to ensure that the data is read correctly the BBC is left in the interrupt routine until the complete data packet has been transferred. The routine is triggered by data entering the RS423 buffer; the BBC replies by sending the acknowledge flag (06); then SBC sends the data. If data is being recorded, then it is transferred to the 'data buffer' and the

grating position is checked to see if the scan has been completed. The data taking routine is totally transparent to the user, even if the main program were to stop the data would continue to be recorded until the end of the scan is reached.

The interrupt routine also checks the 'command' buffer flag to see if a command is to be sent to the SBC. Finally, the routine passes the signal to the BBC user port, where it is changed into an analogue signal for a chart recorder.

The Main Scanning Program

As well as storing data to disk the program is designed to allow the simple and safe operation of the spectrometer. All the important information, such as wavelength, signal, grating speed, amplifier gain, sidereal time, etc., are clearly presented and most operations only require one or two key strokes.

2.8 Operation of the Spectrometer

2.8.1 Scanning

The scans are usually taken using 9.38 Hz sky chopping with the signals being read every 10 cycles. Both upper and lower beam scans are taken, particularly when working at L, in case there are any background signal gradients on the sky. Since a DC motor is used, the grating is driven at constant speed whilst the data is taken. The speed is such that, typically, 5 to 6 samples are taken across one resolution element so the spectra are sufficiently oversampled.

2.8.2 Setting and Driving the Grating

Despite using an antibacklash worm and wheel, and having the encoder inside the cryostat, backlash could still cause problems. When scanning, the grating must always be driven in the same direction (generally increasing fine encoder reading) and when setting a position it should always be approached from the same direction.

2.8.3 Wavelength Calibration

When calculating the wavelength from the encoder reading, the grating rule is used, ie

$$N\,\lambda = 2d\sin(aX + b) \tag{2.2}$$

N = Order

λ= Wavelength

d= Line spacing (in this case about 300 lines per mm)

$aX + b$ = Grating angle, X being the encoder value

To calibrate the wavelength a helium lamp is used. The line at 1.086 μm is viewed in 2nd, 3rd and 4th orders and the 2.056 μm line in the 2nd order. The number of lines per mm on the grating is well known at room temperature but the grating will contract when it is cold so increasing the value. To determine the values of d, a and b, graphs of $\arcsin(\frac{N\lambda}{2d})$ verses encoder position are calculated for various values of d. The one that gives the best straight line is used; this is usually between 300 and 303 lines per mm. The fit is very accurate, with the correlation coefficient being better than 0.99999.

2.8.4 Working Magnitude Ranges

The limiting magnitude will vary with the window to be used and the prevailing weather conditions but when scanning, a safe working limit is about +2.5 mag at K. If accurate line measurements are required then it will be closer to +1 mag or many repeats will have to be made.

2.9 Current Spectrometer Upgrades

Both the data acquisition system and the cryostat are currently being upgraded. In July 1989, work started on upgrading the detector readout system to low noise integrating amplifiers made by Infrared Laboratories. This system is totally different from the TIAs currently used and require at least 16 bit A-Ds to digitize the signal. An Archimedes micro computer will be used for data storage and on line reduction.

Work has also started on improving the vacuum seal around the drive shaft. The drive shaft is continually rotating whilst observations are taken causing the seal to leak. A separate vacuum chamber is to be put around the warm motor shaft so the pressure difference across the Wilson seal, and hence it is hoped the leak rate, will be dramatically reduced.

2.10 CGSII on UKIRT

The cooled grating spectrometer mark 2 is a common user 1 to 5 micron instrument that is operated on the 3.8m United Kingdom Infrared Telescope in Hawaii. It uses a linear InSb detector array, which has seven, 200 micron square detectors, with the distance between adjacent centres being 230 microns. When I observed with it in November 1988, they were read out using TIAs and reset amps, although it has since been upgraded to the Infrared Laboratories' integrating amplifiers.

The instrument contains 2 back to back gratings giving nominally the following spectral resolutions

J	300
H	430
K	650
L	460
M	780

The actual resolution is dependent on the aperture used ($\approx$ 1" to $\approx$ 5") and the size of the seeing disk, and at K it can be as low as 350. The spectral resolution is approximately matched to the detector size.

The grating is driven using a stepper motor which also gives the position: there is no internal encoder. When scanning, the grating is still whilst the detectors are integrating. After the signals have been read the spectrum is stepped either a quarter, a third, a half or

the whole length of the detector block, depending on the amount of oversampling required. Therefore, the order in which the channels appear in the final spectra is dependent on the amount of oversampling, and there are missing points at either end of the scan. For 4 times oversampling (as used in November 88) the order of the channels is

1 x x x 2 x x 1 3 x x 2 4 x 1 3 5 x 2 4 6 1 3 5 7 2 4 6 .....

..... 1 3 5 7 2 4 6 x 3 5 7 x 4 6 x x 5 7 x x 6 x x x 7

x is a missing point.

2.10.1 Data Format

The data is stored in a DBS file which can be converted to ASCII using software at the telescope. The upper and lower beam scans are not presented separately but are co-added to form a single file (it is claimed that UKIRT is on a good enough site to do this). If many repeats are taken, then as well as saving the individual files, the co-adds of all the files will also be saved.

The header contains the file name, gains, time, airmass, etc. The actual data is in the form

Wavelength, Signal, Error

The wavelength is the nominal value only and is good to a fraction of the resolution. If a very accurate wavelength calibration is required it can be corrected using scans of Kr or Ar lines.

The signal has had the gain normalized using their nominal values which are claimed to be very accurate.

The error is the difference between the upper and lower beam.

Chapter 3

An Absolute Determination of the Near Infrared Flux From Vega

An attempt was made in July 1987 to directly measure the absolute flux from Vega in the near infrared. The project was a collaboration between A.J Booth, D.E.Blackwell and D.Petford from Oxford, M.J.Selby and myself from ICSTM and S.Arribas from the Instituto de Astrofisica in Tenerife.

3.1 Introduction

The accurate determination of the absolute flux from a star in the infrared has proved very difficult, but for some projects like the IRFM it is vital. Only one star needs to be accurately measured since the absolute flux for other stars can be determined by ratioing. The star that is generally chosen for absolute calibration is Vega because it is the standard calibration star, being defined as zero magnitude at all wavelengths.

The majority of absolute flux calibrations in the infrared have used indirect methods and/or model atmosphere calculations. To calibrate Vega, Johnson used the solar constant with stars of similar spectral type to the sun, and then relative photometry. Strecker (1979)

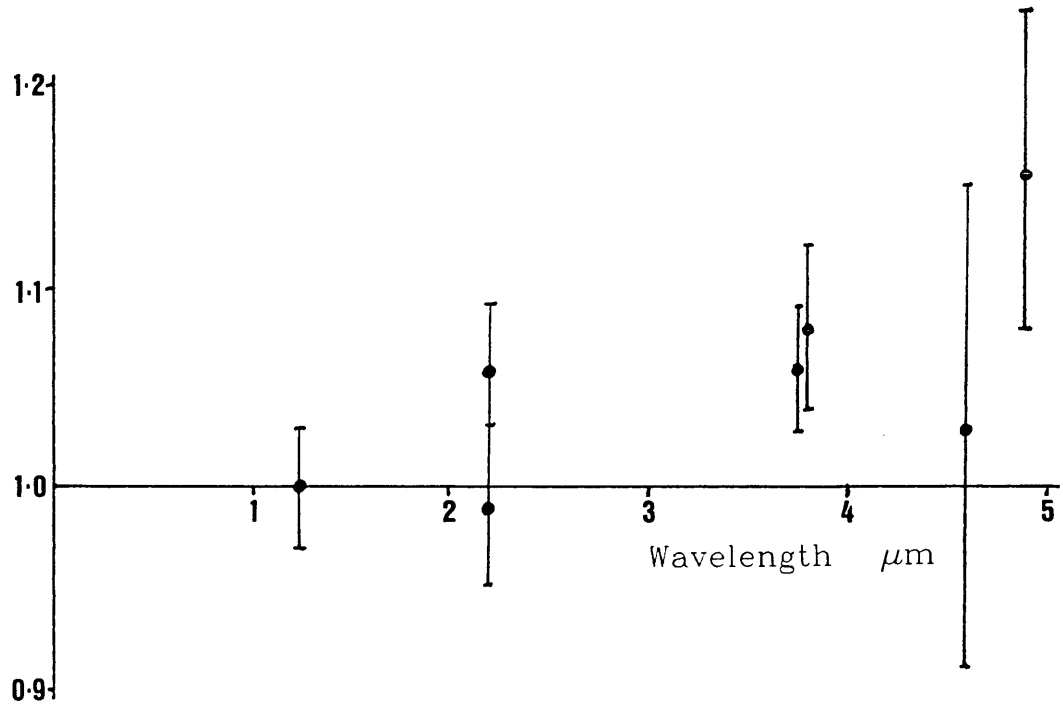

Figure 3.1: Ratio of Observed to Model Vega Fluxes

used a model atmosphere developed by Oke and Schild (1970). The most important models at present are those of Dreiling and Bell (1980) and Kurucz(1979), although other models give similar results. In developing any model, assumptions have to be made about the stellar atmosphere, and in particular the temperature profiles. If these are incorrect then errors must be introduced. It is therefore important that direct measurements are made to confirm the models.

To date, only the ICSTM/Oxford group has published attempts at a direct absolute calibration of Vega. They compared the flux from Vega with that from a known source mounted at the telescope. Various wavelengths have been attempted, defined either by narrow band filters or by using CGS1. A group at KPNO has also attempted a direct absolute calibration. They placed their source 2.6km away on a neighbouring mountain, but found it difficult to calibrate the horizontal extinction so have not published their results. The direct absolute calibrations measured by ICSTM/Oxford have found a wavelength dependent excess over the models. The excess starts at about 2μm climbing to 11% by 5 μm. Table 3.1 shows the measured and model fluxes and figure 3.1 shows their ratio.

Table 3.1: The Infrared Flux from Vega

Wavelength (μm)	Measured flux ($10^{-10} W m^{-2} \mu m^{-1}$)	Model flux ($10^{-10} W m^{-2} \mu m^{-1}$)
1.24	30.6 ±3%	30.6
2.20	3.92 ±4%	3.96
2.20	4.19 ±3%	3.96
3.76	0.544 ±3%	0.5111
3.80	0.528 ±4%	0.490
4.6	0.242 ±12%	0.234
4.92	0.210 ±7%	0.180

It was decided to refine the instrumentation used in previous attempts made by ICSTM and Oxford to try to reduce the errors, particularly the systematic errors, to below 1%.

3.2 The ICSTM/Oxford Method

The method used for the absolute calibration of Vega relies on the optics making the calibration source appear identical to the star at the detector. A re-imaging optical system is used with either the telescope's focus or the aperture of the calibration source at its focus (figure 3.2). The system used in 1987 is different from that used previously. Mirrors are used for the re-imaging rather than warm lenses (which will have far higher backgrounds) and the source is physically moved to the focus instead of using a 45 degree mirror to divert the beam.

The flux from the star is calculated at each wavelength using

$$F = \frac{B_s A S_{Vega}}{f^2 T R S_{source}} \tag{3.1}$$

F = Flux from Vega ($W m^{-2} \mu m^{-1}$)

B_s = Flux from the source ($W m^{-2} strad^{-1} \mu m^{-1}$)

S_{Vega} = Measured signal from Vega (volts)

S_{source} = Measured signal from the source (volts)

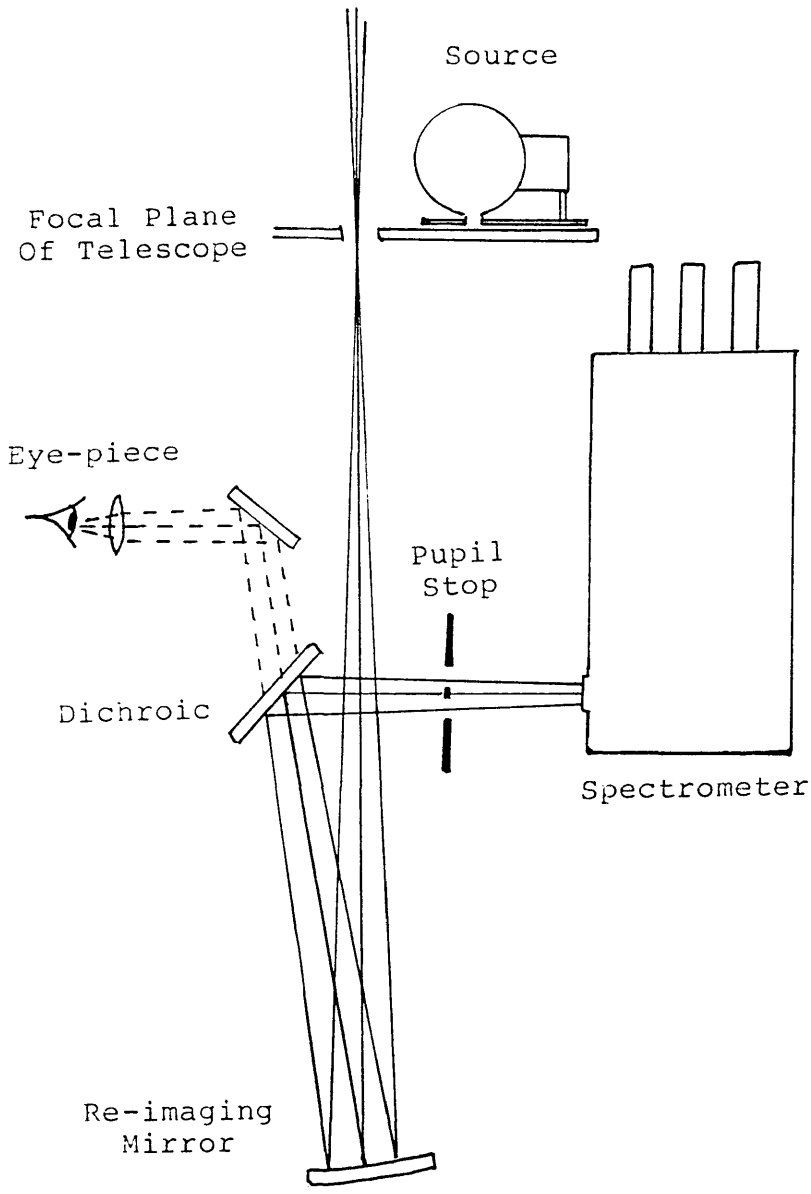

Figure 3.2: The Re-imaging Photometer Cage

The pupil stop is at the focus of the re-imaging mirror. It allows the detector to see only the telescope mirror and none of the supports. This makes the solid angle in which the detector can see the source identical to that in which it can see the star.

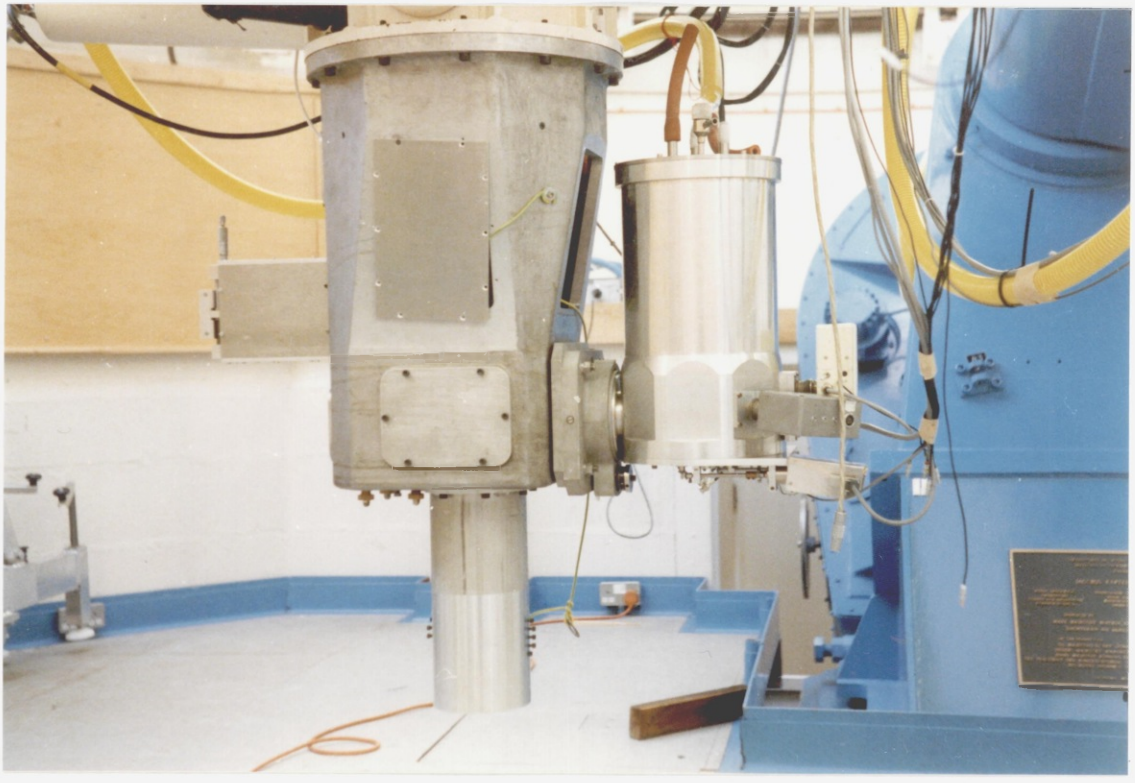

Figure 3.3: CGS1 on the JKT.

This shows CGS1 mounted on the re-imaging photometer cage on the JKT in La Palma. CGS1 is using the side looking outer.

f = Focal length of the telescope (m)

A = Area of the source pin hole (m^2)

T = Transmission through the atmosphere

R = Reflectivity of the telescope mirrors

3.3 The Calibration Source

The calibration source must have very good long term stability. Its flux must be reproducible not only from night to night during the observations, but also later when it is accurately calibrated in a laboratory. Therefore, at the wavelengths to be calibrated, the source should be on the Rayleigh-Jeans part of its flux curve, so the flux is less dependent

on temperature.

$$F_{RJ} \propto \frac{T}{\lambda^4} d\lambda \tag{3.2}$$

The source used in this attempt was a quartz bulb run off a very stable power supply.

The flux reaching the detector passes through a pin hole which is of a similar size to the seeing disk of the star (in this case 0.6mm) so that the two appear identical to the detector. However, the angular diameter of Vega at the earth is about 3.4 milliarcseconds, so despite being at nearly 10,000K, the flux from the star will only be $\frac{1}{1000}$th that of the source, or less. The linearity of the electronics cannot be guaranteed over this range, so it is necessary to attenuate the signal. In the past this has been achieved using MgO diffusers (which were found not to scatter uniformly), a low temperature source (which was too unstable) and finally glass and plastic slides. In the July 87 observations an integrating sphere was used. It has three main functions:

- It reduces the flux from the bulb.
- It increases the size of the source so that it appears the same size as the seeing disk.
- It distributes the radiation such that there will be equal flux in equal solid angles so the detected flux is not dependent on the angle of the aperture.

The output from the sphere looks like a dilute black body at the same temperature as the bulb. The bulb and integrating sphere used in July 1987 gave a source/Vega ratio of between 1 and 100 over 1 to 5 microns.

The source used at the telescope was calibrated against a furnace (designed by NPL) with a very accurately known emissivity, both before and after the observations. This means that the actual flux distribution from the source does not have to be predictable, only reproducible.

3.4 The Detector System

The ICSTM CGS1 was used to take the measurements. A spectrometer with a resolution of 500 has a number of advantages over a photometer using narrow band filters.

- Essentially the monochromatic flux is being measured rather than the integral over the filter profile.
- The IRFM relies on the continuum flux being measured. A spectrometer allows the continuum regions in the stellar spectra to be isolated so avoiding all the major absorption lines.
- The best parts of the atmospheric windows can be isolated allowing the atmospheric extinction to be more accurately calculated.
- There is a larger choice of possible wavelengths that can be easily observed.

In order to operate with the re-imaging optics, the spectrometer had to be converted from a bottom looking to a side looking cryostat. This entailed placing a 45 degree flat on the copper can above the filter wheel. Unfortunately, this pushes the focus further into the cryostat so a slower beam has to be used, and it makes alignment considerably more difficult.

On the 1m JKT, CGS1 had a 20" field of view on the sky with a very good image profile. It is important that the sky aperture is much larger than the seeing disk of the star. This is to reduce the risk of losing flux from the star through bad tracking, wind bounce or the seeing flaring.

3.5 The Reflectivity of the Mirrors

Clean aluminised mirrors are usually about 96% reflecting in the near infrared, so some of the flux will be lost through reflections off the primary and secondary telescope mirrors. A reflectometer was built at Oxford to measure the reflectivity of the telescope mirrors. It compares the reflectivity with that of a calibrated gold mirror. Measurements were taken over a grid of points on both mirrors and the averages calculated, after making an allowance for their curvature. The reflectivity of the JKT's mirrors was found to be 85% at 2μm.

3.6 The Focal Length of the Telescope

As can be seen in equation 3.1 the focal length squared is used in the calculation of the absolute flux. In order to keep the errors below 1% the focal length must be measured to better than 0.5%.

The simplest and probably most accurate method for calculating the plate scale of a telescope, hence its focal length, is to time the transit of a star between two slits using the rotation of the earth. This measurement is taken a number of times and the average calculated. The focal length of the JKT is 15.01m.

3.7 Airmass Calibration

The flux from Vega is generally defined as the flux reaching the top of the atmosphere. Therefore, the amount of flux absorbed by the atmosphere must be calculated.

From the thesis of C.M.Mountain, the simplest model of transmission through the atmosphere is

$$T_{(\lambda)} = e^{-\gamma l} \tag{3.3}$$

l is the distance travelled through the atmosphere.
γ varies with wavelength and composition of the atmosphere.

Hence the signal

$$S_{(\lambda)} = C_{(\lambda)} e^{-\gamma l} \tag{3.4}$$

$C_{(\lambda)}$ is the Signal reaching the top of the atmosphere.

It is difficult to define the actual distance through the atmosphere that the light travels, since this will change with height above sea level, atmospheric conditions, etc. Instead, it is usually described in terms of the airmass A (figure 3.4).
Introducing the airmass into equation 3.4

$$LogS = logC - \gamma A \tag{3.6}$$

This works well as long as there are no atmospheric lines present.

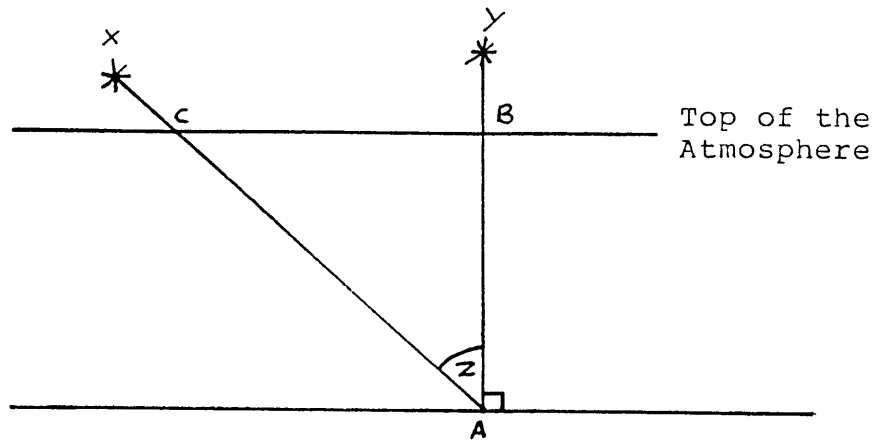

Figure 3.4: Airmass

If the curvature of the earth is ignored and the atmosphere is assumed to be uniform with a definite boundary, as shown, then the parallel plane approximation for the earth's atmosphere can be used. The distance through the atmosphere which the light from star X travels is AC and for a star in the zenith it is AB. The airmass (A) of star X is defined as

$$A = \frac{AC}{AB} = \frac{1}{\cos Z} \tag{3.5}$$

Where Z is the zenith angle.

This approximation is acceptable for zenith angles less than about 60° *or* 70°.

To calculate what the signal at a particular wavelength would be without losses in the atmosphere, the star is measured at a number of different airmasses between 1 and 2.5 during the night. A linear regression, calculated using a least square fit, is used to estimate the signal at zero airmass (figure 3.5).

The above process only works well when there are very stable atmospheric conditions during the night. These are normally only obtainable on high dry sites, such as La Palma, which are above most of the atmospheric water vapour.

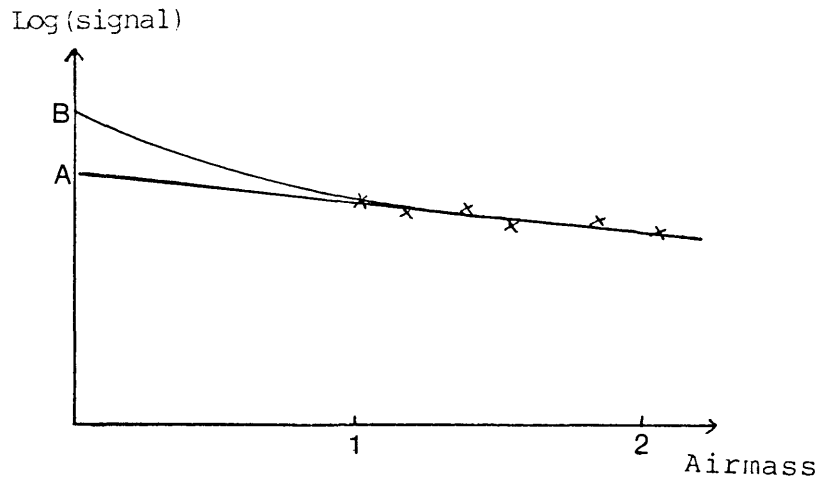

Figure 3.5: Extrapolation to Zero Airmass

The signal is measured a number of times between one and two airmasses. The signal at zero airmass is calculated by a linear extrapolation of the logarithms of the signal. This works well if there are no atmospheric lines since they make the plot non-linear. However, when the lines become completely saturated the plot returns to being approximately linear. Therefore, if the lines saturated close to an aimass of zero, the error will be small.

3.8 The Observations

The measurements of Vega and the source were taken without sky chopping. The removal of the background signal was achieved by nodding the telescope on and off the star or by sliding a shutter between the bulb and the integrating sphere when observing the source (figure 3.6).

A series of measurements of the star were taken at various zenith angles to allow accurate airmass determination. The source was observed at the same zenith angle as the star to try to calibrate the effect of differential flexture.

Figure 3.6: Method of Observation

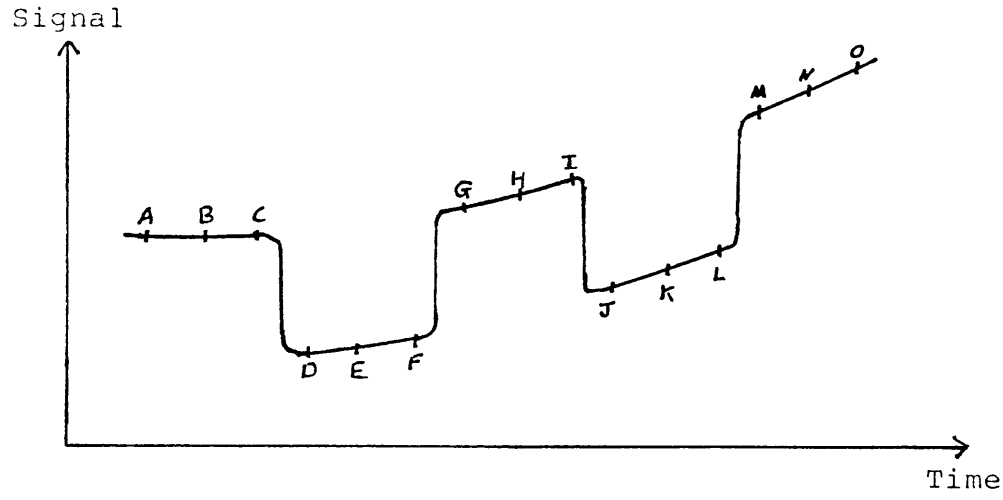

Above is a simulated chart recorder trace. The signals are measured between A & C, D & F, G& I, etc. the output being recorded every second for 20 seconds in each case. The actual signal from the star/source is the difference between the upper and lower traces. The measurements are repeated until the desired S/N has been reached.

Since the measurements are taken DC there will be drifting in the signal levels, especially at longer wavelengths. If the signal were simply calculated using $S_{AC} - S_{EG}$ *etc. (where* S_{AC} *is the average signal between A and C) then errors could be introduced, and the calculation of the S/N for that run become uncertain. Instead, each period of 20 seconds is treated as 2 periods of 10 seconds. The data is processed so the last 10 seconds of the star being IN the aperture and the first 10 seconds of the star being OUT of the aperture are handled separately from the other half of the cycle. ie*

$$S_{IN-OUT} = Average(\, S_{BC} - S_{DE},\, S_{HI} - S_{JK}, \ldots) \tag{3.7}$$

$$S_{OUT-IN} = Average(\, S_{GH} - S_{EF},\, S_{MN} - S_{KL}, \ldots) \tag{3.8}$$

The first and last series of measurements are always on the star. The S/N is calculated for IN-OUT and OUT-IN separately and the run stopped when both have reached the required accuracy. The final signal is calculated by summing the two averages.

3.9 The Problems

Unfortunately, the observations ran into a large number of technical problems which severely limited the accuracy of the final results. The problems ultimately stem from using a completely new photometer cage, a new CGS1 cryostat and a new data acquisition system on an unfamiliar telescope. The situation was further exacerbated by technical problems with the telescope (dirty mirrors, poor declination drive and a broken mirror support).

The major source of error came from differential flexture between the photometer cage and the telescope. This caused a severe loss of signal beyond a zenith angle of 30° which could not be calibrated using the source. This made an airmass calibration impossible.

The use of a quartz bulb for the calibration source is acceptable at wavelengths shorter than about 2.5 μm since the majority of the flux comes from the hot filament. However, longwards of this, most of the flux comes from the far cooler envelope which is not on the Rayleigh-Jeans part of the curve so is very sensitive to temperature change.

3.10 Results

The absence of an accurate airmass calibration makes the calculation of the absolute flux impossible at most wavelengths. However, previous airmass calibrations demonstrate that near 2.2μm the extinction is only about 3% per airmass with good observing conditions. The weather at La Palma during the run was excellent so it is felt justified to use this value with the results at 2.250 μm. The measured flux from Vega at 2.250μm is $3.81\text{x}10^{-10}\text{Wm}^{-2}\mu\text{m}^{-1}$ with an error of 4%. This is within 1% of the value expected at this wavelength from the previous absolute calibrations.

3.11 Future Absolute Calibration Attempts

It is important that the direct absolute calibration of Vega is repeated in the near infrared, but with significant improvements to the method. It is proposed that a future attempt

makes use of the unique properties of the 4.2m WHT on La Palma. By using the Nasmyth focus, the cryostat, re-imaging optics and furnace will not be tilted as the telescope moves, so removing the differential flexture which caused the problems on the JKT. The amount of space available on the Nasmyth platform will allow a much larger and, it is hoped, a more stable calibration source to be used, possibly the NPL designed furnace at Oxford. Finally, there will be the factor of 16 increase in signal.

Other direct techniques for the absolute calibration of Vega must be developed to add credence to the results already obtained. One possibility could involve calibrating the sun, a G2V star, for which θ is already known, then using the IRFM to calculate T_e. If the temperature spectrum is flat and it agrees with the T_e predicted from the total flux, then it would give a greater confidence in the models of G2V stars.

Chapter 4

The Reduction of Near Infrared Spectra

4.1 Introduction

The shape of the raw spectra is defined by a mixture of the actual stellar spectra, the telluric features and instrumental effects .

The stellar spectra. For the majority of stars in the near infrared this is a Rayleigh-Jean's type continuum flux with absorption lines superimposed.

The instrumental effects. The overall shape of the raw spectra is dominated by the profile of the broadband blocking filter. The shape of the lines in the spectra is dependent on the resolution of the spectrometer. Very high resolutions (eg 10^4) allow the lines to be resolved, so the shape is determined by processes in the star. At medium (eg 500) or lower resolutions the lines are no longer resolved and the shape is approximately the instrumental profile. Many lines become blended, particularly molecular features, and it can be impossible to assign a single transition to a particular feature.

The Telluric features. Molecules, particularly H_2O and CO_2, in the earth's atmosphere absorb strongly at some infrared wavelengths. Figure 4.1 shows a model of the transmission through the atmoshpere developed by C.M.Mountain using the IRTRANS

program of Truab and Stier (1976). This clearly shows a large number of strong atmospheric features throughout the near infrared wavelength range.

In general, the atmospheric features and the instrumental profile are by far the most dominant features. Figure 4.2 shows the raw Vega spectra taken by CGS1 in the J, H, K and L windows. However, because the atmospheric features and the instrumental effects have the same relative strength in all the spectra, they can, in principle, be removed by ratioing with a calibration star whose absolute spectra has already been determined.

$$Absolute\ Spectra\ Star\ A = \frac{Raw\ Spectra\ Star\ A\ \times\ Absolute\ Spectra\ of\ Star\ B}{Raw\ Spectra\ of\ Star\ B} \quad (4.1)$$

(All the spectra must have the same spectral resolution.)

Although, in principle, this is very simple there are major problems.

4.1.1 Atmospheric Extinction

As described in the previous chapter, the amount of extinction depends on the distance through the atmosphere the light travels (ie proportional to airmass) and the composition of the atmosphere (humidity, amount of dust, etc.). When removing the effect of atmospheric extinction from spectra, it is only necessary to have the same amount of extinction in both of the spectra to be ratioed, and unlike the absolute calibration, the signals at zero airmass do not have to be calculated.

From this it is obvious that the best solution is to have the calibration star very close to the star, galaxy, supernova, etc. whose spectra is to be measured, and where possible this is done. However, when attempting spectrophotometry on a large number of stars this becomes impractical, not only because of the time it would take, but because of the lack of accurately measured calibration stars. The solution in this case is to measure one calibration star at a number of different airmasses during the night.

The method preferred by Strecker is to observe the target at the same airmass as one of the calibration measurements. In reducing the CGS1 and CGSII data I have used the linear relation between the logarithm of the signal and the airmass (see chapter 3) to calculate what the 'raw' spectra would have been if the measurement had been taken at

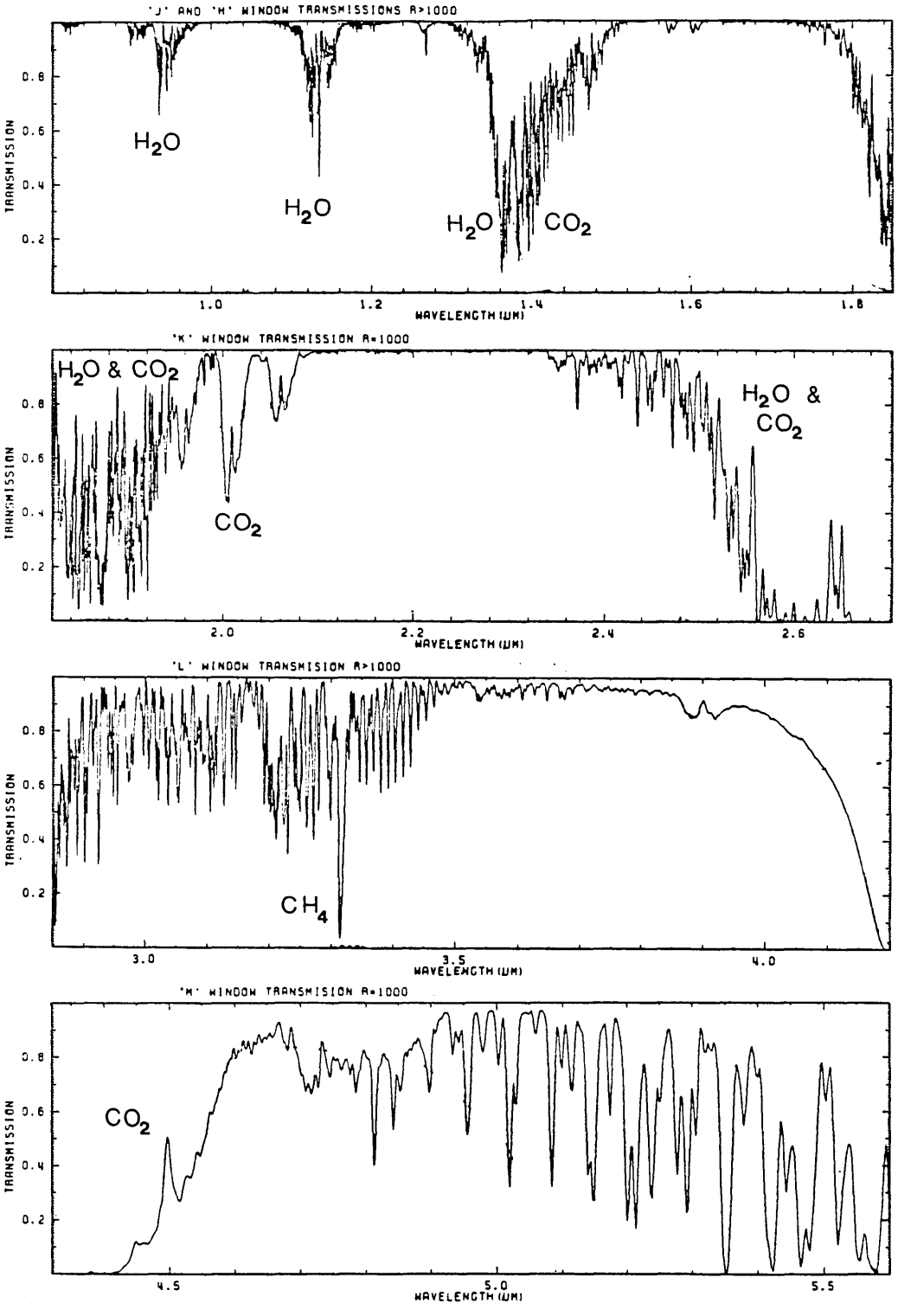

Figure 4.1: Atmospheric Absorption in the Near Infrared

(Adapted from the thesis of C.M.Mountain)

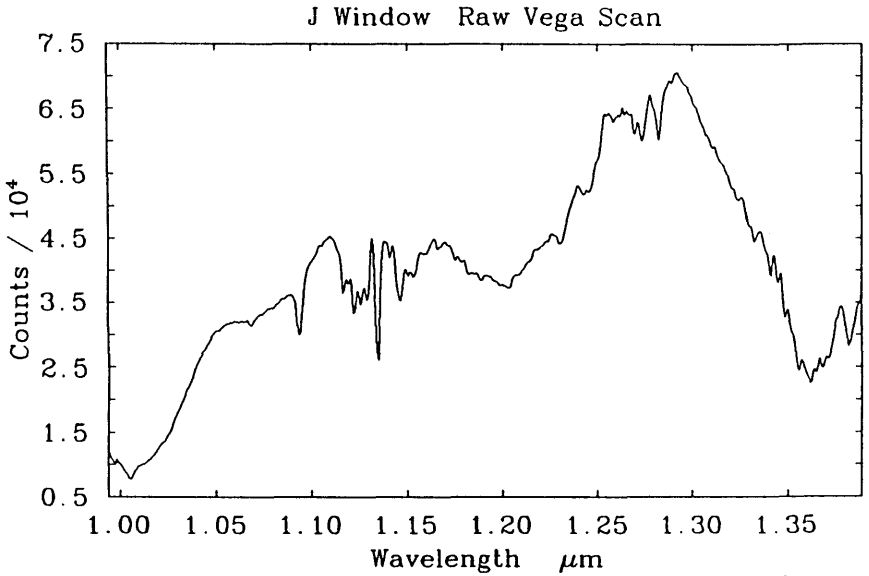

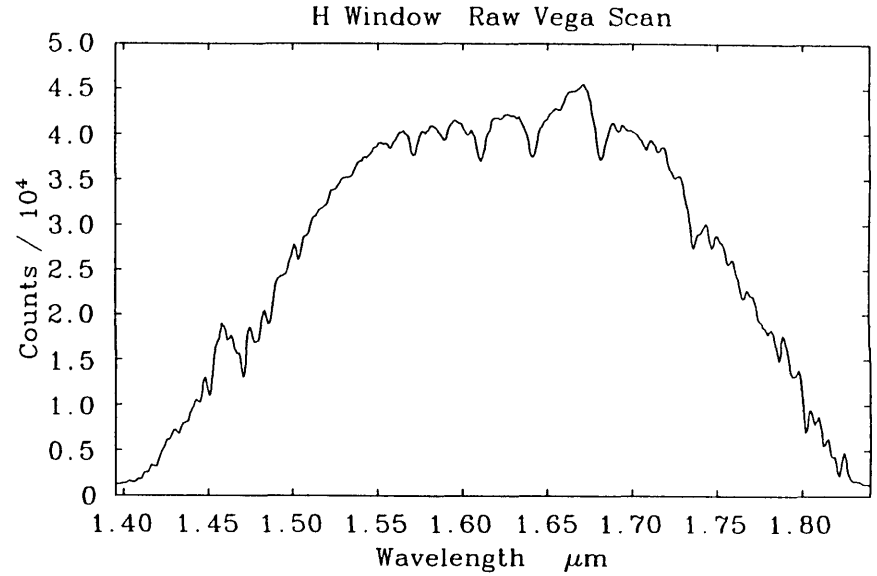

Figure 4.2: Raw CGS1 Scans of Vega

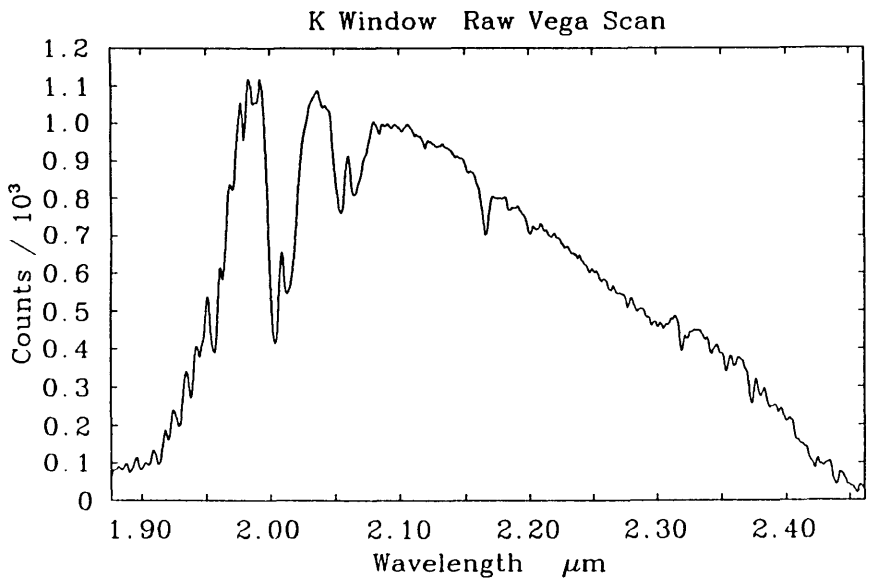

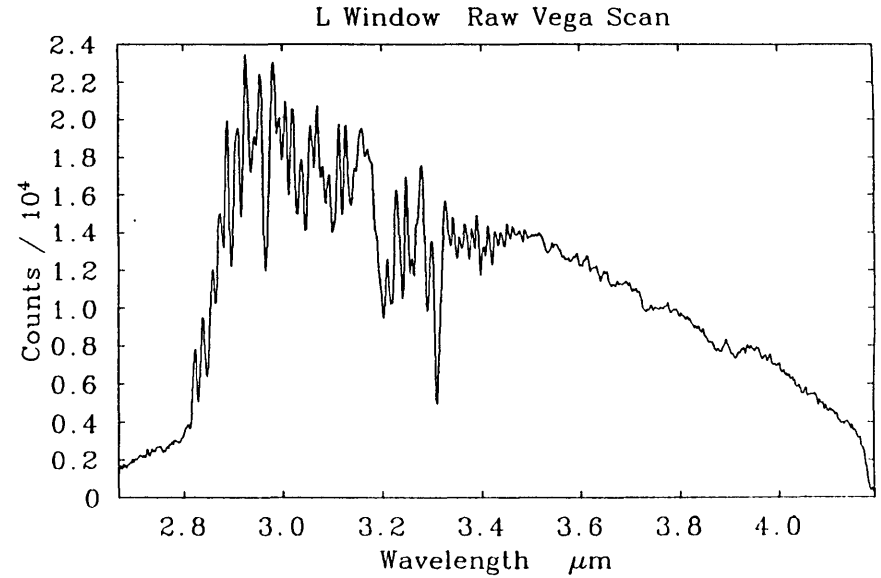

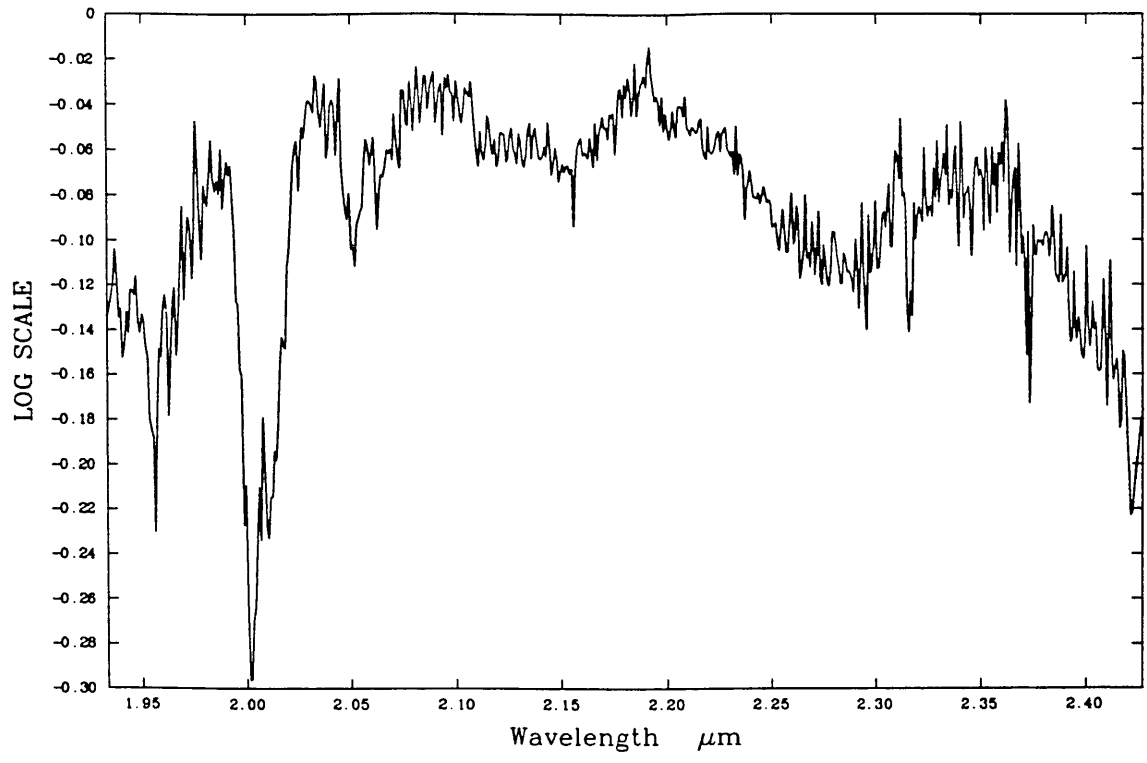

Figure 4.3: CGSII K Window Airmass Spectrum

an airmass of 1. It is better to interpolate the effect at an airmass of 1 rather than at zero airmass because of the effect of saturated atmospheric lines.

Firstly, the airmass calibration spectra are smoothed to decrease the rms noise at each point, then the $\log_{10}$ is taken. The gradient of airmass verses $\log_{10}$ signal is calculated using a least square fit for each wavelength. Where applicable upper and lower beams are treated separately and their results averaged.

The result is to produce an 'airmass spectrum', ie the change in the $\log_{10}$ of the signal for a change in the airmass of one at every wavelength. Figures 4.3 and 4.4 show the airmass spectra for CGS1 and CGSII in the K window.

The airmass spectra is then used to extrapolate all the specta taken on a particular day, to a airmass of one. The correction at each wavelength is calculated using

$$\log_{10} S_1 = (1 + G(1 - A)) \log_{10} S_a \tag{4.2}$$

S_1 = Signal at an airmass of 1

S_a = Signal at an airmass of A

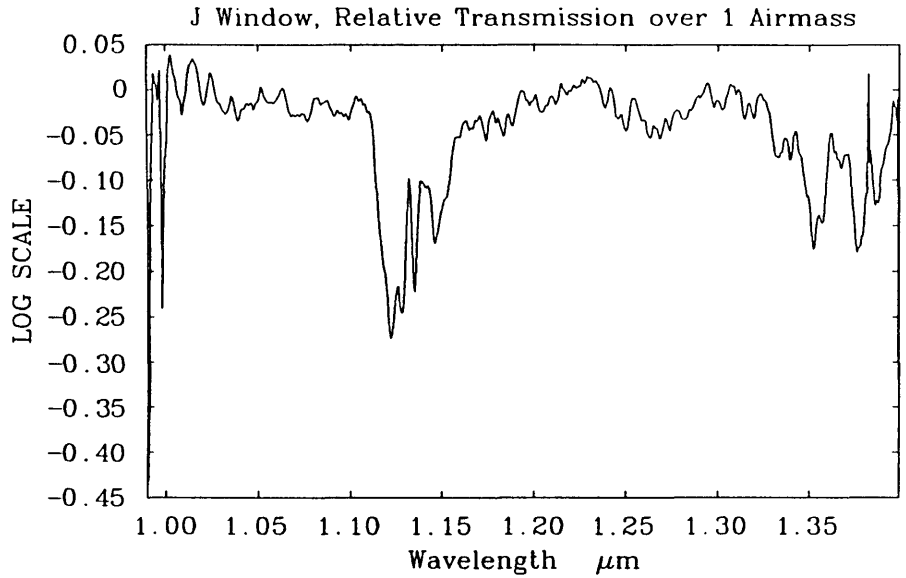

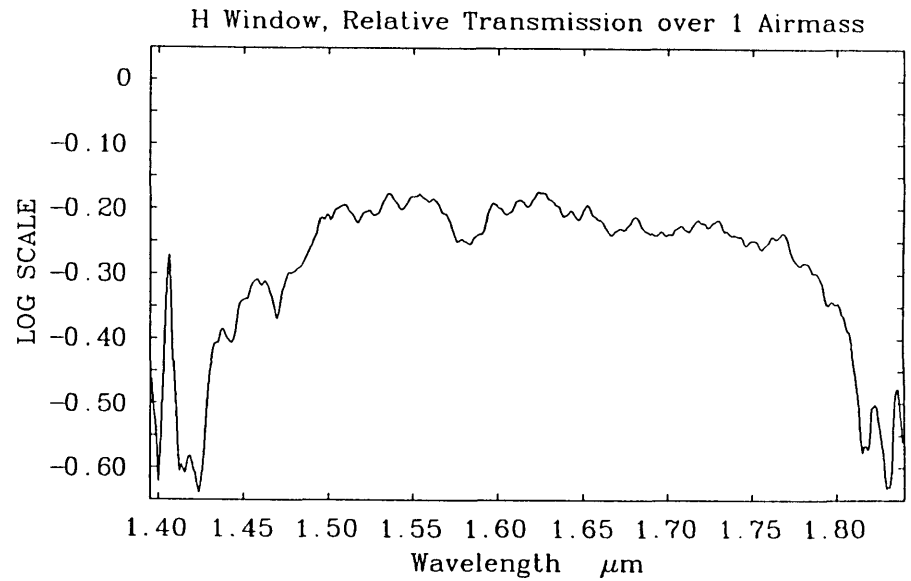

Figure 4.4: CGS1 Airmass Spectra

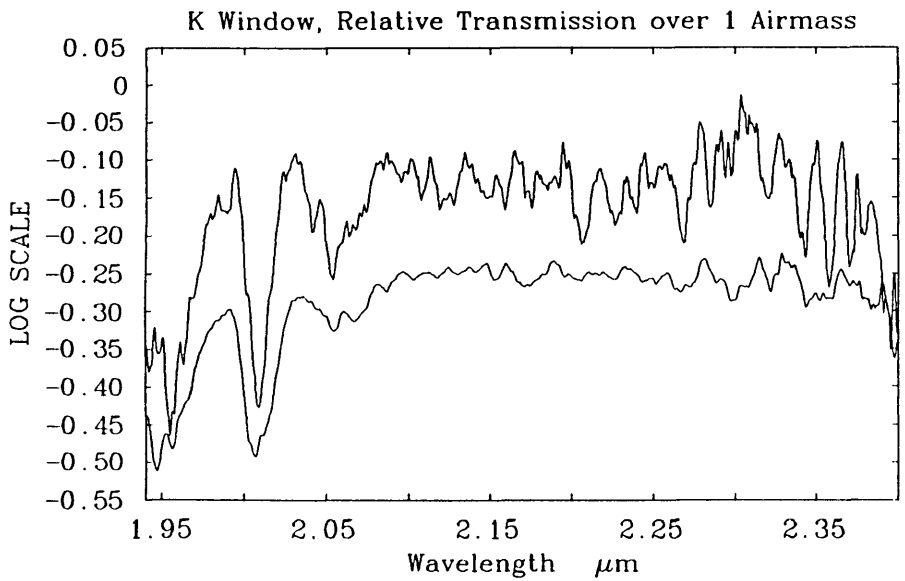

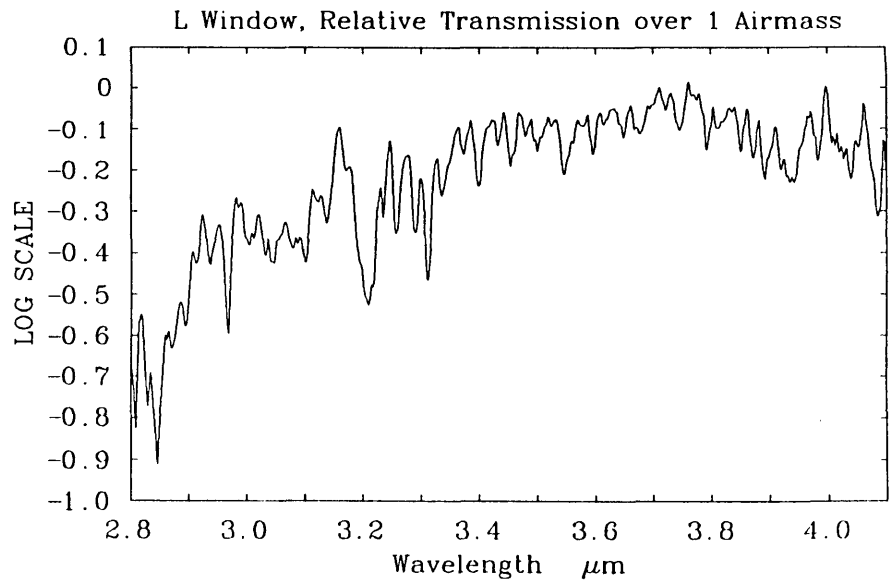

G = Gradient from the airmass spectra$^{\mu m}$

A = Airmass at which the observations were taken

Both these methods rely on the observing conditions being very stable during the night. Generally when working on high dry observing sites, a sufficient number of nights are suitable for this work. However, only in exceptional circumstances will an airmass calibration taken on one night be useful for calibrating a second night's observations.

The Effect of Dust

Tenerife is relatively close to the Sahara desert and one of the problems of working in the Canaries is the dust clouds which blow over, particularly during the summer. On occasions the dust can be so thick that all but the brightest stars are invisible. Although the dust attenuates the signal, it tends to make the atmosphere very stable, so reliable data can be obtained in all but the poorest conditions. The K window airmass spectra in figure 4.4 shows the effect of changing dust in the atmosphere. The lower spectrum was obtained through relatively heavy dust. The effect is to attenuate the signal uniformly at all wavelengths.

4.1.2 The Absolute Calibration Spectrum

As I have describe earlier, there are many problems in accurately defining the continuum spectrum of the main calibration star, Vega, in the near infrared. A decision has to be made whether to use the model atmospheres or the direct measurements as the absolute Vega spectrum. I have used the model developed by Kurucz but corrected for the measured excess found in the direct absolute calibration experiments (figure 4.5). The absolute spectra has a very high spectral resolution, considerably higher than CGS1's, therefore the absolute spectra must be convolved with the spectrometer's line profile. Since the spectral resolution changes with wavelength and grating order, a separate profile has to be be made for each window. The result is to produce an absolute calibration spectrum with the same spectral resolution as the spectrometer (figure 4.6).

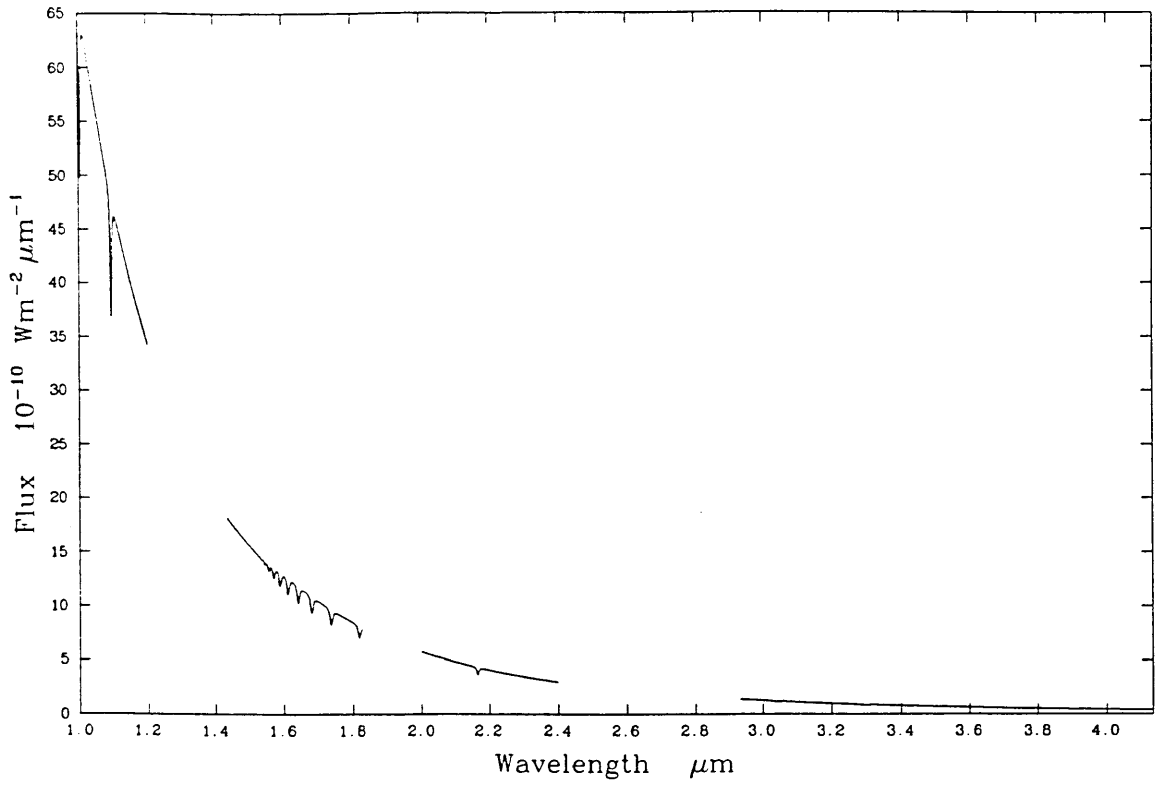

Figure 4.5: Model Vega Spectrum

The strong hydrogen lines in Vega have lead to some observations being calibrated using F and G stars. Although they are cooler than Vega, hydrogen absorption lines are still present in their spectra. Allowance must be made for these, otherwise there is a severe risk that the final result will be dependent on the calibration star. The use of cooler stars has a further disadvantage. Since the temperature of Vega is around 10,000K there are only hydrogen absorption lines in its near infrared spectrum. Below about 6000K other absorption lines (eg neutral metal lines) start to become significant so must be present in the model spectra.

Many spectra are not presented in terms of absolute flux; instead the ratio with a hot calibration star is used. Where possible this is Vega after having the hydrogen lines removed. This has the advantages that no models are involved and by presenting the data as a ratio most of the λ^{-4} Rayleigh-Jeans type wavelength dependence will be removed, making the blocking features more obvious. Often they are presented as normalized ratios (ie the integrated fluxes are normalized), which makes the comparison of spectra from different stars considerably simpler.

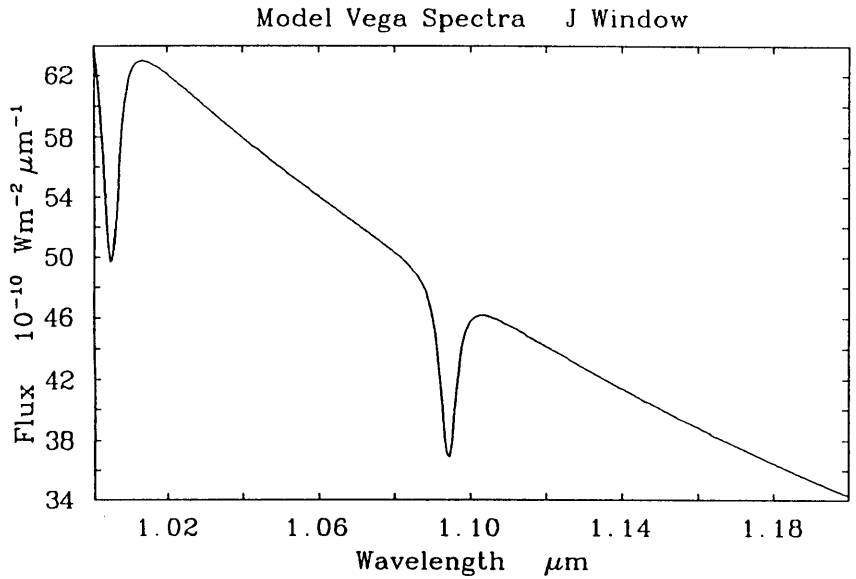

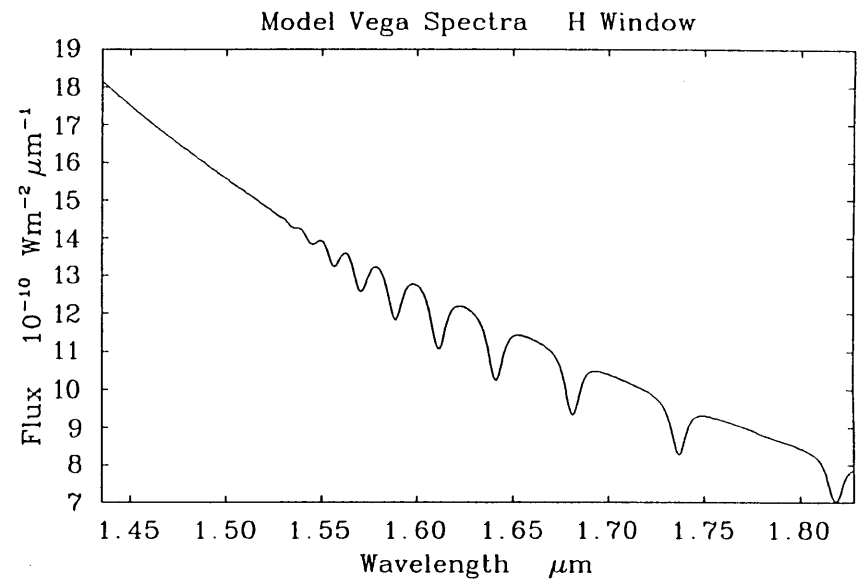

Figure 4.6: Model Vega Spectrum at a Reduced Resolution

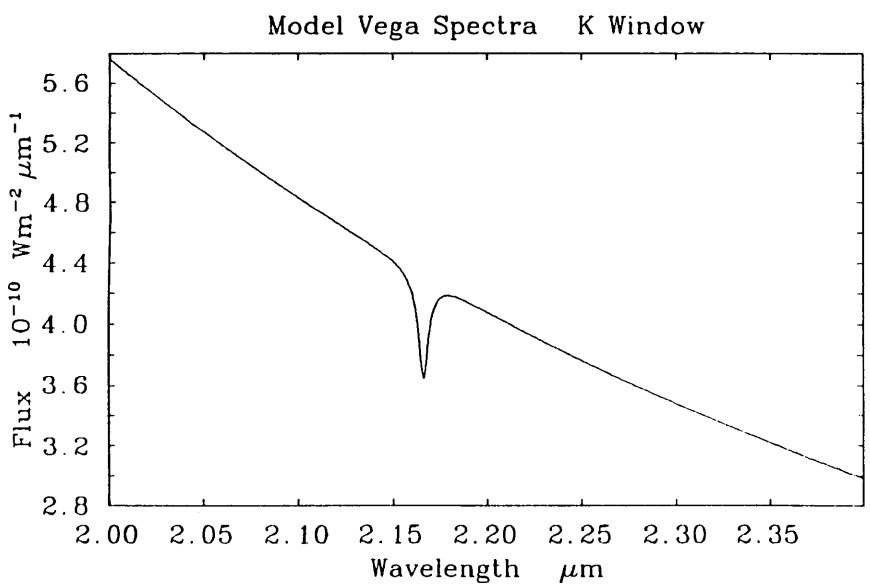

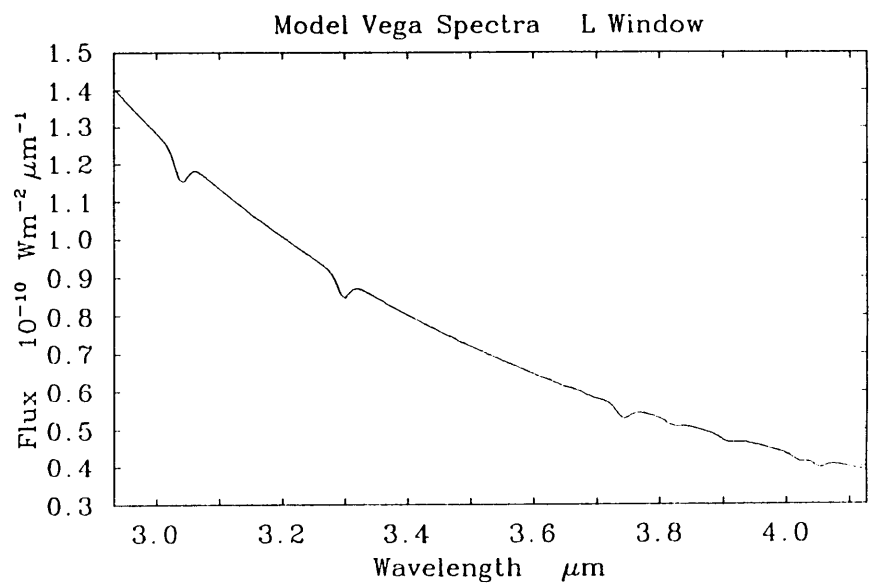

There are two basic methods for removing some of the hydrogen lines from the spectra of hot calibration stars. If there is no coincident telluric feature (eg Brackett gamma) the line can be removed from the raw spectra by interpolation. The second method ratios the calibration star with a star that should show no (eg IRC+10216), or at the least, very weak hydrogen lines (ie K5 stars or later). The shape and depth of the line can be taken from the ratio, then used to remove the feature from the raw spectrum. This will only work if there is no coincident line in the spectrum of the cool star. If neither of these methods are applicable then either a model will have to be used or the hydrogen lines left in.

4.2 Wavelength Registration

As described in chapter 2, accurate wavelength registration is crucial. Unfortunately, poor grating encoding is not the only cause of the relative shifts between spectra. The movement of the star in the aperture, the seeing changing, flexture in the optics as the telescope tilts, etc., can also produce them, and the amount of shifting may not be constant across a spectrum. It is, therefore, important that these shifts are removed before the spectra are ratioed.

The method that I have developed for the removal of the relative shifts in wavelength uses cross correlation to align the atmospheric features from one spectrum with those of the 'wavelength calibration' spectrum. The calibration spectrum should have good absolute wavelength registration and a high signal to noise ratio. The wavelength range common to the calibration spectrum and the spectra to be aligned is cut into 7 overlapping quarters (figure 4.7). The average shift in each section is calculated by cross correlation: this result is taken as being the shift at the centre of that section. The amount that a particular wavelength needs to be shifted is calculated using a linear interpolation between the shifts at the centres of the two sections in which it lies. This method significantly reduces the errors introduced by the relative shifts between spectra so they are generally below those from the other sources. This technique only works because the raw spectra are at a high signal to noise; are over relatively large spectral ranges and there are a large number of strong atmospheric lines in all windows.

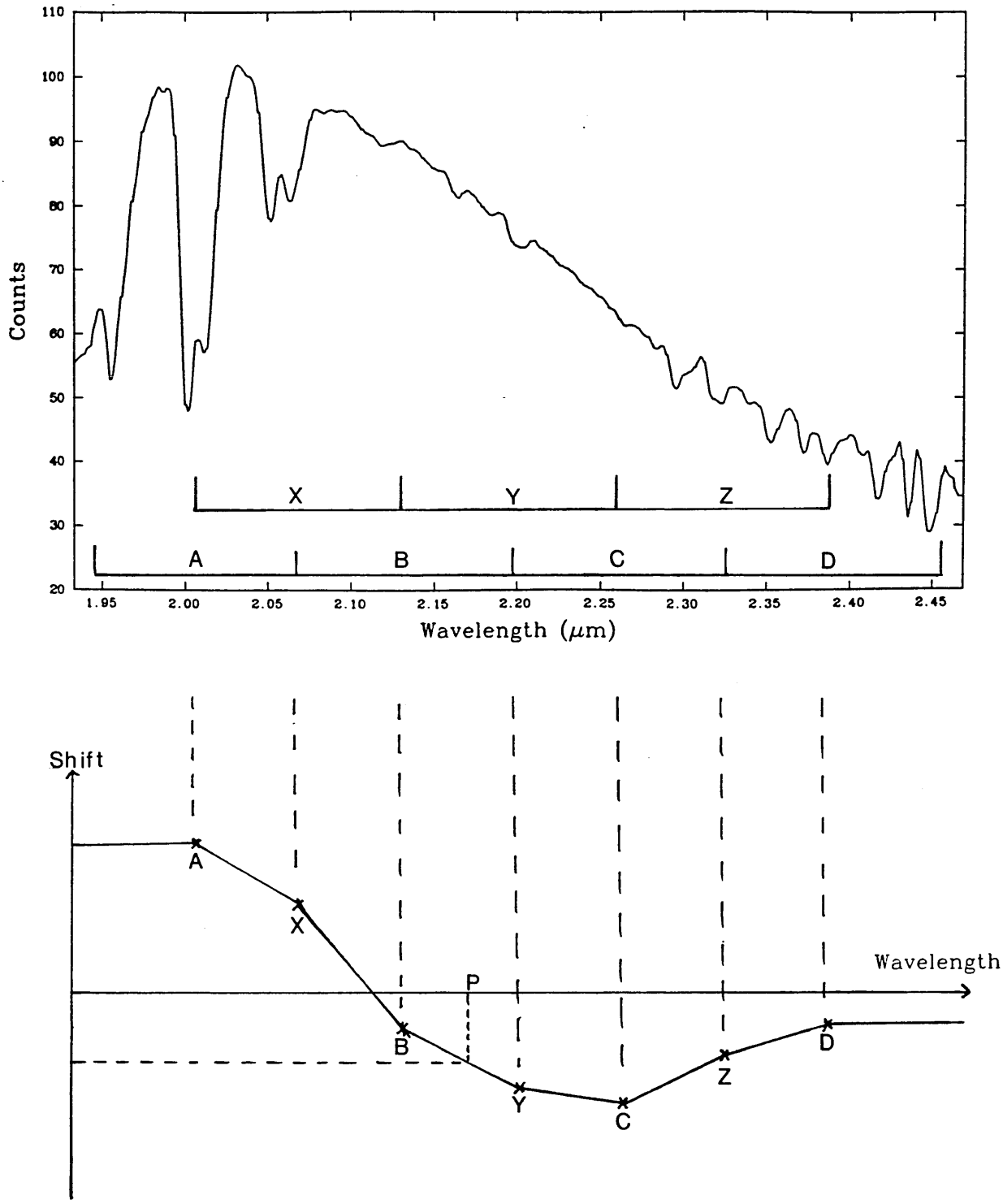

Figure 4.7: Cross Correlation.

The shift calculated by cross correlating each section against the wavelength calibration spectrum is taken as being the shift at the centre of the respective section. The shift at a position P is calculated using a linear interpolation between the closest centres.

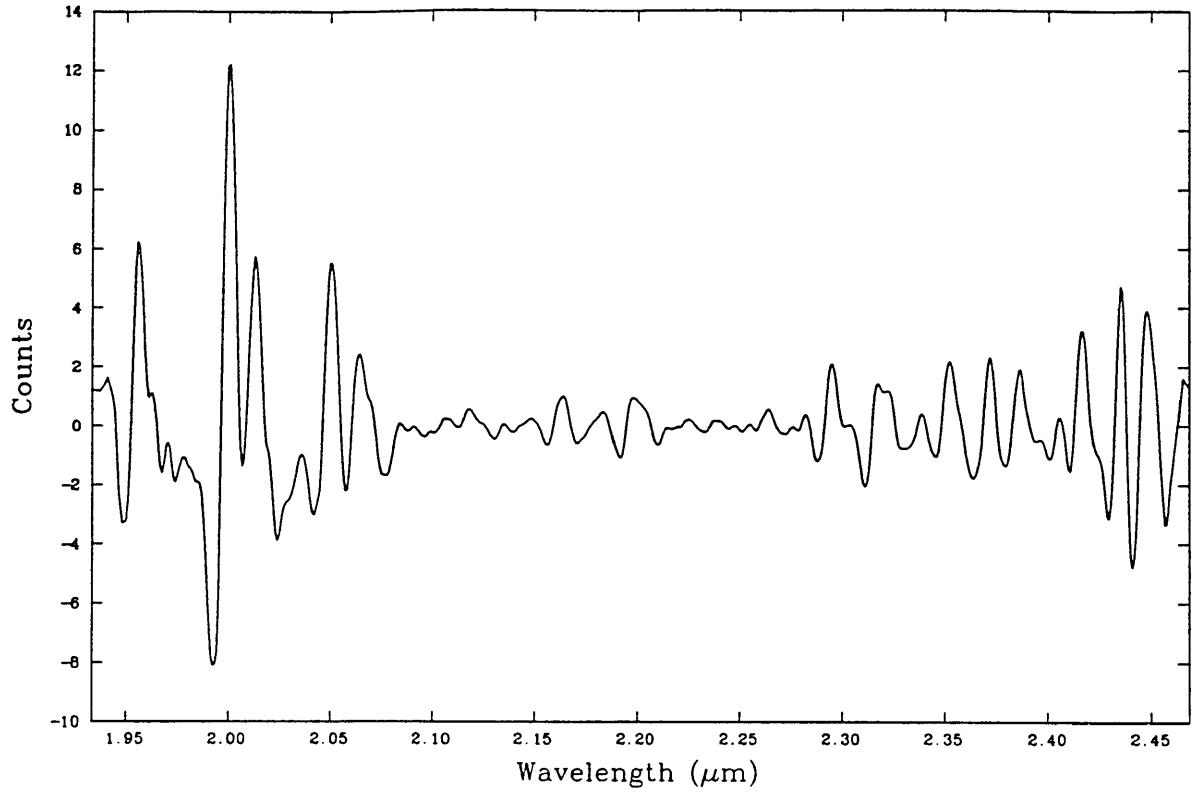

Figure 4.8: The effect of the High Pass Filter

This is the same spectum as in figure 4.7 after a high pass filter has been applied to it.

4.2.1 Cross Correlating

The wavelength registration in the ~~the~~ raw spectra is best defined by the position of lines, in particular their edges, and very poorly by the overall shape. Therefore, before cross correlating a 'high pass' filter is applied to the spectra. This removes the DC offset and any features larger than about 3 times the width of the line profile, so making the lines the dominant features (figure 4.8).

4.3 The Spectral Reduction Software

In July 1988 an Archimedes 440 micro computer was obtained to improve the 7 channel data acquisition system. Having a 20Mb hard disk, 4 Mb of RAM and a relatively powerful micro processor, it can deal with large amounts of data very quickly: in many cases being faster than a Micro VAX. I have written the spectral reduction package for the Archimedes

as part of the upgrades of the data acquisition system for the spectrometer. Included in the package are many routines, not available on STARLINK, that were developed to deal with problems specific to grating spectrometers. The majority of the spectral reduction for CGS1 and CGSII data has been done using the Archimedes.

4.4 The Data Sets

The majority of the CGS1 data presented in this thesis was taken on the 1.5m TCS (Tenerife) by A. Zadrosny, I. Hepburn and C. Lazaro in June 1985. A selection of carbon stars and bright, single, non-variable stars were observed at J, H, K, and L. Further data was obtained by S. Arribas and myself in May 1988, however, bad weather and instrumental problems limited the observations to 1 night. Observations were taken in the K window of bright single non-variable stars.

In November 1988 observations of single, bright, non-variable stars were made using CGSII on UKIRT by S.Arribas, A. DeMenezes and myself. Bad weather limited us to observing only on two nights and in the K window. November 12th had good observing conditions but on November 16th the seeing was poor. Unfortunately, when we were observing channel 6 was dead so four times over sampling had to be used to ensure there would be sufficient data points across the final spectra.

4.5 Decoding CGS1 Data

Since the majority of the data decoded was taken in 1985 using the 4 channel data acquisition system, I will describe the method used for decoding this data set. Decoding the 1988 data is virtually identical, except for the initial transfer of data to the computer.

- The data is transferred from the Cristie digital Tape recorder to the computer using the RS232 link. The data is converted from ASCII to numbers and the coarse and fine encoders are combined to give a single grating position.
- Occasionally there are points which have been corrupted. 'Bouncing' on the data bus of the digital rack can make the grating appear to go backwards or alter positive

to negative signals. These errors are easily spotted and corrected.

- An information file is then written for each raw spectrum and the data is put into stacks, one for each day.

The data is now in a format that can be handled by the spectral reduction package.

As described earlier the data is taken with the grating being driven at constant speed so the distance between data points in terms of encoder position will be approximately constant, whereas in terms of wavelength it will not. Therefore, when dealing with CGS1 data, it is preferable to use encoder position until the final spectra are produced.

- It is simpler and quicker to work with files which have the same encoder scale. However, the way CGS1 is operated means that the raw scans will not be in this form. A regularly spaced encoder scale is defined for each window then all the scans are converted to the relevant scale using a 4th order Laplace interpolation.
- The effect of using different post amplifier gains is removed. Ideally the gains should be calibrated at the telescope; however, there appears to be an error in the gain calibration taken during the observing run as the results are inconsistent, and differ considerably from previous gain calibrations for that post amplifier. Therefore, I have used the nominal gains.
- All the raw spectra are checked for regions which have an unexpected loss of flux, usually caused by the star moving out of the aperture. These regions are deleted.
- A cross correlation calibration spectrum is chosen for each window. All the spectra are shifted onto the relevant calibration spectra so that the atmospheric features match, using the cross correlation method described in section 4.2.
- The effect of airmass is removed (see section 4.1.1).
- Since the data was taken from a good high observing site, the upper and lower beams will be very similar. This allows the upper and lower beam scans for each star to be averaged producing a single raw spectra at better S/N.
- The encoder positions are converted to wavelength using the method described in chapter 2.

The result is a processed spectrum for each star which can be ratioed with the processed spectrum of the absolute calibration star, Vega.

When many of the brighter stars are ratioed with Vega, a significant proportion of the noise comes from the raw Vega spectra. However, in many of the windows Vega will have been observed on many nights whilst the other star may not. Therefore, it would be advantageous if all the raw spectra of Vega taken in a particular window could be combined to produce a spectrum with a higher signal to noise. The spectra of Vega cannot simply be co-added since the observing conditions, in particular the airmass calibration, will change between nights. However, when observing conditions are comparable, the difference between the spectra taken on different nights in the good parts of the atmospheric windows will vary relatively slowly in wavelength; typically over a wavelength scale three or four times the spectral resolution of CGS1. Therefore, by applying a low pass filter to the spectra, with a cut off at about 3 times the width of the instrumental profile, a smoothed version is produced which still contains the information on the differences between nights. By ratioing these smoothed spectra, the difference between them can be calculated. This can then be used to make a spectra taken on one night 'appear' that it was taken on another night.

For example, consider two separate nights, A and B, when observing conditions were comparable and measurements were taken in the same window. After the processes described earlier in this chapter have been performed the result will be a calibration Vega spectrum for each night (V_A and V_B), both at an apparent airmass of 1. To improve the S/N for the calibration of night A, the Vega spectrum from night B is to be added to it. It is therefore necessary to alter V_B to make it appear that it was taken on night A, ie produce a spectra $V_{(B\,to\,A)}$.

- Apply the low pass filter to V_A to produce V_{AS}
- Apply the Low pass filter to V_B to produce V_{BS}
- Divide V_{AS} by V_{BS} to give the difference spectrum $D_{\frac{AS}{BS}}$
- Then $V_{(B\,to\,A)} = V_B \times D_{\frac{AS}{BS}}$

The above method works very well in the good parts of the K and L atmospheric windows. It offers a significant increase in the S/N for each point in the spectra without decreasing

the spectral resolution. However, if this technique were applied to the poorer parts of the atmospheric windows, with strong telluric features, (eg 2.8 to 3.4μm) then the noise would probably be increased.

4.6 Decoding CGSII Spectra

Discussions with the scientist in charge of CGSII indicated that the instrument is very rarely used for taking spectra over whole windows, so I have had to discover the quirks in the CGSII data for myself and work out suitable routines to remove them.

As described earlier, the data comes as ASCII files on VAX computer tape with a header containing the information for each file and then the data (position counter, wavelength, signal and error). The data is transferred to the Archimedes using KERMIT then the format is converted for the spectrum analysis program.

4.6.1 The Multi-channel Response

The dominant feature of raw CGSII spectra is its 'jaggedness' (figure 4.9). This is caused by each of the seven channels having a slightly different response, so a cyclical pattern is imposed on the spectra. This is a feature of all multi-channel instruments since it is impossible to make all the detectors, electronics and optical paths identical for each channel. This multi-channel effect must be removed before ratioing the spectra because there are a number of possible errors they can introduce.

Changing Gains

When taking the spectra of stars of different magnitudes, the amplifier gain is altered to maximise the signal without saturating the electronics. If the gains do not change by exactly the same amount on all channels, extra noise will be introduced when ratioing stars measured using different gains.

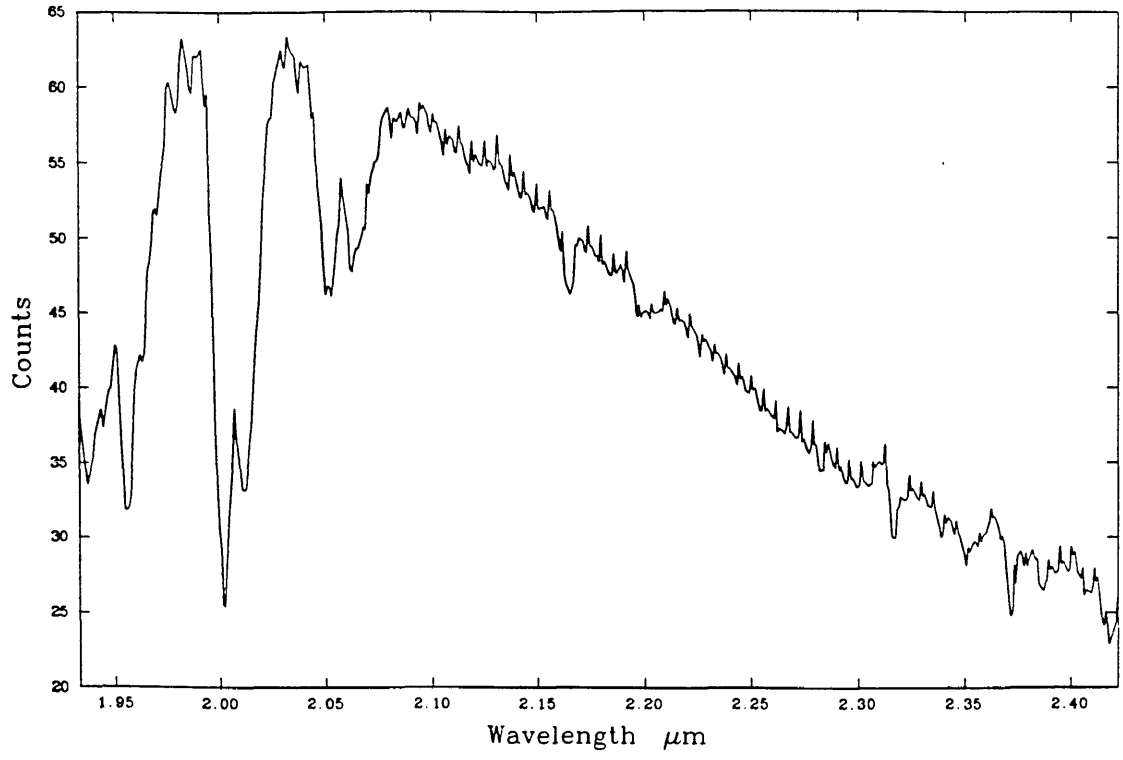

Figure 4.9: Raw CGSII Scan of BS458

Cross Correlation

If two raw spectra were cross correlated against each other the dominant factor would be the cyclical pattern. Since by the very way the instrument is operated the cyclical pattern for each spectra will exactly match, nothing would be gained and any shifts would remain.

Positioning of the Star in the Aperture

As the telescope moves around the sky the optics will flex. This causes the position of the maximum signal to shift slightly in the aperture and probably alters the beam profiles. The net effect is to alter the optical paths. This can have large effects on the differential response between the channels, particularly when there is poor seeing such as on November 16th. After taking three spectra of BS458 it was realised that the system was not peaked up (figure 4.10); so after peaking up the star was re-measured (figure 4.9). Figure 4.11 shows the ratio of the peaked and not peaked co-adds. There are three obvious effects

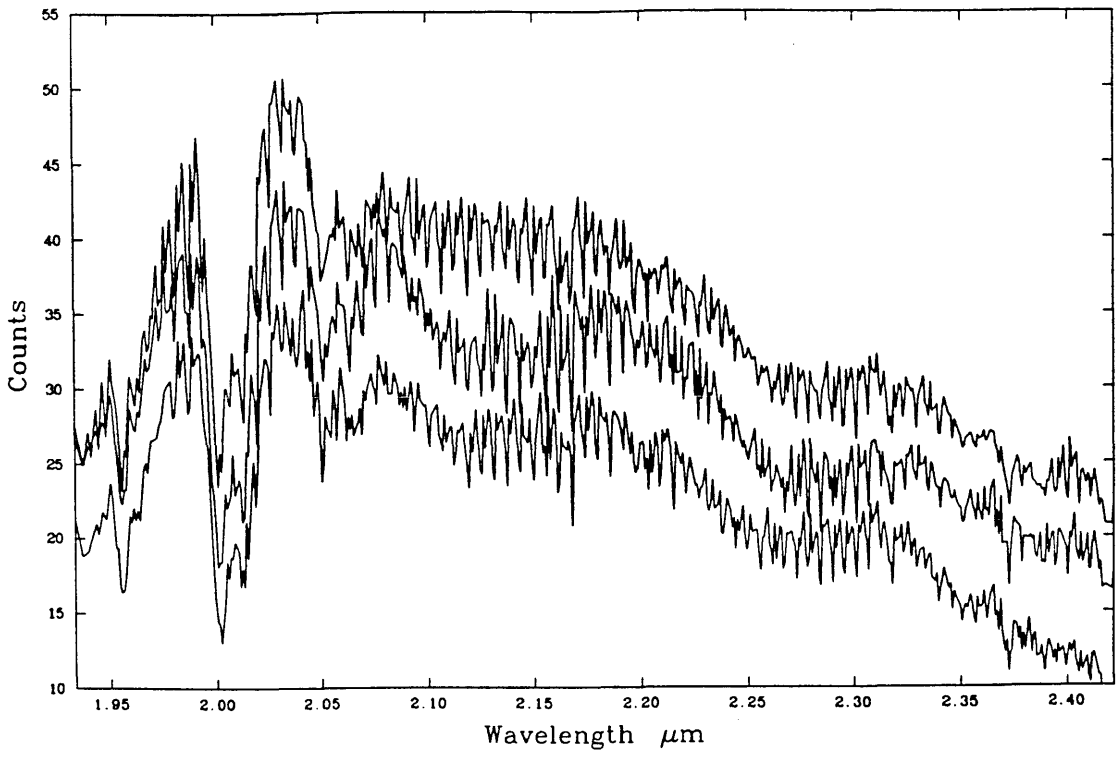

Figure 4.10: Individual Off Centred Scans

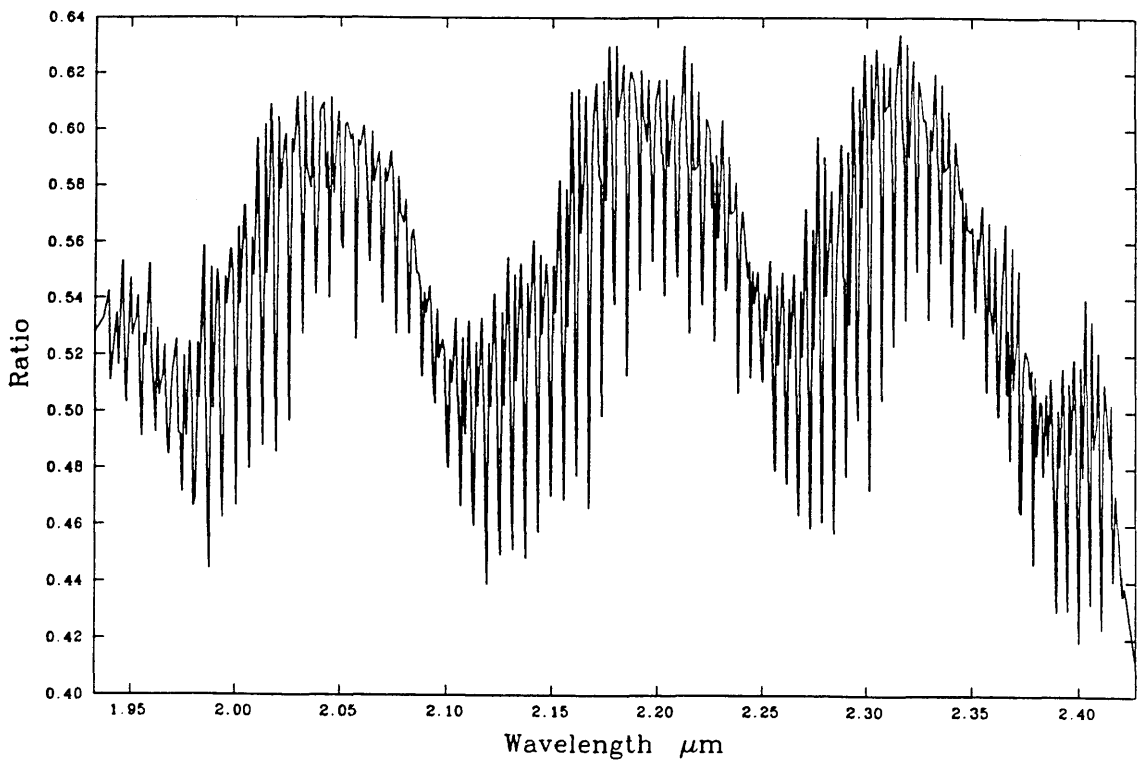

Figure 4.11: Ratio of Centred to not Centred Scans

- The differential response alters with the position of the star on the aperture.
- The differential response alters with grating position.
- A long period sine wave is introduced (I will deal with this later).

This is an extreme case, but all the scans taken on November 16th show this effect to some degree and there are signs of this in the November 12th data when the seeing was considerably better. I am unsure of the exact cause of these effects; however, it is not due to bad tracking because the three unpeaked scans are nearly identical; so it must be associated with changing optical paths inside the cryostat.

4.6.2 Removing the Multi-Channel Response

The differential response must be removed without otherwise altering the spectra, in particular, decreasing its spatial resolution.

- Due to the way that CGSII operates, there will be points missing at the end of the spectra (see chapter 2). The routine is made simpler if these points are included (they are marked as missing points).
- A window smooth is performed over 7 points. Since the instrument is a 7 channel device, if 7 adjacent points are averaged together the effect is to remove the differential response (figure 4.12). This cannot be used alone as it reduces the spectral resolution.
- The original spectra is divided by the smoothed version. The result is a spectra containing the differential response which needs to be removed and the 'high frequency' part of the absorption lines, particularly the strong telluric lines which must be retained (figure 4.13).
- The differential response varies with wavelength, so it is not enough simply to calculate it for each channel by averaging every 7th point. Instead, the differential response at every point in the spectra must be calculated. As figure 4.13 shows, the differential response varies smoothly with wavelength, so at any point it is approximately the average of the differential responses over the closest 7 points measured

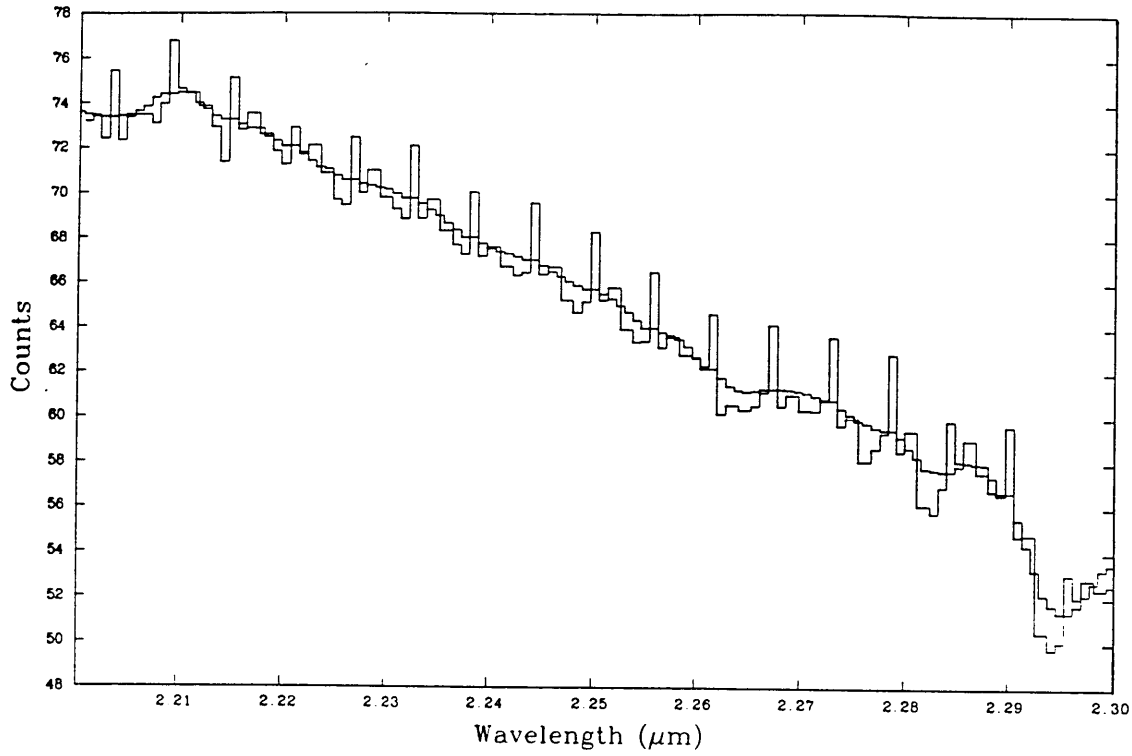

Figure 4.12: Original and Window Smoothed Spectra

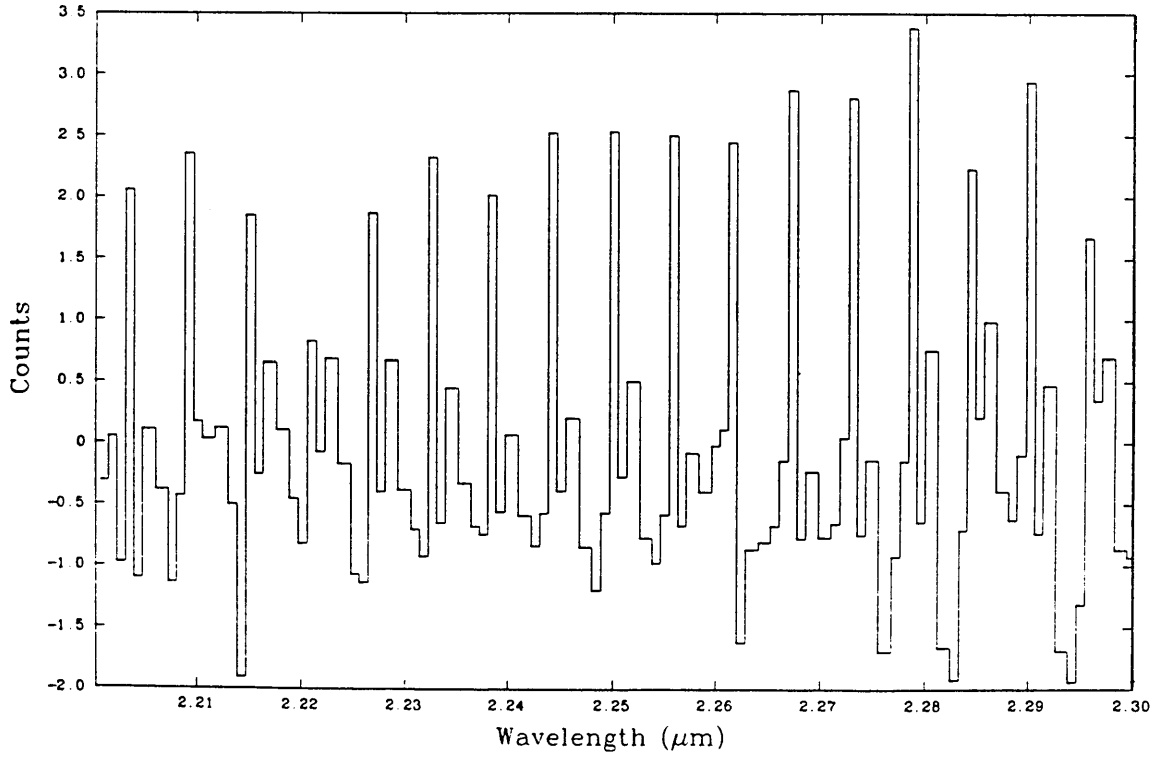

Figure 4.13: Their Difference

by that channel. By using 7 points the effect of absorption lines, which will only affect 1 point, is greatly reduced.

- The original spectra is then divided by the spectra of the differential response to produce the corrected version.

Figure 4.14 shows this technique applied to the raw spectrum of BS996. It success is demonstrated by comparing the power spectra of the original and 'corrected' versions of the raw spectrum (Figure 4.14). In the main, it is only those frequencies associated with the differential response that are removed and the spectral resolution is only slightly reduced. There are other techniques that would also correct the differential response, for example, altering the Fourier Transform of the spectra then taking the inverse Fourier Transform to get the corrected version. The method I have developed has the advantages of being simpler, quicker and fully automatic, requiring no user intervention, which is important when dealing with large numbers of spectra.

4.6.3 Continued CGSII Spectral Reduction

- The shifts in the spectra taken with CGSII are generally smaller than those of CGS1, but if they are not removed the noise will still be increased. The shifts are taken out using cross correlations as described earlier.
- The spectra are corrected for airmass.
- The spectra are ratioed with hot stars which have had the hydrogen lines removed.

Many of the spectra now show this long period sine wave described earlier. This is particularly true for the spectra taken in the poorer observing conditions. This long period sine wave must be removed, but without altering the DC levels and slopes in the ratioed spectra.

4.6.4 Removal of the Long Period Sine Wave

As I have demonstrated earlier this sine wave is linked to the grating position, but appears to be caused by the star being placed in a different position in the aperture. The period

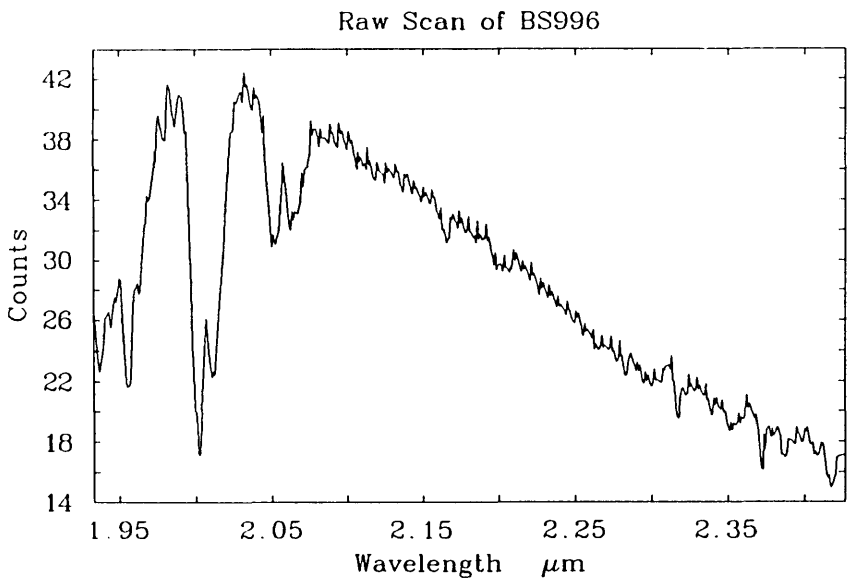

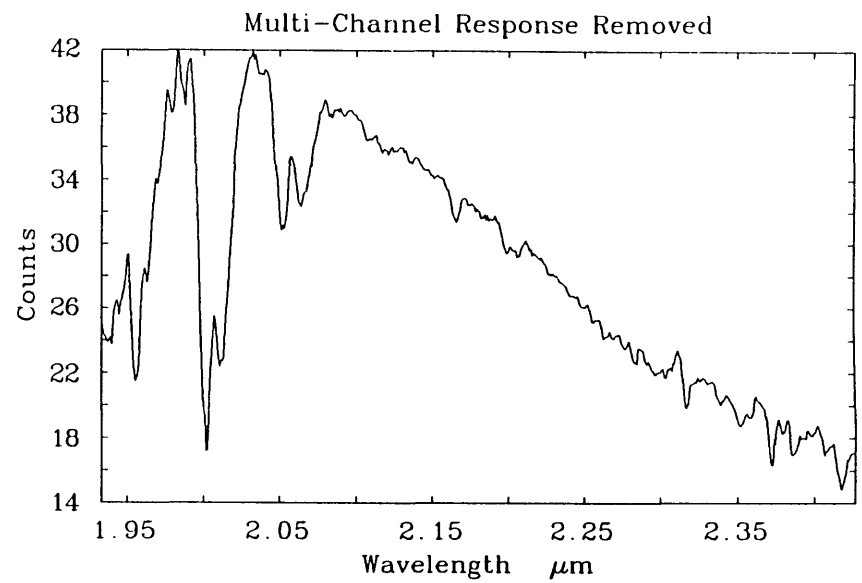

Figure 4.14: Method Applied to BS996

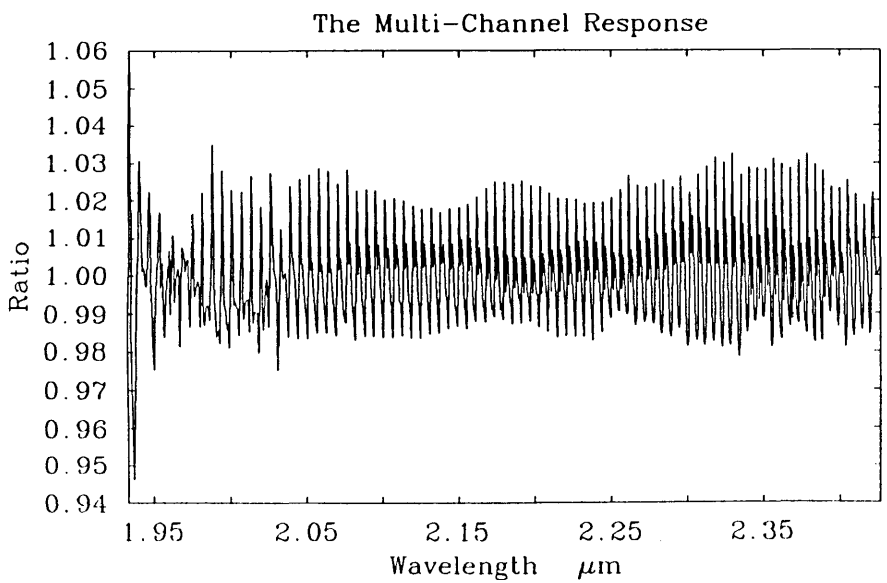

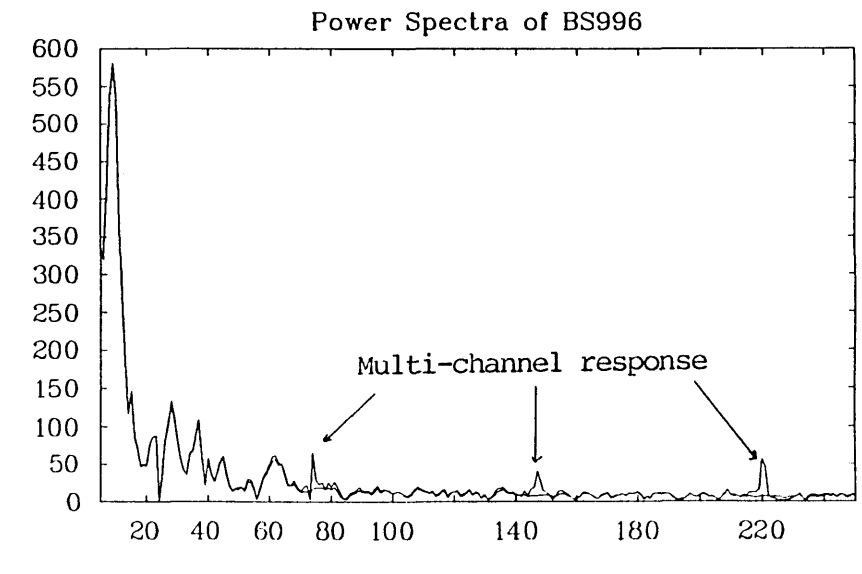

of the sine wave is 6 to 7 detector block lengths or about 210 wavelength positions when 4 times oversampling.
I have used a very simple method to remove the sine wave.

- Any strong features in the ratioed spectra are cut out.
- A band rejection filter, centred on the period of the sine wave, is applied to the ratioed spectra.
- The strong lines are replaced.

Figure 4.15 shows the effect of the method for the two scans of BS458.

Unfortunately, when the sine wave is prominent in the ratioed spectra it also causes the slopes to alter. It has proved impossible to calculate accurately the amount that the slopes are modified.

4.7 Comments on Data Sets

The data produced by CGSII has a considerably higher S/N than the CGS1 data which is to be expected since CGSII was used on a 3.8m and not a 1.5m telescope. However, in general, the spectrophotometric qualities of CGS1 appear considerably better, particularly in bad weather. The ratios of αBoo to Vega for the CGS1 data and the CVF spectra of Strecker (1979) are within 5% between 1.2 μm and 4.1 μm (figure 4.16). Therefore, while CGSII shows a large number of lines CGS1 is considerably more accurate at measuring the continuum fluxes.

4.8 Guidelines for future Spectrophotometry

When attempting spectrophotometry there are a number of way in which the observations can be made more successful.

- Observe as near to the zenith as possible because it reduces flexture in the optics and makes the errors introduced by airmass considerably less.

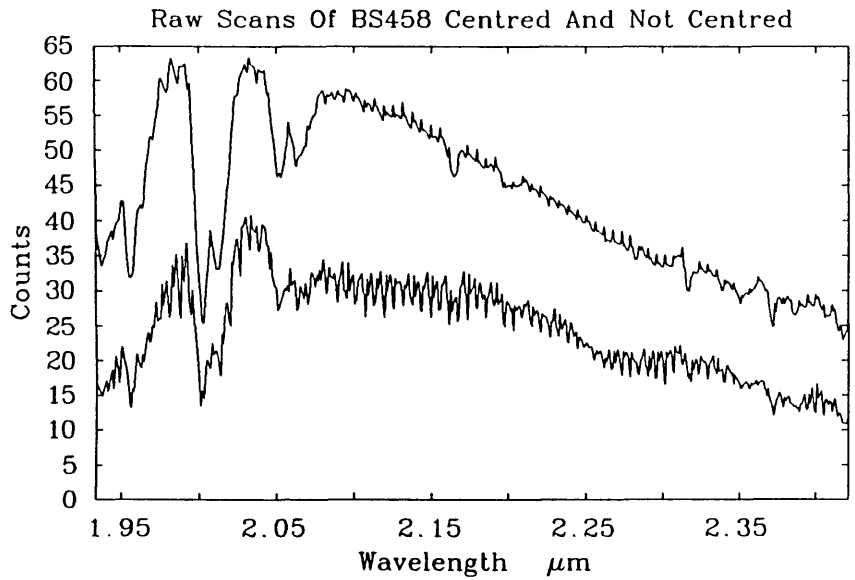

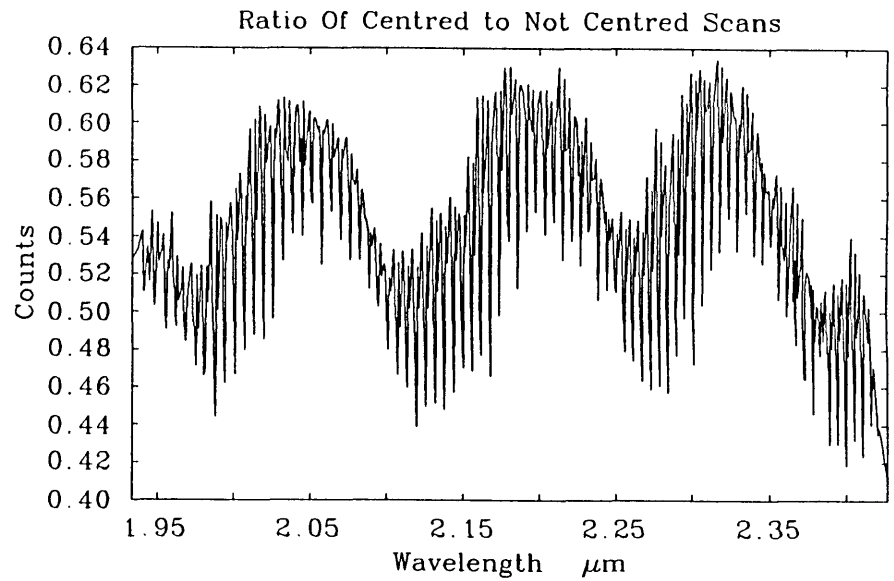

Figure 4.15: The Method Applied to BS458

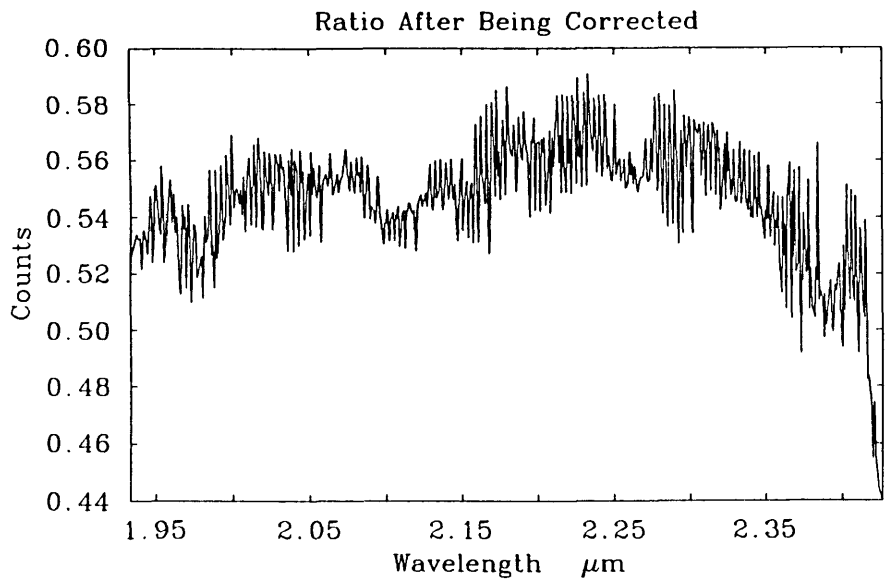

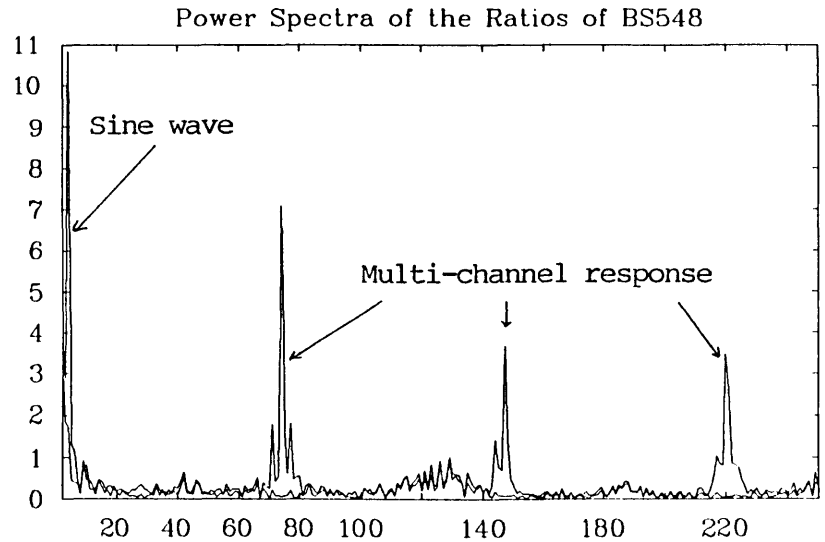

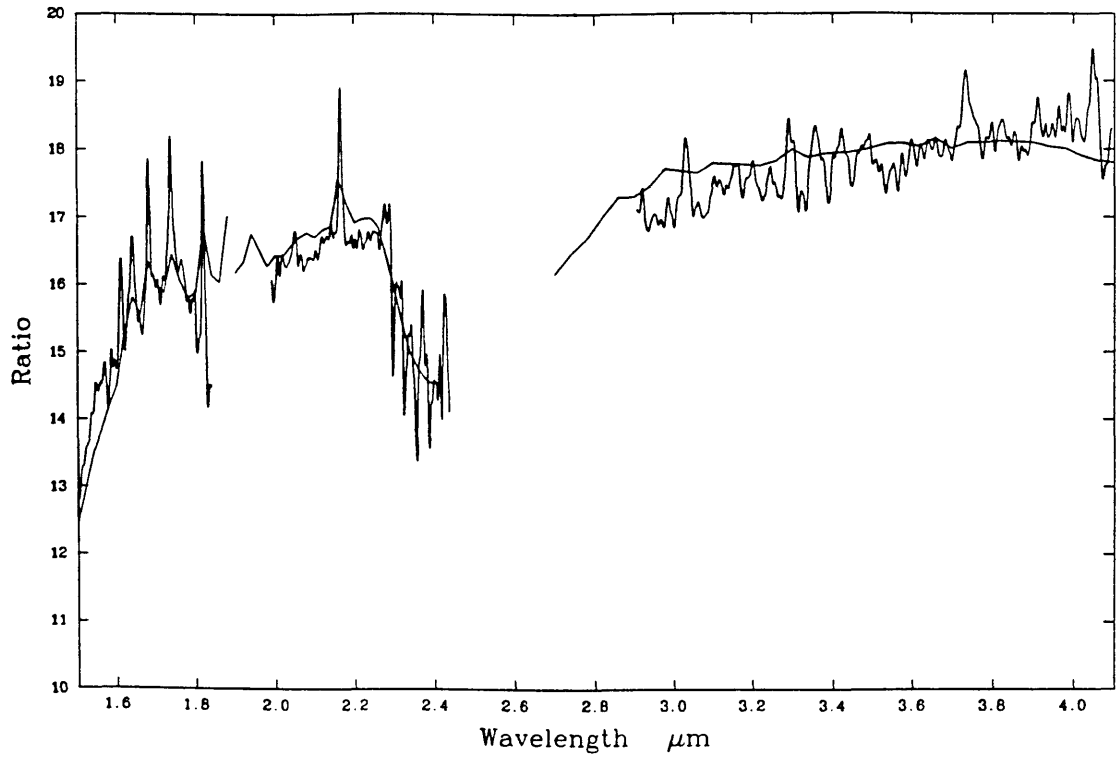

Figure 4.16: The Ratio of αBoo to Vega for CGS1 and Strecker's Data Sets

- It is a waste of time to go too far into the edges of the window as the flux falls off very quickly, so rapidly decreasing the S/N.
- Do not observe stars that are too faint unless they are very important. A signal to noise ratio per point of about 5 to 10 is the minimum that should be used.
- When using CGS1 in the J, H or K windows, always pump the liquid nitrogen as it adds a factor of 2 to the S/N ratio.
- If the seeing is poor when using CGSII, restrict the observations to a very small area of sky around the zenith.
- Keep a very close check on how the instrument is performing as an accuracy of a few per cent is very difficult to achieve. Check the raw spectra very closely for poor tracking, excess noise, unexplained dips, especially if it is a calibration. If there appears to be a problem, repeat the scan.
- Peak up the signal on every star.
- Try to repeat scans later that night or on another night so that there will be some confirmation of the results.

Chapter 5

Near Infrared Spectra and the Application of the IRFM

The spectra presented in this chapter have been analysed as described in chapter 4. Only the data obtained by CGS1 and CGSII has been used, and none of the spectra have been altered to take into account previous measurements.

5.1 The CGS1 Normalized Ratioed Spectra

Presented on the following eight pages are all the spectra taken with the ICSTM CGS1 on the 1.5m TCS since 1985 in the J,H, K and L windows. The spectra have been fully reduced as described in chapter 4, then ratioed with Vega. Vega has not had its hydrogen absorption lines removed so they appear as 'emission lines' in the spectra of the cooler stars. The ratios have been normalized and a DC offset introduced so three spectra can be displayed together without confusion. This allows a more compact presentation of the spectra. The spectra are in order of spectral type so the effect of changing temperature can be clearly seen. The full J window is shown despite the order overlap longwards of 1.2 μm.

CGS1 SPECTRA

J Window

Ratioed with VEGA

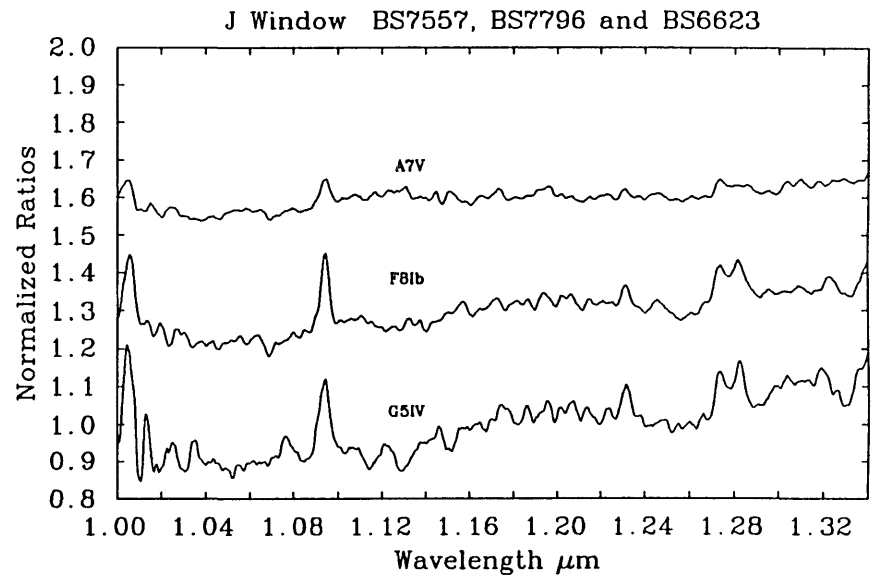

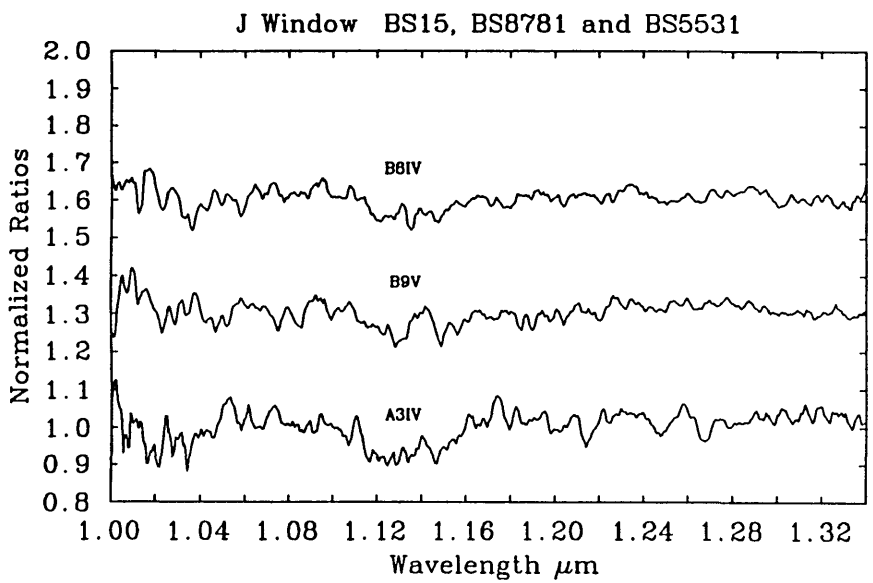

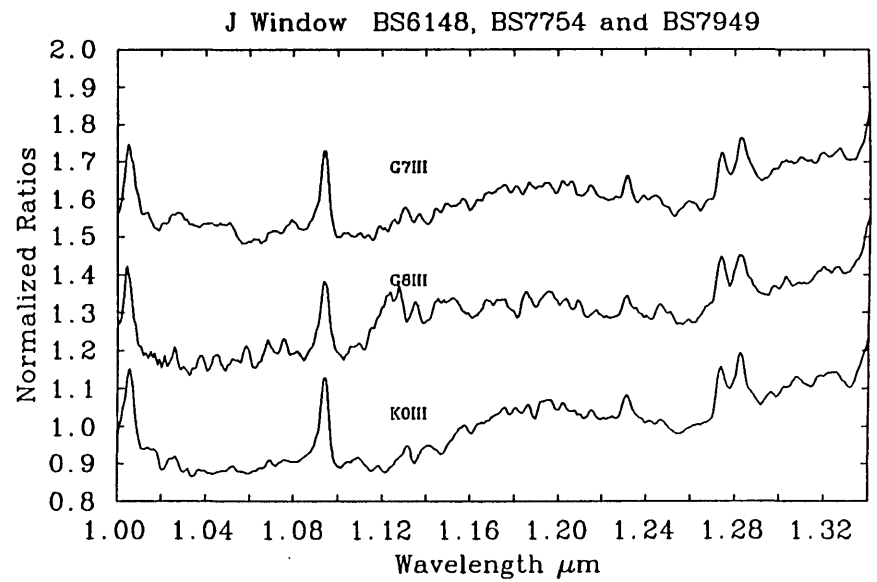

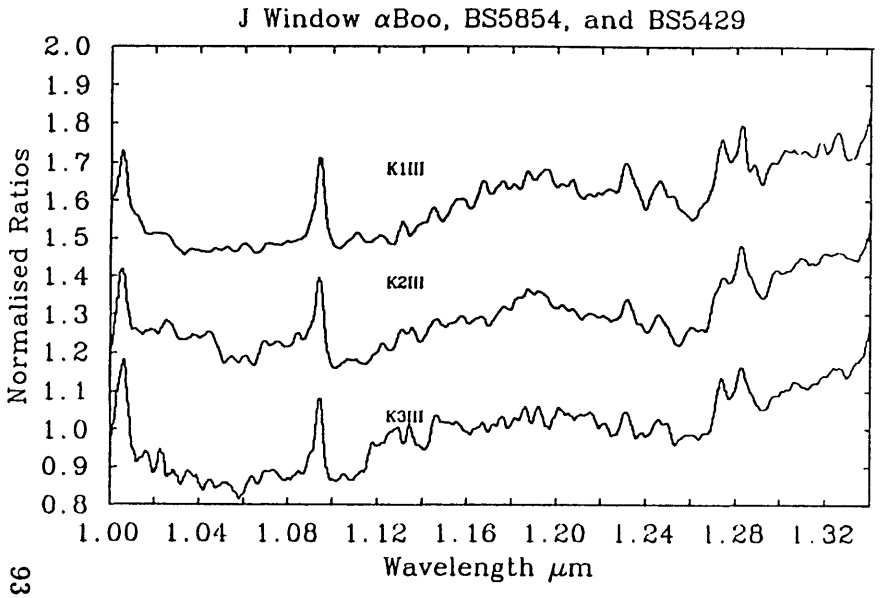
J Window αBoo, BS5854, and BS5429
Normalised Ratios
2.0
1.9
1.8
1.7
1.6
1.5
1.4
1.3
1.2
1.1
1.0
0.9
0.8
K1III
K2III
K3III
1.00 1.04 1.08 1.12 1.16 1.20 1.24 1.28 1.32
Wavelength μm

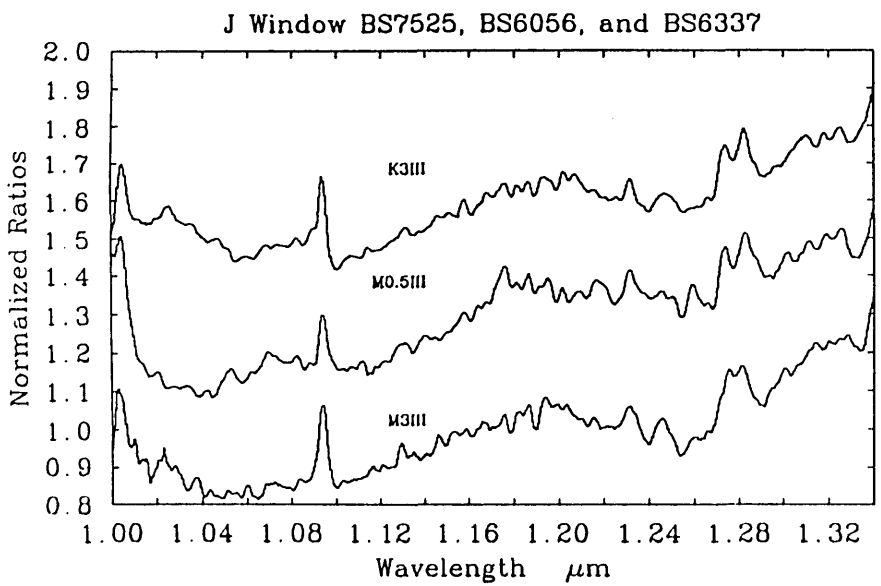
J Window BS7525, BS6056, and BS6337
Normalized Ratios
2.0
1.9
1.8
1.7
1.6
1.5
1.4
1.3
1.2
1.1
1.0
0.9
0.8
K3III
M0.5III
M3III
1.00 1.04 1.08 1.12 1.16 1.20 1.24 1.28 1.32
Wavelength μm

CGS1 SPECTRA

H Window

Ratioed with VEGA

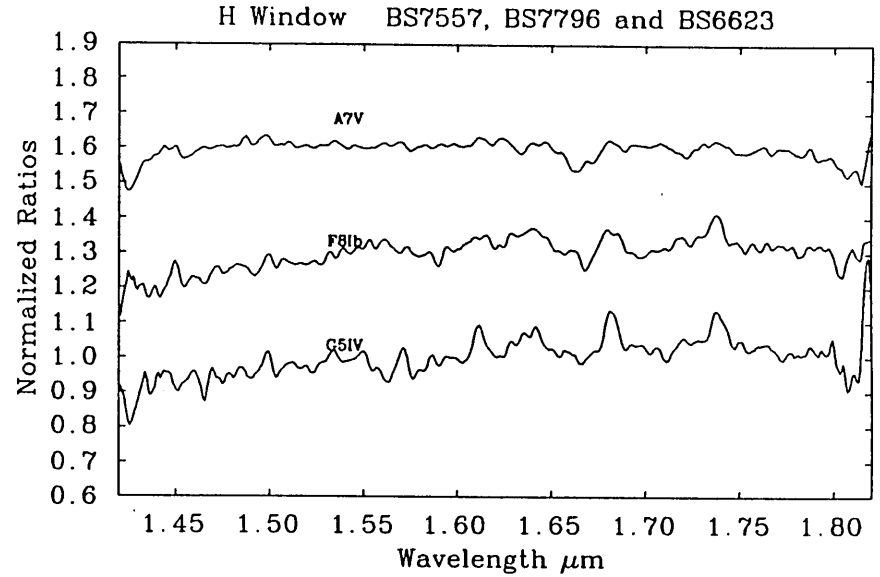

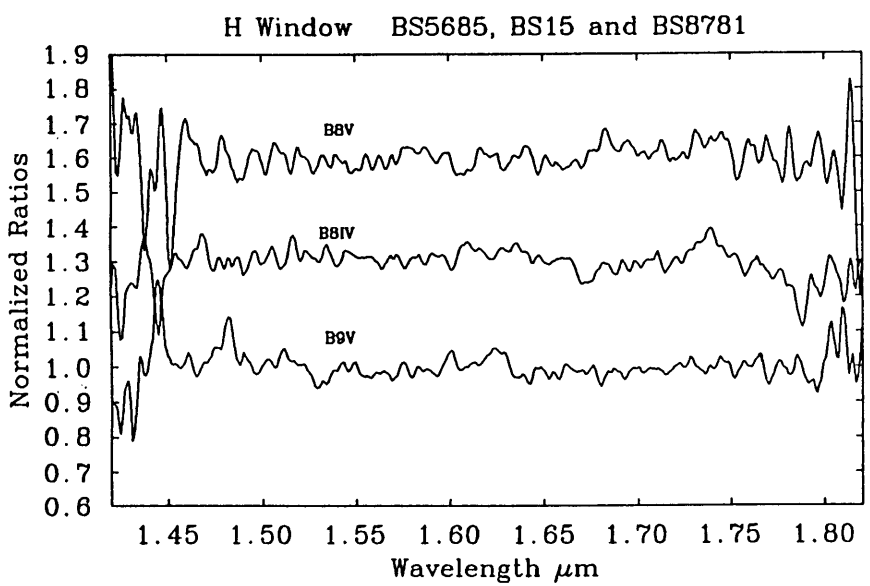

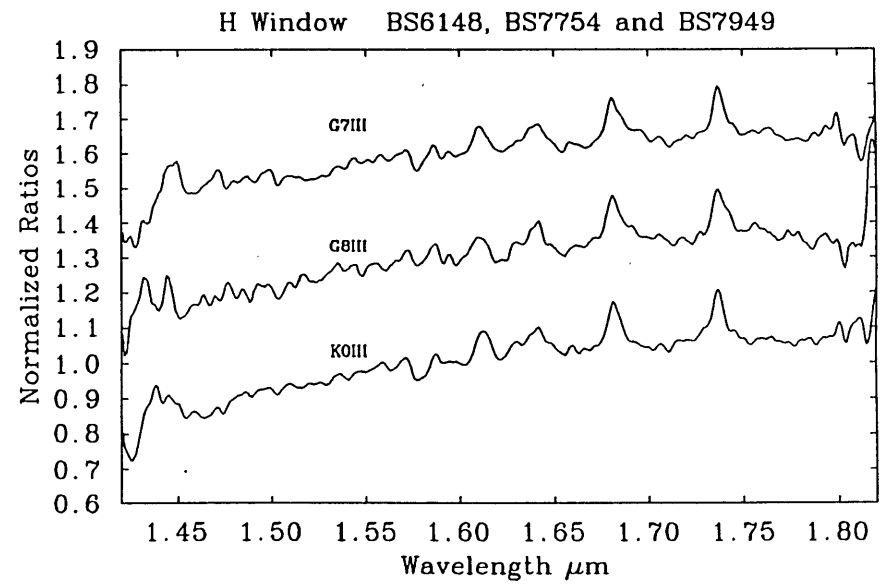

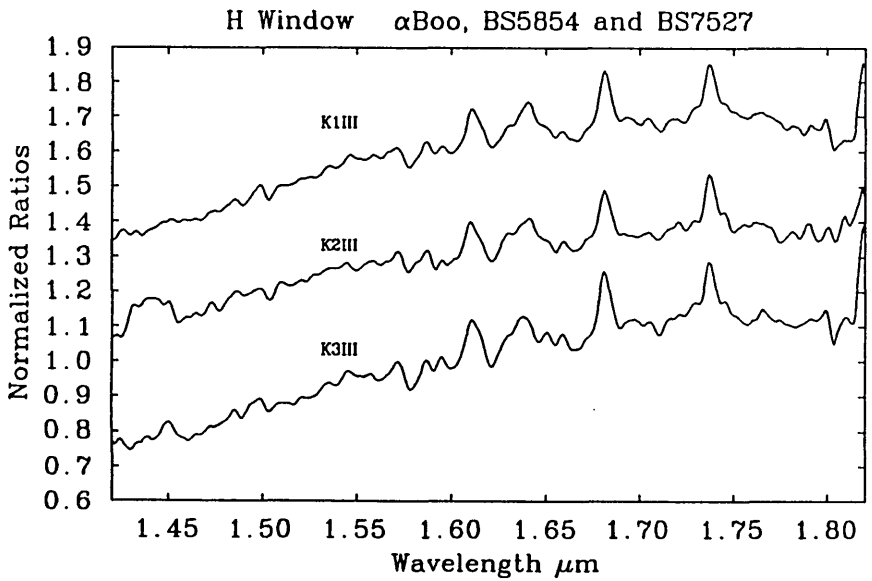
H Window αBoo, BS5854 and BS7527
Normalized Ratios
1.9
1.8
1.7
1.6
1.5
1.4
1.3
1.2
1.1
1.0
0.9
0.8
0.7
0.6
K1III
K2III
K3III
1.45 1.50 1.55 1.60 1.65 1.70 1.75 1.80
Wavelength μm

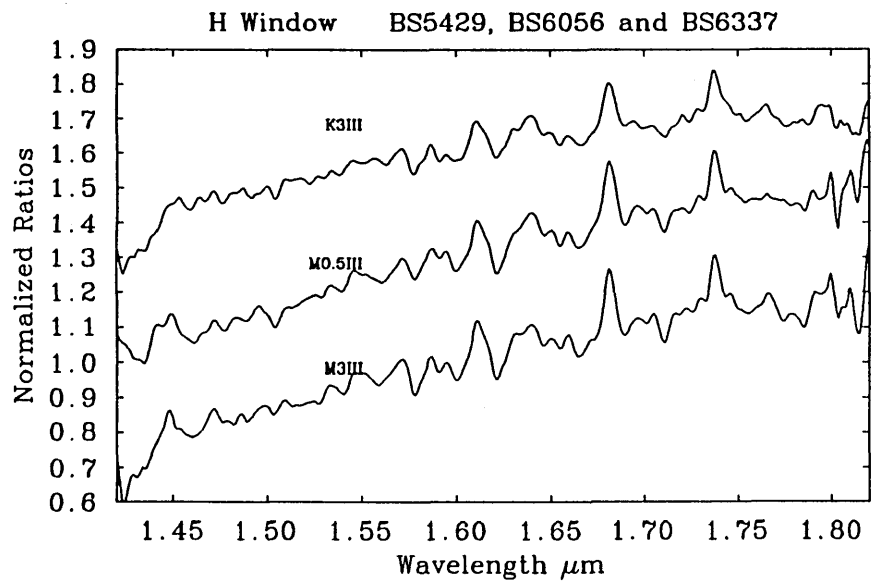
H Window BS5429, BS6056 and BS6337
Normalized Ratios
1.9
1.8
1.7
1.6
1.5
1.4
1.3
1.2
1.1
1.0
0.9
0.8
0.7
0.6
K3III
M0.5III
M3III
1.45 1.50 1.55 1.60 1.65 1.70 1.75 1.80
Wavelength μm

CGS1 SPECTRA

K Window

Ratioed with VEGA

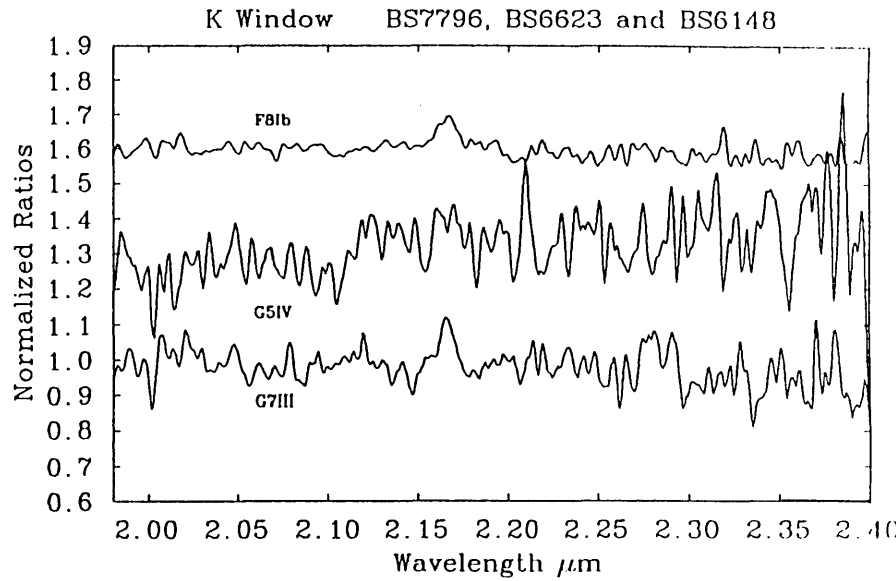

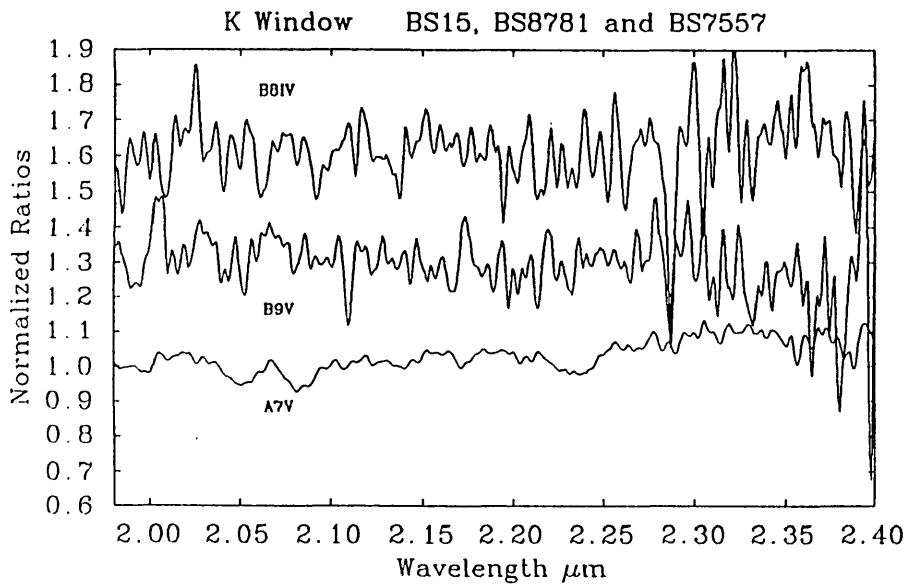

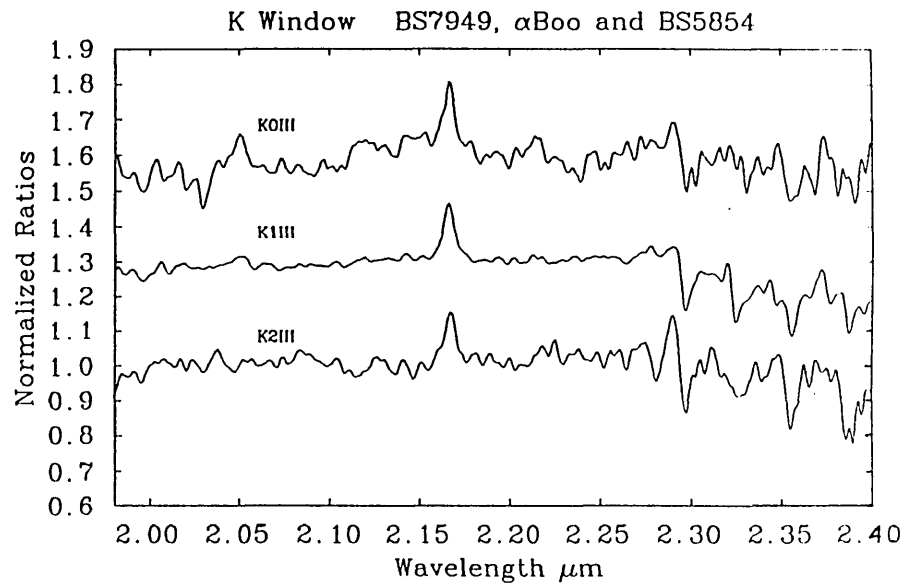

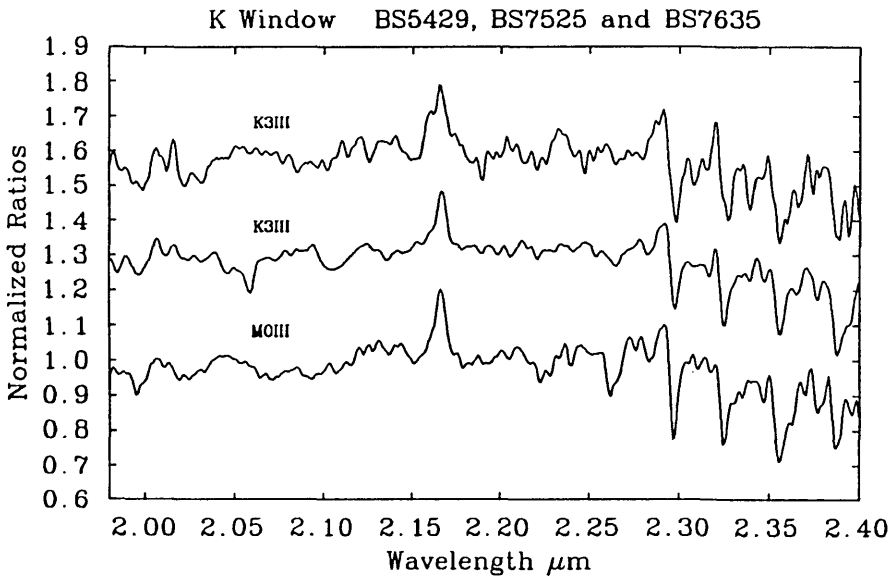
K Window BS5429, BS7525 and BS7635
Normalized Ratios
1.9
1.8
1.7
1.6
1.5
1.4
1.3
1.2
1.1
1.0
0.9
0.8
0.7
0.6
K3III
K3III
M0III
2.00 2.05 2.10 2.15 2.20 2.25 2.30 2.35 2.40
Wavelength μm

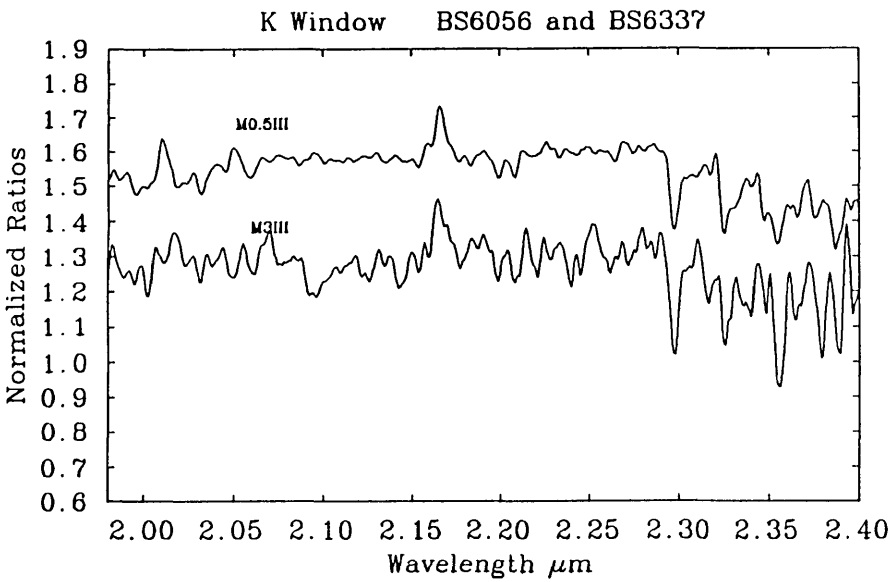
K Window BS6056 and BS6337
Normalized Ratios
1.9
1.8
1.7
1.6
1.5
1.4
1.3
1.2
1.1
1.0
0.9
0.8
0.7
0.6
M0.5III
M3III
2.00 2.05 2.10 2.15 2.20 2.25 2.30 2.35 2.40
Wavelength μm

CGS1 SPECTRA

L Window

Ratioed with VEGA

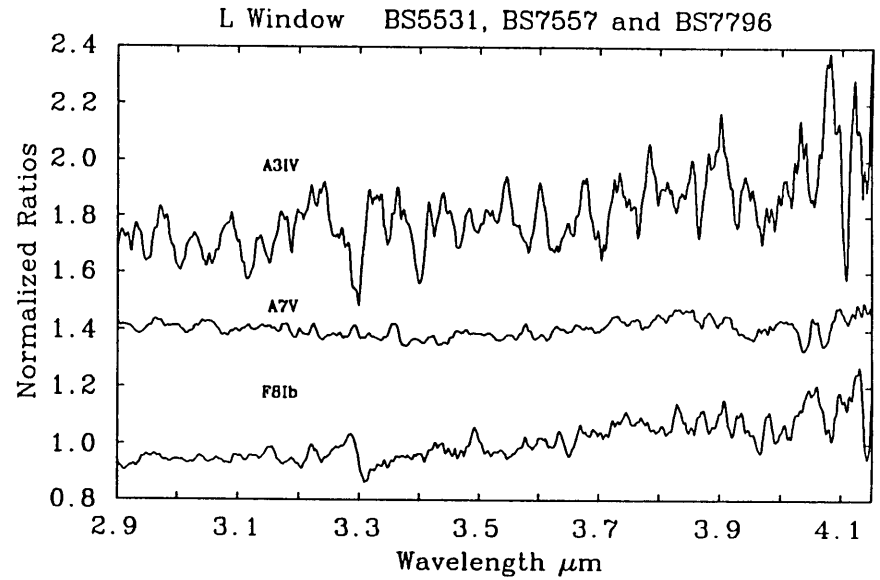

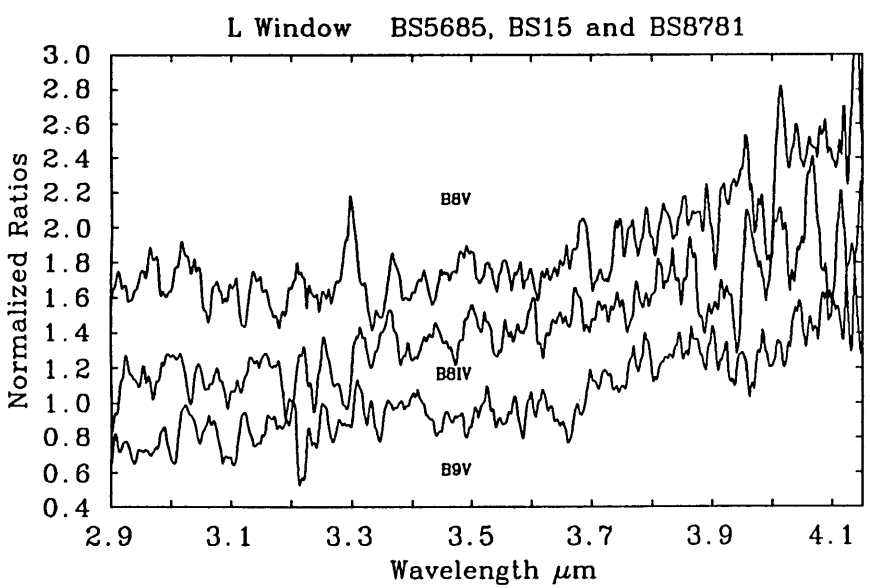

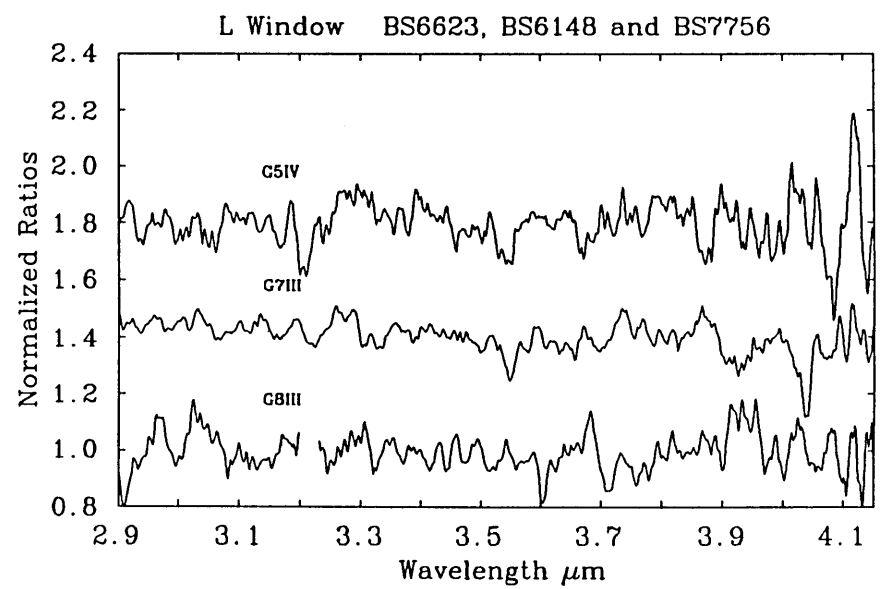

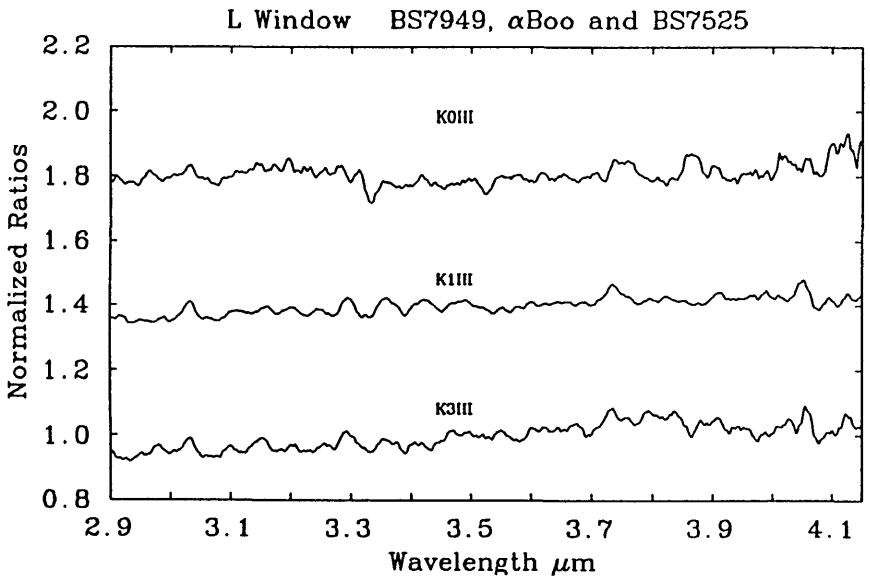
L Window BS7949, αBoo and BS7525
Normalized Ratios
2.2
2.0
1.8
1.6
1.4
1.2
1.0
0.8
K0III
K1III
K3III
2.9
3.1
3.3
3.5
3.7
3.9
4.1
Wavelength μm

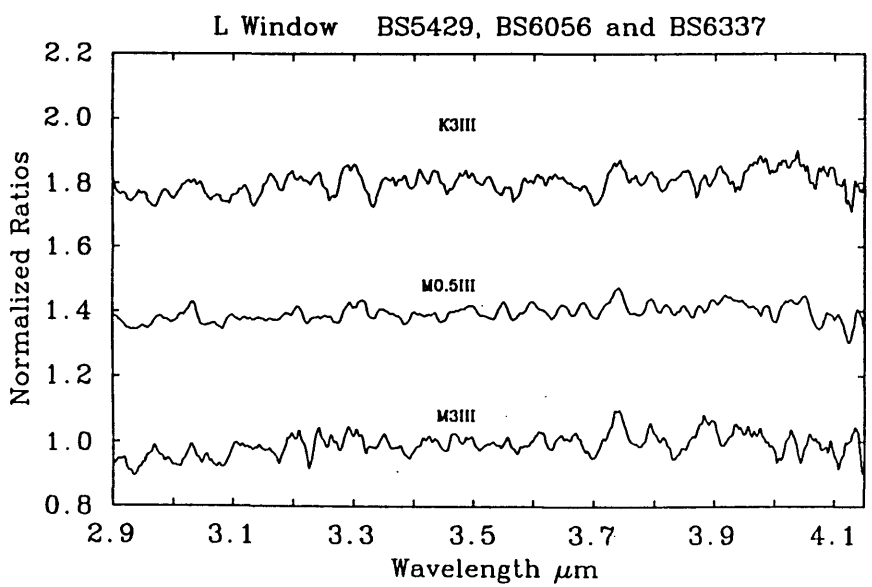
L Window BS5429, BS6056 and BS6337
Normalized Ratios
2.2
2.0
1.8
1.6
1.4
1.2
1.0
0.8
K3III
M0.5III
M3III
2.9
3.1
3.3
3.5
3.7
3.9
4.1
Wavelength μm

5.2 The CGSII Normalized Ratioed Spectra

On the next 4 pages are presented all the spectra taken on UKIRT with CGSII on the 12th and 16th of November 1988. The spectra are presented in the same manner as the CGS1 ratios except the spectra from November 12th has been ratioed with the A0V star BS3314 and the spectra from November 16th have been ratioed with the AIII0 star BS2540. Both stars having been corrected for their hydrogen absorption lines.

CGSII SPECTRA

Taken on November 12th 1988.

The spectra have been ratioed with the A0V star BS3314

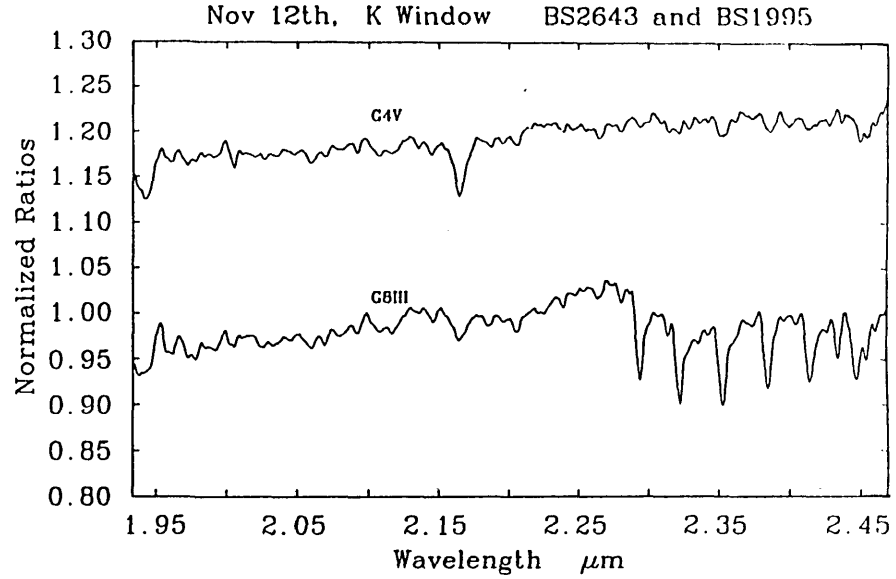

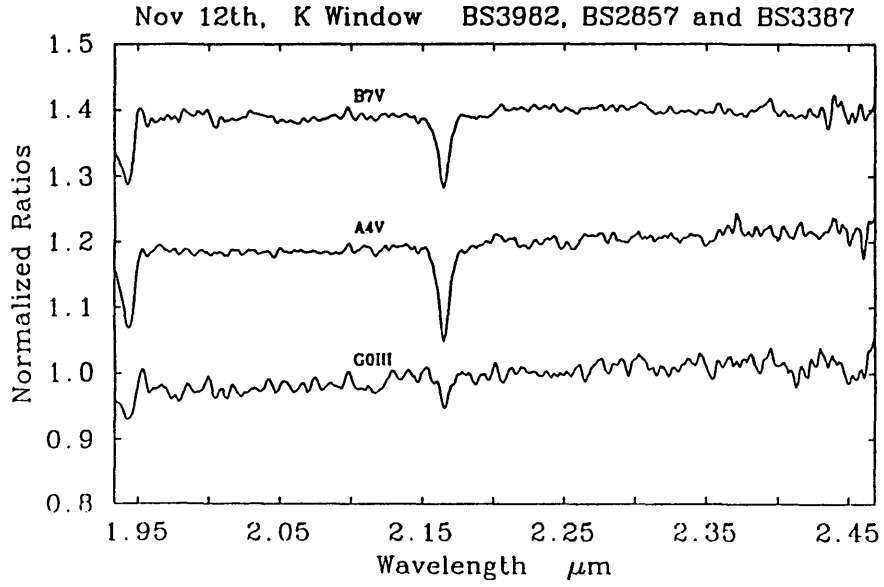

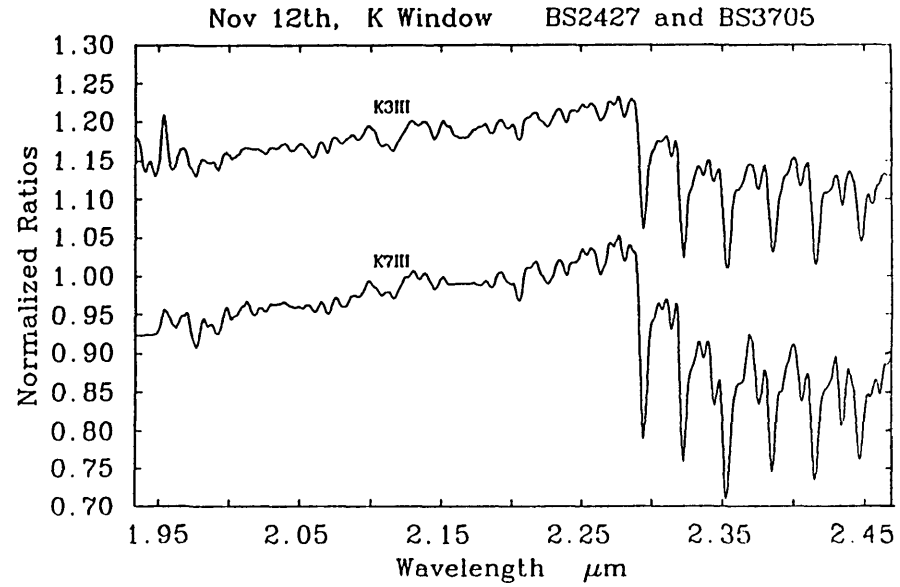

CGSII SPECTRA

Taken on November 16th 1988

The spectra have been ratioed with the A3III star BS2540

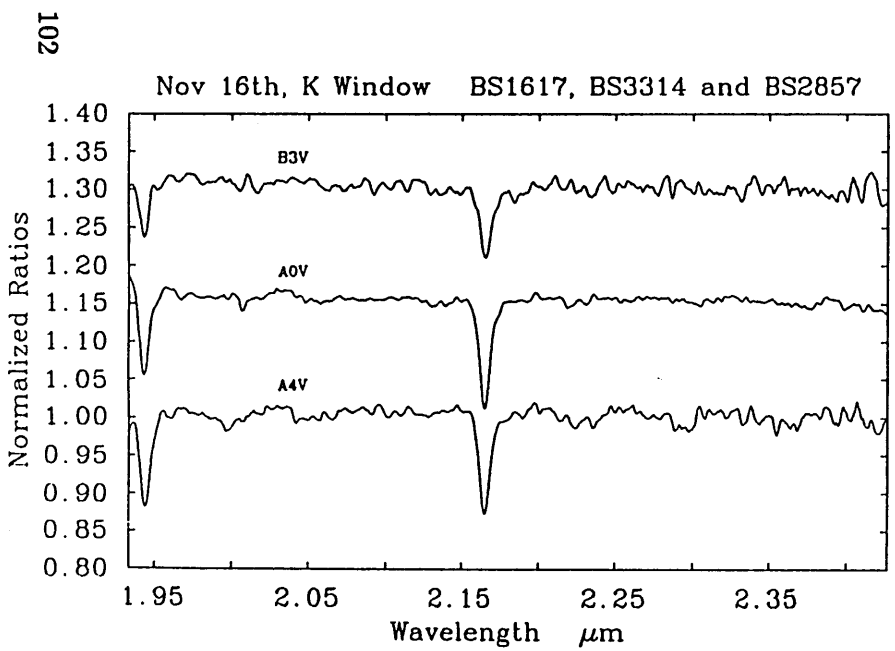

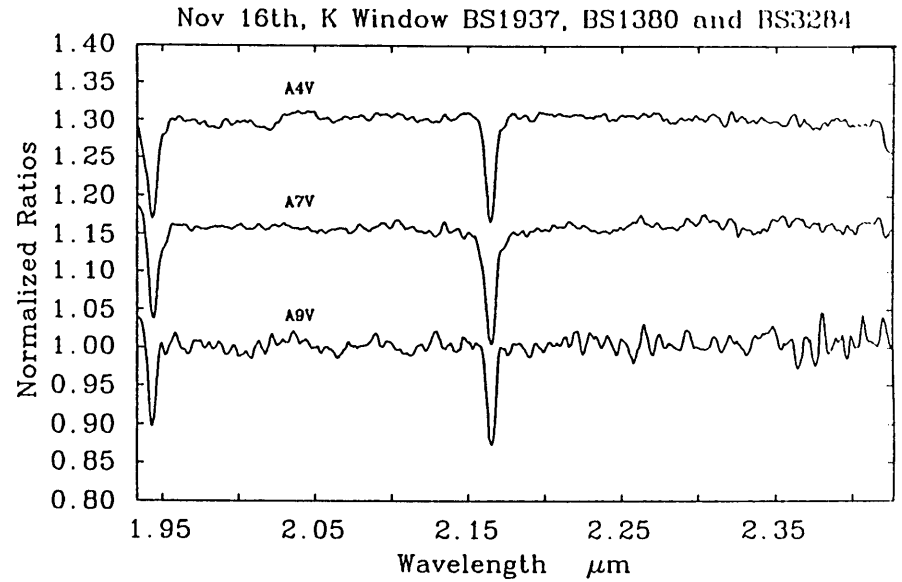

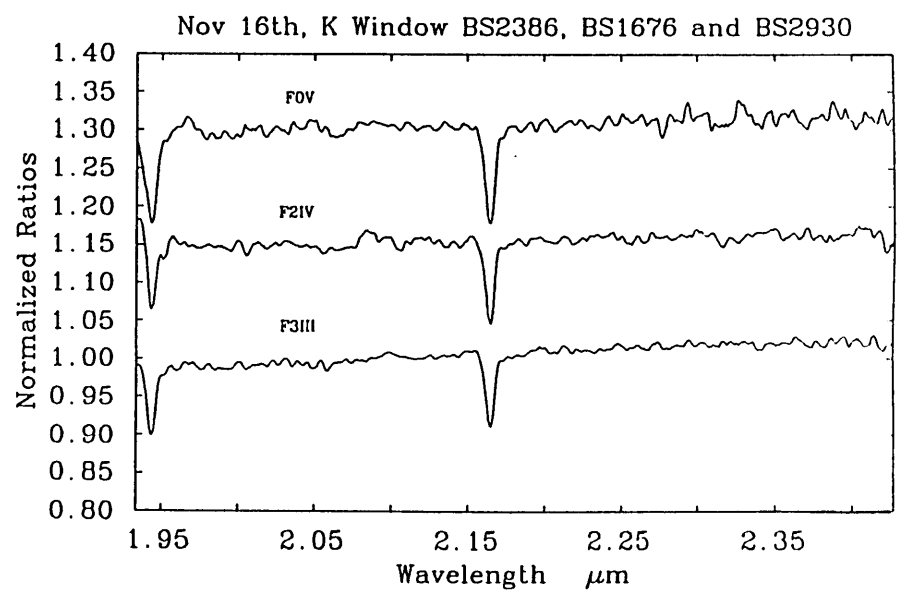

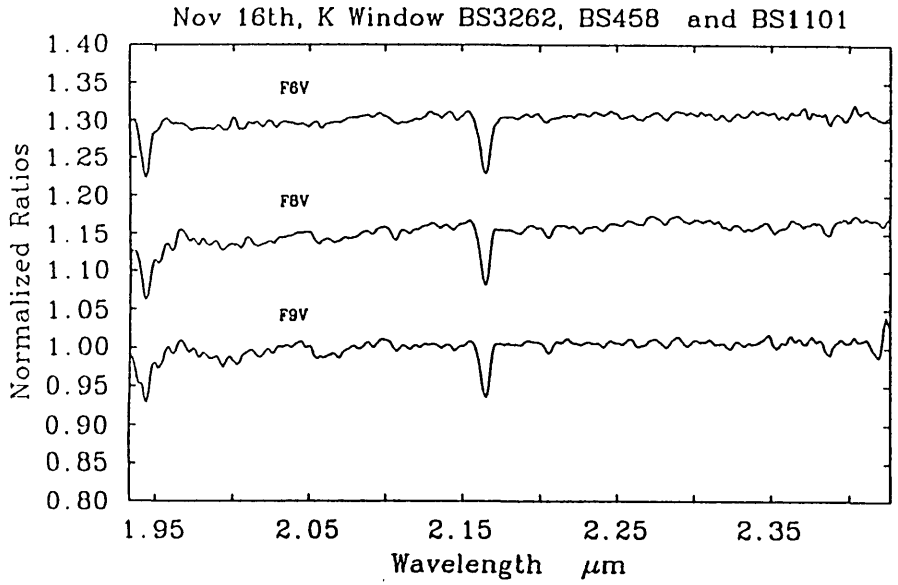
Nov 16th, K Window BS3262, BS458 and BS1101
F6V
F8V
F9V
Normalized Ratios
1.40
1.35
1.30
1.25
1.20
1.15
1.10
1.05
1.00
0.95
0.90
0.85
0.80
1.95
2.05
2.15
2.25
2.35
Wavelength μm

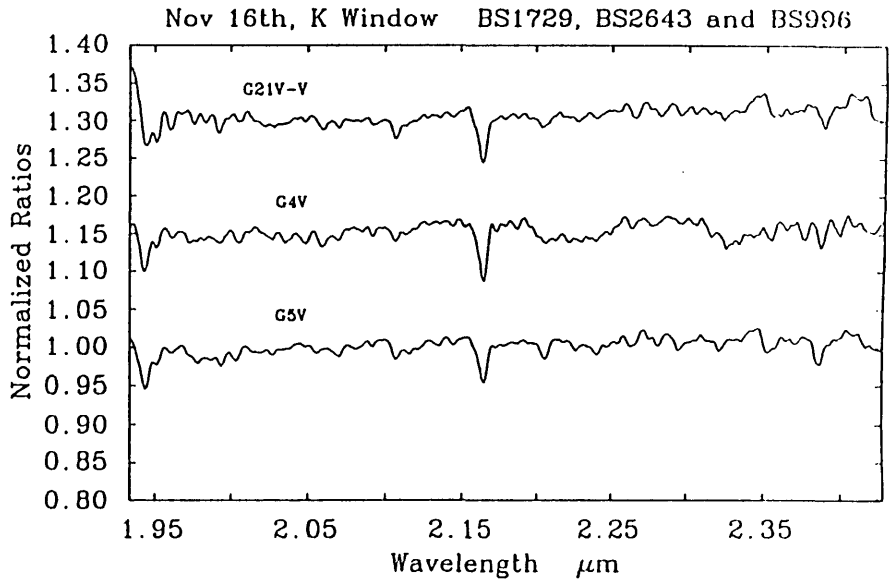
Nov 16th, K Window BS1729, BS2643 and BS996
G2IV-V
G4V
G5V
Normalized Ratios
1.40
1.35
1.30
1.25
1.20
1.15
1.10
1.05
1.00
0.95
0.90
0.85
0.80
1.95
2.05
2.15
2.25
2.35
Wavelength μm

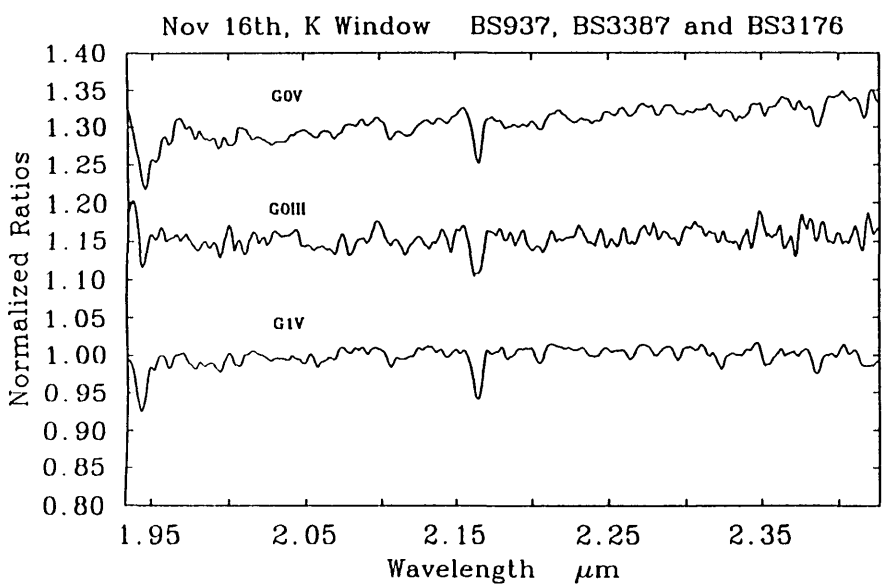
Nov 16th, K Window BS937, BS3387 and BS3176
G0V
G0III
G1V
Normalized Ratios
1.40
1.35
1.30
1.25
1.20
1.15
1.10
1.05
1.00
0.95
0.90
0.85
0.80
1.95
2.05
2.15
2.25
2.35
Wavelength μm

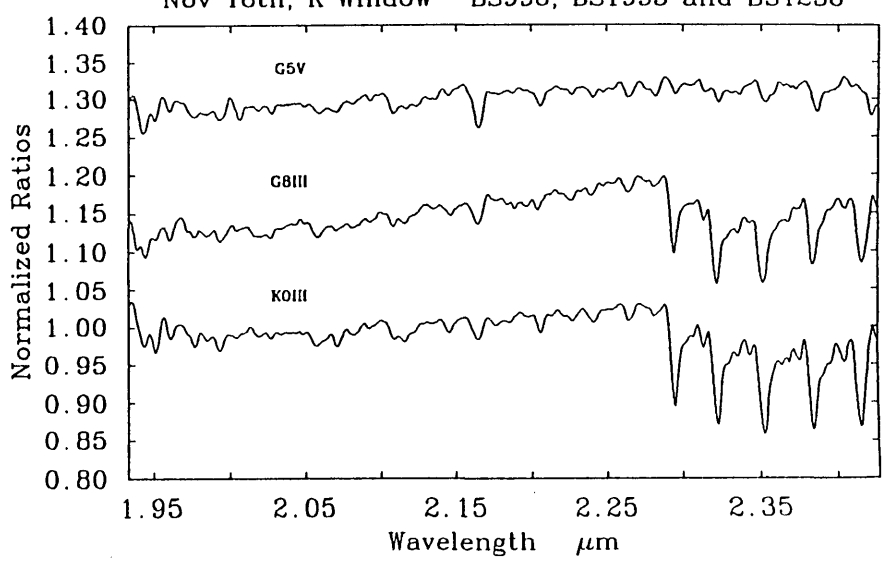
Nov 16th, K Window BS996, BS1995 and BS1256
G5V
G8III
K0III
Normalized Ratios
1.40
1.35
1.30
1.25
1.20
1.15
1.10
1.05
1.00
0.95
0.90
0.85
0.80
1.95
2.05
2.15
2.25
2.35
Wavelength μm

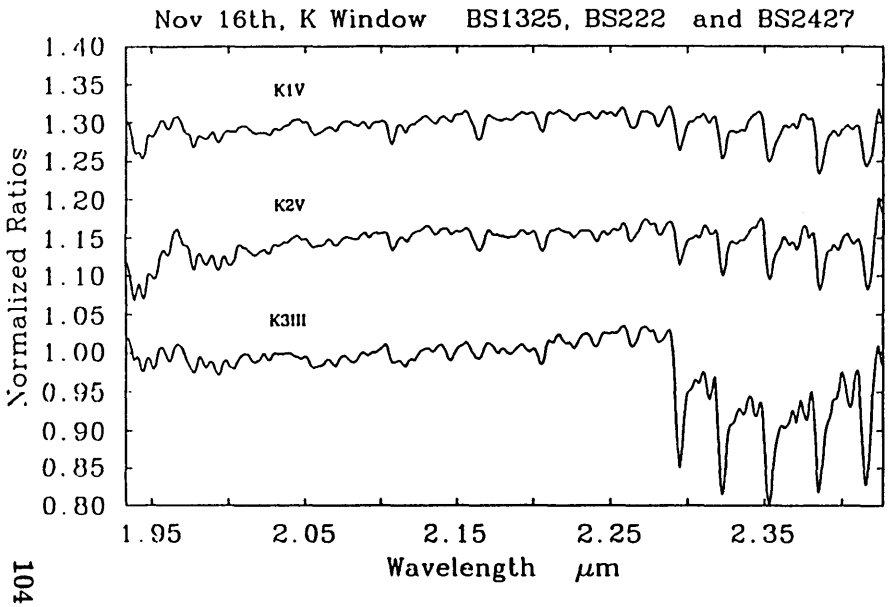
Nov 16th, K Window BS1325, BS222 and BS2427
K1V
K2V
K3III
Normalized Ratios
1.40
1.35
1.30
1.25
1.20
1.15
1.10
1.05
1.00
0.95
0.90
0.85
0.80
1.95
2.05
2.15
2.25
2.35
Wavelength μm

5.3 The Absolute Spectra

On the following 4 pages are presented the 1 μm to 4.1 μm absolute spectra with their flux in units of $Wm^{-2}\mu m^{-1}$. Only the CGS1 data is presented in this form since the CGSII data only covers the K window and there are some problems with the quality of the photometry. The absolute calibration spectra used was that developed by Kurucz, but corrected for the infrared excess found by the direct absolute flux calibration. The spectra are presented in order of spectral type. Only the part of the J window which does not show order overlap has been included. The dominant error in the spectra is caused by the uncertainty in the absolute spectra of Vega.

ABSOLUTE SPECTRA

Taken with CGS1

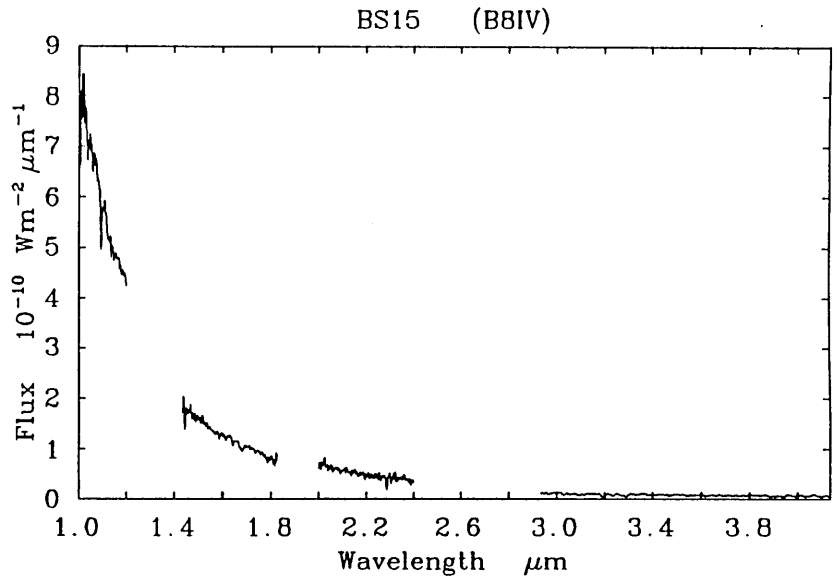

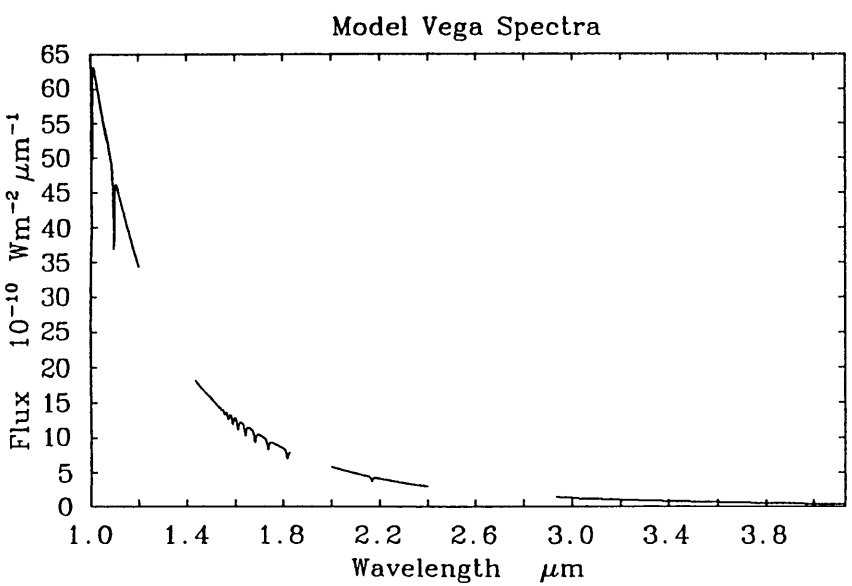

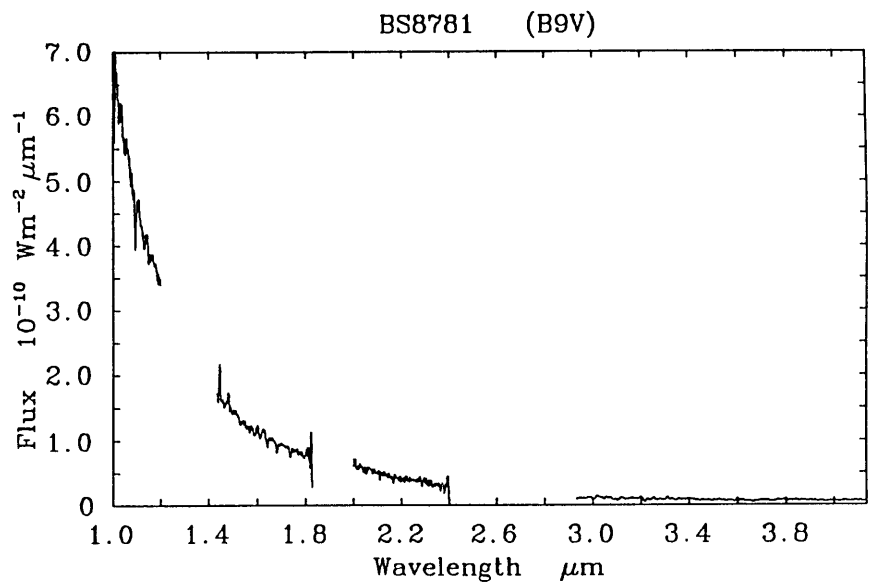

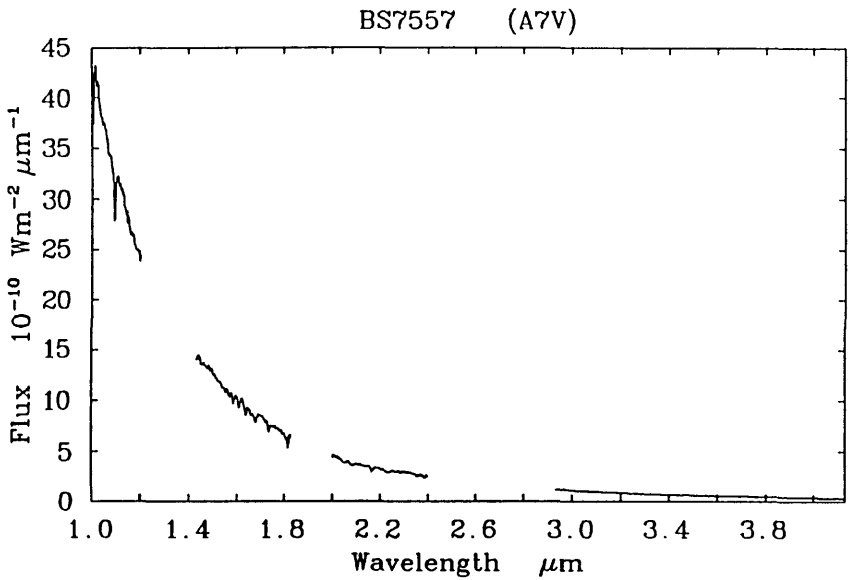
BS7557 (A7V)
Flux 10^{-10} Wm^{-2} μm^{-1}
Wavelength μm

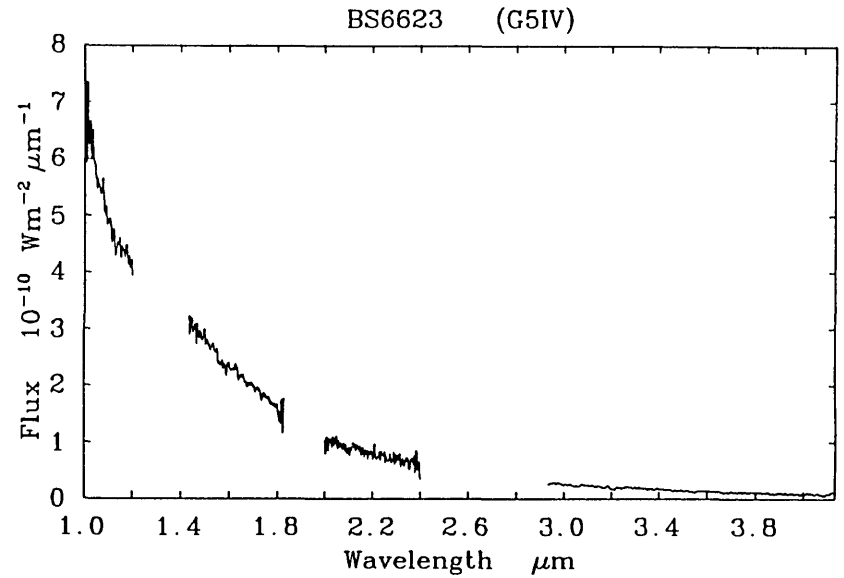
BS6623 (G5IV)
Flux 10^{-10} Wm^{-2} μm^{-1}
Wavelength μm

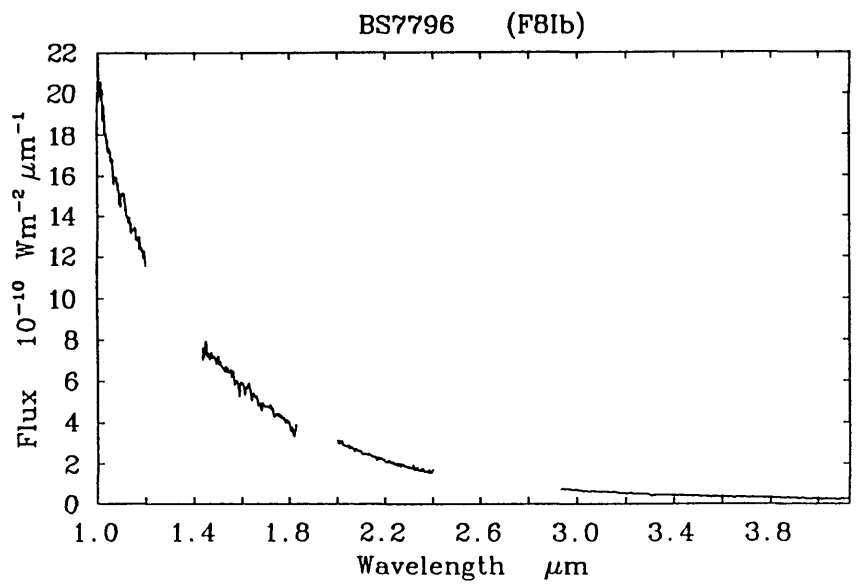
BS7796 (F8Ib)
Flux 10^{-10} Wm^{-2} μm^{-1}
Wavelength μm

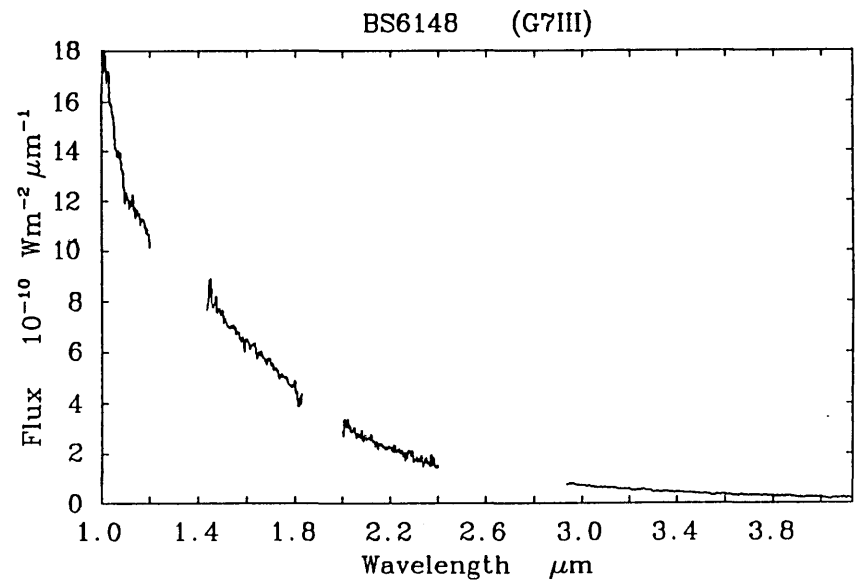
BS6148 (G7III)
Flux 10^{-10} Wm^{-2} μm^{-1}
Wavelength μm

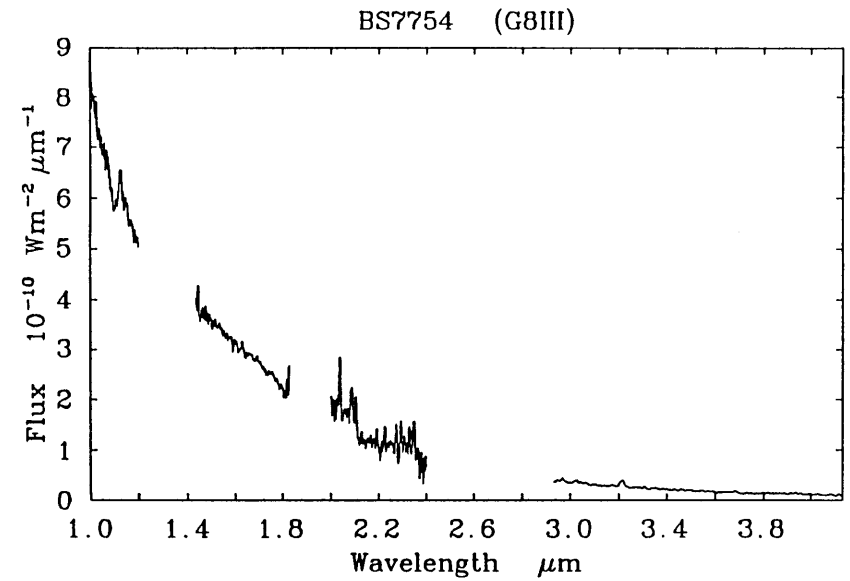
BS7754 (G8III)
Flux 10^{-10} Wm^{-2} μm^{-1}
Wavelength μm

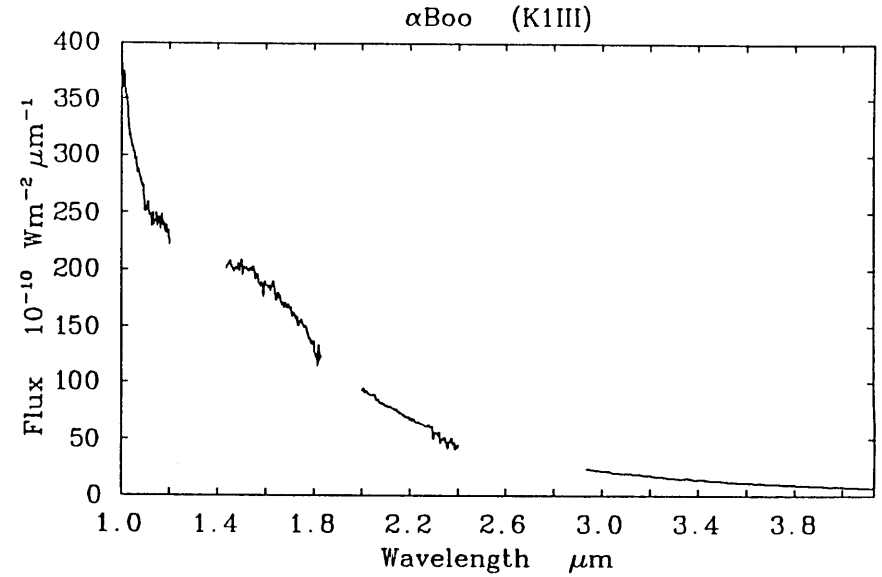
αBoo (K1III)
Flux 10^{-10} Wm^{-2} μm^{-1}
Wavelength μm

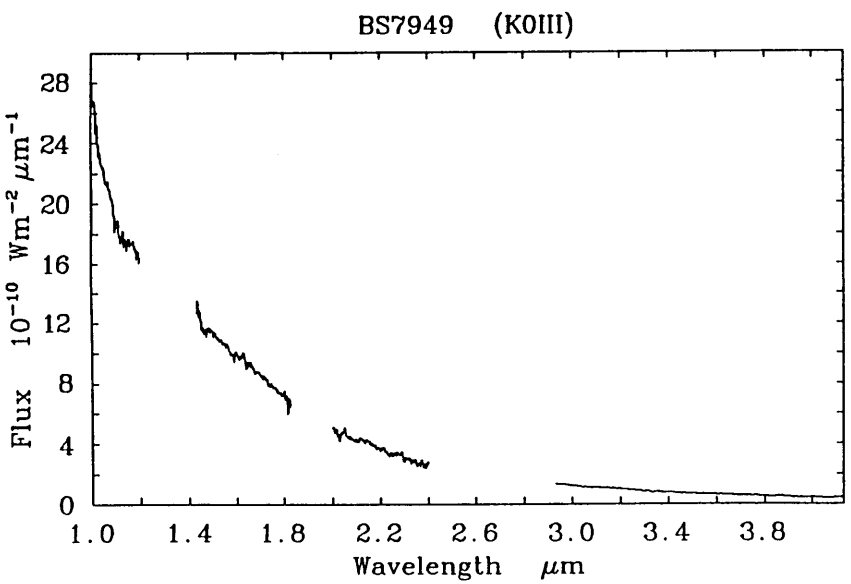
BS7949 (K0III)
Flux 10^{-10} Wm^{-2} μm^{-1}
Wavelength μm

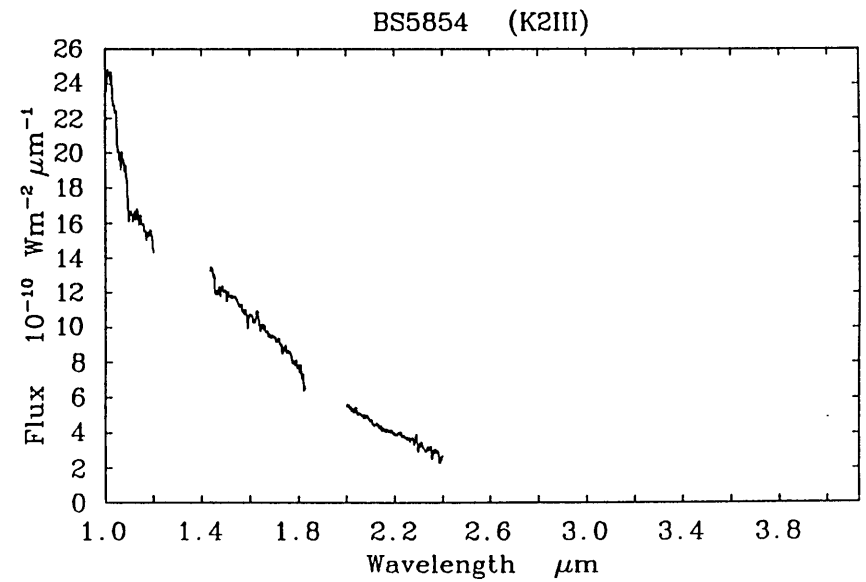
BS5854 (K2III)
Flux 10^{-10} Wm^{-2} μm^{-1}
Wavelength μm

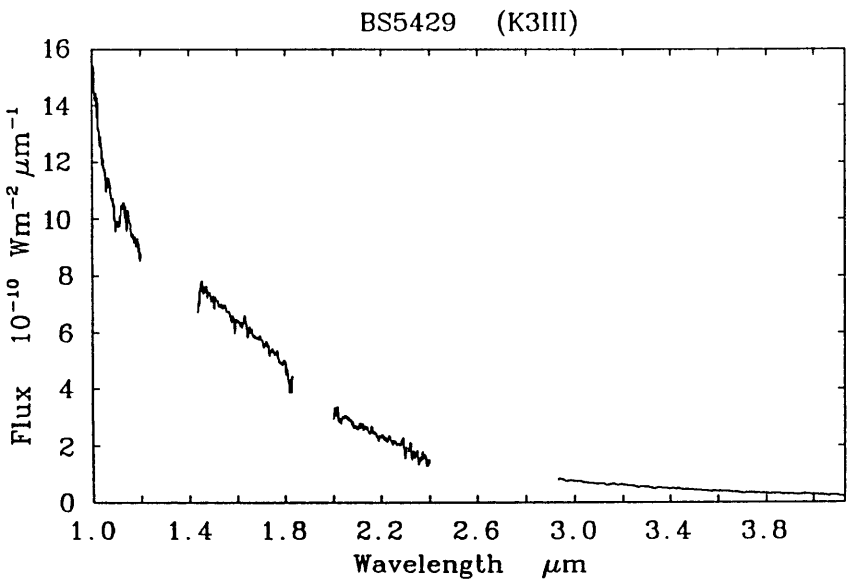
BS5429 (K3III)
Flux 10^{-10} Wm^{-2} μm^{-1}
Wavelength μm

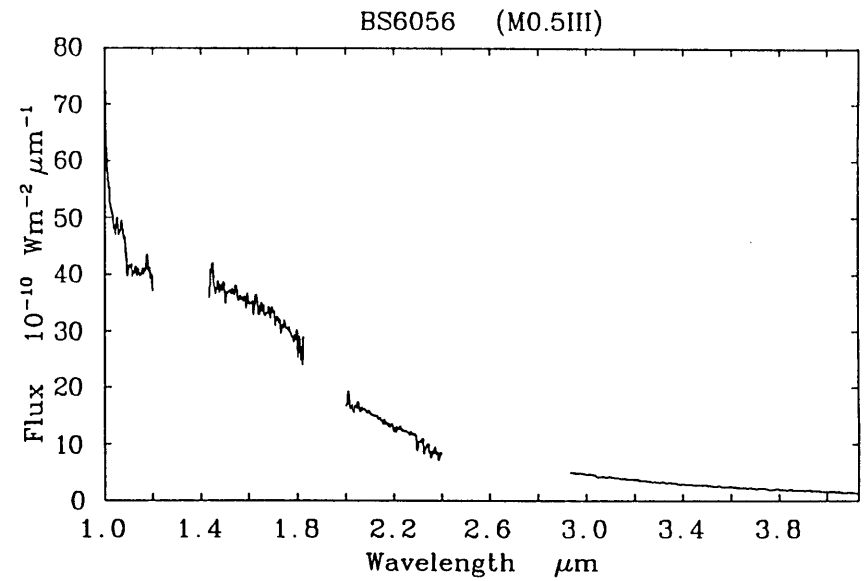
BS6056 (M0.5III)
Flux 10^{-10} Wm^{-2} μm^{-1}
Wavelength μm

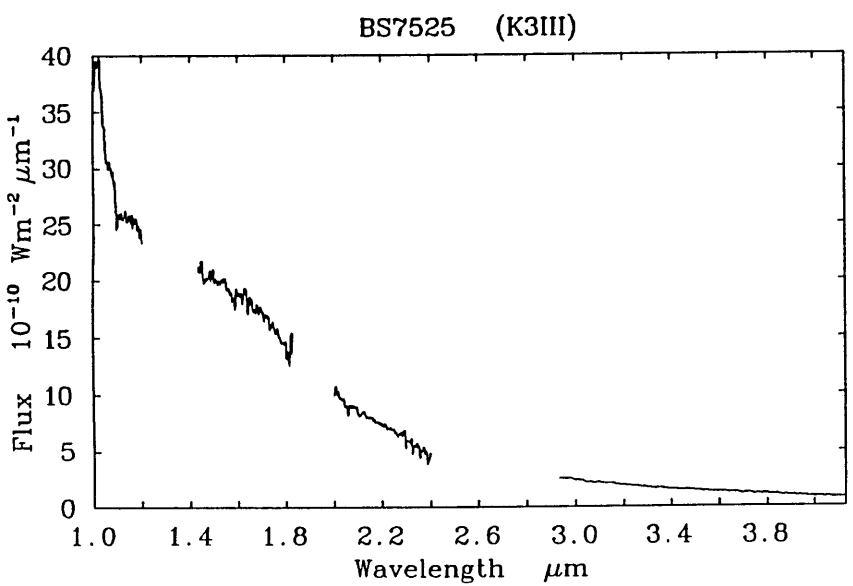
BS7525 (K3III)
Flux 10^{-10} Wm^{-2} μm^{-1}
Wavelength μm

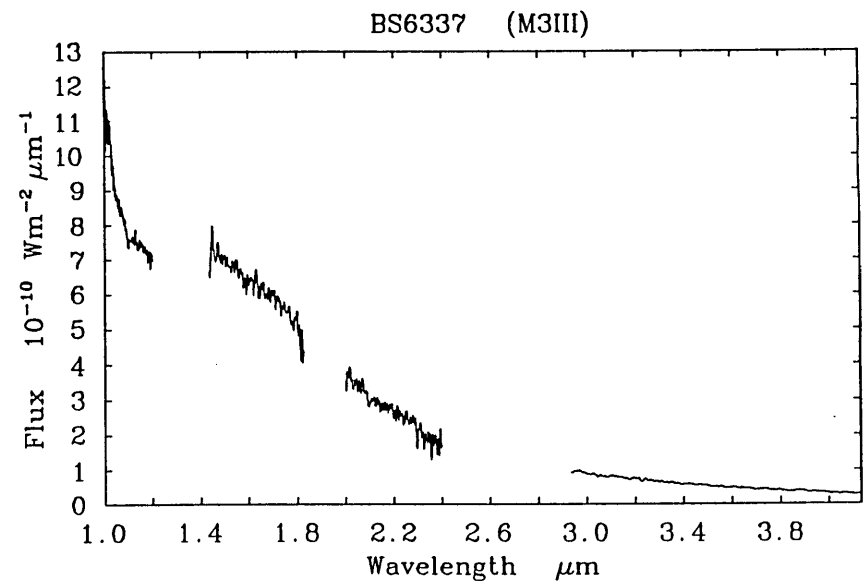
BS6337 (M3III)
Flux 10^{-10} Wm^{-2} μm^{-1}
Wavelength μm

5.4 The Spectral Lines

As expected, the hydrogen lines dominate the spectra of the hot stars whereas the cooler ones show the neutral metal lines and strong CO lines at 2.3 microns. (Appendix A lists all of the lines that have been identified). However, by using a resolution of only about 500 many lines become blended, particularly in the H window, and it then becomes impossible to assign a feature to a particular atom or molecule.

The better S/N of the CGSII spectra means that it is preferable to use this data set when measuring the strength of lines. The strength of three lines has been measured: Brackett γ at 2.166 μm, the Na doublet at 2.2062 μm and the CO band head at 2.293μm. Generally the B γ and the Na doublet are not blended with other lines so it is possible to measure their equivalent widths. This is the ratio of the area of the absorption line to the estimated continuum level at that wavelength. It is independent of both spectral resolution and flux so can be used to compare results taken with different instruments. The CO band head is blended with other CO lines so this technique could not be used. Instead, the relative depth of the line has been measured. It is difficult to estimate the accuracy of the results but, in general, they are better than 10%. The line strengths are listed in table 5.1 and shown in figures 5.4 to 5.6.

The relative strength of the hydrogen and sodium are independent of luminosity class. However, the giants have considerably stronger CO features than the dwarfs of the same spectral type.

5.5 The 3.4μm to 4μm Excess in the B Stars

Most normal stars are well on the Rayleigh-Jeans part of their flux curves by 3 μm so the ratios with Vega are approximately flat. However, this is not the case for the three B stars that were measured. As can be seen in figures 5.7 and 5.8 all three stars show a similar excess over Vega, which is considerably larger than that shown by Arcturus, a K1III star. This excess approximates to a black body at a temperature of about 500K a few hundred times larger than the star.

Table 5.1: Line Strengths

Name	Type	B γ ($10^{-4}\mu$m)	Na ($10^{-5}\mu$m)	CO (Relative %)
BS3705	K7III	0	17	23.6
BS2427	K3III	1	11.5	16.2
BS222	K2V	1.6	14	5.1
BS1325	K1V	2.1	12.5	5.3
BS1256	K0III	1.6	11	12.4
BS1995	G8III	2.8	9.4	9.3
BS996	G5V	3.4	12	2.2
BS2643	G4V	4.8	9.4	1.0
BS1729	G2IV	4.2	9	1.3
BS3176	G1V	4.4	11	1.5
BS3387	G0III	4.5		2.1
BS937	G0V	3.8	8	1.3
BS1101	F9V	4.4	8	0.9
BS458	F8V	4.9	8	0.6
BS3262	F6V	5.9	7	0
BS2930	F3III	6.1	6	0
BS1676	F2IV	7.1	4	0
BS2386	F0V	9.2	0	0
BS3284	A9V	9.1	0	0
BS1380	A7V	11	0	0
BS1937	A4V	10.2	0	0
BS2857	A4V	10.5	0	0
BS3314	A0V	11	0	0
BS3982	B7V	9.5	0	0
BS1617	B3V	7	0	0

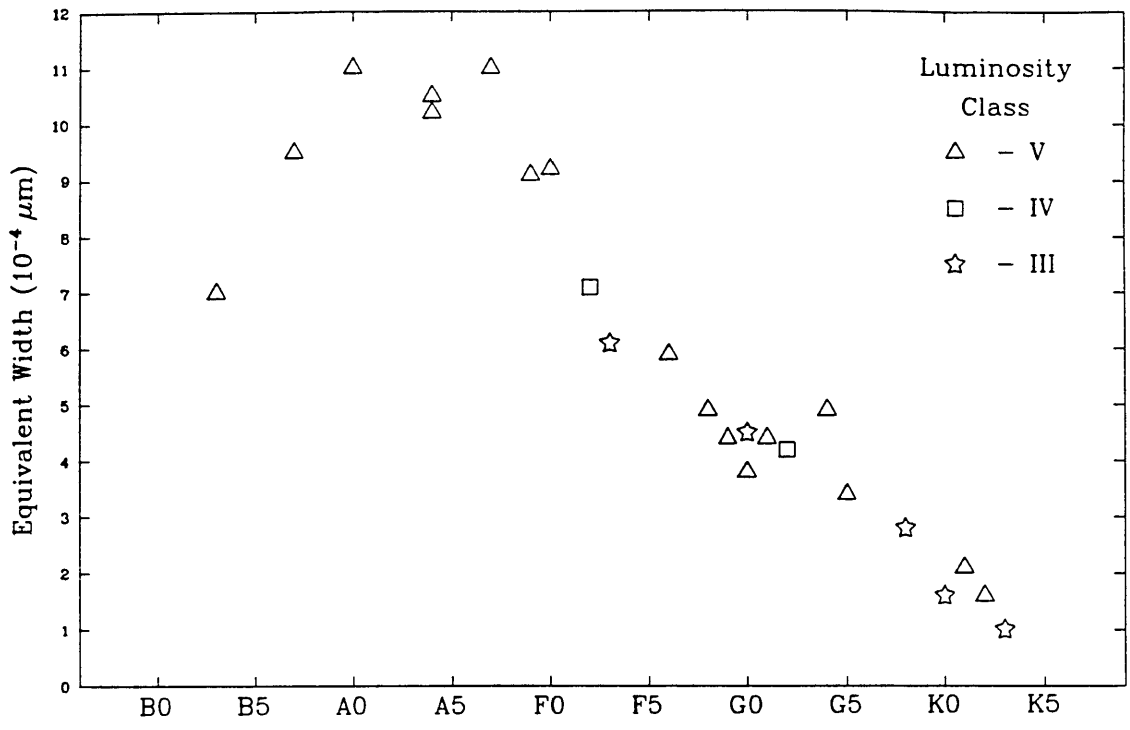

Figure 5.4: Equivalent Width of Brackett Gamma.

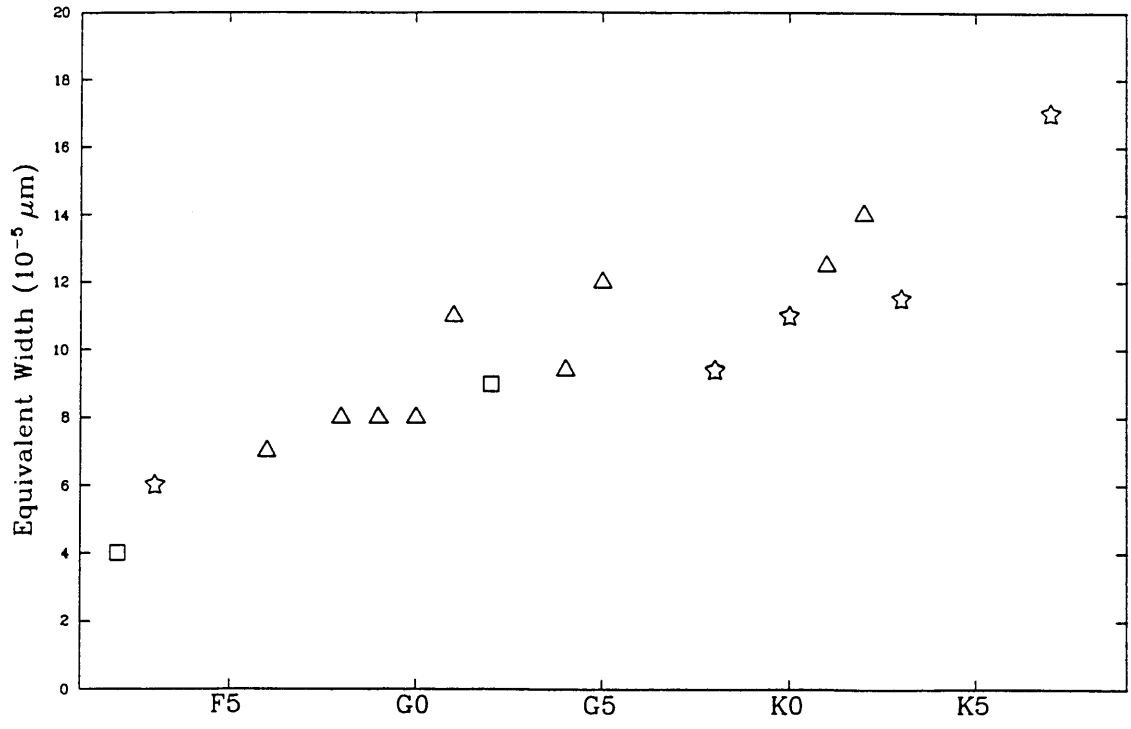

Figure 5.5: Equivalent Width of the Na Doublet.

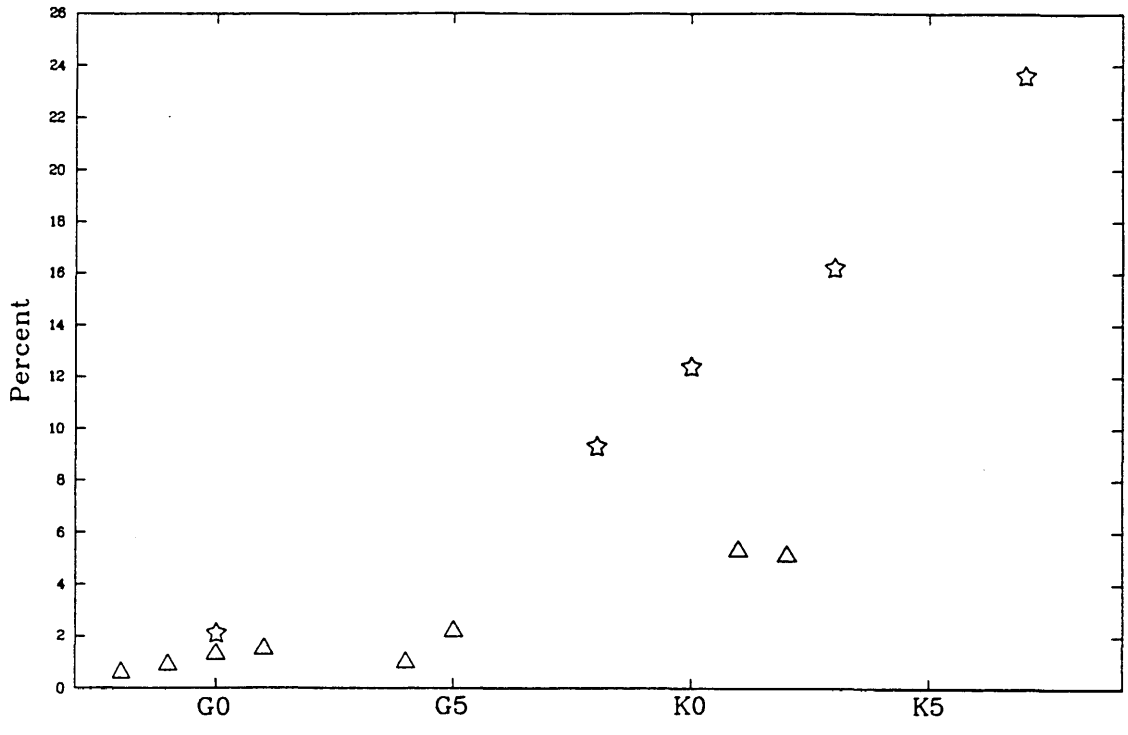

Figure 5.6: Relative Strength of the CO Band Head.

IRAS showed that a number of early type stars had an infrared excess which was linked to the presence of a circumstellar dust cloud. However, this usually required the stars to be rapidly rotating and the 3 B stars in this sample are not. If it is not due to dust then it will have to be an effect in the photosphere. It is necessary to extend the measurements into the M window to give a better indication as to the source of the excess.

At present there must be some doubt as to the validity of this result, as there is the possibility that it is an instrumental or atmospheric effect, since the S/N for each point is low. However, other stars taken on the same night at a similar S/N do not show an excess; also I have done a number of tests on the data at various stages in the reduction, all of which indicate the excess is real. There is some supporting evidence for the excess from narrow band photometry taken for use with the IRFM (Selby et at 1987). The L filter is centred on about 3.6 μm and it is noticeable that when the IRFM is applied to the early type stars, their temperatures are lower in the L window than in the K. It is important that more spectra of early type stars are taken between 3 and 5 microns to confirm this result.

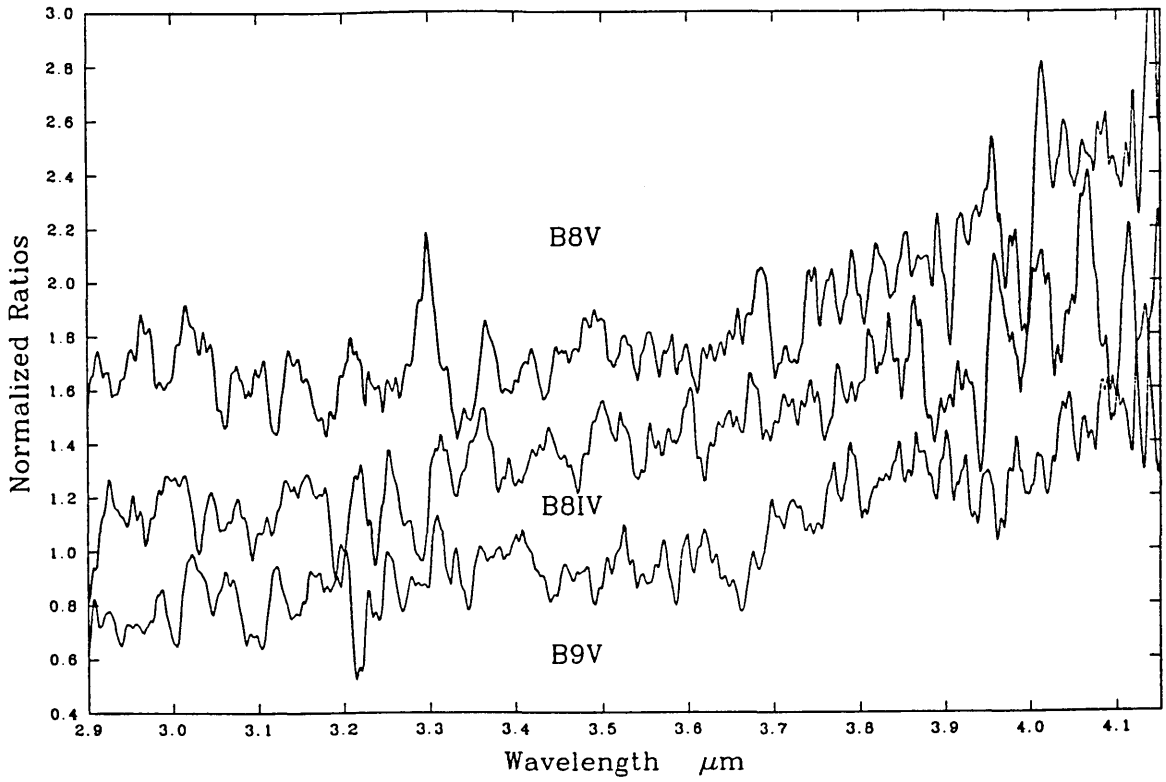

Figure 5.7: Ratio of the 3 B Stars with Vega

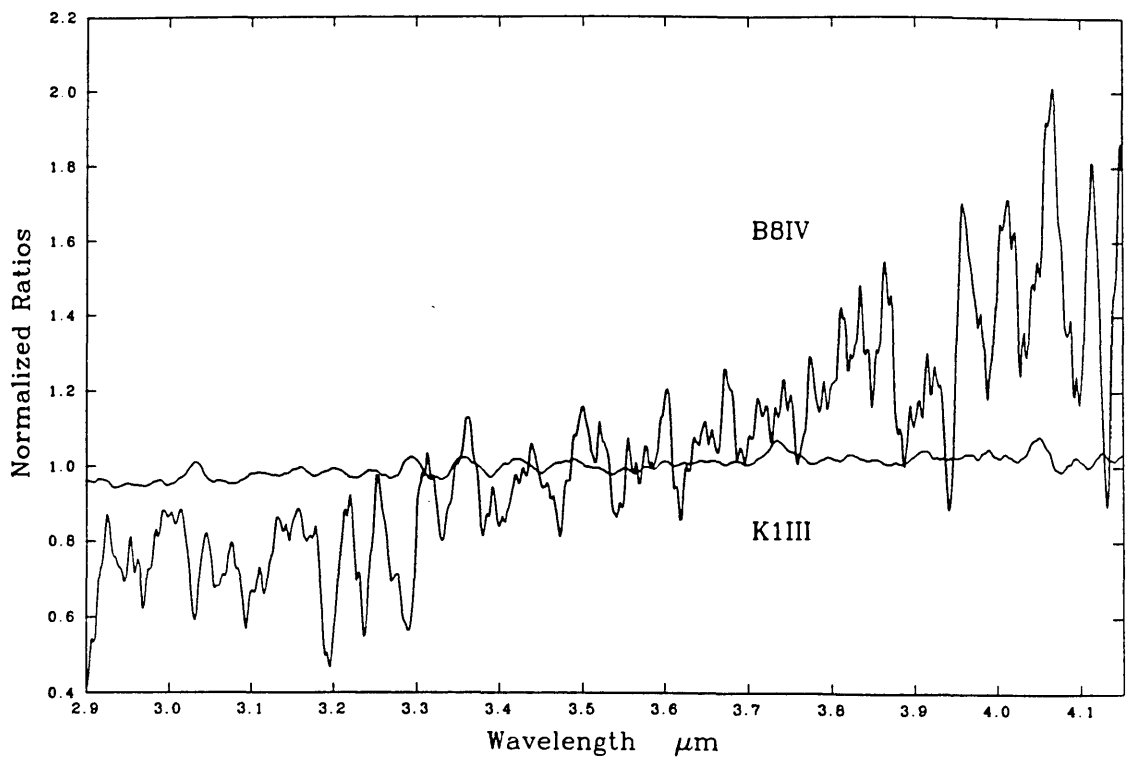

Figure 5.8: Comparison of the ratios of αBoo and BS15 to Vega.

5.6 The Effect of Line Blocking on Photometry

As described in chapter 1 the IRFM relies on the continuum flux being measured but line blocking reduces the observed flux. Figures 5.9 and 5.10 show the K and L filters' profiles used for the measurement of the 180 stars observed with the 4 channel (Selby et al 1987) superimposed on the spectrum of αBoo. Both filters include hydrogen lines for the hotter stars, Bγ in the K window and Pfδ in the L. There are no strong blocking features in the L filter for the cool stars although there are a number of neutral metal lines in the K filter.

Star	Percentage of Continuum Flux Measured	
	K	L
A0V	99.5	99.5
F0V	99.5	99.5
G0V	99.5	99.7
K0V	99	99.8
K7III	98	

(Error about 0.2%)

Therefore, the blocking features make a small but measurable effect when the IRFM is applied to previous photometry.

5.7 The Application of the IRFM

5.7.1 The Absolute Vega Calibration

The decision whether to use the model or direct absolute flux calibration for Vega, when applying the IRFM, is based solely on which is likely to give a more constant temperature and angular diameter with wavelength. Figure 5.11 shows the IRFM applied to αBoo after being calibrated by the direct measurements of Vega and the model fluxes of

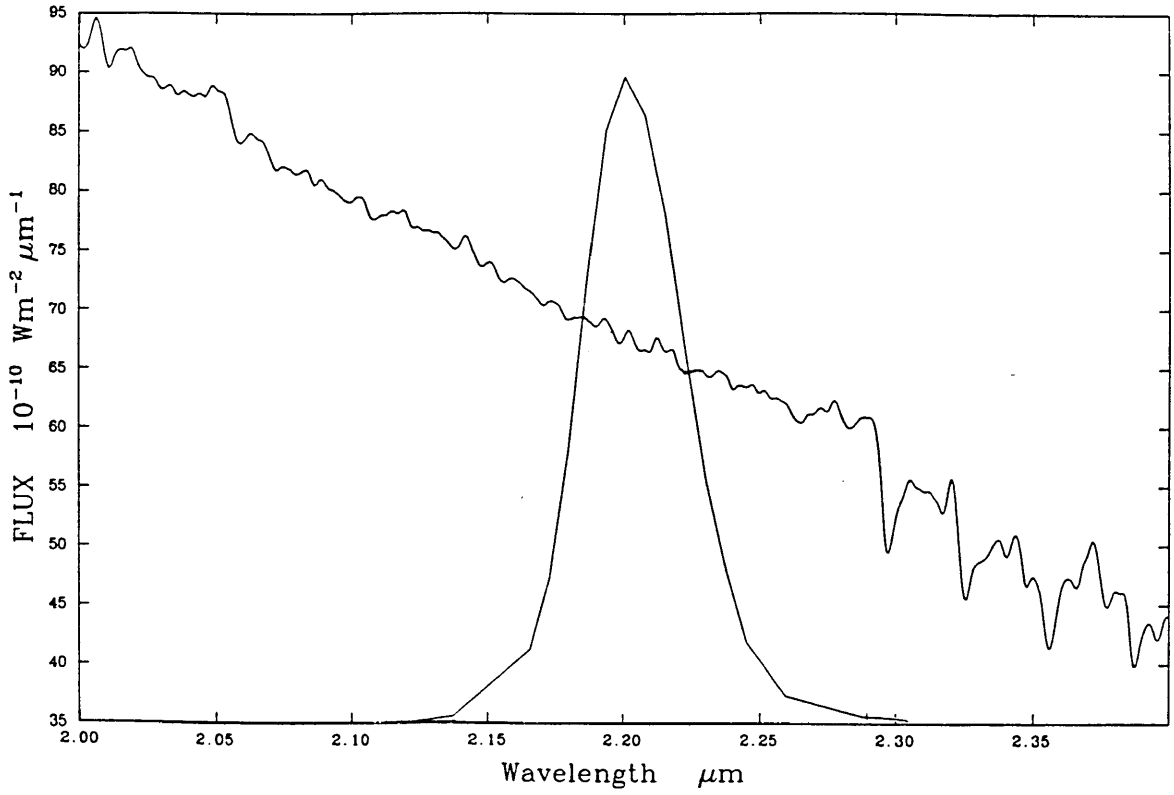

Figure 5.9: K Filter

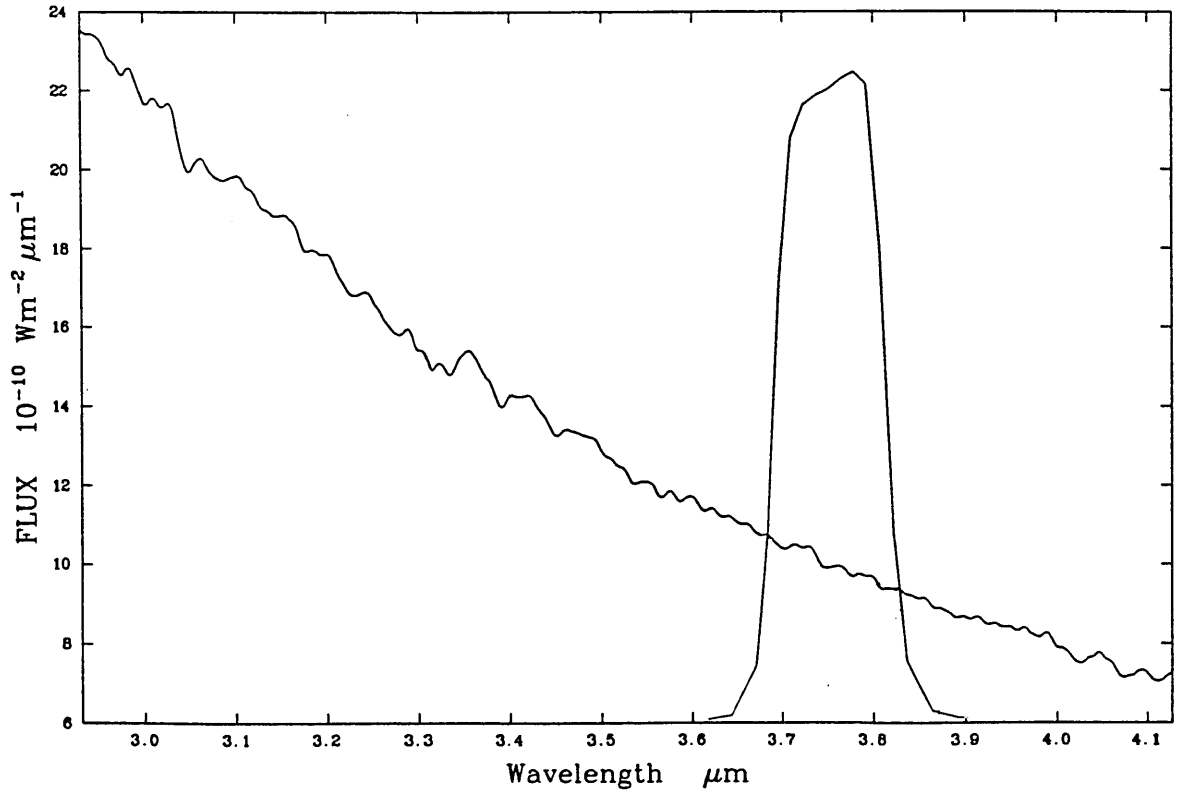

Figure 5.10: L Filter

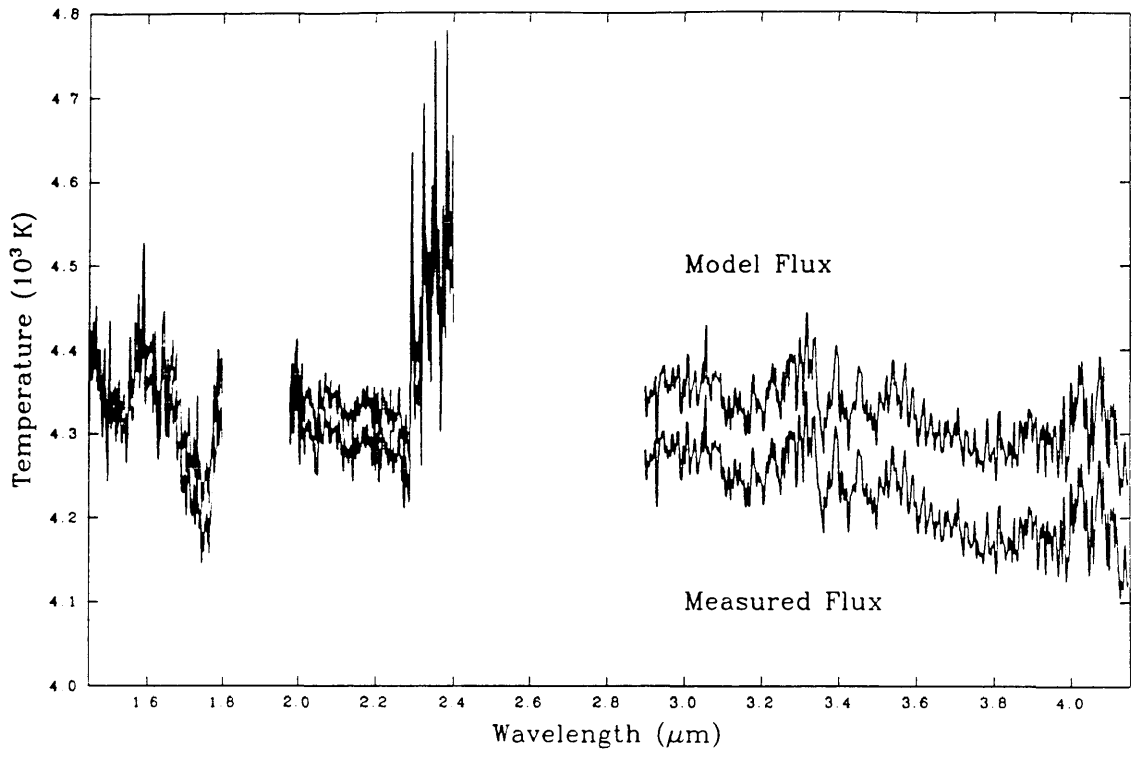

Figure 5.11: The Difference that the Absolute Vega Calibration Makes to the IRFM

Dreiling and Bell. The temperatures calculated using the Dreiling and Bell model were found to be less dependent on wavelength, so these fluxes have been adopted. However, I must stress that by using the model fluxes it does not necessarily mean that they are more accurate, it only means that the models are consistent with each other (see section 5.8).

5.7.2 The Model Atmospheres

The MARCS code has been used to calculate the model infrared fluxes for effective temperatures of 3500K to 6000K at $\log g$ of 2 and 4500K to 5500K at a $\log g$ of 4 and assuming a solar metal abundance (figure 5.12). The limits are defined by the class of stars on which the IRFM is to be applied in this case. It is important that only continuum model fluxes are used with the IRFM; so four to five wavelengths in each atmospheric window are chosen, such that they miss all of the major blocking features. The ratio of total flux to monochromatic flux is calculated at every wavelength for every model atmosphere to produce the table described in section 1.4.4.

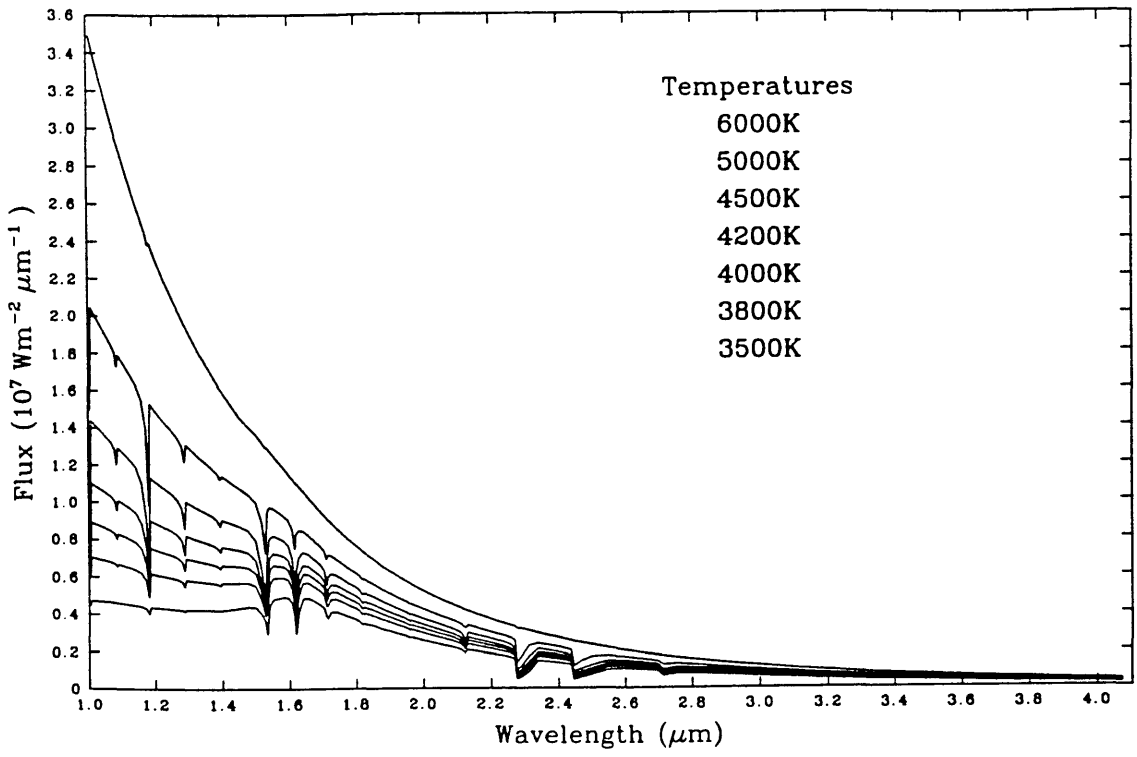

Figure 5.12: The MARCS Code Models for $\log g = 2$

5.7.3 The Total Fluxes

Difficulty in finding accurate total fluxes has limited the application of the IRFM to 9 stars. The total fluxes used have been taken from Blackwell et al (Submitted) and are listed in table 5.2.

5.7.4 The Calculation of T_e and θ

The IRFM has been applied to the spectra using the second method described in chapter 1. Laplace interpolations were used to calculate the intermediate positions on the table of $\log g$, $\log T_e$, $\log \lambda$, and $\log R$. The IRFM has only been applied between 1.4μm and 4.1 μm because, for the majority of the stars in the sample, their fluxes are off the Rayleigh-Jeans curve shortwards of this, making the method less accurate.

Table 5.2: Total Fluxes.

Star	Type	Flux (Wm^{-2})
BS5340	K1III	4.921×10^{-8}
BS5429	K3III	1.665×10^{-9}
BS5854	K2III	3.324×10^{-9}
BS6056	M0.5III	7.124×10^{-9}
BS6148	G7III	2.392×10^{-9}
BS6337	M3III	1.262×10^{-9}
BS6623	G5IV	1.176×10^{-9}
BS7525	K3III	4.524×10^{-9}
BS7754	G8IIIb	1.177×10^{-9}

5.7.5 The Calculated Values of T_e and θ

The spectra of T_e and θ verses wavelength are presented on the next nine pages. The mean values of T_e and θ are listed in table 5.3.

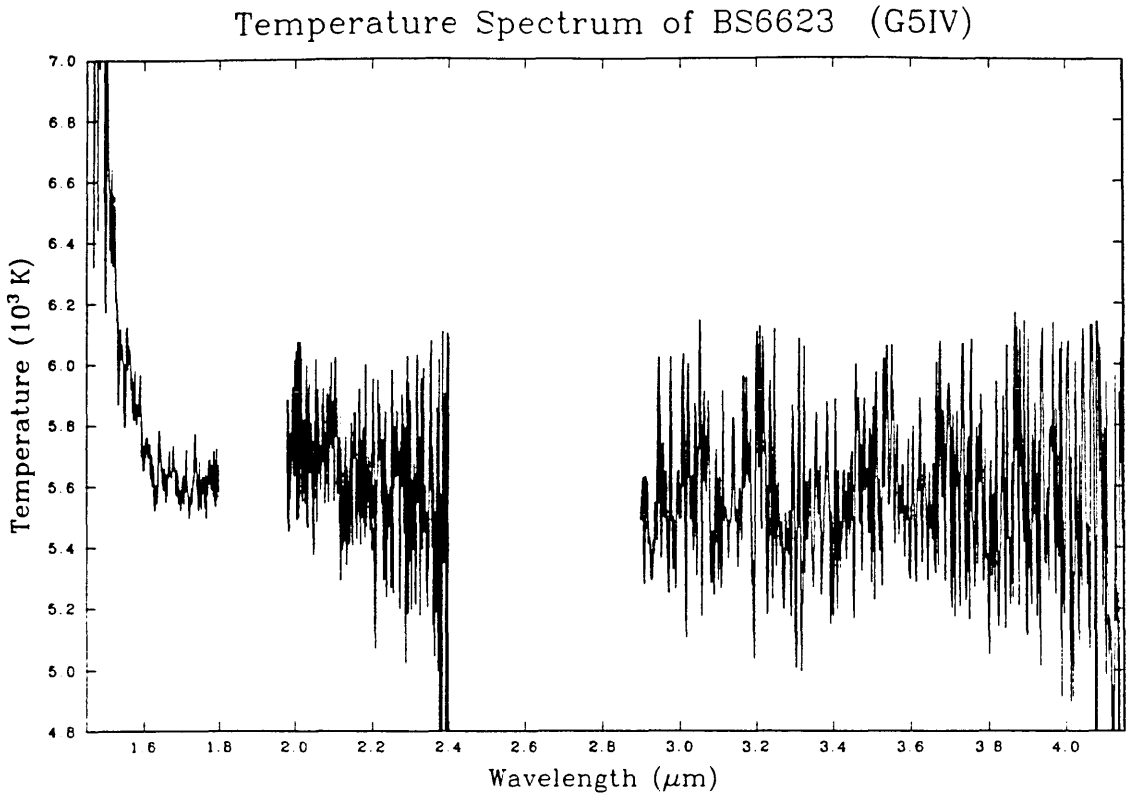
Temperature Spectrum of BS6623 (G5IV)
Temperature (10^3 K)
7.0
6.8
6.6
6.4
6.2
6.0
5.8
5.6
5.4
5.2
5.0
4.8
1.6
1.8
2.0
2.2
2.4
2.6
2.8
3.0
3.2
3.4
3.6
3.8
4.0
Wavelength (μm)

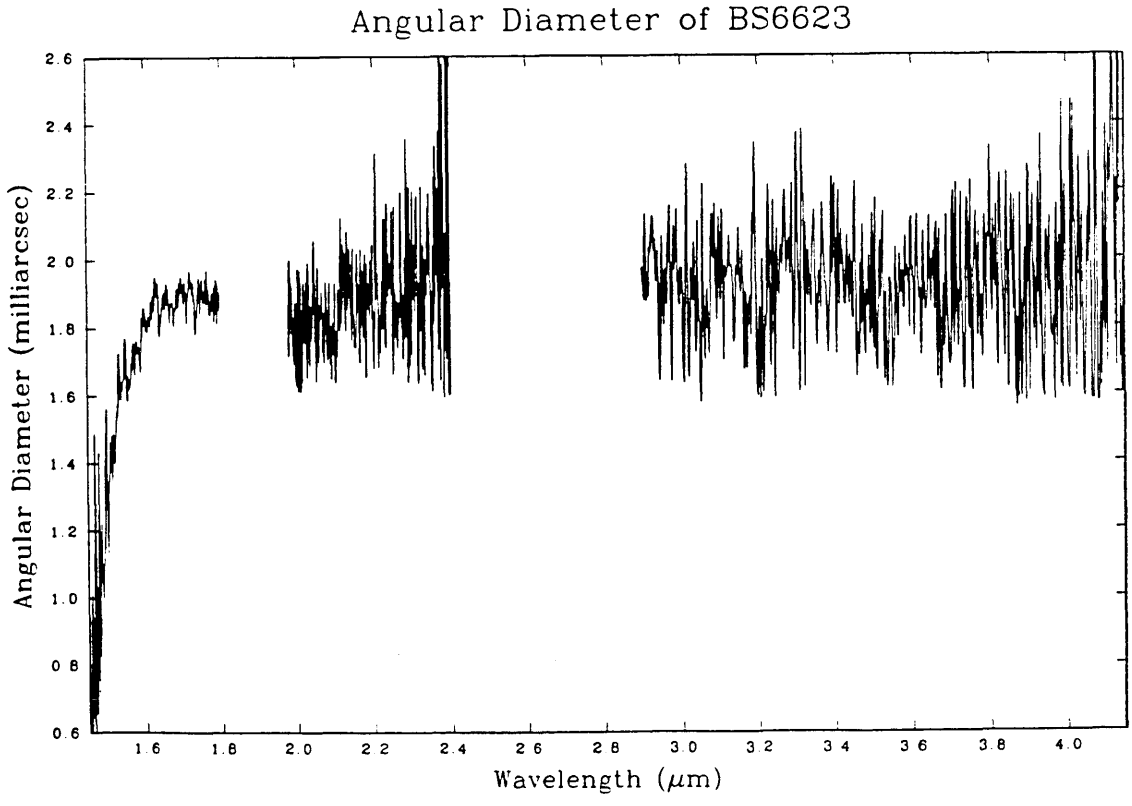
Angular Diameter of BS6623
Angular Diameter (milliarcsec)
2.6
2.4
2.2
2.0
1.8
1.6
1.4
1.2
1.0
0.8
0.6
1.6
1.8
2.0
2.2
2.4
2.6
2.8
3.0
3.2
3.4
3.6
3.8
4.0
Wavelength (μm)

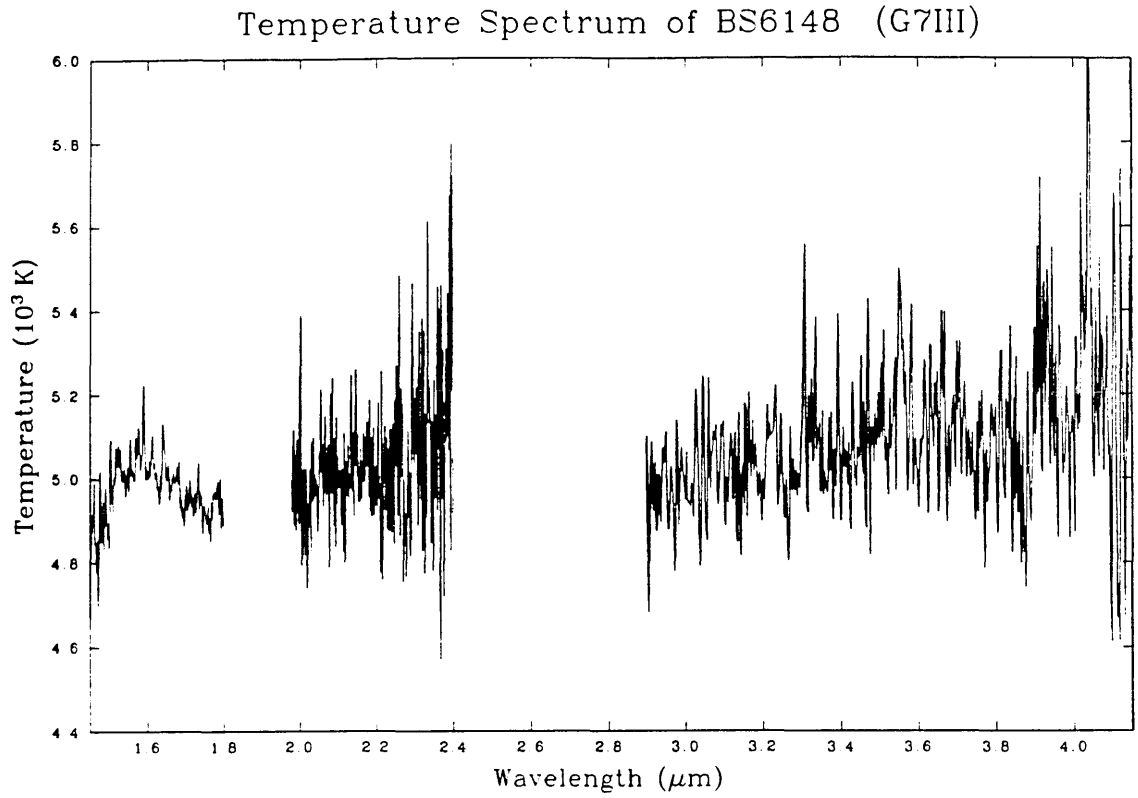
Temperature Spectrum of BS6148 (G7III)
Temperature (10^3 K)
6.0
5.8
5.6
5.4
5.2
5.0
4.8
4.6
4.4
1.6
1.8
2.0
2.2
2.4
2.6
2.8
3.0
3.2
3.4
3.6
3.8
4.0
Wavelength (μm)

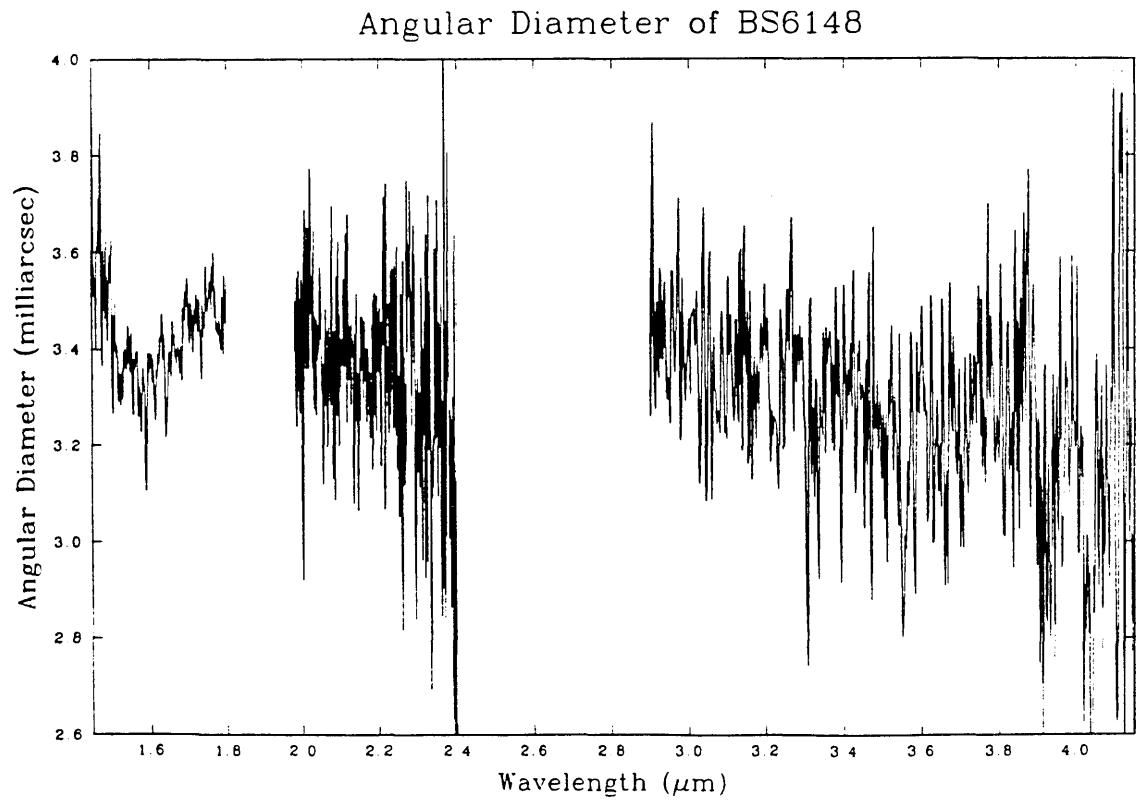
Angular Diameter of BS6148
Angular Diameter (milliarcsec)
4.0
3.8
3.6
3.4
3.2
3.0
2.8
2.6
1.6
1.8
2.0
2.2
2.4
2.6
2.8
3.0
3.2
3.4
3.6
3.8
4.0
Wavelength (μm)

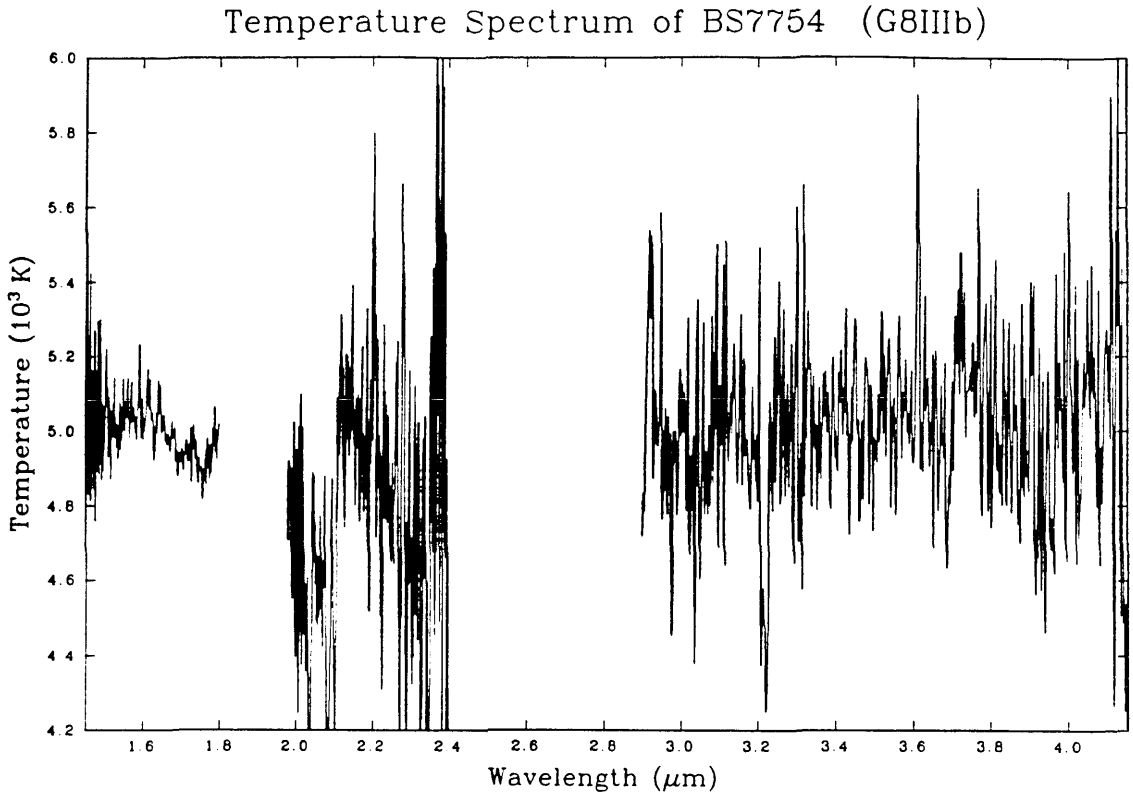
Temperature Spectrum of BS7754 (G8IIIb)
Temperature (10^3 K)
6.0
5.8
5.6
5.4
5.2
5.0
4.8
4.6
4.4
4.2
1.6
1.8
2.0
2.2
2.4
2.6
2.8
3.0
3.2
3.4
3.6
3.8
4.0
Wavelength (μm)

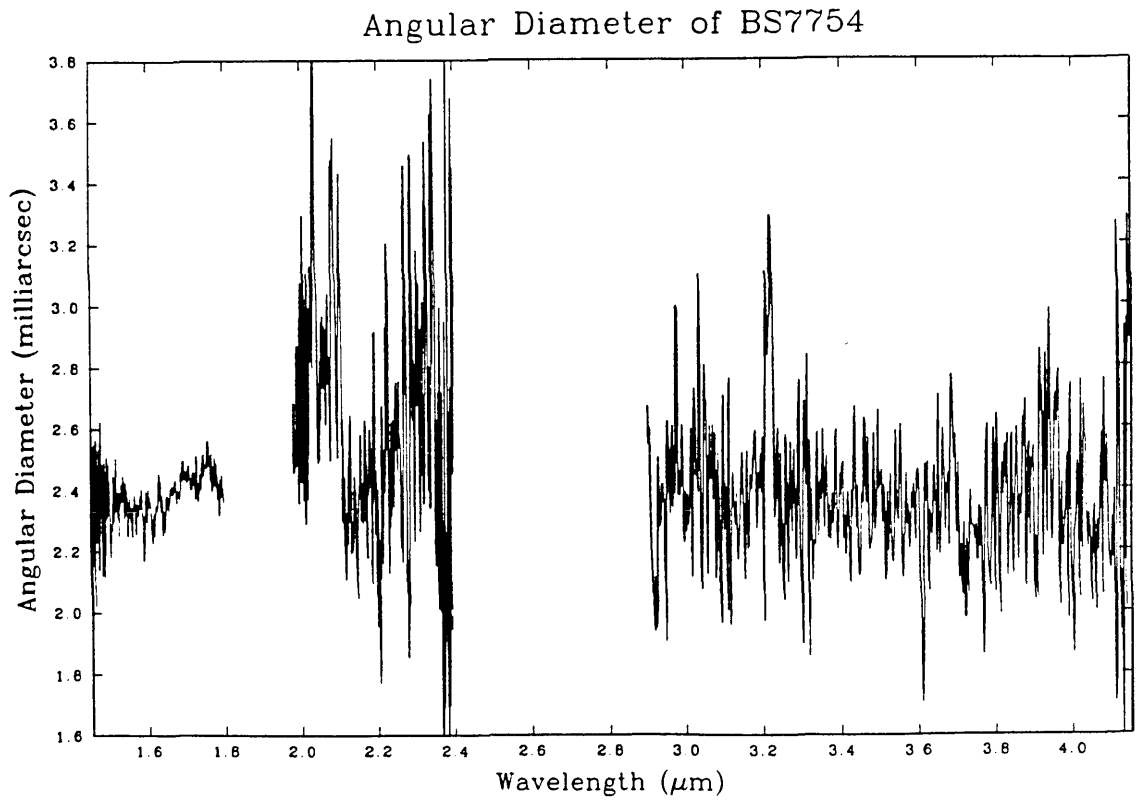
Angular Diameter of BS7754
Angular Diameter (milliarcsec)
3.8
3.6
3.4
3.2
3.0
2.8
2.6
2.4
2.2
2.0
1.8
1.6
1.6
1.8
2.0
2.2
2.4
2.6
2.8
3.0
3.2
3.4
3.6
3.8
4.0
Wavelength (μm)

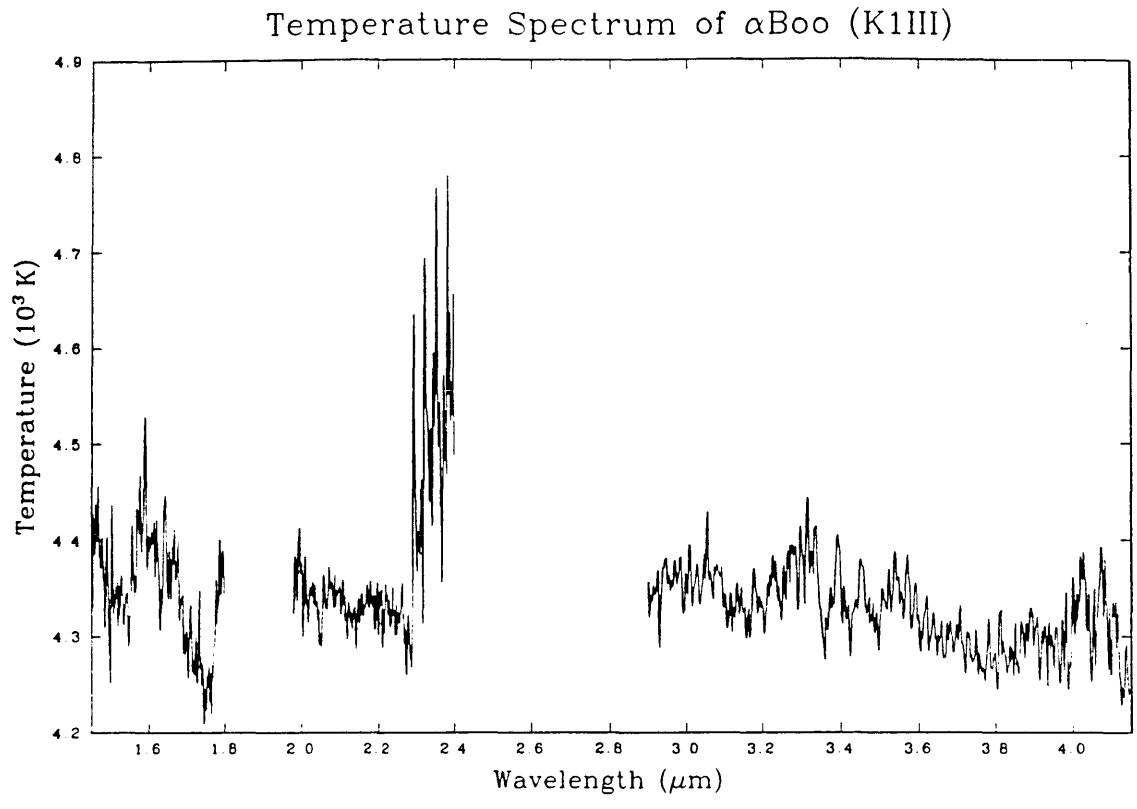
Temperature Spectrum of αBoo (K1III)
Temperature (10^3 K)
4.9
4.8
4.7
4.6
4.5
4.4
4.3
4.2
1.6
1.8
2.0
2.2
2.4
2.6
2.8
3.0
3.2
3.4
3.6
3.8
4.0
Wavelength (μm)

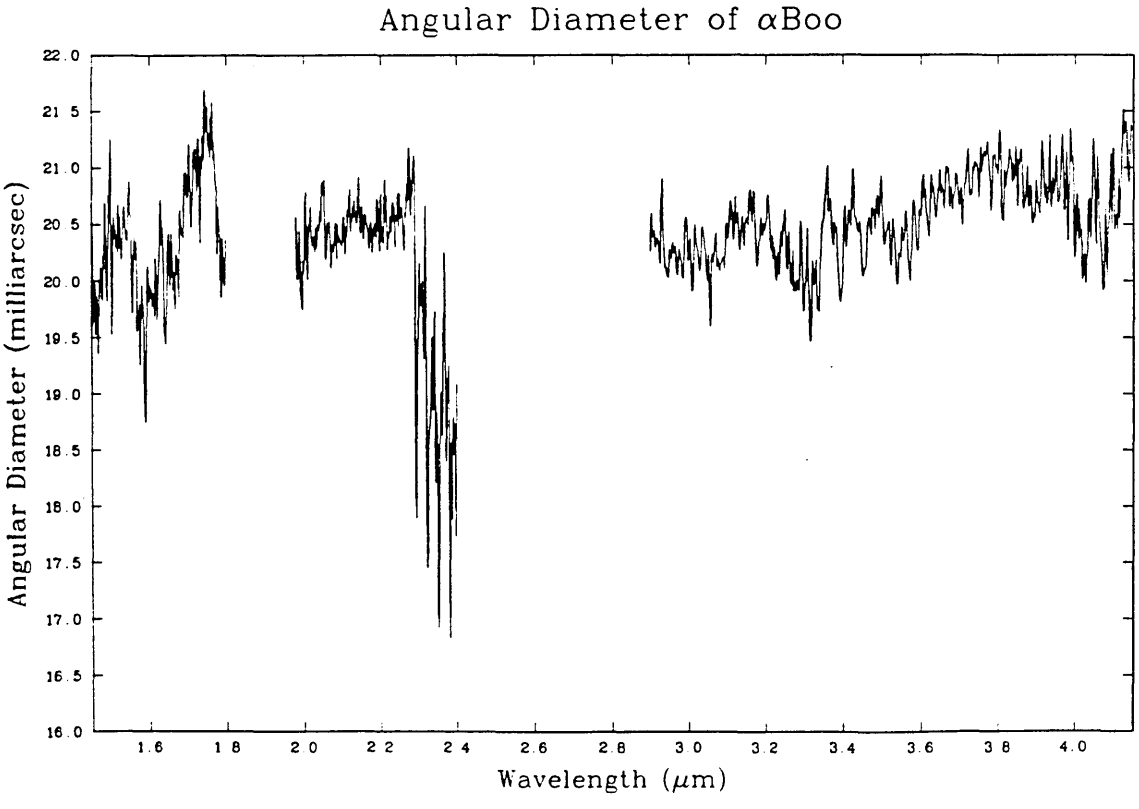
Angular Diameter of αBoo
Angular Diameter (milliarcsec)
22.0
21.5
21.0
20.5
20.0
19.5
19.0
18.5
18.0
17.5
17.0
16.5
16.0
1.6
1.8
2.0
2.2
2.4
2.6
2.8
3.0
3.2
3.4
3.6
3.8
4.0
Wavelength (μm)

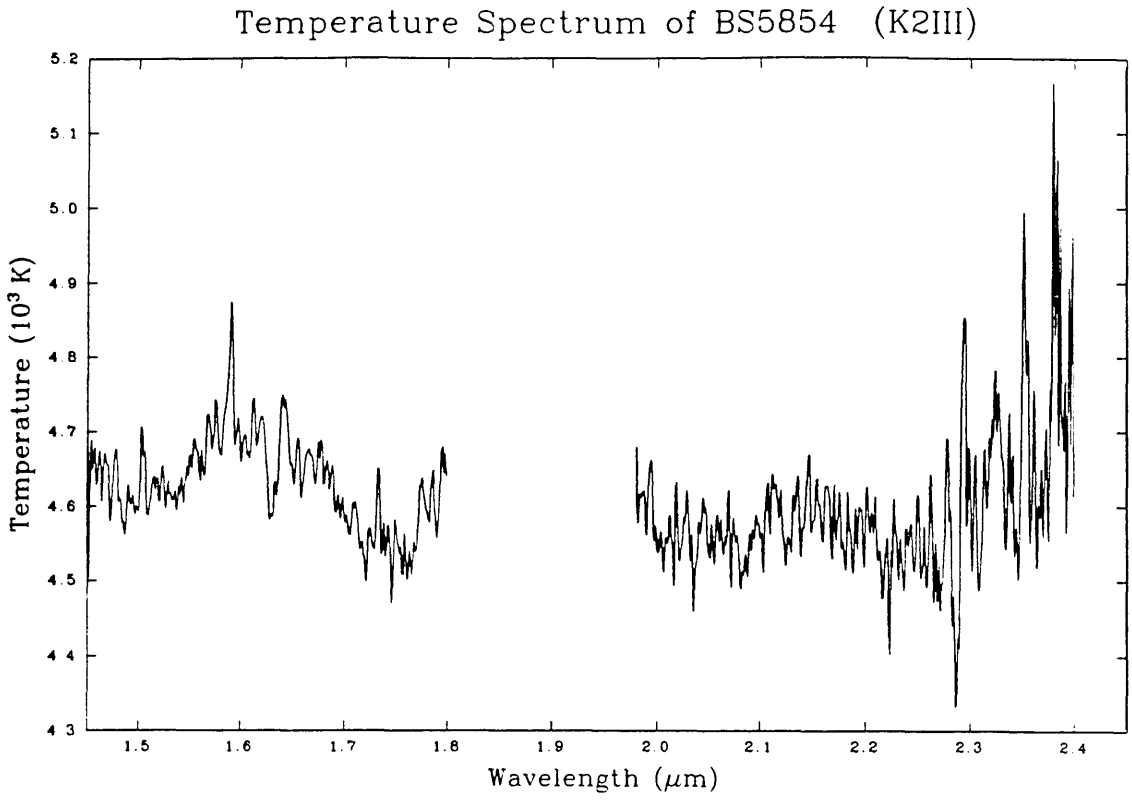
Temperature Spectrum of BS5854 (K2III)
Temperature (10^3 K)
5.2
5.1
5.0
4.9
4.8
4.7
4.6
4.5
4.4
4.3
1.5
1.6
1.7
1.8
1.9
2.0
2.1
2.2
2.3
2.4
Wavelength (μm)

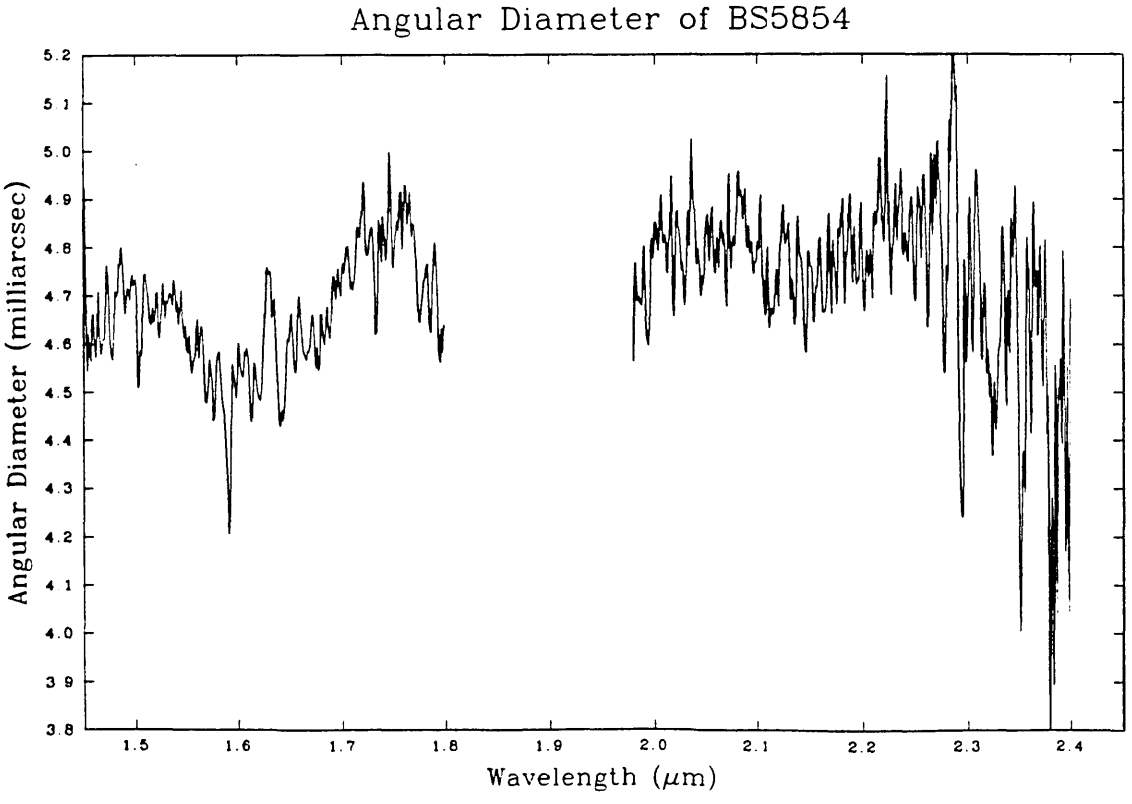
Angular Diameter of BS5854
Angular Diameter (milliarcsec)
5.2
5.1
5.0
4.9
4.8
4.7
4.6
4.5
4.4
4.3
4.2
4.1
4.0
3.9
3.8
1.5
1.6
1.7
1.8
1.9
2.0
2.1
2.2
2.3
2.4
Wavelength (μm)

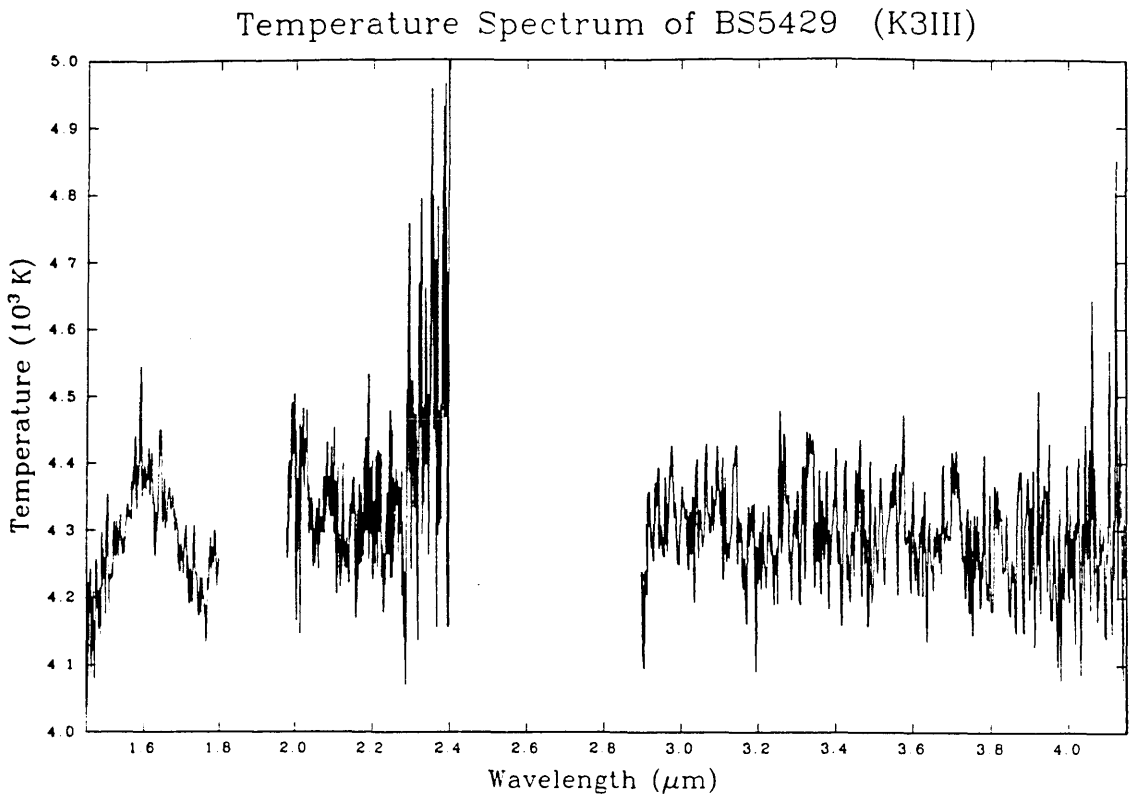
Temperature Spectrum of BS5429 (K3III)
Temperature (10^3 K)
5.0
4.9
4.8
4.7
4.6
4.5
4.4
4.3
4.2
4.1
4.0
1.6
1.8
2.0
2.2
2.4
2.6
2.8
3.0
3.2
3.4
3.6
3.8
4.0
Wavelength (μm)

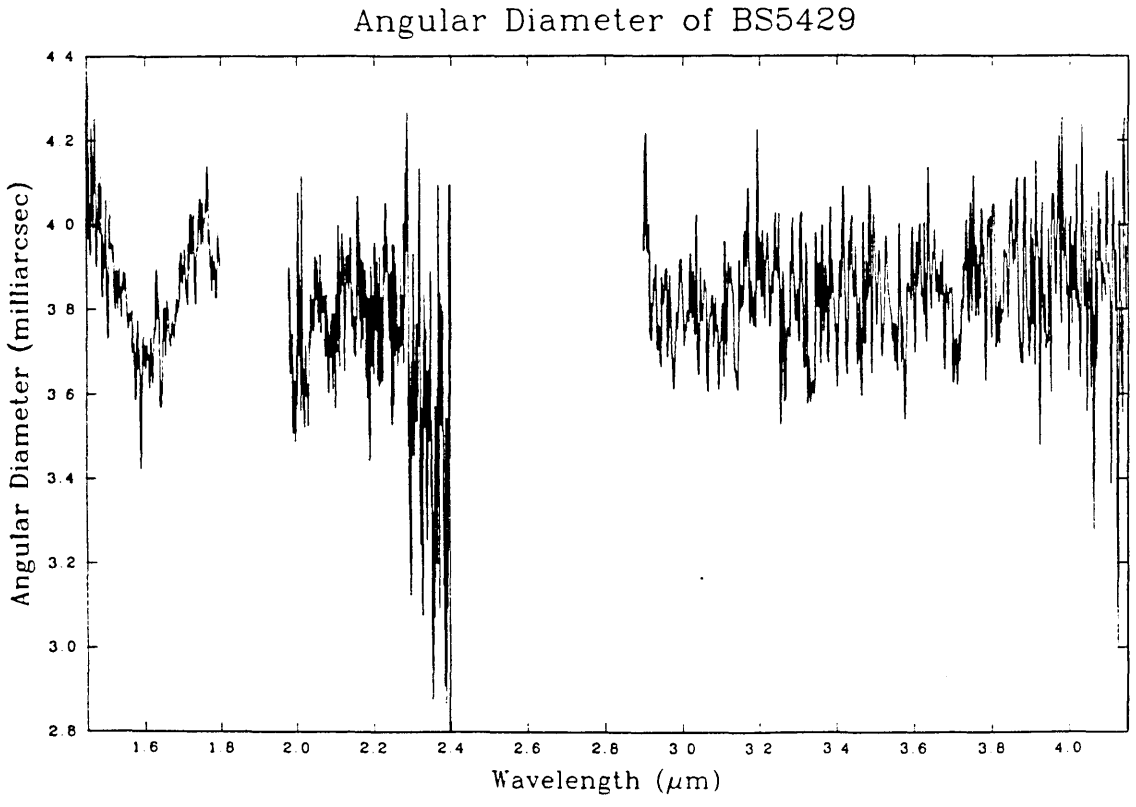
Angular Diameter of BS5429
Angular Diameter (milliarcsec)
4.4
4.2
4.0
3.8
3.6
3.4
3.2
3.0
2.8
1.6
1.8
2.0
2.2
2.4
2.6
2.8
3.0
3.2
3.4
3.6
3.8
4.0
Wavelength (μm)

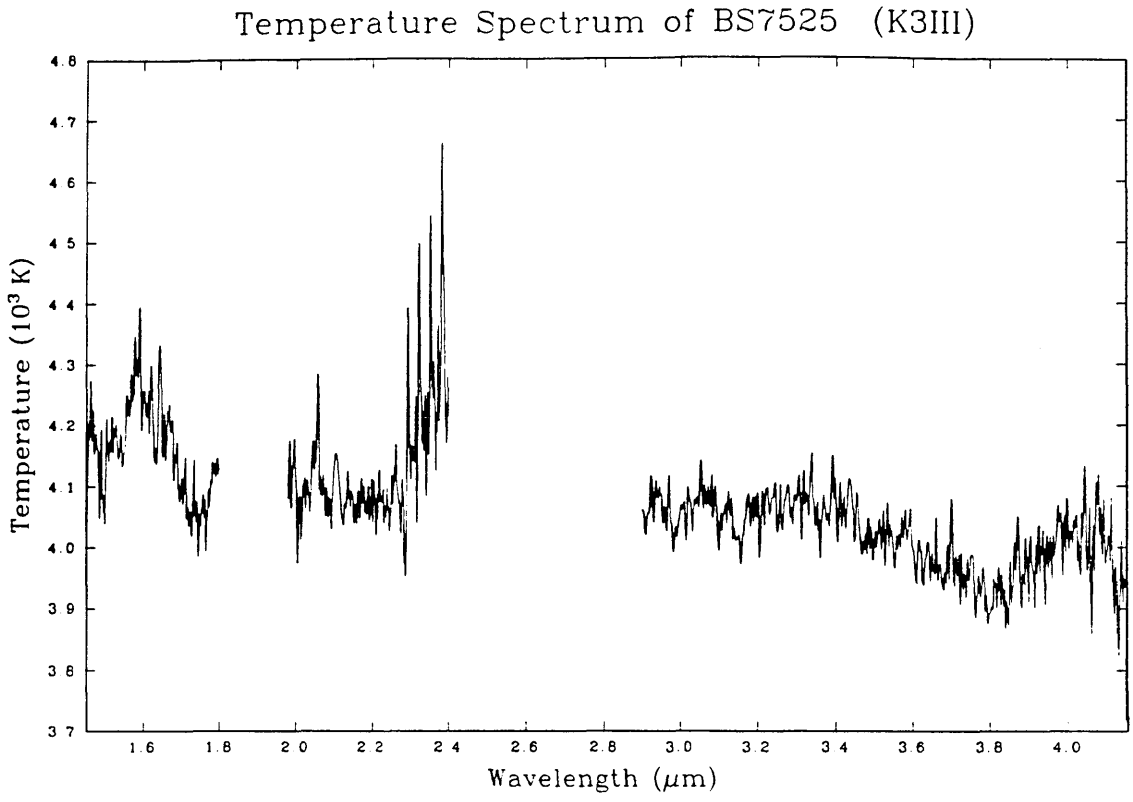
Temperature Spectrum of BS7525 (K3III)
Temperature (10^3 K)
4.8
4.7
4.6
4.5
4.4
4.3
4.2
4.1
4.0
3.9
3.8
3.7
1.6
1.8
2.0
2.2
2.4
2.6
2.8
3.0
3.2
3.4
3.6
3.8
4.0
Wavelength (μm)

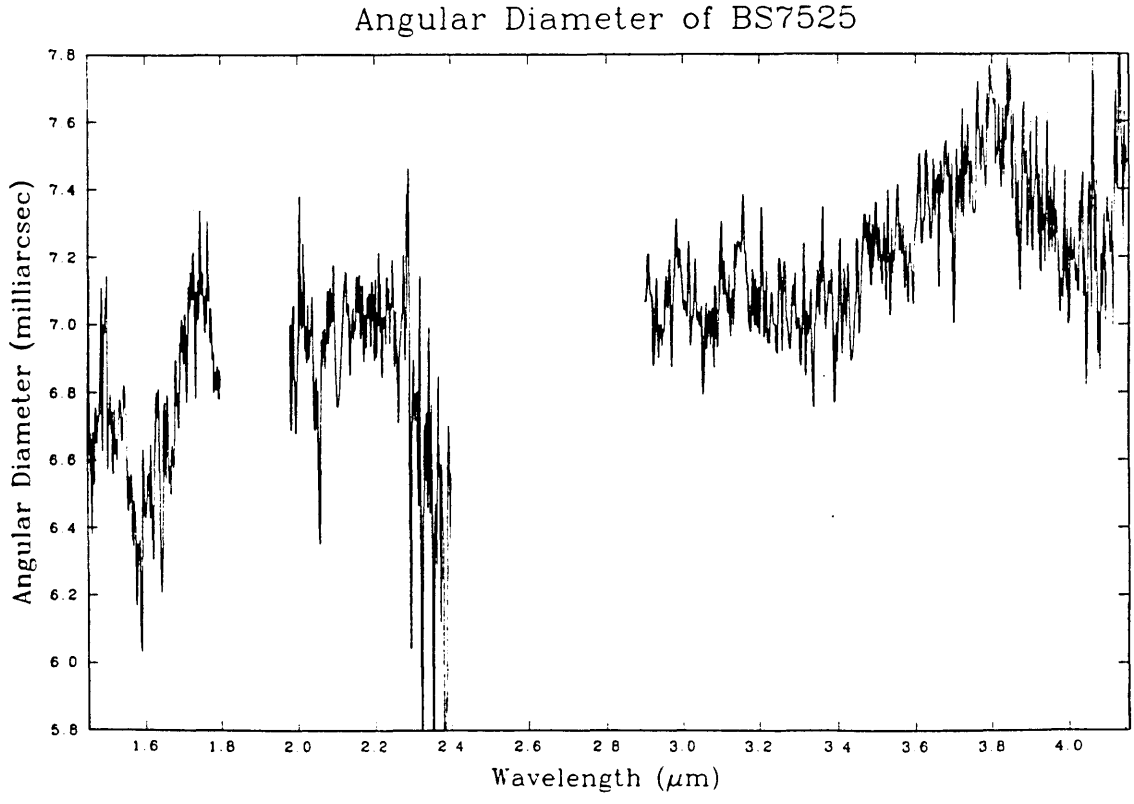
Angular Diameter of BS7525
Angular Diameter (milliarcsec)
7.8
7.6
7.4
7.2
7.0
6.8
6.6
6.4
6.2
6.0
5.8
1.6
1.8
2.0
2.2
2.4
2.6
2.8
3.0
3.2
3.4
3.6
3.8
4.0
Wavelength (μm)

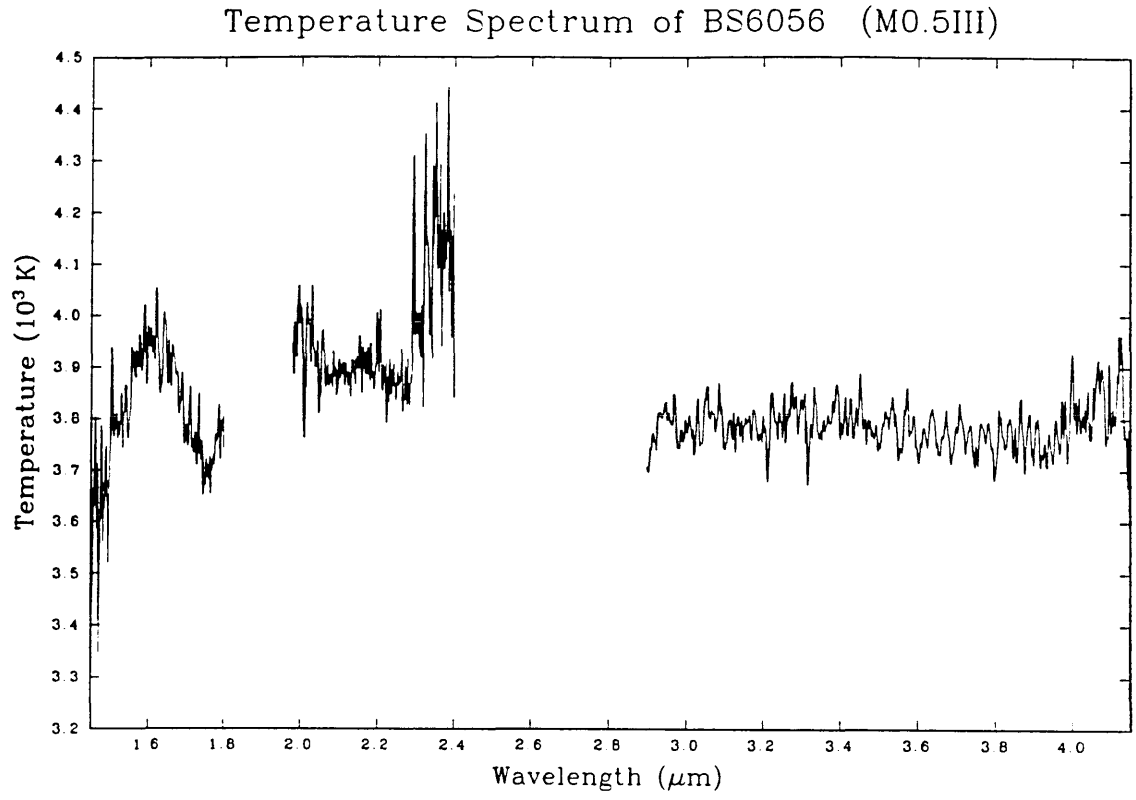
Temperature Spectrum of BS6056 (M0.5III)
Temperature (10^3 K)
4.5
4.4
4.3
4.2
4.1
4.0
3.9
3.8
3.7
3.6
3.5
3.4
3.3
3.2
1.6
1.8
2.0
2.2
2.4
2.6
2.8
3.0
3.2
3.4
3.6
3.8
4.0
Wavelength (μm)

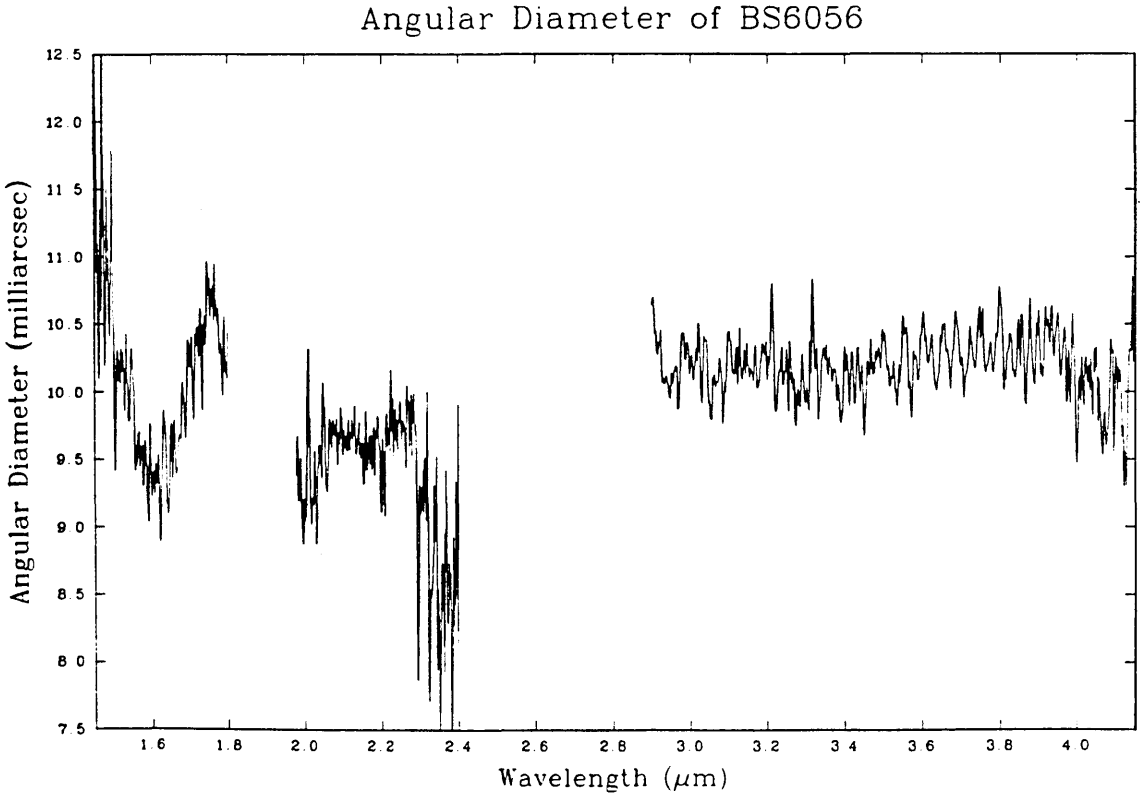
Angular Diameter of BS6056
Angular Diameter (milliarcsec)
12.5
12.0
11.5
11.0
10.5
10.0
9.5
9.0
8.5
8.0
7.5
1.6
1.8
2.0
2.2
2.4
2.6
2.8
3.0
3.2
3.4
3.6
3.8
4.0
Wavelength (μm)

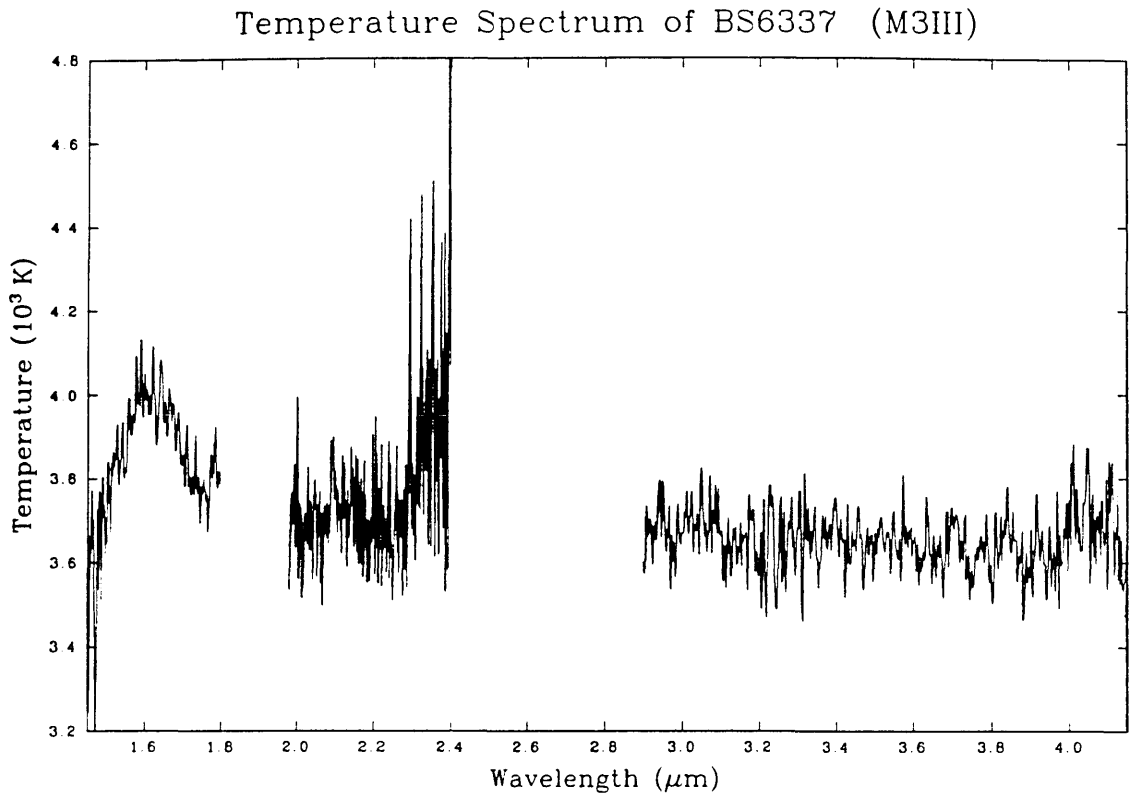
Temperature Spectrum of BS6337 (M3III)
Temperature (10^3 K)
4.8
4.6
4.4
4.2
4.0
3.8
3.6
3.4
3.2
1.6
1.8
2.0
2.2
2.4
2.6
2.8
3.0
3.2
3.4
3.6
3.8
4.0
Wavelength (μm)

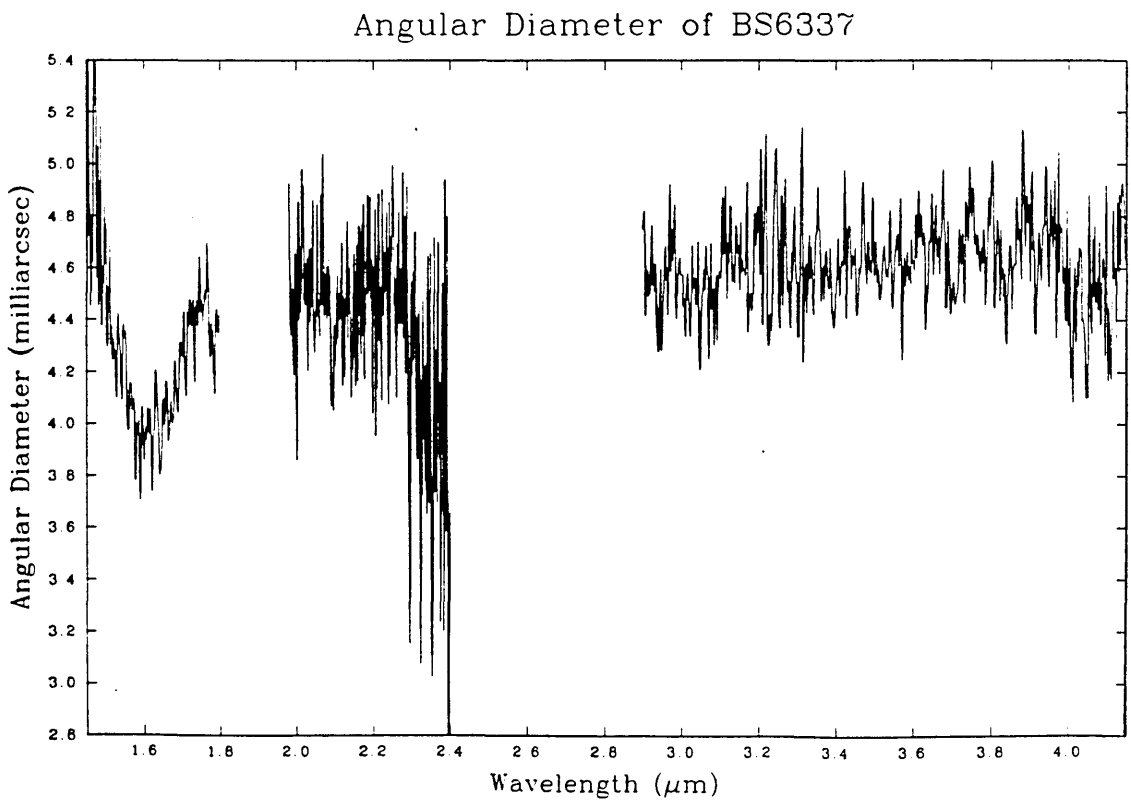
Angular Diameter of BS6337
Angular Diameter (milliarcsec)
5.4
5.2
5.0
4.8
4.6
4.4
4.2
4.0
3.8
3.6
3.4
3.2
3.0
2.8
1.6
1.8
2.0
2.2
2.4
2.6
2.8
3.0
3.2
3.4
3.6
3.8
4.0
Wavelength (μm)

Table 5.3: Temperatures and Angular Diameters

Star	Type	H		K		L	
		T_e	θ	T_e	θ	T_e	θ
BS6623	G5IV	5627	1.66	5673	1.85	5561	1.94
BS6148	G7III	4974	3.42	5008	3.38	5097	3.27
BS7754	G8IIIb	5006	2.37	4794	2.61	5020	2.38
BS5340	K1III	4348	20.33	4334	20.4	4325	20.11
BS5854	K2III	4630	4.66	4564	4.79		
BS5429	K3III	4282	3.859	4327	3.77	4292	3.84
BS7525	K3III	4160	6.738	4089	6.97	4018	7.12
BS6056	M0.5III	3803	10.16	3904	9.59	3786	10.19
BS6337	M3III	3846	4.30	3701	4.50	3652	4.61

Temperature in Kelvin and θ in milli-arcseconds

As expected, many of the absorption features are clearly visible, particulaly the CO bands around 2.3 μm. These have the effect of locally increasing T_e and decreasing θ. When calculating the mean values of T_e and θ the areas with major lines have been ignored. In general, the agreement in temperature between the windows is better than 3% and where large differences do occur there is usually an obvious cause (eg problems at the edges of the windows). The results vary little from those obtained using narrow band photometry (Blackwell et al 1989).

As can be seen in the plots, the IRFM works well in the K and L windows but shortward of this there are definitely problems with the model. At the transition from bound-free to free-free opacities (1.6μm), the temperatures vary with wavelength. This could be partly due to using the incorrect values of $\log g$ or metalicity, but I believe that the major problem is in the models themselves. The spectra certainly demonstrate that great care must be taken when applying the IRFM in the H window and, in general, it is better to use the windows longwards of 1.8μm.

5.7.6 Future use of Spectrophotometry with the IRFM

To date 1 to 4 μm spectra have been obtained for only about 15 stars and so the most important immediate task is to increase this number. The ultimate aim is to have high quality spectra of single, non variable stars covering every spectral type and luminosity class. This will allow a more detailed examination of the accuracy of the model spectra, in particular for defining the wavelength ranges in which the IRFM can be applied.

In general, the absolute photometric properties of spectrometers are poor, certainly when compared with pure photometer systems; whereas the relative photometry across a spectrum can be good. So whilst the magnitude at a specific wavelength may be inaccurate, the relative difference in flux between two wavelengths is considerably better. Photometry, using known filter profiles, exists for all the stars whose spectra have been taken. Integrating the spectra, after they have been multiplied by the filter profiles, is equivalent to the photometry so should give an identical result. Any significant difference will be due to errors in the absolute photometric accuracy of the spectra and where necessary corrections can be made. It is expected that using this technique will significantly improve the absolute accuracy of the final spectra.

When the IRFM is applied to certain stars the temperature and angular diameters are found to alter with wavelength. There is a number of possible causes, such as the presence of a cool companion, interstellar extinction, circumstellar dust clouds, etc., and high quality spectra will be able to distinguish between them.

5.7.7 Conclusion

High quality spectrophotometry is a valuable diagnostic tool for the IRFM. As well as being able to give angular diameters and temperatures directly, it clearly defines the areas in which the IRFM could become inaccurate due to problems in the stellar models or the star's spectrum. Also, spectrophotometry can be used to improve the accuracy of previous applications of the IRFM to photometry, particularly for cooler stars, by measuring the amount of line blocking with spectral type, so allowing corrections to be made.

5.8 The Absolute Vega Flux

As yet, it is impossible to say whether the model or direct measurements of the absolute flux of Vega are more accurate. Both the spectra and the paper of Blackwell et al (submitted) suggest that at present it is better to use the model Vega fluxes when applying the IRFM, since the results are less dependent on wavelength. However, as stated earlier, all that this means is that the models are consistent with themselves.
From equations 1.6 and 4.1

$$F_s = \frac{F_{MV} \times S_s}{S_V} = \frac{\theta^2}{4} F_{ms} \tag{5.1}$$

where F_s = Flux from the star

F_{MV} = Model Vega flux

F_{ms} = Model stellar flux ie $f(T_e, g, \lambda, m)$

F_s = Absolute flux from the star

S_V = The measured signal from Vega

S_s = The measured signal from the star

Therefore

$$\frac{S_s}{S_V} \propto \frac{F_{ms}}{F_{MV}} \tag{5.2}$$

If the long wave excess in the B stars is confirmed by other measurements then there must be a high possibility of Vega also having an excess since it is only about 10% cooler. When more spectra of early stars are taken, it would be valuable to include Vega and a number of other A type stars to see if they show a similar excess.

Chapter 6

Sky Surveys And Galactic Structure

6.1 Introduction

It is not known when the first maps of the sky were developed by primitive man, but in all the recorded early societies the study of the sky formed an integral part of their cultures. The stars were grouped into constellations which represented animals, gods, kings, etc. and in this way their relative positions became fixed. A great deal of time and energy was devoted to the study of the stars because they offered a valuable frame of reference for both time and position. The Greeks and Egyptians both used the position of Sirius at sunrise or sunset to define their calendars. All the great seafaring nations, such as the Phoenicians and Polynesians, used the position of the stars to define directions and latitude. In fact, many of the great observatories, such as those at Greenwich or Paris, were expressly set up to fix the position of the bright stars to aid navigation. Stars have continued to be used in a similar way up to the present day. Despite having atomic clocks and satellite navigation, the transit of stars is still used as the final arbiter of time and position.

6.2 Sky Surveys

The data from sky surveys tends to be presented in two formats, either as a catalogue and/or as a 'map'. Catalogues deal with specific objects: they give the position and some of their attributes (eg magnitude) so are presented as lists. They are used mainly when dealing with distinct objects such as a star or galaxy. Maps are basically images of the sky showing the distribution of flux with position to the spatial resolution and limiting magnitude of the survey. Therefore maps are better than catalogues at representing areas of sky. For example, the distribution of stars and dust in an open cluster is considerably simpler to understand when looking at a picture rather than a list of numbers.

6.2.1 Visible Star Catalogues

The School of Alexander was one of the foremost scientific/philosophical institutions in the Ancient Greek world. It was pupils of this school who produced amongst the first star catalogues. Timocharis & Aristyllus, Hipparcus and Ptolemy compiled catalogues between the third century BC and the second century AD which defined the positions of up to 1000 of the major stars and divided them into the 6 magnitudes visible to the naked eye. Cataloguing the positions of stars has continued until the present day. Some of the more notable catalogues are those by Flamsteed and Hevelius in the mid 17th century and by Lacaille and Brabley in the 18th century. Primarily, they were to aid navigation although after the work of Kepler and Newton they were required as a reference frame for the study of the motion of planets, comets and asteroids. Probably the most used star catalogues at present are the Bright Star Catalogue which lists all stars to a visual magnitude of +6 and the Smithsonian Astronomical Observatory catalogue which has a limit of +9.

6.2.2 Visible Sky Maps

The advent of telescopes allowed astronomers to see stars hundreds of times fainter than was possible with the naked eye, although it was not until Herschel in the late 18th century that the first 'deep sky' survey was carried out. He used star counts to determine the

distribution of stars in various parts of the sky and showed that the majority were centred in what is now known to be the galactic plane. Difficulties in recording the information meant that the best star map of that period was probably in Herschel's head.

The development of photography in the mid-19th century could not make an impact on large scale deep sky surveys until telescopes were designed which gave large fields of view. It was not until 1930 that the Schmidt telescope was developed. This allows many square degrees of sky to be imaged with a high spatial resolution (about an arcsecond) and faint limiting magnitude (typically +18 at I). A major problem with Schmidt plates is that the response is logarithmic and can vary over the surface of the plate. This makes it difficult to determine magnitudes to an accuracy of better than 1 magnitude. Many surveys have been carried out which now cover the whole sky at a number of wavelengths between about 400nm and 900nm, perhaps the most famous of which are the Palamar and UK Schmidt surveys.

6.3 Sky Surveys at other Wavelengths

Over the past 50 years or so, advances in electronics and detector design, coupled with the ability to get above the earth's atmosphere, now make it possible to take astronomical observations over the whole EM spectrum.

6.3.1 Infrared Surveys

To date, the existing near infrared surveys either cover a large area of sky at a poor spatial resolution and/or a poor limiting magnitude, or cover very restricted areas of sky.

The Two Micron Sky Survey carried out at Cal. Tech (Neugebauer and Leighton 1969) was the first major near infrared survey. It covered 77% of the sky at K with a limiting resolution of +3 mag. Just over 5000 sources were detected, most of which were in the galactic bulge area. Since the late 70's a number of balloon-borne surveys have been carried out by groups from the Max Plank Institute, Nagoya and Kyoto (Hofmann 1977,1978, Maihara 1978, Ito 1976,1977, Hayakawa 1976,1977,1978,1979,1981). These measured the surface brightness of the galaxy at 2.4 microns using beam sizes of about one degree.

Imperial College and the IAC have carried out a number of very restricted surveys, mainly around the galactic centre at K and H. They had spatial resolutions of between 15 and 30 arc seconds and sensitivities of about +10 mag. at K. A group in South Africa (Glass et al 1986) have made a 2 by 1 degree map of the galactic centre at J,H and K. They achieved a spatial resolution of about 10 arcseconds and a limiting magnitude of about +11 at K.

The AFGL 4 colour sky survey (Price and Walker 1976) was the first to use longer infrared wavelengths. The survey used rockets and covered most of the sky at 4.2, 11.0, 19.8 and 27.4 microns. 2363 sources were detected.

The IRAS survey is probably the most prestigious infrared survey yet carried out. It covered over 90% of the sky at 12, 25, 60 and 100 microns but with a spatial resolution around 1 arcminute. The data has been published both as a map and as a point source catalogue. The catalogue contains some 246,000 sources of which 65% are stars, most of these are in the galactic bulge region.

6.3.2 Other Wavelengths

There have been a large number of radio surveys. Generally, they map spectral lines such as HII, HI, CO,CS, OH, NH3, etc.

The atmosphere absorbs gamma ray, X-ray and UV radiation so it is necessary to use either balloons, sounding rockets or a satellite to observe in these wavelength ranges. X-ray and gamma ray experiments have spatial resolutions in the order of degrees because imaging is impossible at these wavelengths. The surveys carried out are usually of the galactic bulge and plane. UV radiation can be imaged in the same way as the visible so high spatial resolutions can be achieved. There have been many successful satellites such as IUE and TD1. The data is usually presented in catalogues.

6.4 Galactic Structure

It is now well established that the galaxy is a typical type Sb2 spiral. There are 4 main components

- The nuclear region or core which is only about 1 pc across. It contains a point like and highly energetic object at the core of the radio source Sgr A west with many radio, infrared and X-ray sources surrounding it. In 1987 a lunar occultation has provided more detail on the number and position of the infrared sources (I.S. MacLean).
- The central bulge. This is approximately spherical with a radius of 2 Kpc. It contains mainly old stars.
- The disk. This has a radius of 25Kpc but is only 600 pc thick. It contains the spiral arms and dust lanes.
- A relatively few halo stars. These have a spherical distribution centred on the bulge and reach out to about 15 Kpc.

Although the gross structure of the galaxy has been determined there is still very little detailed information on the large scale distribution of stars in the galaxy.

It is only relatively recently that the position of the sun in the galaxy has been accurately determined. Herschel gave the first real estimation of its position. He used star counts and came to the conclusion that the sun must be towards the centre. Unfortunately, he did not realise the effect of interstellar extinction which makes the technique unusable. It was not until 1918, when H.Shapley used the distribution of globular clusters to show the shape and size of the galaxy, that it was conclusively shown that the sun was actually a considerable distance from the centre. The distance of the sun from the centre of the galaxy is now generally given as 10 Kpc although some sources suggest that 8.6 Kpc is a better figure.

6.4.1 Interstellar Extinction

The majority of the gas and dust in the galaxy gathers along the galactic plane. Therefore, interstellar extinction quickly becomes a major problem when looking in this region.

The equation relating the apparent and absolute magnitude of a star is

$$m = M - 5 + 5\log r + Ar \tag{6.1}$$

m = Apparent magnitude

M = Absolute magnitude

r = Distance in pc

A = Extinction in mag pc^{-1}

At K the extinction is quoted as being 0.2 mag per Kpc compared with 1.9 mag per Kpc for the visible. Therefore, when looking at the centre of the galaxy the near infrared loses only 2 magnitudes to extinction, compared with nearly 20 magnitudes in the visible. There is also a further loss of about 20 magnitudes to the inverse square law, so even the very brightest supergiants will have an apparent magnitude of +26 in the visible so could not be observed. However, at 2.2 microns its apparent magnitude would be around +6 putting it within the detection limits of even the smallest telescopes. In reality, the dust distribution is not uniform and tends to form clumps, so there are areas where the extinction is far less. Even so, it has been found that visible wavelengths are unsuitable for work beyond about 4 Kpc, in the galactic plane. The majority of the information on galactic structure has come from infrared and radio surveys.

6.4.2 The Radio Galaxy

Radio waves show negligible interstellar extinction so can be used to observe the entire galaxy. The dominant features in the radio sky are HII region and supernova remnants. However, clouds of cool neutral hydrogen also are detectable and these have proved the best spiral tracers. The first large scale maps of the spiral structure of the galaxy were made by comparing kinematic models with measurements of the Doppler shift in the 21cm HI line (Schmidt-Kaler 1976).

6.4.3 The Infrared Galaxy

The near infrared is the best wavelength range in which to study the distribution of stars in the galaxy because most stars are still high on the Rayleigh-Jeans part of their flux curves. Two basic techniques have been used to measure star distribution: integrated surface brightness using large sky apertures and counting discrete infrared sources.

The balloon observations by groups from the Max Plank Institute, Nagoya and Kyoto have determined the average surface brightness of the galaxy on the scale of degrees at 2.4 microns. The results clearly show the central bulge, the disk and some of the fine structure. (Hayakawa et al 1981)

Grasdalen and Gaustad (1971) compared the Two Micron Sky Survey with the Dearborn Catalogue of faint red stars. 93% of the IRC sources were found in this catalogue with a peak around M4. Although there are nearly 1500 times as many red dwarfs as giants in the vicinity of the sun (Astrophysical Quantities) the absolute magnitude of the giants is in the range -5 to -7 compared with 5 to 7 for the dwarfs (ie over 10,000 times brighter). Therefore, the majority of the stars detected by the Two Micron Survey ~~Survey~~ were M giants, and it will be the same for any infrared survey in the galactic plane.

The restricted surveys carried out by Imperial College and the IAC attempted to determine the galactic structure using star counts. The surveys were complete to H=10.5 mag and K=9.5 mag, the limits being caused by confusion rather than the instrumentation. This corresponds to detecting M3III stars out to 6-7 Kpc. Some 800 star were detected within these limits in the 0.18 deg^2 surveyed. Evidence was found for a population of highly reddened objects, which are probably supergaints, within 70pc of the galactic centre.

6.5 The Proposed 2.2μm Galactic Survey

Recent developments in near infrared array technology now make it feasible to attempt to survey large areas of the sky in the near infrared, using a reasonably high resolution and achieving a faint limiting magnitude. It is still impractical to attempt to cover the whole sky, so the most interesting area to map must be the galactic bulge and plane. Such

a survey would not only add greatly to our understanding of the galactic structure but would also be an invaluable source of information when developing observing programmes in the galactic plane.

Chapter 7

The ICSTM 7 Channel Linear Infrared Camera

The ICSTM 7channel linear infrared camera was designed and built in 1986/7 at Imperial College by M.Selby, I.Hepburn and the technicians of the astrophysics group. It was developed because there was a 7 element detector array and a suitable liquid nitrogen cryostat available at that time. It has since been used to search for brown dwarfs and as the detector system for the 2.2 micron galactic survey.

7.1 Design Aims

When designing the instrument a number of observational and practical considerations were taken into account.

- A pixel size of about 15" was chosen (assuming the 1.5m TCS was to be used). This would allow a relatively large area of sky to be mapped quickly.
- The instrument should have the best limiting magnitude possible. Therefore, the detector must only see sky and not the telescope structure.
- The instrument should be developed using existing equipment, ie cryostat, optics and detector.

7.2 The Cryostat

The 7 channel cryostat was originally a spare for the 4 channel photometer. It has a single nitrogen chamber and can operate at either liquid or solid nitrogen temperatures. The window is in the side of the instrument which allows a simpler optical arrangement to be used.

7.3 The Optical Layout

The 7 channel has a re-imaging optical system (figures 7.1 and 7.2). The optical arrangement is based on a concave spherical mirror, 5cm focal length, which images the 1.4mm by 11.2mm entrance slit at its centre of curvature onto the seven 200 micron square detectors via two zinc selenide lenses. The lenses give the required optical conversion to make the detectors image the whole slit. The image of the primary mirror is formed at the focus of the re-imaging mirror. By placing a cooled aperture or pupil stop, exactly the same size as the image of the primary, at this position, all the radiation which comes from the telescope surrounds is masked and the detector can only see the primary mirror. This significantly reduces the amount of background radiation falling on the detector, so improves the sensitivity.

The cryostat does not have a filter wheel so is limited to a single filter; currently this is a standard K filter. The filter is placed directly behind the pupil stop so no unfiltered radiation can fall onto the detectors.

7.4 The Detector

The 7 channel linear detector array was constructed by Cincinnati Electronics. It consists of seven 200 micron square InSb photovoltaic detectors, with an interdetector gap of 30 microns. The seven detectors have separate anodes but a common earth. Each detector is operated in a separate Hall type transimpedence amplifier circuit. There are two pre-amp boxes which fit onto the side of the cryostat. They hold the warm parts of the circuits.

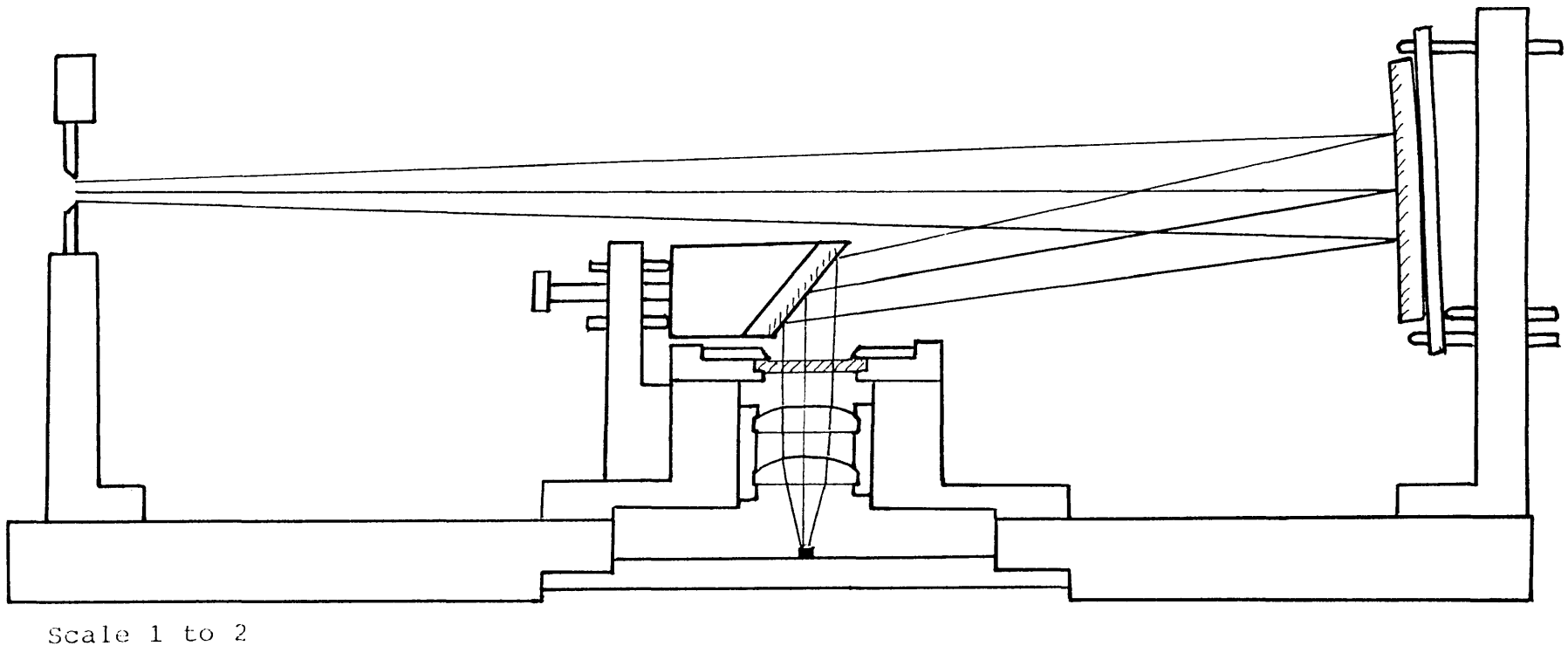

Figure 7.1: The 7 Channel Optical Configuration

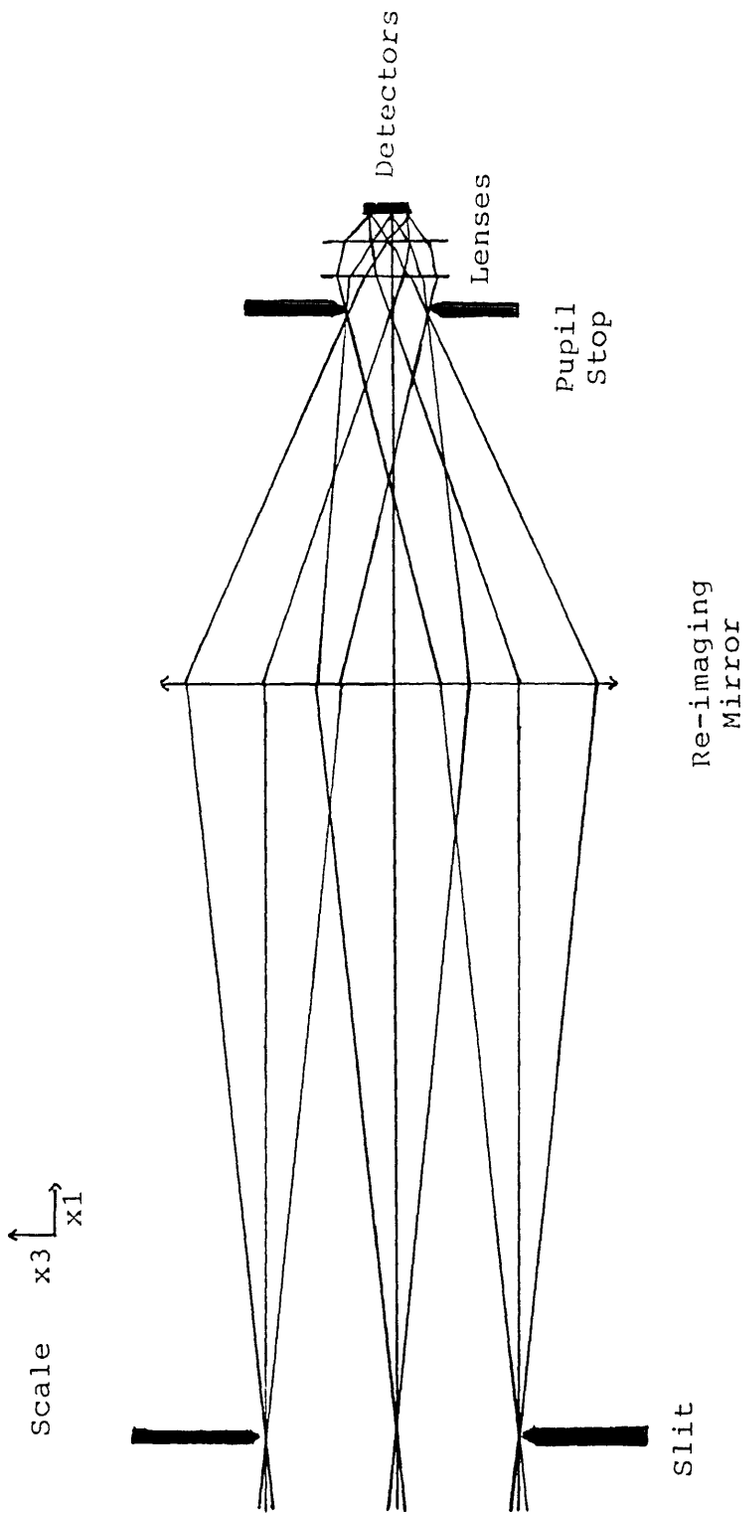

Figure 7.2: The Equivalent Optical Layout

The circuits are powered using rechargeable batteries.

7.5 The 7 Channel Data Acquisition System

The 7 channel data acquisition system was designed and built at Imperial College by the electrical technicians of the Astrophysics group between 1984 and 1986.

The 7 channel data acquisition system has 3 main parts: the analogue rack, the digital rack and the user computer (figure 7.3).

7.5.1 The Analogue Rack

This is a standard 19.5 inch mains powered rack which is mounted on the telescope as close to the cryostat as feasible. 7 lemo cables connect each post amplifier to the respective pre-amplifier.

Each of the 7 channels has a separate post amplifier module. The amplifiers can be used either AC, when chopping, or DC. In this case an offset voltage can be applied to the outputs. There is a choice of 8 possible amplifier gains which range from x0.33 to x1000. The values can be set remotely. The outputs have a 20Hz single pole low pass filter to reduce the unwanted high frequencies, particularly 50Hz pickup.

There are 8 (1 spare) 100 KHz voltage to frequency converters. These produce a train of pulses whose frequency is dependent on the applied voltage. They are set up so that -10v produces no output, 0v produces 50 KHz and +10v produces 100 KHz. A digital signal is in effect noise free, so there will be no degradation of signal between the analogue and digital racks, which are usually many metres apart.

In tests the amplifiers and V to Fs have proved to be very linear with gains close to their nominal values.

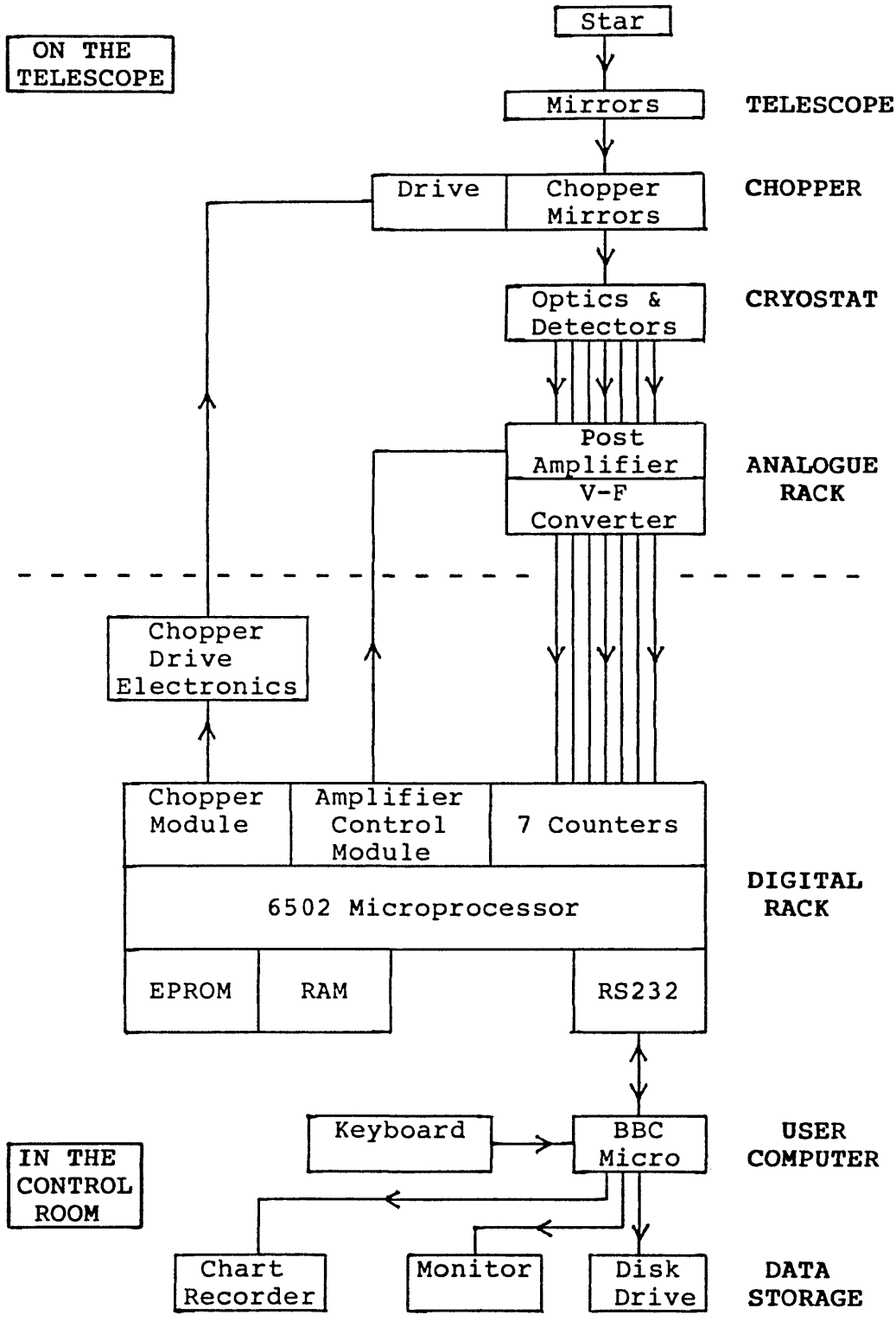

Figure 7.3: Data Flow in the 7 Channel Data Acquisition System

7.5.2 The Digital Rack

This is a double layer, 19.5 inch rack which is powered by the mains and is usually operated in the control room. It is linked to the analogue rack via 8 BNC cables for the signals, and 1 multi core cable to control the gains. The digital rack is controlled by a 6502 microprocessor board which communicates with the other modules in the rack using the ICSTM 'Astrobus' data bus system. The microprocessor board also has the 1MHz crystal oscillator which provides the clock signal for all the other modules in the rack. An 8k eprom emulator holds the machine code program which controls the microprocessor.

The signals from the V to F converters are sent to 8 bi-directional counters. These are 24 bit counters which, under software control, can be made to count up, down or reset to zero. The counter can be frozen by applying +5v to one of the pins (eg when reading out) and a module has been built, which is controlled by the hardware timer on a 6522 VIA, to do this.

The rack produces the square wave timing signal which runs the sky chopper, using a free running hardware counter on a 6522 VIA. The period can be varied by altering the starting value on the counter.

The other modules in the digital rack are the post amplifier gain control module and the RS232 module for communication with the user computer. The RS232 is a standard serial interface which is available on most computer systems from main frames to personal computers. The system has a number of possible baud rates, but in order to transfer the information as quickly as possible the 9600 baud rate is used (just over 1200 bytes per second). The user computer is usually operated close to the digital rack, but it is possible to have them hundreds of metres apart: this could be very useful when working on some telescopes.

7.5.3 The User Computer

At present the user computer is a BBC microcomputer, although, in principle, it could be any computer with an RS232 or RS423 serial interface. The purpose of the user computer is to take the data from the digital rack; store the data; present the data in an easily

understood format and pass commands to the digital rack.

The BBC uses a 6502 microprocessor and has between 6 and 27 K bytes of RAM for user programs. Although this is now considered limited, it is sufficient to control the instrument and provide a small amount of on line data reduction. The BBC is a very simple computer to program. Full documentation on all the external ports is provided and it is possible to have direct access to memory locations from high level languages such as BASIC. The BBC can operate a large number of peripherals, including floppy and hard disk drives for the data storage and a high resolution colour monitor for its presentation. An 8 bit digital to analogue converter has been fitted to the user port (6522 VIA bi-directional port) which can drive a chart recorder.

The major advantage of using two computers, rather than just one, is that the primary functions of the computers can be different. The primary function of the digital rack is to control the instrument, in particular, to make sure the counters are read at the correct times and nothing must prevent this. The primary functions of the user computer are to pass information between the user and the digital rack, and to store the data.

7.6 Phase Sensitive Detection

The sky and telescope both look like 300K black bodies, so at infrared wavelengths they will produce a significant contribution to the detected flux. The signal from the background sources must be removed if accurate measurements are to be made. The simplest way to remove the background signal is to observe the object, which includes the backgrounds, and then the background alone (ie an adjacent area of sky which contains no sources). Subtracting the latter from the former gives the signal from the object, assuming both observations were taken under the same conditions. It is possible to do this by moving the whole telescope, but since the sky emission varies with time it could be too slow (telescopes take many seconds to settle after being moved so require long integrations in each position if they are to be used efficiently). The standard methods employed are to either 'chop' the secondary mirror or to use a focal plane chopping system, similar to the two mirror system used at the 1.5m TCS. Generally, a chop frequency of between 3 and 20 Hz is employed. Chopping the signal has a second advantage since the signal will now

be at the chop frequency and not at zero Hz. The detector noise power spectrum is 1/f in nature so will be considerably less at the higher frequencies.

7.6.1 The Advantage of Digital Phase Sensitive Detection

The PSD with the 7 channel data acquisition system is performed digitally. This has 2 major advantages. Firstly, it is feasible to build a high quality digital 7 channel PSD system at a relatively low cost, whilst a comparable analogue system would be considerably more expensive. Secondly, analogue systems usually have low pass filters on their outputs, typically about 1 Hz, but digital systems do not require this. Therefore, digital systems react far faster to changing input signals, which could be useful for the removal of noise spikes. In tests the 7 channel PSD system performed at least as well as analogue systems.

7.6.2 Phase Sensitive Detection with the 7 Channel Data Acquisition System

The phase sensitive detection is achieved by having the counters counting up when the star is observed and down when observing the sky alone.

The timing for the counters comes from the counter disable 6522 VIA. For the majority of the time the output is low so the counters operate, but there is a periodic short disable pulse (at present its duration is fixed at 2ms). The period of this pulse is exactly half the chop period. (Figure 7.4). Since both the chopper and counter disable VIAs use the same clock, the phase between them will remain fixed unless it is deliberately altered. When the counter disable pulse goes from low to high, so freezing the counters, an interrupt is called which will alter the direction of count and if necessary reads and resets them. The counters can integrate for over half a minute without needing to be read and reset, but in general, they are read out every 10 chop cycles. Although integrating on the counters has the advantage that it does not use any CPU time, it is important to have a number of readings for each object observed as this allows a standard deviation to be calculated.

The data acquisition system has 16 possible chop rates between 7Hz and 60Hz, but to date it has always been run at 9.38Hz. By not using a multiple of the mains frequency it is

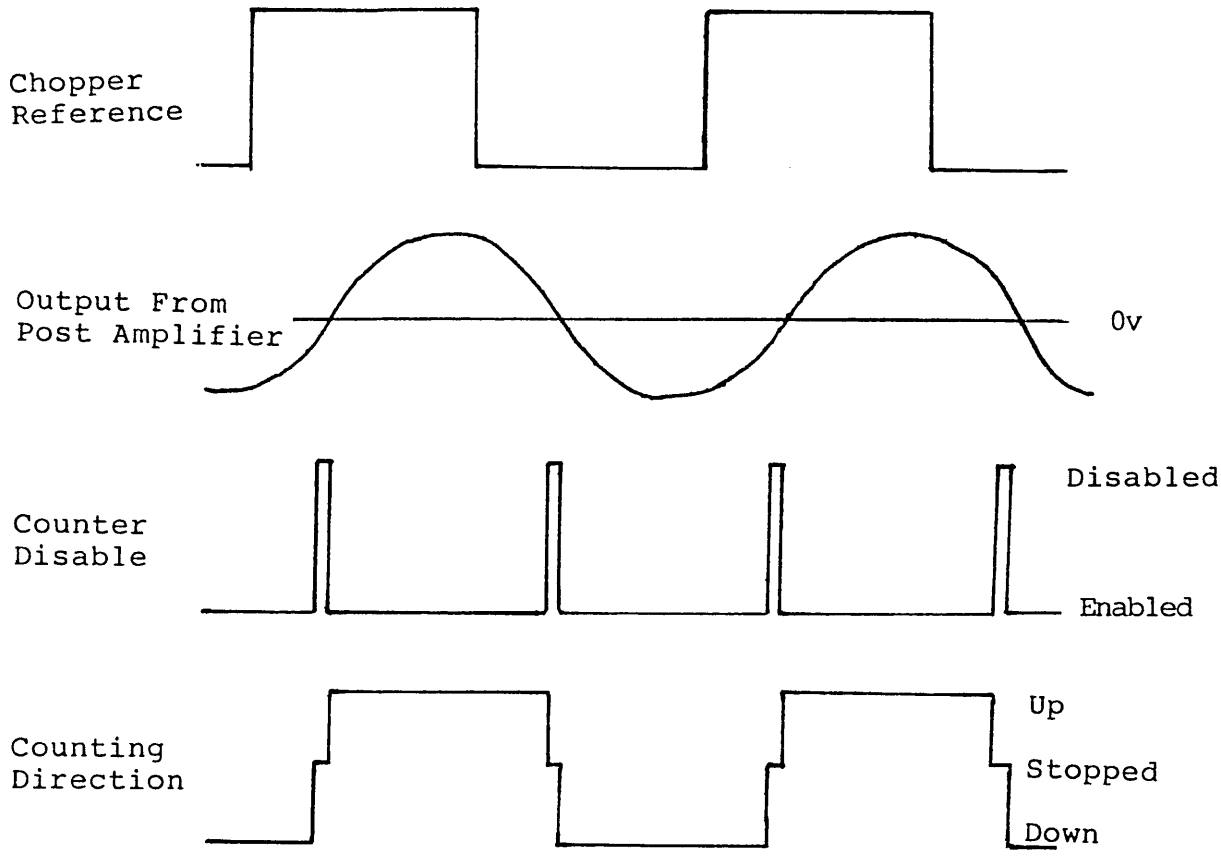

Figure 7.4: Chopper and Counter Timing Diagram.

hoped to reduce the effect of 50 Hz pickup. When working at this frequency the counters are disabled under 4% of the time.

It is important to be able to alter the phase between the counter disable and the chopper, since low pass filters will cause a phase shift in the signal between the detector and V to F converters. The alteration in phase in achieved by lengthening or shortening the time between consecutive counter disable pulses, by a set amount, until the maximum signal is found.

When the system is required to operate DC, ie without chopping, the counters are

operated in the same way as when chopping, except they always count up.

7.6.3 The Advantage of Voltage to Frequency Converters

For this particular application, V to F converters have a significant advantage over analogue to digital converters or digital volt meters. The V to F converters continuously sample the signal for the whole observation, whereas the A-Ds or DVMs sample the signal at a specific instant in time. Therefore, the alias bands for the V to F are considerably smaller than for an A-D or DVMs, so the effect of any high frequency noise, especially 50 Hz pickup, is greatly reduced. A-Ds must sample at a frequency at least twice that of the highest frequency in the noise, therefore low pass filters are essential to keep the data rates at a manageable level.

7.7 The Software

The original 7 channel software was developed by M. Bartholomew and M. Hooker. I have significantly improved this so the system is easier to use and can operate at higher sample speeds.

7.7.1 The Digital Rack Software

This has three main parts: the set up, the interrupt and none interrupt routines.

The Set Up Routine

This initialises all the modules so that they are in their default states, ie 7 channels; chopping mode; chop rate 9.38Hz; a post amp gain of one and the RS232 set to 9600 baud with the interrupts turned off.

The Interrupt Routine

This is either called by the counter disable VIA or the RS232.

When it is called by the 6522 VIA, the counter direction is changed if chopping is being used. If the correct number of chop cycles has passed, the counters are latched, read out then reset. The data is then sent to the 'output buffer' along with the gains. The RS232 is set to interrupt on its output buffer being empty and the value & 38 is sent to tell the user computer that there is data to be transferred.

When the RS232 interrupt is called, a check is made to see if the user computer has acknowledged that data is ready to be sent. If it has not, another data ready signal is sent. If an acknowledgement has been received the next byte on the output buffer is sent. After the last byte has been sent, the interrupt is turned off.

The None Interrupt Routine

This takes the commands from the BBC and acts on them. For the majority of the time the routine is looking for data entering the RS232, in particular, checking for the acknowledgement from the user computer.

7.7.2 The BBC Software

The BBC software is again divided into interrupt and none interrupt routines.

The Interrupt routine

This is triggered by data entering the RS423. The BBC then remains in the interrupt routine until all the data has been sent; in this way there is no possibility of data being lost. The BBC sends an acknowledge character (& 06) to tell the digital rack that it is ready to receive the data, and then the data packet is transferred. If data is being stored the routine transfers the data to the 'data buffer'.
The interrupt routine then checks the 'command buffer' to see if there is a command to be

sent to the digital rack. By only sending commands directly after receiving data, numbers and not just ASCII characters can be sent without the possibility of their being mistaken for an acknowledge character. Numbers are faster to send and easier to handle.
Finally, the routine passes one channel to the user port to be output on a chart recorder.

The None Interrupt Routine

This is written in BASIC and is designed to make the interface between the user and data acquisition system as simple as possible. The routine displays the data as it comes from the digital rack, along with other necessary information, such as the post amplifier gains and chop frequency. After a series of measurements have been made the mean and standard deviations for each channel are displayed and the data stored to disk. The entry of commands is also simple and reliable; as they are entered they are passed to the 'command buffer' where they wait until the next data package has been received before being transferred.

7.8 The BBC to Digital Rack Commands

The commands all start with an ASCII character and then the data where necessary. (x represents a real number.)

S Starts the timers. Must be the first command sent.

G x x x x Sets the seven post amplifier gains. The value of the gain number and varies between 0 and 7 so two gains are sent in each byte.

C x Sets the chop frequency. x varies from 0 to 15.

I x Sets the number of half chop cycles before the signal is read. x must be even and in the range 2 to 254.

X x sets the number of channels to be used. x takes a value between 1 and 7.

F Allows the phase to be set. Enter **1** or **2** to alter the phase between the counter enable and the chopper. When satisfied enter **Return** to leave routine.

U The up/down counters only count up (ie working DC).

D The up/down counters count up and down (ie chopping).

7.8.1 The Digital Rack to BBC Data Packet

When 7 channels are being used, the data packet sent from the digital rack to the BBC is

Byte Number	
1	Number of bytes in the packet
2	Number of channels
3-6	The post amplifier gains, two values per byte
7-9	Channel one's data
10-12	Channel two's data
13-27	Channels three to seven's data

If a command was sent to the SBC since the previous data packet was transferred it is now echoed back to the user computer. For example, if the data is to be transferred after every 4 chop cycles then

28	I
29	8

7.9 Commissioning the 7 Channel

The 7 channel was commissioned on the 1.5m TCS in March 1987 using a K filter. The 1 sigma one second limiting magnitude of the system is between +12.5 and +13 on all channels. The image profiles are excellent, having a flat top of about 10" and a half width of about 12". The centres of the detectors are spaced by 15".

7.10 The Data Acquisition Up Grades Required for the 2.2 Micron Galactic Survey

When it was proposed to attempt the survey (see chapter 8) it was realised that the existing data acquisition system could not cope with the large amount of data that would be produced. About 10 samples per second would need to be continuously read and stored for periods of hours. The original system can operate at this sample rate, but for only about 1 minute, after which time the data must be stored. The BBC would require longer than 0.1 seconds for this, so data would be lost.

I have extended the data acquisition software so that there is a second method for the transfer of data. The system defaults into the original data transfer routine so the gains, chop frequency, etc., can be set. However, when observations are to be taken there is now an option to transfer data in blocks of up to one hundred sets of 7 counter readings. By receiving large blocks the BBC will have many seconds to deal with the data without the possibility of more arriving.

7.10.1 Changes to the Digital Rack Hardware

The only change necessary to the hardware is the inclusion of an 8k byte ram buffer for the intermediate storage of the data. The software treats it as two 4k buffers so one is filled whilst the other is being read out.

7.10.2 Changes to the Digital Rack Software

When the command is sent to begin transferring the data in blocks, a flag is set which re-routes the interrupt routine. Instead of transferring the data directly to the output buffer, it is held in one of the temporary storage buffers. After a specific number of samples, the data ready flag is set and data is read to the other buffer.

The data is transferred to the RS232 as a complete block but without using interrupts. Again, the data ready character is sent to the BBC, and data is not transferred until the acknowledge has been received.

7.10.3 Changes to the BBC Software

The BBC interrupt routine is also re-routed when transferring the data in blocks. As before, the BBC remains in the interrupt routine whilst the data is being received; this can be up to 2 seconds. The data is stored on a 10k buffer.

At present there are three possible routines for storing the data, either to a floppy disk, a hard disk or dumping the data to another computer via an IEEE interface. The IEEE is a parallel interface and has a transfer rate of over 50k bytes per second.

7.10.4 Digital Rack to BBC Data Block

The data block sent from the digital rack to the BBC when 7 channels are in use is

The header

1	& FF
2-5	Gains
6-7	Number of bytes to be sent

The data block

Data block counter (1 byte)

1	channel 1,	channel 2,	- - - - - - channel 7
2	channel 1,	channel 2,	- - - - - - channel 7
3	channel 1,	channel 2,	- - - - - - channel 7
:	:	:	:
:	:	:	:
100	channel 1,	channel 2,	- - - - - - channel 7

2 byte check sum

When reading out 10 times per second, the maximum value on a counter will be 10,000 so can be held in less than two bytes. Therefore, there is the option of storing the data in 2 or in 3 bytes to cut down the amount of information to be saved. When working at 10 samples per second, a 100 sample block is sent every 10 seconds and contains 1.5k bytes. It takes the RS232 about 2 seconds to transfer the data, and the BBC about a further second to store it. Therefore, there is sufficient time to display at least some of the data. This system has been heavily used in the last 2 years and since all the bugs have been removed, it has not lost any data.

7.10.5 New BBC to Digital Rack Commands

All the comands to set up the data block are sent whilst the computers are in the original data transfer mode.

P x1 x2 Sets the shape of the data block. x1 is the number of bytes stored for each counter reading (1 to 3). x2 is the number of sets of readings in the block (1 to 100).

A Starts the data being transferred in larger blocks.

N Returns to the data being transferred as before.

7.11 Future Upgrades of the 7 Channel

At present there are no definite plans to upgrade the 7 channel. However, it is hoped in the near future to optically isolate the analogue and digital racks to remove the earth loop so reducing 50 Hz pickup. Eventually, it is intended to convert to the integrating amplifiers developed by Infrared Laboratories.

Chapter 8

The 2.2μm Galactic Survey

A collaborative project between Imperial College (London) and the Instituto de Astrofisica (Tenerife) has been instigated to map most of the galactic bulge and plane at 2.2μm. The ultimate goals are to fill the gap between the IRAS and Schmidt I plate surveys for a large area of the most interesting part of the sky and to provide detailed information on the large scale distribution of stars in the galaxy. The survey will be carried out using the ICSTM 7 channel linear infrared camera on the 1.5m TCS. It is a long term project and is currently in its second year. To date, the majority of the effort has been in developing the infrastructure for the survey rather than reducing the data into its final format.

8.1 Why The Choice of 2.2μm

In deciding the best window for the survey a number of practical and scientific considerations were taken into account.

- The survey must be at a wavelength that is considerably longer than 0.9 μm, otherwise it would be repeating the Schmidt I plate surveys.
- Star distribution in the galaxy is one of the major motivations behind this survey. In the infrared, fluxes from stars are on the Rayleigh-Jeans curve so fall rapidly with increasing wavelength. Beyond 2.2 μm the drop in flux would be greater than the drop in interstellar extinction so not as many sources would be detected.

- The sky emission increases very steeply beyond 2.2 μm and at these longer wavelengths it would dominate the detector noise.
- InSb detectors are probably at their most sensitive in the K window.

8.2 Personnel Involved with the Project

The personnel involved with the project are M.J.Selby and myself from ICSTM and F.Gazon from the IAC. At least two new students are expected to start this year. ICSTM has provided the cryostat and data acquisition system: the IAC provides the telescope and the data storage facilities.

8.3 The Telescope

The 1.5 m Telescopio Carlos Sanchez (TCS) on Tenerife, which is now run by the IAC, will be used for the survey. It was built to test the principles of thin mirror telescopes in the early 70's and has been operated successfully in the near infrared since then. The quality of the images is reasonably good, with the seeing disk being typically 3" to 4"; however, the tracking and pointing are poor. It is situated on a dry site 8000ft above sea level and generally enjoys good weather during the summer months when the survey will be carried out. It is only 29 degrees from the equator so will allow the galactic centre to be mapped, albeit at a high airmass. The survey will require 3-4 months every year if it is to be completed on a reasonable time scale and the IAC have agreed to allocate the necessary telescope time. It is difficult to envisage how other telescopes on comparable sites could be used for such long periods of time.

8.4 The Detector and Data Acquisition System

The ICSTM 7 channel linear infrared camera (see chapter 7) will be used for the survey. In order to be able to digitize the noise, hence achieve the best limiting magnitude, the post amplifier gains are set to 1000. An IBM PC with a 40Mb hard disk is linked to the

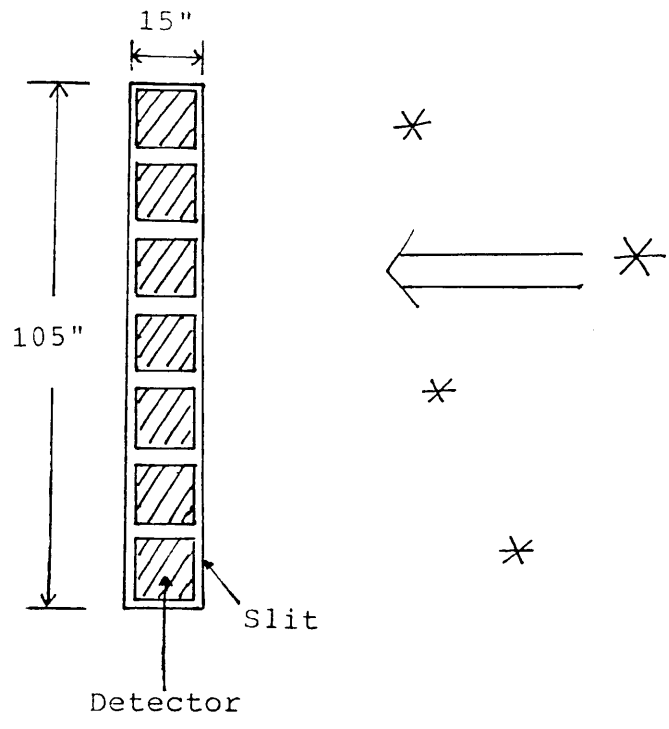

Figure 8.1: Method of Observation

The rotation of the earth moves the sky through the detectors. The apparent angular velocity of the sky is $15 \cos\delta$ *arcsec* sec^{-1}, *where* δ *is the declination.*

BBC via the IEEE to allow the large amount of data to be easily stored.

8.5 Method of Observation

The survey is carried out with the linear detector array aligned along the declination axis and the telescope stationary (figure 8.1). The rotation of the earth moves the sky through the detectors more smoothly and at a rate better known than that of any telescope drive. By knowing the exact starting position of the scan, the position of any point along it can be accurately determined from the elapsed time. The counters are read out about 10 times per second to ensure there is significant oversampling of the point object profiles. This allows the positions of sources to be determined to about 3" and match filtering techniques to be used in the data reduction. On average, each scan is two and a half hours long so it

passes through the entire galactic plane and reduces the length of time lost in repositioning the telescope. It is important that each strip of sky is repeated with the detectors moved 7.5" in declination to allow for the dead space between the detectors, otherwise there is a high possibility that sources will be missed and others reduced in strength. Also, by overlapping the scans there will be a check on the quality of the data. Up to 50% of the sources should appear identical in both scans so poor weather, problems with the cryostat, etc., can be identified by comparing them. It is vital that there is a check on the quality of the data if the survey is to be reliable.

Individual sources pass through the ~~the~~ slit in about 1 second. Since the 1/f noise for the InSb detectors at 1 Hz is small, the survey can be carried out without sky chopping. This makes the data reduction considerably easier and maximises the spatial resolution so reducing confusion problems. Since the high frequencies are no longer required, a 10 Hz low pass filter has been introduced into the detector circuit by putting a capacitor across the load resistor. This will reduce the 50 Hz pick up, hence the noise. Further, by working DC, an offset can be introduced into the post amplifiers to increase the dynamic range of the system.

The method being used is the only way large areas of sky can be covered quickly and accurately with a linear detector system. It is also by far the simplest and safest way to observe. By not driving the telescope or the chopper there will be no tracking errors: the telescope will not move out of the dome's slit: it does not matter if the observers fall asleep (as long as they wake up in time for the next scan) and there is less equipment to go wrong.

8.6 Setting up the Scan

Every starting position that will be used during the survey has been determined and given a reference number. They are 105" apart in declination and are about 1 hour from the centre of the galactic plane.

It is very important that the exact starting position is known so that scans can be successfully overlapped to remove the dead space between the detectors. The telescope is

positioned at the start of a scan by offsetting from the closest SAO star, generally within 8 arc minutes. Initially, the offsetting used the guide camera and SAO star alone. (The guide camera has a limiting magnitude of about +15 and a 3.5 arcminute field of view. A 5" reticule has been placed on the monitor so relative positions can be defined.) This works well when the starting position is close to the SAO star. However, when it is more than 3.5 arc minutes, it is inadvisable to attempt to go there directly since blind offsetting on the TCS is very inaccurate, and other faint stars visible in the TV camera have to be used to define intermediate positions. Each intermediate position will increase the error in the starting position. Whilst this method is probably accurate to about 4" it can take time and it is easy to make a mistake that will go unnoticed.

A better method was introduced in 1989 which uses the Schmidt plates. The area around the starting position is digitized and then stored on computer tape. The starting position is then marked, the offsets from the nearest stars brighter than +15 are calculated and a hard copy made (figure 8.2). The starting position is now directly defined in relation to the fainter stars visible in the TV camera as well as the SAO star. Therefore, the exact locations of the intermediate positions are known and the final accuracy of the starting positions is always better than 2".

8.7 Calibration of the Scans

The accurate photometric calibration of the scans is crucial to the success of the project. This will be attempted in two ways

- Before and after each scan a 'calibration run' is performed. This consists of letting a standard calibration star, typically between +4.5 and +7 magnitudes, run across each detector in turn (figure 8.3). Where possible it is performed at approximately the same declination as the scan, although the lack of calibration stars is a problem. As well as calibrating the photometry these scans also show the effect of crosstalk between channels. When a bright star passes through a detector there will be about a 1% response from the other channels. This is mainly caused by radiation scattering inside the cryostat. The calibration runs allow the size of this effect to be accurately measured, so offers the possibility of removing it in the data reduction. Finally, the

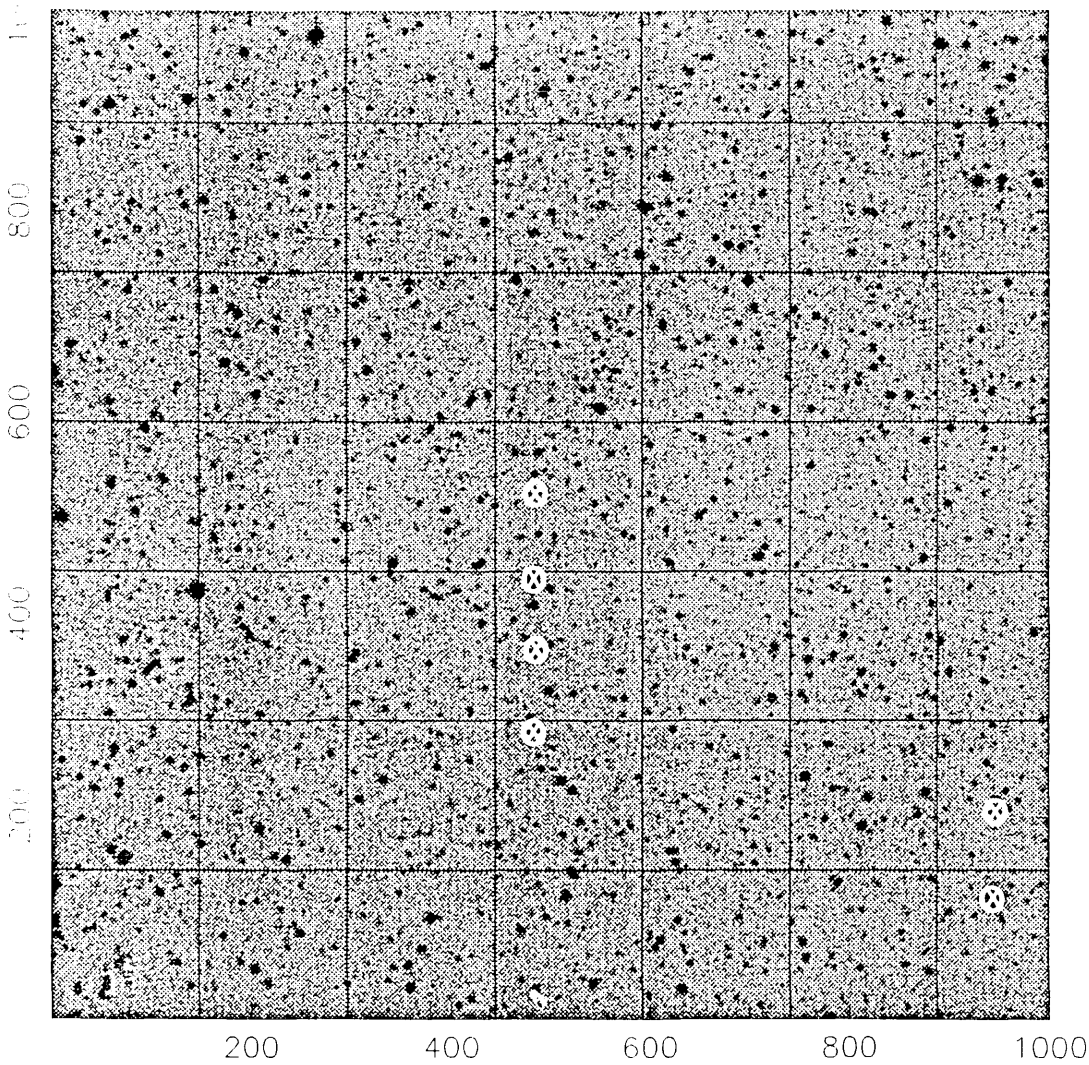

Figure 8.2: A Typical Computer Star Map.

The starting positions are marked with crosses

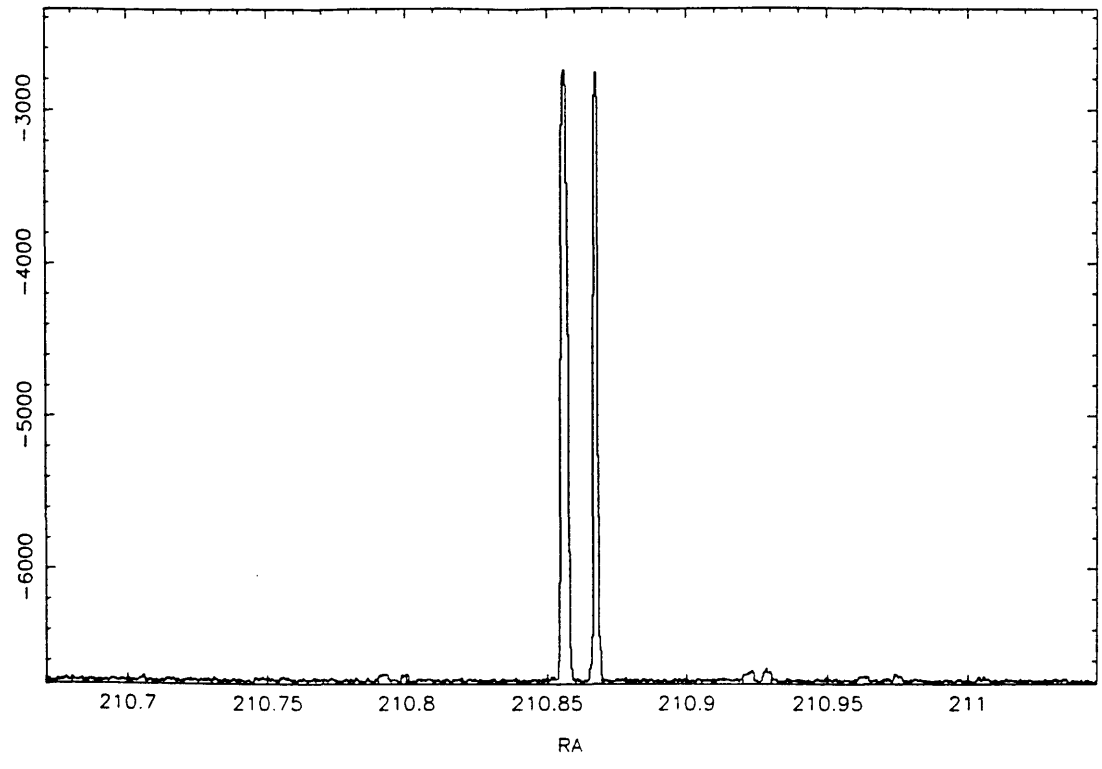

Figure 8.3: A Calibration Run on Channel 4

The left-hand of the two peaks is the calibration run. The right-hand peak is produced by the telescope as it moves back to the start. The smaller 'bumps' are produced by the cross talk as the star moves through other channels.

calibration runs can be used for the match filtering, although the profile will have to be altered if the calibration run is taken at a different declination to the scan.

- It is intended to carry out accurate photometry on a number of the sources detected using a standard photometry system.

It is hoped that the final photometric accuracy of the survey will be approximately 0.1 magnitudes.

8.8 Logging the Scans

The information on each scan must be accurately recorded so there is no possibility of confusion occurring between scans. A short information block is saved on the beginning of the data file. The title indicates whether the file is a scan (SC) or a calibration (CB),

which scan/calibration during the night (A,B,C,...) and the date. The other information saved is the amplifier gain, and the scan reference number or calibration star. The weather conditions, performance of the instrument, etc., is recorded separately in the observing log book.

8.9 Data rates and Storage

Sampling 7 channels 10 times per second with 2 bytes per channel produces 9K bytes of data per minute. Therefore, a typical scan will be over 1 mega byte long and a full night's observing will require about 4 Mb of storage space. The only way in which this amount of data can be successfully handled is to dump it directly to a hard disk as it is taken. Hard disks are reliable, have very fast access times and a storage capacity of typically 40 Mb. At the end of the night's observing the data is transferred to a VAX/ Data General readable tape in a standard FITS format.

8.10 Reducing the Data

To date very little work has been done in reducing the data, although this is altering now that the observational side is working well.

The data is reduced in many different ways depending on which facet of the data is being examined, eg point or extended objects; however, the initial reduction of the raw data is the same. Firstly, the data is 'deglitched' to remove any noise spikes. This is possible since they have an easily recognisable shape. Then the DC offset is removed from the data so the background level is approximately zeroed and the signals become positive. Figure 8.4 shows a complete single channel scan that passed close to the galactic centre. Figure 8.5 shows two small sections close to the galactic centre for all 7 channels. The channels have been separated by the introduction of DC offsets.

The initial method to be used for point source detection is match filtering. This is probably the most sensitive method for the detection of a known signal shape in the presence of noise. A calibration beam profile (which is the instrumental profile) is convolved

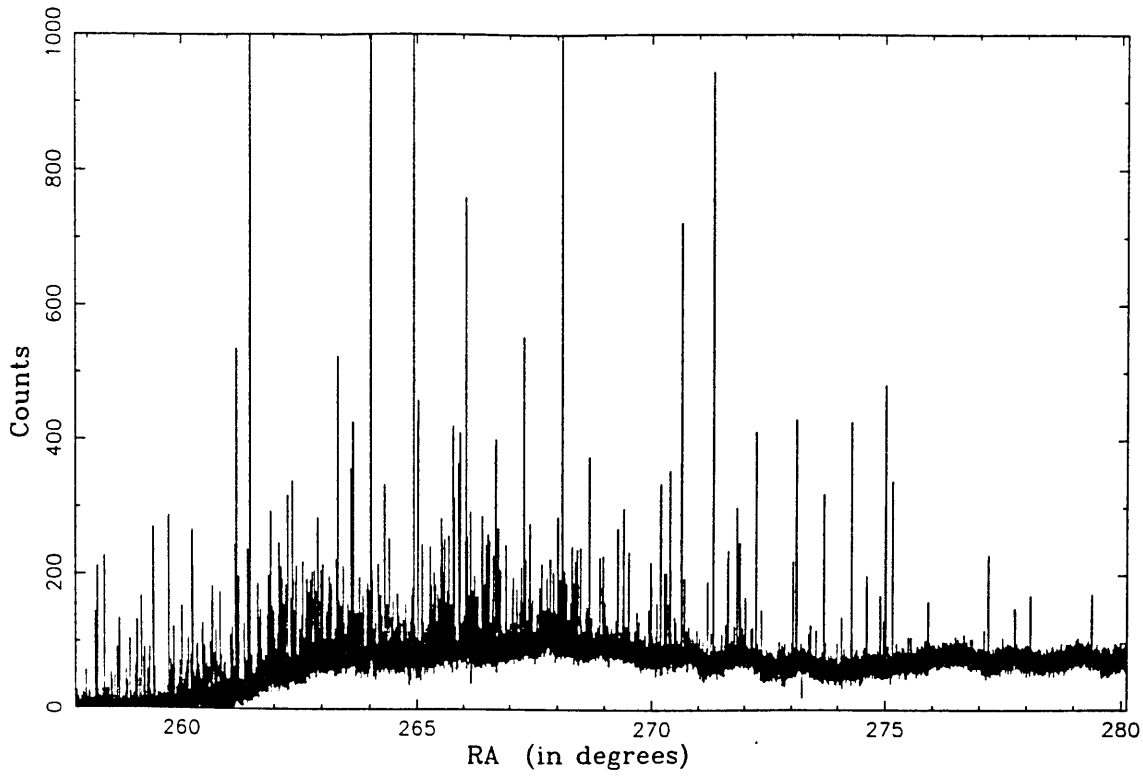

Figure 8.4: Complete Scan Near the Galactic Centre

with the scans after allowing for any difference in declination. If S(x) is the observed scan and I(t) is the instrumental profile then

$$C(x) = \int_{-t_0}^{t_0} S(x+t)I(t)\,dt \tag{8.1}$$

The signal has been smoothed to give the best possible signal to noise ratio. The positions and strengths of sources can now be determined by looking at peaks alone.

Unfortunately, match filtering reduces the spatial resolution which is a problem, particularly towards the galactic centre. Figure 8.6 shows this effect and sources which are clearly multiple stars in the original data are merged to form an extended source. There are a number of possible ways of detecting these multiple sources. One possibility is to examine the shape of the source in the raw data and compare it with the point source profile. Another is to look for changes in the slope of the source: if the slope changes sign more than once it is an indication of a multiple source.

A number of other routines will be applied to the data. They may offer ways of increasing the S/N whilst maintaining the spatial resolution which will be important for crowded areas of sky.

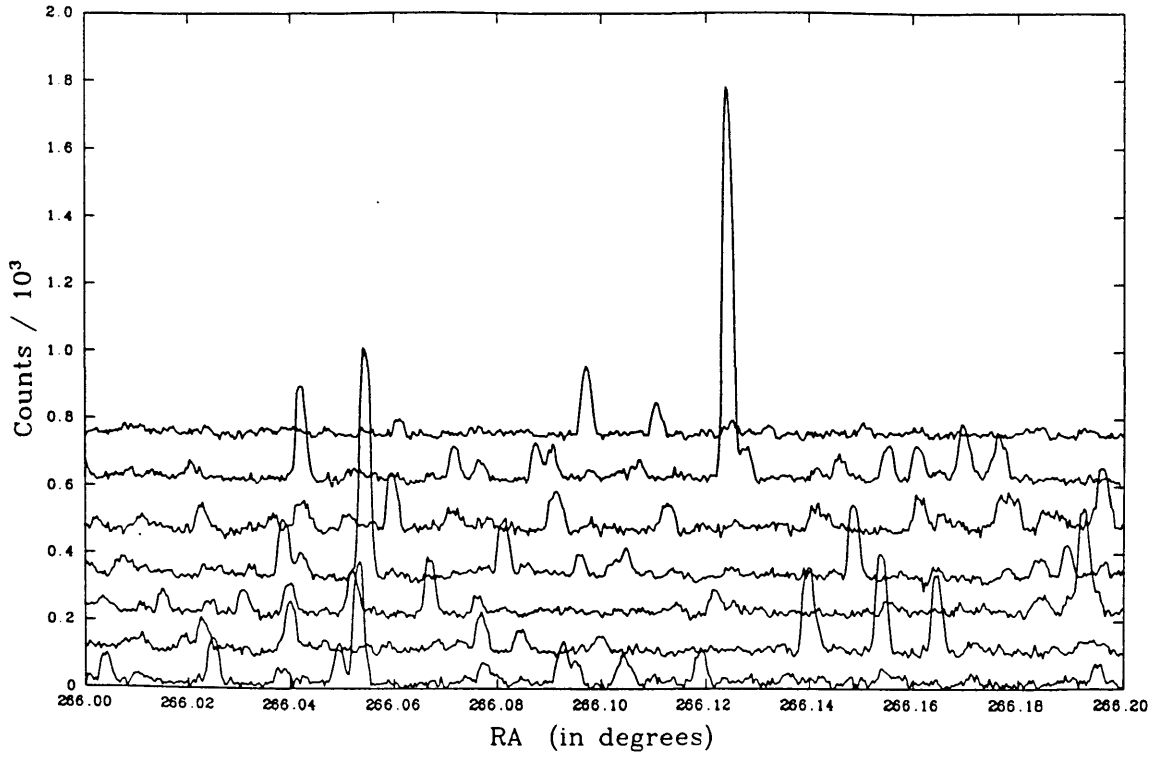

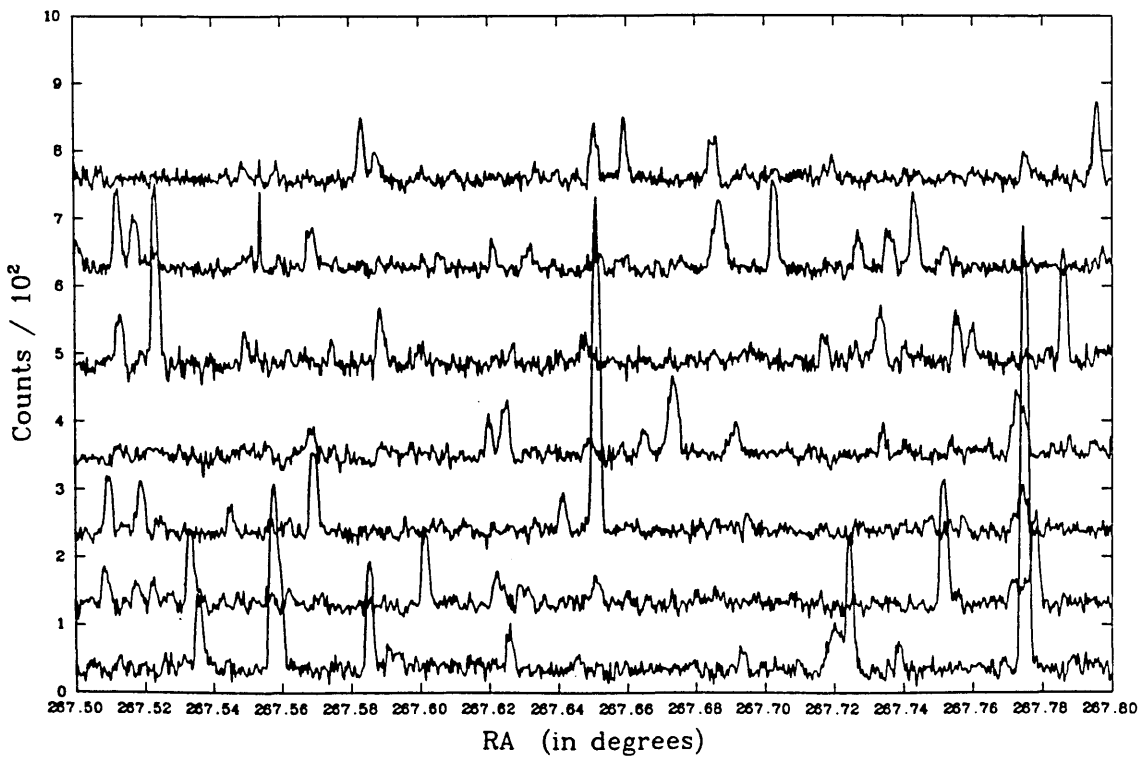

Figure 8.5: 2 Parts of a Scan Close to the Galactic Centre

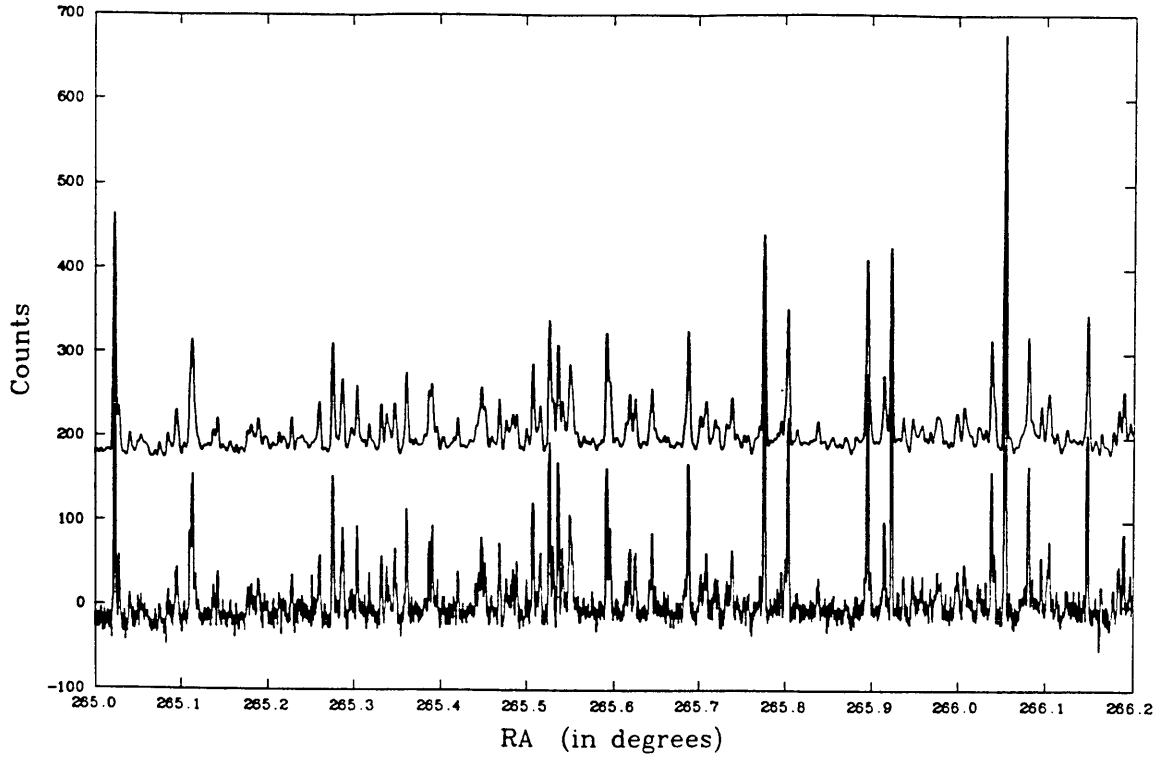

Figure 8.6: The Effect of Match Filtering on the Spatial Resolution

To date, no real attempt has been made at detecting extended sources. This will be considerably more difficult than detecting point sources because DC drifting in the electronics and patchy sky transmission will cause spurious effects. However, a number of extended sources are clearly present on the scale 15" to 1'-2', although until more detailed work is performed it is impossible to determine what they are. It is expected that many of the detections will instigate follow up observing programmes in the infrared and at other wavelengths.

8.11 Limiting Magnitude and Spatial Resolution

The 1 sigma limiting magnitude of the survey is approximately +12.5, although this will vary with channel and observing conditions, and the spatial resolution is between 10 and 15 arc seconds. Previous results suggest that with these limits, the survey will be confusion limited in areas with high star densities. This is when there is a high probability of there being two or more sources detected simultaneously in one channel, so only the brighter one is recorded. The result is to significantly reduce the number of fainter sources detected,

so the survey is complete at the limiting magnitude of the equipment. Towards the centre of the galaxy the confusion limiting magnitude will be about +10.

8.12 Time Scale for the Survey

The survey was started in the summer of 1988 and will run for at least 5 years. We do not expect to have covered the whole galactic bulge and disk in this time, but this is the furthest that can be planned ahead in terms of instrumentation, telescope time, etc. Also in about 1993 the ISO (the Infrared Satellite Observatory) will be launched, and both M.J.Selby and F.Gazon are co-investigators on the project. The survey will be an invaluable aid for the development of observing programmes in the galactic plane. It is expected that the project will have built up its own momentum by 1993 so will continue after this date.

8.13 Data Presentation

The data will be presented in three formats

- A map of the galactic plane will be produced with a spatial resolution of about 10" and a 1 sigma limiting magnitude of +12.5.
- A point source catalogue.
- An extended source catalogue.

The data will only be presented in a computer readable format. It is estimated that the final point source catalogue will contain some ten million sources, about 50 times more than IRAS. Therefore, it is inconceivable to publish the data in printed format.

8.14 What Will be Detected

Perhaps the most interesting aspect of taking the data is the comparison between the TV guide camera and the signals on the detectors. Possibly only 10 per cent are common to both. There are a large number of very bright (8th mag or less) infrared detections which have no visible counterpart. This indicates that the majority of sources detected by the survey are very red objects.

Previous results indicate that the majority of sources detected will be M giants. Assuming the survey has a magnitude limit of +10 in the crowded areas of the sky, a M3III star will be detected to a distance of about 8 Kpc, which is just short of the galactic bulge. The supergiants, though, should be detectable throughout the galaxy.

The 2.2μm sky survey (1969) detected one BN object and a number of dust shrouded stars in only 5000 sources. The survey should detect BN objects at over 3Kpc so many more, possibly thousands, could be discovered, along with tens of thousands of shrouded stars.

The survey will provide much information on the size and distribution of dust clouds in the galaxy. The near infrared shows the dust clouds by a reduction in the number of detections whereas the far infrared sees them in emission. Much information on the structure of dust clouds will be gained by the comparison of the 2.2μm and IRAS surveys.

A large number of extended objects will be detected: these will include compact HII regions, planetary nebulae and globular clusters.

8.15 Comparison with Other Equipment

When proposing this project, the first response of many astronomers was, "Why not use a large 2D CCD array, like IRCAM on UKIRT?". These arrays have over 3000 pixels with a two arcminute square field of view, so at first sight it might be expected that they could complete the survey far faster than a 7 channel device. This is not the case.

There are two ways in which IRCAM could be used to map an area, either to take

a snapshot of each area or to scan. In order to map at sidereal rate using the snapshot mode, one frame would have to be taken every 8 seconds. It would take about this long to reposition the telescope and let it settle, so only a small proportion of the time would be spent taking data. Further, it is unlikely that sources could be positioned as accurately as when scanning at sidereal rate.

To achieve a good photometric accuracy when scanning, at least 3 samples are required per pixel. A pixel on IRCAM is about 2" square; therefore, when working at sidereal rates about 20 samples per second are required. TIAs, as used in the 7 channel, typically produce the equivalent of 1000 electrons per root second amplifier/detector noise and no read out noise. However, the noise on IRCAM is dominated by the readout for integrations of less than about 5 seconds, each readout producing around 450 electrons. Therefore, IRCAM operates best when used for long integrations: higher sample rates rapidly increase the noise. Also, when scanning at sidereal rate there would be the problem of handling over 100K bytes per second.

The conclusion must be that a 2D array camera, like IRCAM on UKIRT, could not perform the survey significantly faster than the 7 channel working at sidereal rate, although a better spatial resolution and limiting magnitude could be achieved. Since it is inconceivable that any telescope other than the 1.5m TCS would allocate the required time, the use of 2D array camera is out of the question at the moment.

8.16 Future Up Grades to the Instrumentation

When carrying out a long term project it is important that the equipment is altered as little as possible so the quality of the data remains constant. However, it is hoped that in the future a 32 element linear array camera will become available which will speed up the survey.

8.17 Future Work

Obviously the most important tasks in the near future are to fully reduce the data and continue with the observations. However, there are a number of complementary projects which could be started that would significantly add to the quality of the survey.

One of the hardest tasks will be cross-referencing the survey with others carried out at different wavelengths, particularly the IRAS and Schmidt plate all sky surveys. There have been discussions with the Royal Observatory Edinburgh about the possibility of using their plate measuring machines to produce a computer data base for the I,R and V plates of the galactic plane with a similar spatial resolution as the galactic survey. This would allow computers to carry out colour differencing on huge numbers of stars as well as providing complementary data bases to the 2.2 μm galactic survey.

At present there is no back up observing programme in the event of the 7 channel becoming unavailable during a run. This could be an optical misalignment, a vacuum leak, etc., which would require the instrument to be stood down for one or two nights whilst the problem is sorted out. One possible back up programme would be to use the ICSTM 4 channel photometer system. This simultaneously measures J,K,L and M windows, although it is proposed to alter this to J,H,K and L, and it can be run using the same data acquisition system and telescope mount as the 7 channel, so conversion between the two would be very fast. The project would be to make 4 wavelength maps of small areas of the galaxy (about 10 arcminutes square) with a spatial resolution and limiting magnitude similar to that of the survey. This would allow infrared colour differencing on a large number of sources, which will indicate their spectral type and distances.

Appendix A

List of Detected Absorption Lines

Only those the features which have been definitely identified and can be attributed to one or two absorption lines are included. The line positions have been taken from Kleinmann 1986 and Montgomery 1969.

The Hydrogen Lines

Wavelength	Name	Transition
0.932	P ζ	9 to 3
0.955	P ϵ	8 to 3
1.005	P δ	7 to 3
1.094	P γ	6 to 3
1.282	P β	5 to 3
1.588	B κ	14 to 4
1.611	B ι	13 to 4
1.641	B θ	12 to 4
1.681	B η	11 to 4
1.737	B ζ	10 to 4
1.818	B ϵ	9 to 4
1.945	B δ	8 to 4
2.166	B γ	7 to 4
4.052	B α	5 to 4
2.873	Pf η	11 to 5
3.039	Pf ζ	10 to 5
3.297	Pf ϵ	9 to 5
3.740	Pf δ	8 to 5

P=Paschen B=Brackett Pf=Pfund

The other lines detected

Lines	Wavelength (μm)
Na	1.140
Fe	1.160
Mg	1.188
Si	1.198
Si	1.203
Mg/Si	1.208
Si	1.227
Fe	1.475
Fe	1.499
Fe	1.529
Si/Ti	1.559
Mg	1.575
Si	1.588
Fe	1.611
Fe	1.643
Si	1.668
Al	1.6719
Fe	1.701
Mg	1.723
Si	1.723
Fe	2.071
Si	2.091
Mg	2.106
Al	2.116
Si	2.135
Ti	2.178
Si	2.187
Na	2.208
Fe	2.227

Fe	2.238
Ca	2.265
Mg	2.281
Co	2.292
Co	2.322
Na	2.338
Co	2.343
Co	2.352
Co	2.373
Co	2.383
Co	2.403

Appendix B

Comparison of Instantaneous and Integration Sampling Theory

Consider a signal g(t) which has a frequency spectrum G(f) that is to be sampled every 'a' seconds

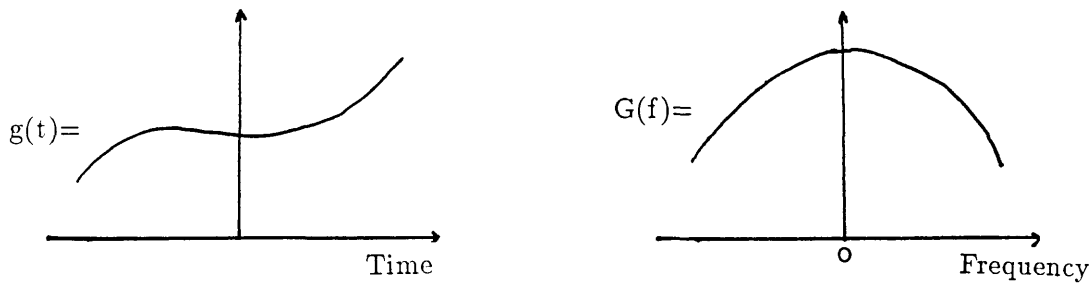

Instantaneous Sampling

When the signal is sampled instantaneously every **a** seconds it is the equivalent of multiplying the function by a Dirac comb of spacing a. The sampled spectrum $g_s(t)$ is

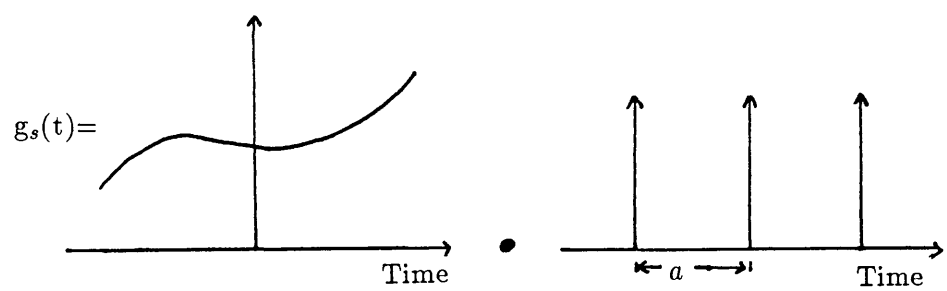

In frequency space this becomes

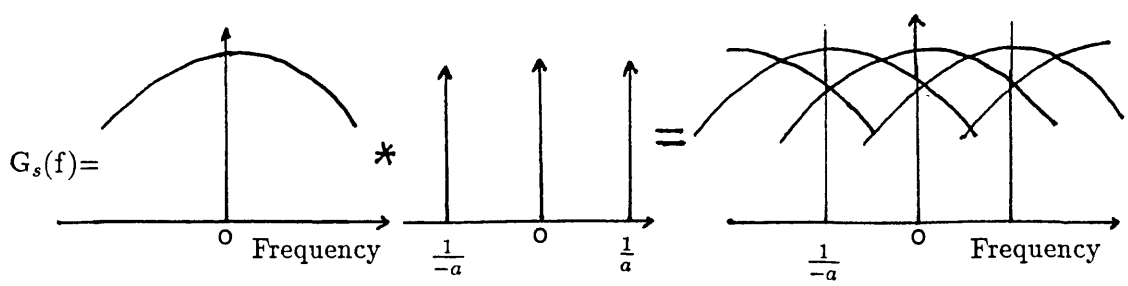

Integration Sampling

When using an integration sampling technique, in effect the function g(t) is being convolved with a top hat function of width **a**. Therefore the function which is to be sampled g'(t) is

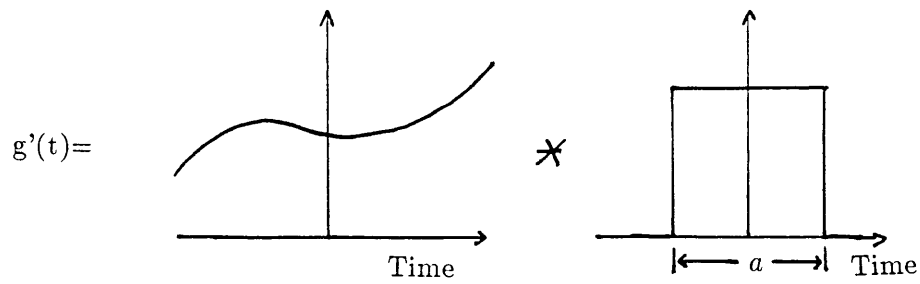

In frequency space

$$G'(f) = G(f) \quad \frac{\sin \pi a f}{\pi a f}$$

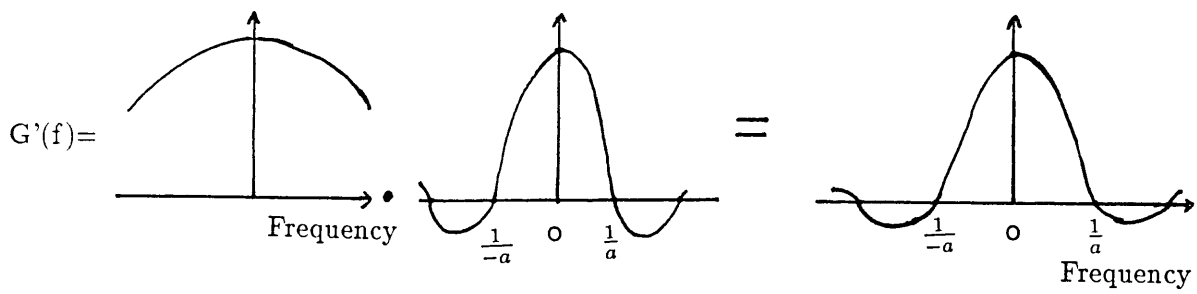

This is sampled as before to produce a spectrum in frequency space of

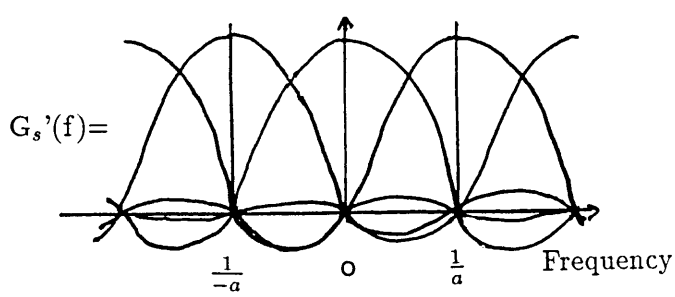

Detected Frequencies

Sampling theory states that the maximum frequency that can be detected is half the sampling frequency, in this case the Nyquist limit is $\frac{1}{2a}$. However, as the above demonstrates the act of sampling can cause the high frequencies to appear below this limit, due to what are called alias bands. These increases the noise. The best way of overcoming the alias bands is to sample at a frequency at least twice that of the highest frequency in the noise,

ie either sample at a faster rate or reduce the bandwidth of the signal. However, this is not always possible as it can lead to unmanageable data rates or there may be some high frequencies which are difficult to remove (eg 50 Hz pick up).

When the signal is undersampled, integration sampling is considerably less sensitive to high frequency noise than is instantaneous sampling. The power spectra, below the Nyquist limit, for both sampling methods are

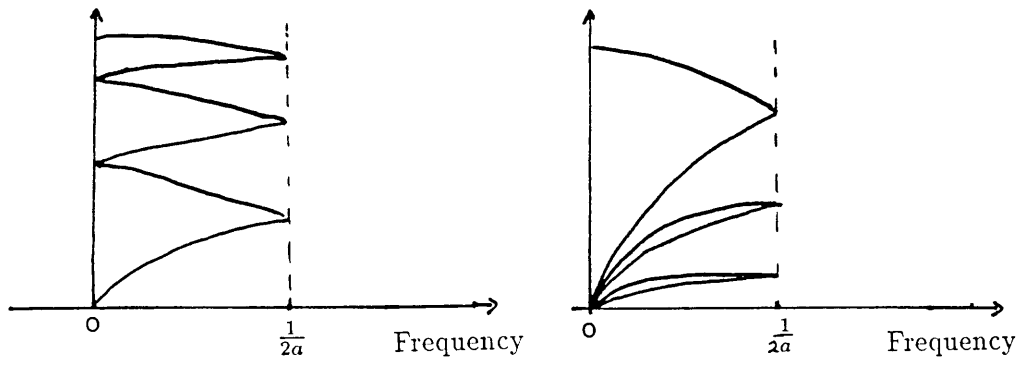

Instantaneous Integrating

Integration sampling reduces the noise at all frequencies since the noise spectrum is multiplied by $\frac{\sin a\pi f}{a\pi f}$, which is always less than one. Further, at multiples of the sampling frequency the noise is reduced to zero. Therefore, if there is only one dominant high frequency in the noise it can be removed by making the sampling period a multiple of the period of the noise. (eg sampling at 10 Hz to remove 50Hz mains pick up).

Appendix C

The Absolute Spectra Of Carbon Stars

For a number of years ICSTM has been collaborating with the IAC in taking spectra of carbon stars with the intention of comparing the results with models. A number of spectra of carbon stars were taken by C.Lazaro, I.Hepburn and A.Zadrosny in July 1985 as well as the bright stars which have been described earlier. I have reduced the spectra of the carbon stars in the same way as the bright stars in chapters 4 and 5. On the next 4 pages are presented the absolute spectra obtained. To date this has been my only involvement with the project.

Carbon stars are very cool having temperatures between 2000K and 3000K and so their flux distributions peak in the near infrared. Their spectra are dominated by molecular lines which are not resolved by CGS1. The major features are

C_2	1.04 μm
CN	1.10 μm
C_2	1.4 μm
C_2	1.75 μm
CO	2.3 μm
HCN & C_2H_2	3.1 μm

CARBON STARS

Taken with CGS1

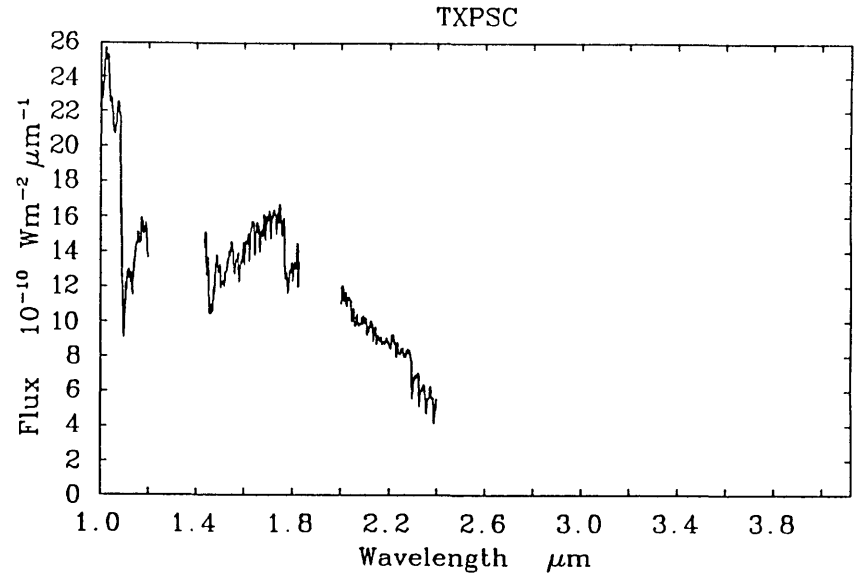

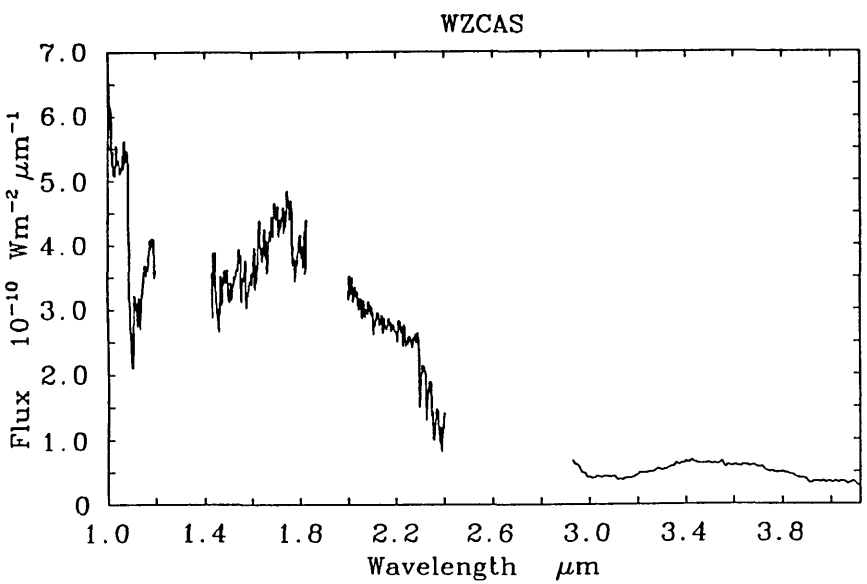

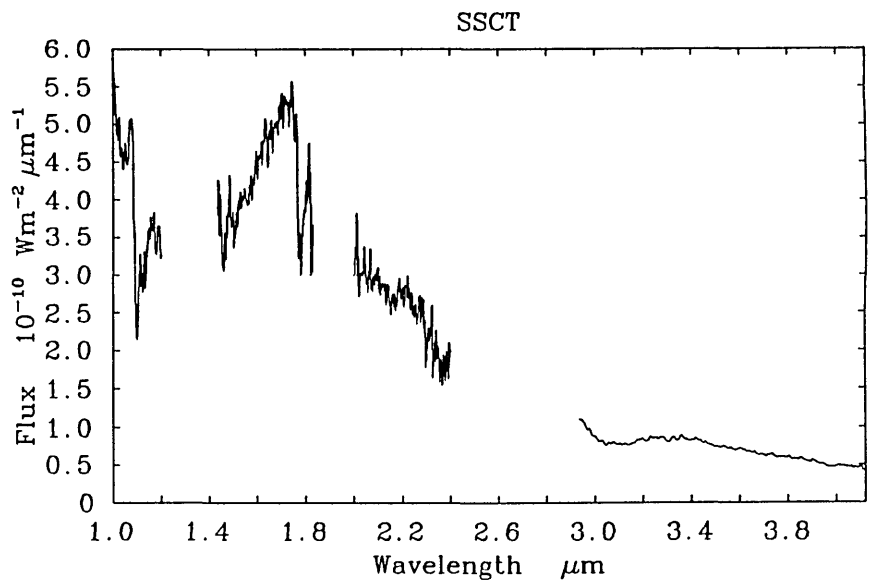

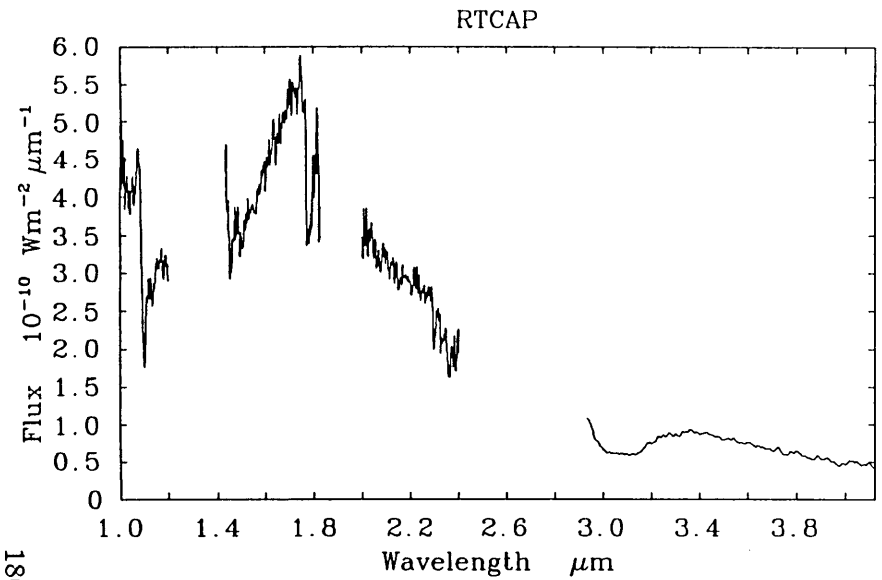
RTCAP
Flux 10^{-10} Wm^{-2} μm^{-1}
Wavelength μm

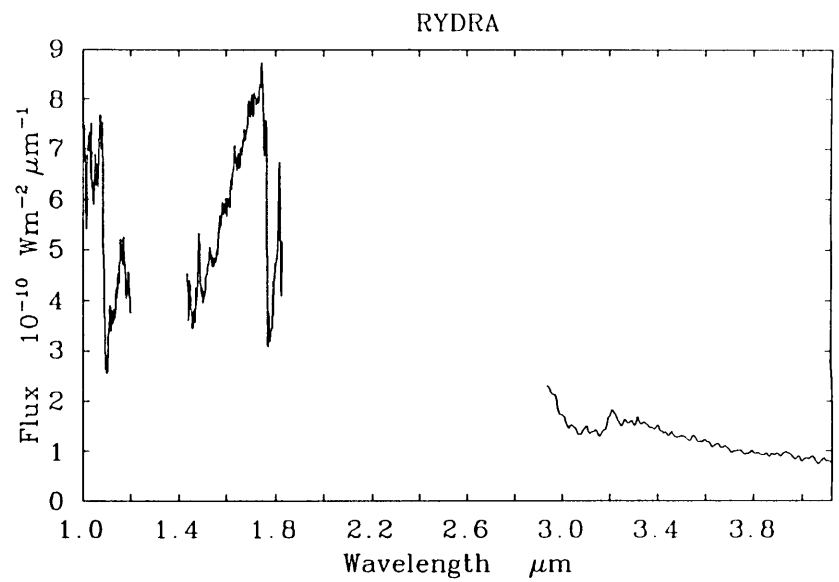
RYDRA
Flux 10^{-10} Wm^{-2} μm^{-1}
Wavelength μm

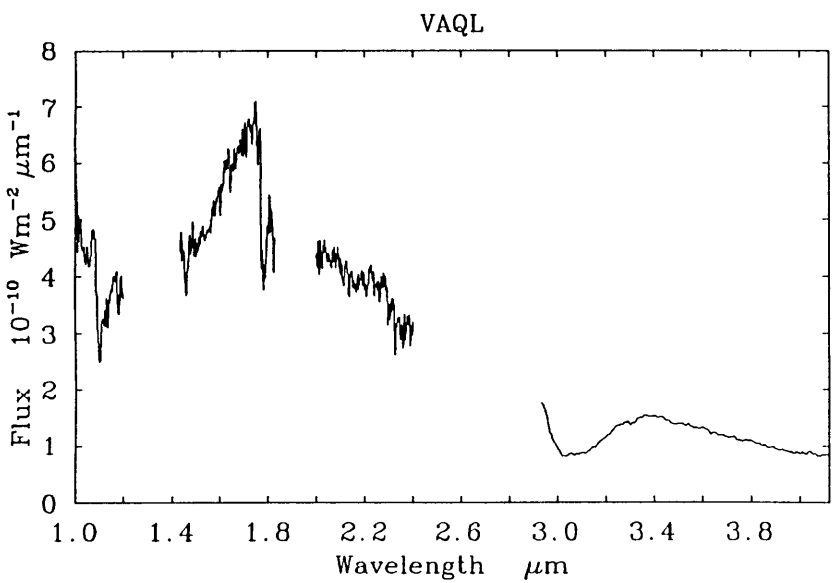
VAQL
Flux 10^{-10} Wm^{-2} μm^{-1}
Wavelength μm

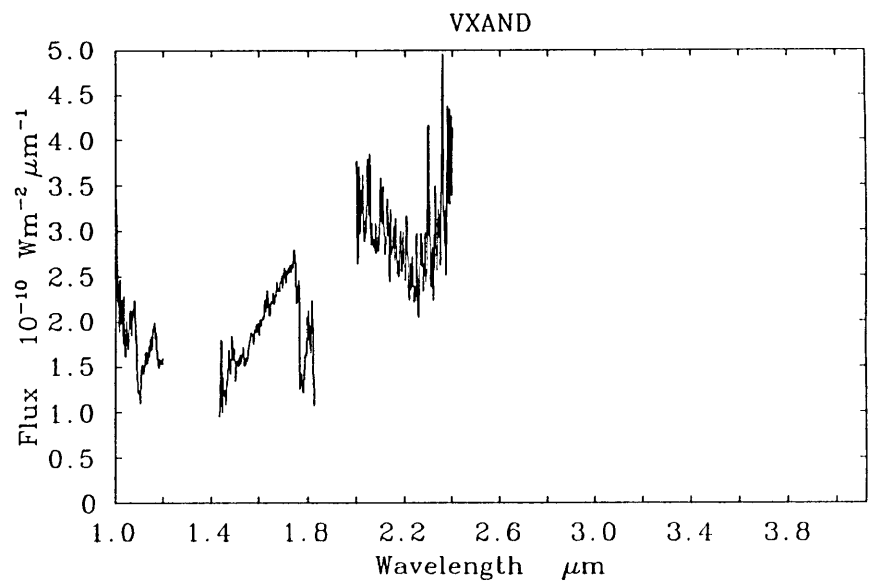
VXAND
Flux 10^{-10} Wm^{-2} μm^{-1}
Wavelength μm

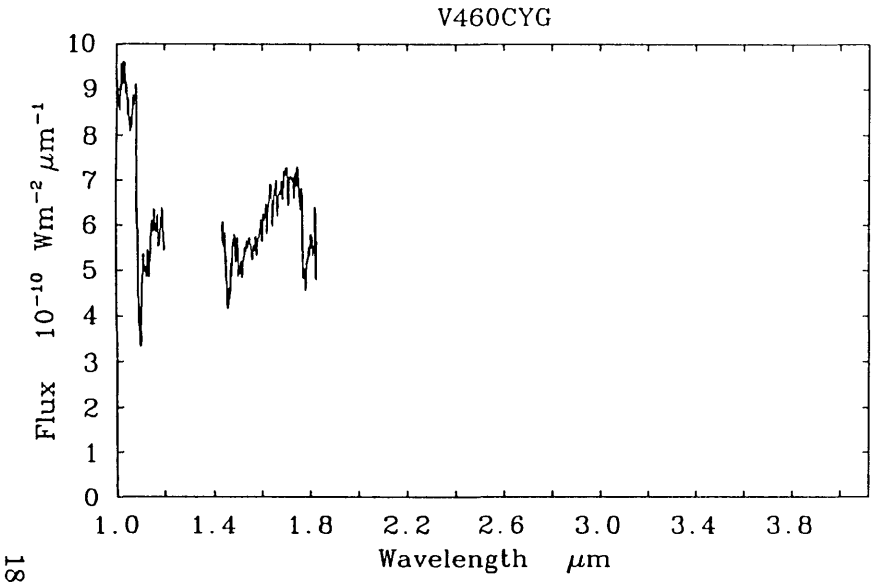
V460CYG
Flux 10^{-10} Wm^{-2} μm^{-1}
0 1 2 3 4 5 6 7 8 9 10
1.0 1.4 1.8 2.2 2.6 3.0 3.4 3.8
Wavelength μm

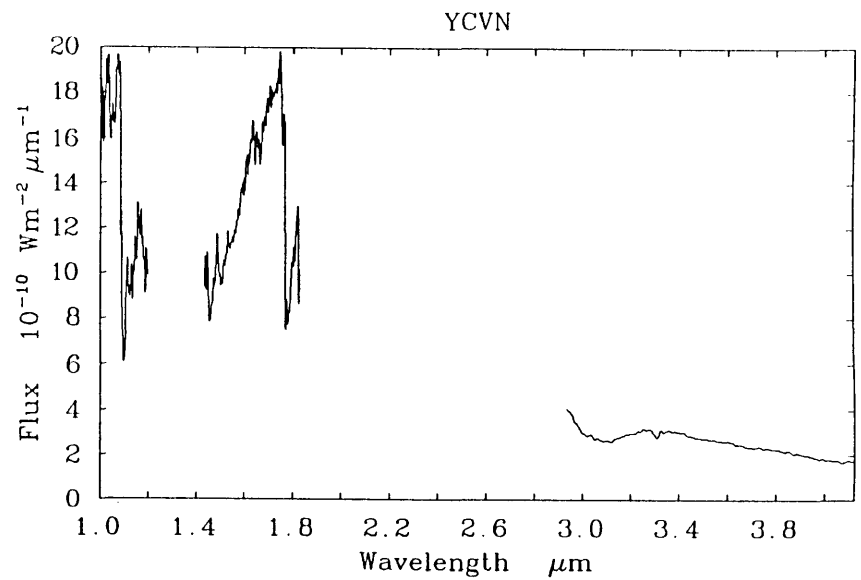
YCVN
Flux 10^{-10} Wm^{-2} μm^{-1}
0 2 4 6 8 10 12 14 16 18 20
1.0 1.4 1.8 2.2 2.6 3.0 3.4 3.8
Wavelength μm

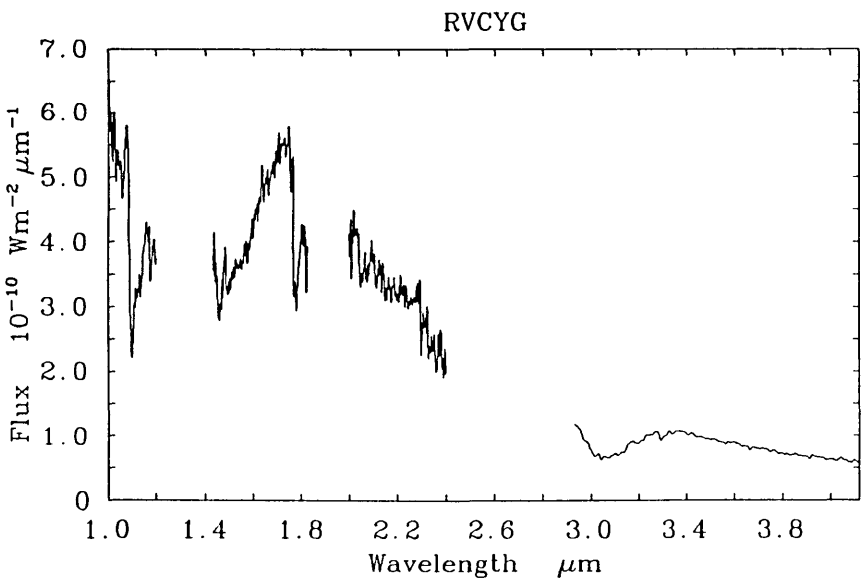
RVCYG
Flux 10^{-10} Wm^{-2} μm^{-1}
0 1.0 2.0 3.0 4.0 5.0 6.0 7.0
1.0 1.4 1.8 2.2 2.6 3.0 3.4 3.8
Wavelength μm

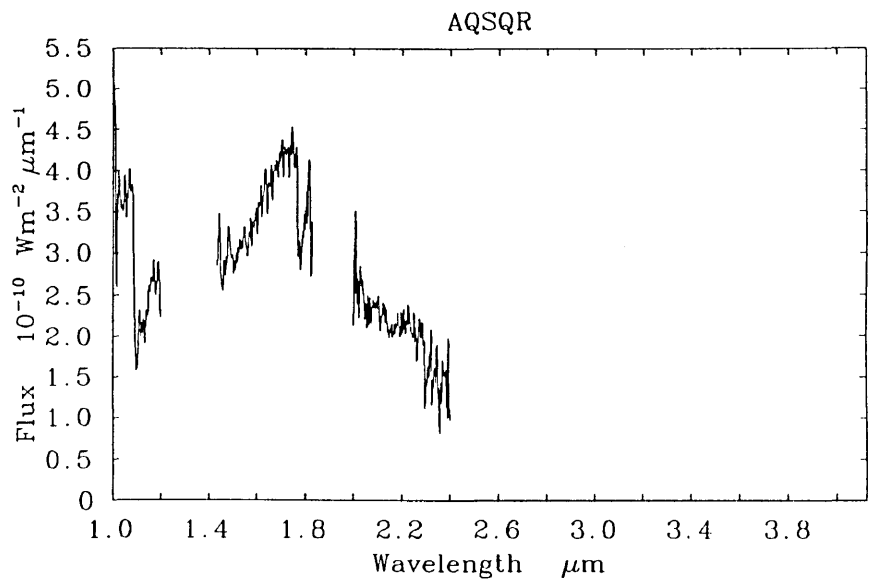
AQSQR
Flux 10^{-10} Wm^{-2} μm^{-1}
0 0.5 1.0 1.5 2.0 2.5 3.0 3.5 4.0 4.5 5.0 5.5
1.0 1.4 1.8 2.2 2.6 3.0 3.4 3.8
Wavelength μm

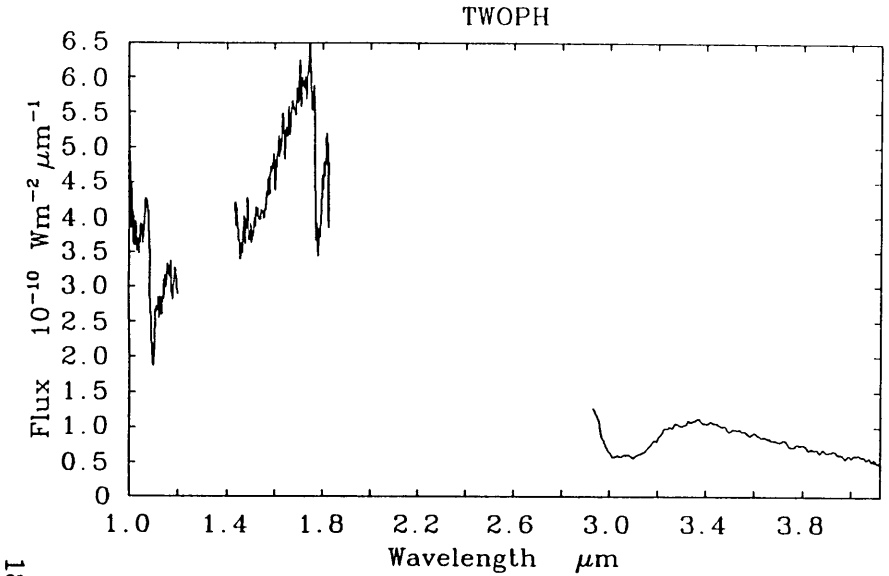
TWOPH
Flux 10^{-10} Wm^{-2} μm^{-1}
Wavelength μm

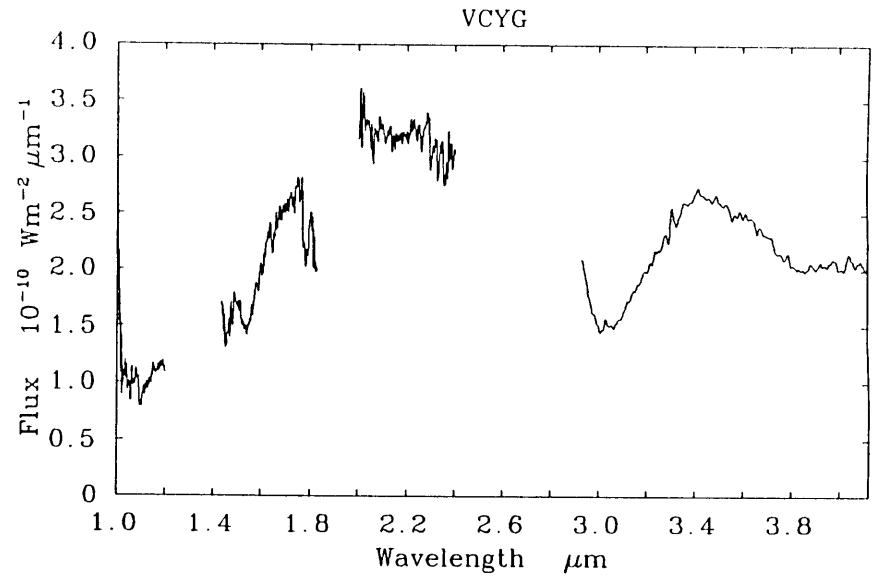
VCYG
Flux 10^{-10} Wm^{-2} μm^{-1}
Wavelength μm

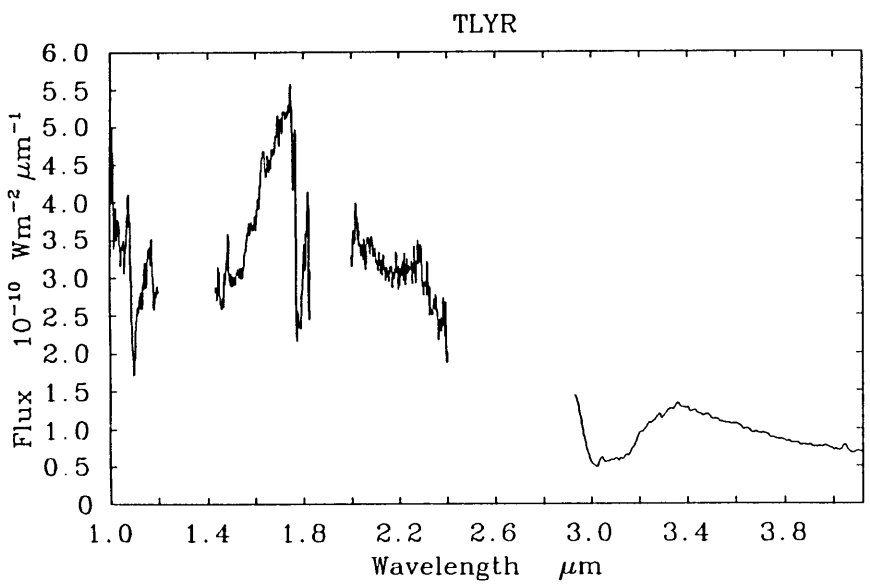
TLYR
Flux 10^{-10} Wm^{-2} μm^{-1}
Wavelength μm

References

Allen, C.W., 1973, *Astrophysical Quantities* , The Athlone Press, 3rd Edition

Beichman, C.A., 1987, *Ann. Rev. Astron. Astrophys.*,**25**, 52

Bell, R.A. and Gustafsson, B. 1989, *Mon. Not. R. Astro Soc.*,**236**, 653

Blackwell, D.E., Ibbetson, P.A., Petford, A.D., and Willis, R.B., 1975, *Mon. Not. R. Astro Soc.*,**171**, 195

Blackwell, D.E., Ibbetson, P.A., Petford, A.D., and Willis, R.B., 1976, *Mon. Not. R. Astro Soc.*,**177**, 219

Blackwell, D.E. and Shallis, M.J., 1977, *Mon. Not. R. Astro Soc.*,**180**, 177

Blackwell, D.E., Shallis, M.J. and Selby, M.J., 1979, *Mon. Not. R. Astro Soc.*,**188**, 847

Blackwell, D.E. and Shallis, M.J., 1980, *Astron. Astrophys.*,**81**, 336

Blackwell, D.E., Petford A.D. and Shallis, M.J., 1980, *Astron. Astrophys.*,**82**, 249

Blackwell, D.E., Booth, A.J., Leggett, S.K., Mountain, C.M. and Selby, M.J., 1986, *Mon. Not. R. Astro Soc.*,**221**, 427

Blackwell, D.E., Petford, A.D., Arribas, S., Haddock, D.J. and Selby, M.J., 1989, *Astron. Astrophys.*, (Submitted)

Carbon, D. and Gingerich, O., 1969, *Proc. Third Harvard-Smithsonian Conference on Stellar Atmospheres*, 377, MIT Press

Code, A.D., Davis, J., Bless, R.C. and Hanbury Brown, R., 1976, *Astrophys. J.*,**203**, 417

Conti, P.S., 1973, *Astrophys. J.*,**179**, 181

Cousins, A.W.J. and Guelke, R., 1953, *Mon. Not. R. Astro Soc.*,**113**, 776

Di Bendetto, G.P. and Conti, G., 1983, *Astrophys. J.*, **268**, 309

Dreiling, L.A. and Bell, R.A., 1980, *Astrophys. J.*,**241**, 736

Evans, D.S., Heydenrych, J.C.R. and Van Wyk, J.D.N., 1953, *Mon. Not. R. Astro Soc.*,**113**, 781

Grasdalen, G.L. and Gaustad, J.E., 1971, *Astron. J.*,**76**, 231

Gezari, D.Y., Labeyrie, A. and Stachnik, R.V., 1972, *Astrophys. J.*,**173**, L1

Glass, I.S., Catchpole, R.M. and Whitelock, P.A., 1987, *Mon. Not. R. Astro. Soc.*,**227**, 373

Gray, D.F., 1967, *Astrophys. J.*,**149**, 317

Gray, D.F., 1968, *Astron. J.*,**73** 769

Gray, D.F., 1981, *Astrophys. J.*,**245**, 992

Hanbury Brown R. and Twiss, R.Q., 1956, *Nature*,**178** 1046

Hanbury Brown, R., 1968, *Ann. Rev Astr. Astrophys.*,**6**, 13

Hanbury Brown, A., Davis, J. and Allen, L.R., 1974, *Mon. Not. R. Astro Soc.*,**167**, 121

Hayakawa, S., et al, 1976, *Nature*,**261**, 29

Hayakawa, S., et al, 1977, *Astron. Astrophys.*,**58**, 325

Hayakawa, S., et al, 1978, *Publ. Astron. Soc. Japan*, **30**, 396

Hayakawa, S., et al, 1979, *Nature*,**279**, 510

Hayakawa, S., et al, 1981, *Astron. Astrophys.*,**100**, 116

Hayes, D.S. and Latham, D.W., 1975, *Astrophys. J.*,**197**, 1015

Hoffleit, D., 1982, *The Bright Star Catalogue*, Yale University Observatoy

Hofmann, W., et al , 1977, *Astron. Astrophys.*,**57**, 111

Hofmann, W., et al , 1978, *Astron. Astrophys.*,**70**, 427

Ito, K., et al, 1976, *Publ. Astron. Soc. Japan*,**28**, 427

Ito, K., et al, 1977, *Nature*,**265**, 517

Johnson, H.L. and Mitchell, R.I., 1975, *Rev. Mex. Astr. Astrofis.*,**1**, No. 3

Jones, A.W., 1982, Ph.D Thesis, University of London

Jones, A.W., Selby, M.J., Prieto, M. and Sanchez, C., 1984, *Astron. Astrophys.*,**138**, 297

Kleinmann, S.G. and Hall, D.N.B., 1986, *Astrophys. J. Suppl*,**62**, 501

Kurucz, R.L., Peytremann, E. and Avrett, E.H., 1974, *Blanketed Model Atmospheres for Early Type Stars*, SAO., Smithonian Institute

Kurucz, R.L., 1979, *Astrophys. J Suppl.*,**40**, 1

Leggett, S.K., 1983, Ph.D Thesis, University of Oxford

Leggett, S.K., Mountain, C.M, Selby, M.J., Blackwell, D.E., Booth, A.J., Haddock, D.J. and Petford, A.D., 1986, *Astron. Astrophys.*,**159**, 217

MacGregor, A.D., 1977, *ICST Detector Testing Contract : Final Report.* Royal Observatory Edinburgh

Maihara, T., et al, 1978, *Publ. Astron. Soc. Japan*,**30**, 1

Mclean, I.S., Aspin, C., Longmore, A.J., and Dixon, R.I., 1988, *Infrared Astronomy with Arrays*, University of Hawaii

Michelson, A.A. and Pease, F.G., 1921, *Astrophys. J.*,**53**, 249

Montgomery, et al, 1969, *Astrophys. J. Suppl.*,**19**, 1

Mountain, C.M., 1983, Ph.D Thesis, University of London

Mountain, C.M, Leggett, S.K., Selby, M.J., Blackwell, D.E. and Petford, A.D., 1985, *Astron. Astrophys.*,**151**, 399

Neugebauer, G. and Leighton, R.B., 1969, *Two-Micron Sky Survey A Perliminary Catalogue*, NASA SP 3047, Washington DC

Oke, J.B. and Schild, R.E., 1970, *Astrophys. J*,**161**, 1015

Petford, A.D., Blackwell, D.E., Booth, A.J., Haddock, D.J., Leggett, S.K., Mountain, C.M, Selby, M.J. and Arribas, S., 1988, *Astron. Astrophys.*,**203**, 341

Popper, D.M., 1967, *Ann. Rev. Astr. Astrophys.*,**5**, 85

Popper, D.M., 1980, *Ann. Rev. Astr. Astrophys.*,**18**, 115

Price, S.D. and Walker, R.G., 1976, *The AFGL Four Colour Infrared Sky Survey*, AGGL-TR-76-0208, USAF Geophysics Laboratory

Ridgway, S.T., Wells, D.C. and Joyce, R.R., 1977, *Astron. J.*,**82**, 414

Ridgway, S.T., 1977, *Astron. J.*,**82**, 511

Ridgway, S.T., Wells, D.C., Joyce, R.R. and Allen, R.G., 1979, *Astron. J.*,**84**, 247

Ridgway, S.T., Joyce, R.R, White, N.M. and Wing, R.F., 1980, *Astrophys. J.*,**235**, 126

Ridgway, S.T., Jacoby, G.H., Joyce, R.R and Wells, D.C., 1980, *Astron. J.*,**85**, 1496

Ridgway, S.T., Jacoby, G.H., Joyce, R.R, Siegel, M.J. and Wells, D.C., 1982, *Astron. J.*,**87**, 808

Ridgway, S.T., Carbon, D.F., Hall, D.N.B and Jewell, J., 1984, *Astrophys. J. Suppl.*,**54**, 177

Saxner, M. and Hammerback, G., 1985, *Astron. Astrophys.*, **151**, 372

Schild, R., Peterson, D.M. and Oke, J.B., 1971, *Astrophys. J.*,**166**, 95

Schmidt-Kaler, T., 1976, *Vistas in Astron.*,**19**, 69

Selby, M.J., Mountain, C.M., Blackwell, D.E., Petford, A.D. and Leggett, S.K., 1983, *Mon. Not. R. Astro. Soc.*,**203**, 795

Selby, M.J., Hepburn, I., Blackwell, D.E., Booth, A.J., Haddock, D.J., Arribas, S., Leggett, S.K. and Mountain, C.M., 1988, *Astron. Astrophys. Suppl.*,**74**, 127

Strecker, D.W, Erickson, E.F. and Witteborn, F.C., 1979, *Astrophys. J. Suppl.*,**41**, 501

Thompson, G.I., Nandy, K., Jamar, C., Monfils, A., Houziaux, L., Carnochan, D.J. and Wilson, R. 1978. *Catalogue of UV Fluxes*

Traub, W.A. and Stier, M.T., 1976, *Appl. Optics*,**15**, 364

Tsuji, T., 1978, *Astron. Astrophys.*,**62**, 29

Tsuji, T., 1981, *Astron. Astrophys.*,**99**, 48

Tsuji, T., 1981, *J. Astrophys. Astr.*,**2**, 95

Tsuji, T., 1981, *J. Astrophys. Astr.*,**2**, 255

Underhill, A.B., Divan, L., Prevot-Burnichon, M.L. and Doazan, V. 1979, *Mon. Not. R. Astro. Soc.*,**189** 601

Underhill, A.B., 1979, *Astrophys J.*,**234**, 528

Underhill, A.B., 1980, *Astrophys J.*,**239**, 220

Underhill, A.B., 1981, *Astrophys J.*,**244**, 963

Underhill, A.B., 1982, *Astrophys J.*,**263**, 741

Underhill, A.B., 1983, *Astrophys J.*,**266**, 718

Wesselink, A.J., Paranya, K. and Devorkin, K., 1972, *Astron. Astrophys. Suppl.*,**7**, 257